Functional integration and structural development of adult newborn hippocampal granule cells

Funktionelle Integration und strukturelle Entwicklung von adult neugebildeten hippocampalen Körnerzellen

Dissertation zur Erlangung des Doktorgrades der Naturwissenschaften

vorgelegt beim Fachbereich Biowissenschaften

Johann Wolfgang Goethe-Universität, Frankfurt am Main

von

Tassilo Jungenitz

aus

Halle/Saale

Frankfurt am Main (2017)

(D30)

Vom Fachbereich Biowissenschaften der

Johann Wolfgang Goethe-Universität als Dissertation angenommen.

Dekanin: Prof. Dr. Meike Piepenbring

Betreuer im Fachbereich: Prof. Dr. Manfred Kössl

Externer Betreuer: Dr. med. habil. Stephan W. Schwarzacher

Gutachter: Prof. Dr. Manfred Kössl, Prof. Dr. Bernd Grünewald

Datum der Disputation:

1. Einführung und Zusammenfassung (Introduction and summary in German language)

1.1. Thema und Fragestellung

Der Hippocampus als Teil des limbischen Systems verbarbeitet sowohl räumliche als auch zeitliche Informationen und spielt eine wichtige Rolle für das deklarative Gedächtnis, also der Speicherung von Informationen über Tatsachen und Ereignisse. Der *Gyrus dentatus* ist eine anatomische Region im Hippocampus und besitzt die einzigartige Fähigkeit auch im adulten Gehirn lebenslang neue Nervenzellen zu generieren. Dieser Prozess wird als adulte Neurogenese bezeichnet und wurde durch Pionierarbeiten von Joseph Altman und Gopal Das in den 1960iger Jahren im *Gyrus dentatus* und in der subventrikulären Zone der lateralen Ventrikel von Säugetieren nachgewiesen (Altman and Das, 1965; Altman, 1969). Seit dieser Erstbeschreibung wurde dieses Phänomen im adulten Gehirn von Singvögeln (Goldman and Nottebohm, 1983; Paton and Nottebohm, 1984; Alvarez-Buylla and Nottebohm, 1988; Alvarez-Buylla et al., 1988; Wilbrecht and Nottebohm, 2004) und in Säugetieren (Gould, 2007; Amrein and Lipp, 2009; Amrein et al., 2011; Bonfanti and Peretto, 2011; Lipp and Bonfanti, 2016), einschließlich des Menschen (Eriksson et al., 1998; Spalding et al., 2013; Bergmann et al., 2015) umfassend beschrieben. Adulte Neurogenese stellt eine besondere Form struktureller Plastizität dar und es wurde gezeigt, dass adult neugebildete Körnerzellen im *Gyrus dentatus* essentiell am Prozess des hippocampalen Lernens und der Gedächtnisausbildung beteiligt sind (Shors et al., 2001, 2002; Snyder et al., 2005; Winocur et al., 2006; Wojtowicz et al., 2008; Deng et al., 2010; Drew et al., 2010; Aimone et al., 2011; Arruda-Carvalho et al., 2011; Sahay et al., 2011a; Denny et al., 2012; Kheirbek et al., 2012; Ben Abdallah et al., 2013; Groves et al., 2013; Agis-Balboa and Fischer, 2014). Es wird vermutet, dass neue Körnerzellen aufgrund ihrer charakteristischen Eigenschaften verstärkt auf neue Informationsmuster reagieren können und darauf spezialisiert sind Muster, die eine hohe Ähnlichkeit zueinander haben zu separieren und diese Unterschiede zu kodieren (eng. *pattern separation*). Eine Beeinträchtigung der Fähigkeit neue Nervenzellen zu generieren kann zu kognitiven Defiziten und

neurologischen Krankheiten führen. Adulte Neurogenese ist ein komplexer Prozess, der Proliferation, Differenzierung und Überleben von neuralen/neuronalen Stamm- und Vorläuferzellen, der strukturellen Entwicklung und funktionellen Integration in das bestehende neuronale Netzwerk des Hippocampus einschließt und durch eine Vielzahl intrinsischer und extrinsischer Stimuli moduliert wird (aktuelle Übersichtsartikel: Zhao et al., 2008; Ming and Song, 2011; Piatti et al., 2013; Cameron and Glover, 2015; Kempermann et al., 2015).

Obwohl bereits eine Vielzahl von wissenschaftlichen Studien zum Verständnis der Entwicklung und Funktion adult neugebildeter Körnerzellen beitragen konnte, bestehen immer noch Unklarheiten darin, wie sich diese neuen Nervenzellen strukturell entwickeln, wann es zu einer funktionellen Integration kommt und wie diese beiden Prozesse miteinander zusammenhängen. In den vorliegenden Arbeiten wurde die strukturelle Entwicklung und synaptische Integration adult neugebildeter Körnerzellen in das bestehende hippocampale Netzwerk der Ratte und Maus unter *in vivo* Bedingungen untersucht. Im Fokus dieser Studien standen folgende Fragestellungen:

(**1**) Doublecortin (DCX) und Calbindin (CB) sind charakteristische histochemische Marker der adulten Neurogenese. Wie gestaltet sich der zeitliche Verlauf ihrer Expression und kann eine Korrelation zwischen struktureller Reifung und funktioneller Integration hergestellt werden?

(**2**) Wie stark ist die histochemische und die strukturelle Diversität zwischen neugeborenen Körnerzellen derselben Generation?

(**3**) Wann erfolgt die synaptische Integration in das adulte neuronale Netzwerk? Und wann kommt es zur Ausbildung synaptischer Plastizität in Folge synaptischer Aktivierungen?

(**4**) Wie ist der zeitliche Ablauf der strukturellen Entwicklung (speziell Dendriten und dendritische Dornenfortsätze) und existieren klar definierte strukturelle Vorrausetzungen für eine erfolgreiche funktionelle Integration?

(**5**) Existiert eine kritische Phase erhöhter Plastizität während der Entwicklung, wie in der Literatur beschrieben?

(**6**) Welche unterschiedliche Formen synaptischer Plastizität zeigen neugebildete Körnerzellen?

(**7**) Unterscheiden sich adult neugeborene Körnerzellen von embryonal oder perinatal entstandenen Körnerzellen in ihrer Morphologie oder Plastizität?

Zur Beantwortung dieser Fragen wurden Methoden aus der Anatomie, Histologie und Elektrophysiologie kombiniert:

(**1**) Der Nachweis neuer Körnerzellen erfolgte entweder durch immunhistologische Färbungen gegen spezifische Marker für unreife und reife Körnerzellen (DCX und CB), Markierungen mit Bromdesoxyuridin (BrdU) oder retro- bzw. adenovirale intrazerebrale Injektionen und Expression von GFP (eng. *green fluorescent protein*).

(**2**) Anschließend wurde eine Elektrophysiologische *in vivo* Stimulation des *Tractus perforans* in der anästhesierten Ratte zur Langzeitpotenzierung (LTP, eng. *long term potentiation*) der Körnerzellsynapsen durchgeführt.

(**3**) Die immunhistologische Analyse der Expression von synaptischen Aktivitäts- und Plastizitätsmarkern in neugebildeten und reifen Körnerzellen erfolgte nach der Stimulation.

(**4**) Eine detaillierte drei-dimensionale Rekonstruktion dendritischer Bäume und Analyse dendritischer Dornenfortsätze an retroviral markierten Zellen wurde durchgeführt.

1.2. *In vivo* Stimulation des Tractus perforans induziert Expression von Plastizitäts-assoziierten Markern in neugeborenen hippocampalen Körnerzellen

(original eng. Titel: "*High-Frequency stimulation induces gradual immediate early gene expression in maturing adult-generated hippocampal granule cells*", (Jungenitz et al., 2014)

In der vorliegenden Arbeit wurde in Urethan-anästhesierten Sprague Dawley Ratten eine zweistündige hochfrequente Stimulationen des medialen *Tractus perforans* durchgeführt, mit dem Ergebnis einer robusten LTP-Induktion an Körnerzell-*Tractus perforans*-Synapsen (Steward et al., 1998). LTP kann in eine frühe, transkriptions-unabhängige und eine späte, transkriptions-abhängige Phase unterteilt werden. Während in der ersten Phase die synaptische Übertragung durch Modifikation von Rezeptoren verstärkt wird, kommt es in der zweiten Phase zur Transkription und Synthese neuer Proteine, die zur Aufrechterhaltung der synaptischen Potenzierung dienen (Clayton, 2000; Loebrich and Nedivi, 2009). Transkriptionsfaktoren und Effektor-Proteine, die innerhalb kürzester Zeit infolge synaptischer Stimulation aktiviert werden, bezeichnet man als *immediate early genes* (IEGs) (Jones et al., 2001; Fleischmann et al., 2003; Reymann and Frey, 2007; Bramham et al., 2010; Chen et al., 2010) und dienten in den vorliegenden Studien als Evaluation einer erfolgreichen LTP-Induktion und Beweis der funktionellen Integration einer Körnerzelle in das adulte hippocampale Netzwerk. Folgende IEGs waren im Fokus dieser Arbeit: Arc, c-Fos, zif268 und pCREB133.

DCX und CB sind histologische Marker, die eine Identifizierung und Unterscheidung in unreife und reife Körnerzellen ermöglichen (Kempermann et al., 2004, 2015; Snyder et al., 2009). Infolge der Stimulation wurden alle reifen CB-positiven Körnerzellen nahezu vollständig aktiviert (ca. 95 %) und zeigten eine starke Expression von IEGs. Trotz dieser umfassenden Aktivierung von Körnerzellen konnte eine stimulations-abhängige Expression von IEGs in DCX-positiven neugeborenen Körnerzellen nicht beobachtet werden. Auch eine weniger robuste und nicht-invasive Stimulation der Tiere, die durch Exploration

einer zuvor unbekannten Umgebung (eng. *novel environment exposure*) (Marrone et al., 2008) erfolgte, führte nicht zu einer Aktivierung DCX-positiver Zellen.

Die frühe Entwicklungsphase DCX-positiver Körnerzellen ist charakteristisch durch ein starkes dendritisches Wachstum geprägt, weswegen sich diese Population morphologisch stark heterogen präsentiert. Dendriten erhalten axonalen Input von präsynaptischen Partnern und ihre Lokalisation wirkt sich deshalb entscheidend auf die Konnektivität eines Neurons aus. Es erfolgte eine Klassifikation neugeborener Körnerzellen anhand des Wachstumsfortschrittes ihrer dendritischen Bäume und Lage innerhalb der einzelnen Schichten im *Gyrus dentatus*. Dendriten innerhalb der Körnerzellschicht erhalten primär Input von lokalen Interneuronen, in der inneren Molekularschicht glutamatergen Input von Mosszellen (assoziativ oder kommissural), in der mittleren Molekularschicht vom medialen und in der äußeren Molekularschicht vom lateralen *Tractus perforans*. Eine Expressions-Analyse von NeuN (*neuronal nuclei, ein* Marker postmitotischer Neurone) und endogen exprimierten Plastizitätsmarkern (pCREB133, zif268) ergab eine enge positive Korrelation mit den definierten morphologischen Stadien. Für eine präzisere Altersbestimmung neugeborener Körnerzellen wurde BrdU systemisch appliziert und anschließend die Expression von Entwicklungs- und Plastizitätsmarkern zu definierten Zeitpunkten analysiert. Es konnte eine starke Zunahme dendritischer Komplexität innerhalb der ersten zwei Wochen und ein rapider Wechsel von DCX- zur CB-Expression zwischen der zweiten und dritten Woche nachgewiesen werden. Infolge der Stimulation konnte ab der dritten Woche eine schwache stimulationsabhängige Expression von c-fos, Arc und zif268 beobachtet werden und nach fünf Wochen waren ungefähr 70 % der neugeborenen Körnerzellen aktivierbar. Es konnte auch nach elf Wochen kein weiterer Zuwachs in der Population neuer und aktivierbarer Körnerzellen beobachtet werden.

Diese Studie liefert starke Indizien für eine enge Korrelation zwischen struktureller Reifung, der Expression charakteristischer Markerproteine, dem Zellalter und der Fähigkeit zur Expression plastizitätsabhängiger Proteine

infolge einer elektrophysiologischen Stimulation des medialen *Tractus perforans*. Solange neugeborene Körnerzellen DCX exprimieren, waren keine Anzeichen synaptischer Aktivierung detektierbar. Erst fünf Wochen nach ihrer Differenzierung zeigten neugeborene Körnerzellen mehrheitlich durch synaptische Stimulation eine Aktivierung plastizitätsabhängige LTP-assoziierter Proteine. Auch nach elf Wochen zeigte die Population neugeborener Körnerzellen im direkten Vergleich reifer CB-positiver Körnerzellen eine schwächere Reaktion auf synaptische Aktivierung.

1.3. Differentielle strukturelle Entwicklung neugeborener Körnerzellen in der Thy1-GFP Maus

(original eng. Titel: "*Differential structural development of adult-born septal hippocampal granule cells in the Thy1-GFP mouse, nuclear size as a new index of maturation*", Radic et al., 2015)

Zur Untersuchung der strukturellen Diversität neugeborener Körnerzellen in der Thy1-GFP Maus wurden BrdU-Markierungen durchgeführt und das bereits angeführte System zur morphologischen Klassifikation DCX-positiver Zellen (siehe 1.2) angewendet. DCX-positive Zellen zeigten ein deutliches und sichtbares dendritisches Wachstum innerhalb der ersten zwei Wochen nach ihrer Entstehung und obwohl nach drei Wochen die Mehrzahl DCX-positiver Zellen einen weit entwickelten morphologischen Phänotyp aufzeigte, konnten einige Zellen mit strukturellen Anzeichen wesentlich früherer Reifegrade detektiert werden. Wie bereits in der Literatur beschrieben (Cameron et al., 1993; Dayer et al., 2003; Kempermann et al., 2003; Snyder et al., 2009), zeigte die Anzahl neugeborener Körnerzellen innerhalb der ersten fünf Wochen eine Abnahme um 80 %. Prox1 (Prospero homeobox protein 1) ist ein Entwicklungs-assoziierter Transkriptionsfaktor der immunhistologisch ausschließlich im Zellkern nachweisbar ist (Lavado and Oliver, 2007; Iwano et al., 2012) und in dieser Studie zur Bestimmung der Zellkerngrößen BrdU-markierter Zellen zu unterschiedlichen Zeitpunkten der Entwicklung diente. Die vorliegenden Befunde bestätigten zentrale Befunde aus der Ratte (siehe 1.2) und demonstrierten eine enge Korrelation zwischen Zellkerngröße, dem

14

dendritischen Reifegrad und dem Alter der Zelle. Innerhalb der ersten vier Wochen konnte eine kontinuierliche Zunahme der Zellkerngröße beobachtet werden, die in zukünftigen Studien zur Voraussage des morphologischen Reifegrades und des Zellalters genutzt werden könnte. Des Weiteren konnte eine schwache, aber tendenziell unbedeutende Migration neugeborener Körnerzellen innerhalb der Körnerzellschicht verzeichnet werden.

Diese Studie konnte noch einmal zentrale Befunde zur strukturellen Entwicklung DCX-positiver Zellen in der Maus bestätigen und präsentiert einen neuen methodischen Ansatz zur schnellen und einfachen Bestimmung des Entwicklungsgrades neugeborener Körnerzellen.

1.4. Neugeborene Körnerzellen zeigen eine kritische Phase dendritischer Plastizität und bleiben strukturell distinkt von perinatal entstandenen Körnerzellen

(original eng. Titel: "*Adult-born hippocampal granule cells exhibit a critical period of dendritic plasticity and remain structurally distinct from perinatally-born granule cells*", Beining et al., 2016)

Eine moderne Methodik zur Identifizierung und morphologischen Charakterisierung ausgewählter Zelltypen ist die Transduktion durch virale Vektoren. In dieser Studie wurde ein rekombinanter retroviraler Vektor, der vom murinen Leukämie-Virus (MMLV) abgeleitet wurde, eingesetzt, um neugeborene Körnerzellen mit GFP zu markieren (van Praag et al., 2002). Retroviren können ausschließlich während der Zellteilung und gleichzeitiger Abwesenheit der Zellkernmembran in ein Ziel-Genom integrieren. Zur Markierung reifer Körnerzellen wurde ein Adeno-assoziierter Virus (AAV) verwendet, der unter Kontrolle des Synapsin-Promotors (Fornasiero et al., 2010; Valtorta et al., 2011) GFP exprimiert. Adult neugeborene Körnerzellen zeigen zwar eine schwache Migration innerhalb der Körnerzellschicht (siehe 1.3), aber dennoch befinden sich ältere Körnerzellen mit erhöhter Wahrscheinlichkeit in den höheren Schichten. Um primär Körnerzellen aus der embryonalen und frühen postnatalen Entwicklung zum Vergleich

heranzuziehen, wurden deshalb ausschließlich AAV-markierte Zellen aus den äußersten zwei Drittel der Körnerzellschicht verwendet. Die Verwendung viraler Vektoren wurde mit elektrophysiologischer *in vivo* Stimulation und LTP-Induktion des medialen *Tractus perforans* kombiniert (siehe 1.2). Der Erfolg der Stimulation wurde durch Expression von Arc und der Ableitung evozierter Feldpotentiale gesichert.

Frontale hippocampale Schnittserien wurden nach erfolgter transkardialer Perfusion und Fixierung des Hirngewebes am Vibratom mit einer Schnittdicke von 300 µm angefertigt, um eine vollständige Rekonstruktion dendritischer Bäume zu gewährleisten. Anschließend wurden GFP-markierte Zellen an einem Zwei-Photonen-Mikroskop aufgenommen, mit Hilfe der TREES toolbox (Cuntz et al., 2011) drei-dimensional rekonstruiert und umfangreich analysiert.

Die strukturelle Analyse von Körnerzellen lieferte überzeugende Indizien für eine überwiegend abgeschlossene dendritische Entwicklung zwischen der dritten und vierten Woche nach Zellmitose. Ein Vergleich mit maturen AAV-GFP-markierten Körnerzellen ergab keine generellen Unterschiede bezüglich der dendritischen Gesamtlänge und Anzahl von Verzweigungen. Im Detail zeigten adult neugeborene Körnerzellen jedoch eine höhere Anzahl kurzer terminaler Segmente in der äußeren Molekularschicht und mehr terminierende Segmente in der inneren und mittleren Molekularschicht. Diese signifikanten Unterschiede wurden mit Hilfe eines Computermodells näher untersucht und die aufgezeigten Unterschiede konnten durch Änderungen charakteristischer morphologischer Merkmale während der perinatalen hippocampalen Entwicklung erklärt werden. Ein direkter Vergleich rekonstruierter Zellen der ipsilateralen (stimulierten) und kontralateralen (nicht stimulierten) Hemisphäre erbrachte keine detektierbaren Unterschiede und resultierte in der Erkenntnis, dass eine stimulationsabhängige LTP-Induktion keine allgemeinen Veränderungen auf dendritischer Ebene erwirkt. Die histologischen Präparate wurden ein zweites Mal am Vibratom auf 50 µm geschnitten, um immunhistologische Färbungen gegen Arc zu ermöglichen. Die Arc-Expression wurde mit allen vorliegenden dendritischen Eigenschaften in Beziehung gesetzt und es konnte eine stimulations-abhängige Reduktion kurzer terminaler

Segmente in der äußeren Molekularschicht in Arc-positiven Körnerzellen der vierten und fünften Woche festgestellt werden.

In dieser Studie werden Befunde aus einer umfangreichen strukturellen Charakterisierung vollständig rekonstruierter Körnerzellen präsentiert, die belegen, dass adult neugeborene Körnerzellen und Körnerzellen aus der embryonalen bzw. frühen postnatalen Entwicklung unterschiedliche morphologische Populationen darstellen. Des Weiteren wurden überzeugende Indizien für eine aktivitätsabhängige strukturelle Plastizität auf dendritischer Ebene während der Entwicklung neugeborener Körnerzellen in einem engen Zeitfenster zwischen vier bis fünf Wochen erarbeitet.

1.5. Strukturelle homo- und heterosynaptische Plastizität adult neugeborener Körnerzellen

(original eng. Titel: "*Structural homo- and heterosynaptic plasticity in adult newborn hippocampal granule cells*", Jungenitz et al., submitted)

Ausgehend von der vorhergehenden Arbeit (siehe 1.4.) lag der Fokus dieser Studie auf der Entwicklung und struktureller Plastizität dendritischer Dornenfortsätze (eng. *spines*). Durch zahlreiche Studien wurde belegt, dass die Dorngröße eng mit der Ausprägung der postsynaptischen Region (eng. *postsynaptic density - PSD*) und deshalb mit der synaptischen Stärke assoziiert werden kann (Reymann and Frey, 2007). Dornenfortsätze zeigen infolge synaptischer Aktivität strukturelle Veränderungen, die in einem direkten Zusammenhang mit der Ausbildung von Langzeit-Potenzierung (LTP, eng. *long term potentiation*) und Langzeit-Depression (LTD; eng. *long term depression*) stehen (Bosch and Hayashi, 2012; Rochefort and Konnerth, 2012). LTP ist assoziiert mit einer Größenzunahme und LTD mit einer Größenabnahme. Es wurde durch *in vivo* Versuche demonstriert, dass eine selektive elektrophysiologische Stimulation des medialen *Tractus perforans* zu einer homosynaptischen LTP-Induktion führt (Steward et al., 1998) und simultan die Induktion einer heterosynaptischen LTD am nicht stimulierten lateralen *Tractus perforans* bewirkt (Abraham et al., 1985, 2007). Dieses Phänomen wird

heterosynaptische Plastizität genannt und wird als ein wichtiger homöostatischer Mechanismus zur Normalisierung der synaptischen Gewichtung innerhalb eines Neurons diskutiert (Chen et al., 2013; Chistiakova et al., 2015).

Wie bereits beschrieben (siehe 1.2 und 1.4), wurden *in vivo* Stimulationen am medialen *Tractus perforans* an Urethan-anästhesierten Ratten durchgeführt und abgeleitete evozierte Feldpotentiale analysiert, die eine homosynaptischen LTP-Induktion am medialen *Tractus perforans* und entgegengesetzt eine Langzeitdepression am nicht stimulierten lateralen *Tractus perforans* aufzeigten. Der Erfolg einer LTP-Induktion wurde zusätzlich durch immunhistologische Färbungen von Arc validiert. F-Aktin und Synaptopodin sind Proteine, die in Dornen lokalisiert und entscheidend in ihrer strukturellen Plastizität involviert sind (Deller et al., 2003; Fukazawa et al., 2003; Jedlicka et al., 2009; Bosch and Hayashi, 2012). Infolge der Stimulation kam es zu einer deutlichen Akkumulation von F-Aktin und Synaptopodin in der stimulierten mittleren Molekularschicht und in den nicht-stimulierten Bereichen der inneren und äußeren Molekularschicht zu einer Abnahme der Expression. Die vorliegenden elektrophysiologischen und histologischen Befunde sind starke Indizien für eine erfolgreiche Induktion homo- und heterosynaptischer Plastizität.

Zur Analyse von Dornenfortsätzen wurden dendritische Segmente viral markierter adult neugeborener und reifer Körnerzellen am konfokalen Mikroskop aufgenommen. Es wurden ausschließlich Segmente mit einer direkten Verbindung zum Zellsoma genutzt, um schichtenspezifische Veränderungen innerhalb derselben Zelle zu detektieren. Die kontralaterale Hemisphäre zeigte keine Beeinflussung durch die verwendeten Stimulationsprotokolle und konnte dadurch als Kontrolle dienen. Neugeborene Körnerzellen zeigten zwischen der dritten und elften Woche eine kontinuierliche Zunahme in Dichte und Größe dendritischer Dornen, die nach elf Wochen das Niveau maturer Körnerzellen erreichten.

Reife Körnerzellen in der ipsilateralen Hemisphäre zeigten infolge der Stimulation eine signifikante Größenzunahme von Dornen in der mittleren

18

Molekularschicht und eine signifikante Größenreduktion in den benachbarten nicht stimulierten Bereichen der inneren und äußeren Molekularschicht. Unter Einbeziehung der vorliegenden elektrophysiologischen und histologischen Ergebnisse, ist dies ein überzeugendes Indiz einer heterosynaptischen Plastizität auf struktureller Ebene. Eine kleine Population von ungefähr 20 % adult neugeborener Körnerzellen zeigte bereits in der dritten Woche die Fähigkeit zur homo- und heterosynaptischen strukturellen Plastizität infolge synaptischer Aktivierung. Nach 5 Wochen kam es zu einem starken Anstieg auf ungefähr 60 % und neugeborene Körnerzellen zeigten keinen Unterschied zu reifen Körnerzellen hinsichtlich Populationsgröße oder Intensität der strukturellen Veränderungen.

Diese Resultate belegen nicht nur erstmalig das Vorkommen heterosynaptischer struktureller Plastizität in neugeborenen Körnerzellen auf Einzelzellniveau, sondern auch, wie durch Computermodelle vorhergesagt (Benuskova and Jedlicka, 2012), an der kommissuralen/assoziativen Körnerzellsynapsen in der inneren Molekularschicht.

1.6. Schlussfolgerung

Die vorliegenden Daten belegen den generellen Verlauf der Entwicklung neugeborener Körnerzellen in zwei unterschiedliche Phasen: frühe dendritische Reifung und späte funktionelle und synaptische Integration. Neugeborene Körnerzellen zeigten ein rasches dendritisches Auswachsen, dass innerhalb der ersten drei bis vier Wochen abgeschlossen war. Während dieses Wachstumsprozesses passieren Dendriten nacheinander die Körnerzellschicht und anschließend die innere, mittlere und äußere Molekularschicht. Dadurch sind sie innerhalb ihrer morphologischen Entwicklungsphasen anatomisch auf spezifische präsynaptische Partner limitiert. Obwohl die Mehrheit der neugeborenen Körnerzellen derselben Generation strukturell homogen war, gab es Unterschiede zu verzeichnen: einige Zellen zeigten ein schnelles Entwicklungstempo und erreichten die äußere Molekularschicht innerhalb der ersten Woche, andere Zellen benötigten für diesen Entwicklungsprozess mindestens drei Wochen oder länger. Die präsentierten Daten zeigen ab der

dritten Woche eine kontinuierliche Zunahme von Dornenfortsätzen und nach elf Wochen erreichten sie eine maximale Dichte und Größenverteilung, die vergleichbar mit Körnerzellen aus der embryonalen oder frühen postnatalen Phase waren.

In der wissenschaftlichen Literatur wird eine transiente kritische Phase beschrieben, in der neugeborene Körnerzellen eine starke Plastizität und sensitivere synaptische Erregbarkeit aufweisen (Schmidt-Hieber et al., 2004; Ge et al., 2007, 2008). Diese Eigenschaften werden als Vorrausetzung für eine kompetitive Integration gegenüber existierenden und integrierten Körnerzellen diskutiert. Des Weiteren können damit charakteristische Funktionen, wie z.B. die Erkennung und Differenzierung ähnlicher Muster (Aimone et al., 2010; Deng et al., 2010), von neugeborenen Körnerzellen erklärt werden. Obwohl die vorliegenden Resultate keine direkten Hinweise auf eine stärkere bzw. sensitivere Plastizität neugeborener Körnerzellen liefern, konnte eine Phase zwischen vier und fünf Wochen identifiziert werden, in der neue Körnerzellen einen sprunghaften Anstieg in ihrer Fähigkeit zur IEG Expression (z.B. Arc und c-fos) und Ausbildung struktureller Plastizität (Dendriten und Dornenfortsätze) zeigten. Dieses Zeitfenster korrespondiert mit Beschreibungen aus der Literatur (Schmidt-Hieber et al., 2004; Ge et al., 2007, 2008).

Vergleichende Studien von neugeborenen und reifen Körnerzellen implizieren, dass beide Gruppen strukturell und funktionell unterschiedliche Populationen repräsentieren. Trotz einer Vielzahl von Daten bleibt es weiterhin unzureichend beantwortet, ob neugeborene Körnerzellen sich im Verlauf ihrer Entwicklung Körnerzellen angleichen, die aus der embryonalen bzw. frühen postnatalen Entwicklung stammen, oder ob sie eine Subpopulation mit individuellen charakteristischen Eigenschaften präsentieren. Die präsentierten Resultate machen deutlich, dass Dornenfortsätze neuer Körnerzellen nach elf Wochen eine vergleichbare Dichte, Größenverteilung und Plastizität aufzeigen, die vergleichbar mit denen vorhandener Körnerzellen sind. Die Fähigkeit zur dendritischen Plastizität nach synaptischer Aktivierung zeigten jedoch nur neugeborene Körnerzellen zwischen der vierten und fünften Woche. Die Stimulation des *Tractus perforans* führte zur Expression von IEGs in fast allen

reifen Körnerzellen, aber nur ungefähr 70 % der adult neugebildeten Körnerzellen zeigten eine Aktivierung.

Diese Ergebnisse implizieren, dass die Integration neugebildeter Körnerzellen kontinuierlich verläuft und obwohl die vorliegenden Daten die Existenz einer dendritischen Plastizität und einen sprunghaften Anstieg synaptischer Plastizität in der vierten und fünften Woche belegen, wurden keine weiteren Hinweise auf eine transiente kritische Phase gefunden. Dendritische Bäume von gereiften adult neugeborenen und reifen Körnerzellen zeigen Unterschiede, die daraufhin deuten, dass neue Körnerzellen eine eigene Subpopulation darstellen. Welche Auswirkungen diese Befunde auf die einzigartige Rolle von neuen Körnerzellen in der hippocampalen Informationsverarbeitung haben, soll Gegenstand zukünftiger Studien sein.

2. List of abbreviations

AAV	adeno-associated virus
abGC	adult newborn granule cell
BP	branch points
BrdU	bromodeoxyuridine
CA	cornu ammonis
CB	Calbindin
DCX	Doublecortin
DG	dentate gyrus
dpi	days post injection
EC	entorhinal cortex
fEPSP	field excitatory postsynaptic potential
GCL	granule cell layer
GC	granule cell
GFP	green fluorescent protein
H	hilus
hif	hippocampal fissure
HFS	high frequency stimulation
hom-het-pos	homo- and heterosynaptic positive
IEG	immediate early gene
IML	inner molecular layer
LPP	lateral perforant path
LTD	long term depression
LTP	long term potentiation

mGCs   mature granule cells

ML   molecular layer

MML   middle molecular layer

MPP   medial perforant path

NSC   neural stem cell

OML   outer molecular layer

PFA   paraformaldehyde

PP   perforant path

Prox1   Prospero homeobox protein 1

RV   retrovirus

SGZ   subgranular zone

STS   short terminal segment

Sub   subiculum

TDL   total dendritic length

TP   termination point

3. Introduction

Hippocampal granule cells (GCs) are continuously generated from neural stem cells throughout life in the mammalian dentate gyrus (DG), a process called adult neurogenesis. There is increasing evidence that adult newborn GCs (abGCs) are essential for hippocampal forms of learning and memory (Shors et al., 2001, 2002; Snyder et al., 2005; Winocur et al., 2006; Wojtowicz et al., 2008; Deng et al., 2010; Drew et al., 2010; Aimone et al., 2011; Arruda-Carvalho et al., 2011; Sahay et al., 2011a; Denny et al., 2012; Kheirbek et al., 2012; Ben Abdallah et al., 2013; Groves et al., 2013; Agis-Balboa and Fischer, 2014). Impaired neurogenesis has been associated with a variety of psychiatric disorders such as depression, temporal lobe epilepsy, and an age-related cognitive decline (Malberg et al., 2000; Drapeau et al., 2003; Eisch et al., 2008; Li et al., 2008; Shruster et al., 2010; Eisch and Petrik, 2012; Fitzsimons et al., 2012; Braun and Jessberger, 2014; Jessberger and Parent, 2015; Lucassen et al., 2015; Miller and Hen, 2015). Furthermore, the perspective of using neural stem and progenitor cells for the development of therapeutic applications that are aimed at neuropathological conditions is encouraging and generates a strong motivation to understand the underlying mechanisms in detail. Adult neurogenesis is a highly complex process comprising processes at the level of proliferation, differentiation, survival, structural development, and functional integration. Various intrinsic and extrinsic stimuli can act as modulators at those levels and consequently, adult neurogenesis is a highly orchestrated process with many facets. In this work, I present novel data on the time course of structural maturation and functional integration of abGCs into the hippocampal network under *in vivo* conditions.

3.1. Anatomy of the hippocampal formation

The hippocampus is a part of the limbic system that has been extensively studied in the brain of rodents. It plays an important role in consolidation of information from short term to long term memory and is associated with spatial memory and navigation (Brun et al., 2008; Fyhn et al., 2008; Moser et al., 2008;

Derdikman and Moser, 2010; Langston et al., 2010; Buzsáki and Moser, 2013; Zhang et al., 2014). It is a frequently used model system because studies benefit from a number of unique anatomical and physiological features that comprise the localization of principal cells in single layers with strictly laminated inputs, mostly unidirectional connectivity, highly plastic synapses, and well established *in vitro* cell culture and *in vivo* techniques.

The hippocampus contains the hippocampus proper which can be further divided into the subregions CA3, CA2, and CA1 (CA - cornu ammonis) and is located within the hippocampal formation that comprises several other related brain regions, including the DG, subiculum, presubiculum, parasubiculum, and entorhinal cortex. Unlike regions of the neocortex, connectivity between principal neurons of the hippocampal formation is largely unidirectionally organized. Multimodal sensory information reaches the hippocampal formation through the entorhinal cortex, which projects axons from the superficial layers (layer II and III) to the DG via the perforant path. Principal cells of the DG, the GCs, give rise to axons called mossy fibers that terminate at CA3 cells, which in turn, provide major input to CA1 via the Schaffer collateral axons. This so called trisynaptic loop is closed either by direct projections from the CA1 field to the entorhinal cortex or by indirect projections via the subiculum, pre- and parasubiculum to the entorhinal cortex. Besides this serial flow of information, the entorhinal cortex is also sending parallel projections to several other fields of the hippocampal formation (e.g. entorhinal cortex layer 2 → CA3) (Andersen et al., 2006) (**Fig. 1a, b**).

The DG is a V- or U-shaped structure that can be divided into three layers. The granule cell layer (GCL) contains densely packed GCs and also a small number of other neuron types such as basket cells at the inner border of the GCL. The molecular layer (ML) is mainly occupied by dendrites of GCs that receive synaptic contacts from axonal terminals of the perforant path and a small number of interneurons. The resting membrane potential of GCs is, in comparison to CA1 or CA3 pyramidal neurons, more hyperpolarized (about -75 mV) (Mody et al., 1992; Spruston and Johnston, 1992; Staley et al., 1992), resulting in a larger threshold for action potential generation and a low

spontaneous firing frequency. Furthermore, the quantity of GCs outnumbers the quantity of pre- (entorhinal pyramidal neurons) and postsynaptic (CA3 pyramidal neurons) partners by an order of magnitude (Boss et al., 1987; Amaral et al., 1990; West et al., 1991; Mulders et al., 1997; Schmidt et al., 2012; van Dijk et al., 2016). This results in a divergence in connectivity from the entorhinal cortex and a convergence in connectivity to CA3. The polymorphic layer (or hilus) is enclosed by the GCL and most prominently contains the mossy cells and GABAergic interneurons. Mossy cells are glutamatergic and give rise to axons that terminate in the inner third of the ipsi- and contralateral molecular layer. GCs at the same septotemporal level are the main source of input to mossy cells, while mossy cells innervate both GCs and GABAergic interneurons at distant levels of the DG. Since mossy cells participate in excitatory and inhibitory circuitries, it is hypothesized that they modulate DG network activity (Andersen et al., 2006; Amaral et al., 2007; Scharfman and Myers, 2012; Jinde et al., 2013).

As stated above, excitatory synaptic contacts of GCs are located primarily in the ML. The ML is highly laminated and receives inputs via the medial perforant path from the medial entorhinal cortex in the middle molecular layer (MML), inputs via the lateral perforant path originating from the lateral entorhinal cortex in the outer molecular layer (OML) and inputs from associated and commissural fibers of mossy cells in the inner molecular layer (IML). It is proposed that the medial entorhinal cortex is involved in processing of spatial information and navigation (Moser et al., 2008; Igarashi, 2016), whereas on the contrary, the lateral entorhinal cortex is more responsive to olfactory, visual, or tactile stimuli (Yoganarasimha et al., 2011; Chao et al., 2016). In addition, GCs receive a variety of other synaptic inputs: neuromodulatory inputs from the septal nuclei (acetylcholine), locus coeruleus (norepinephrine), ventral tegmental area (dopamine), supramammilary region of the hypothalamus (substance P), and the raphe nuclei (serotonin) and GABAergic input via interneurons from e.g. basket and chandelier cells (Freund and Buzsáki, 1998; Andersen et al., 2006; Amaral et al., 2007) (**Fig. 1b, c**).
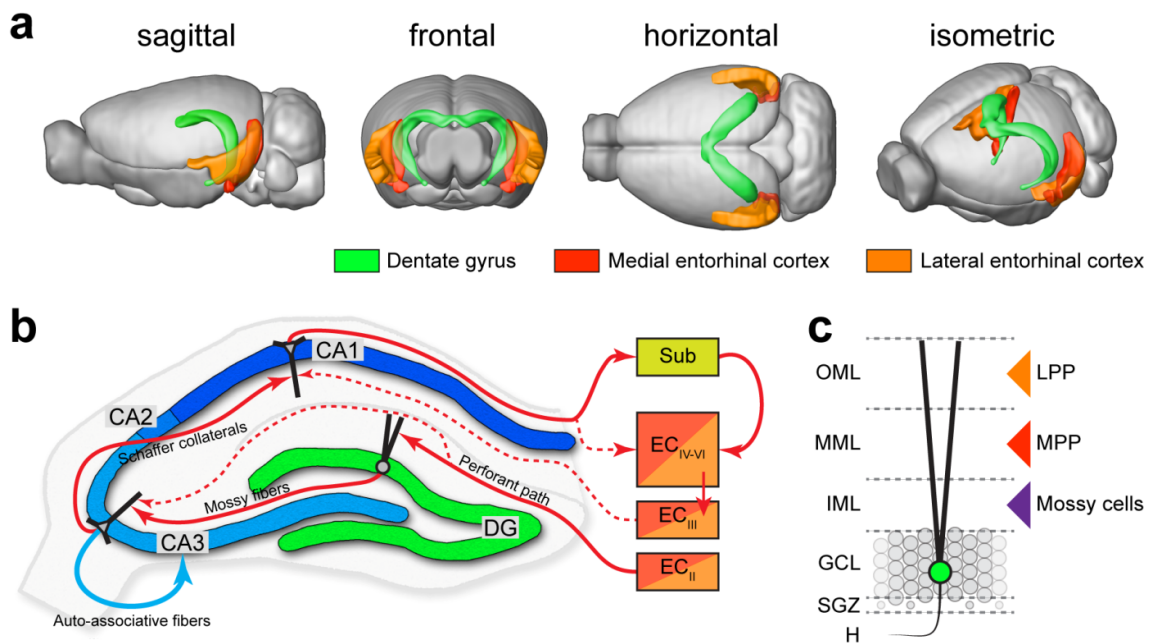
Figure 1. Anatomy of the hippocampal formation. (**a**) The dentate gyrus (DG) is part of the hippocampal formation and is located in the medial temporal lobe of the brain. Main afferent glutamatergic input to the DG is received from the medial and lateral entorhinal cortex (EC). Images adapted from Brain Explorer ® 2 3-D Viewer (http://www.brain-map.org). (**b**) The trisynaptic loop is a relay of glutamatergic synaptic transmission: the DG receives input from the EC (layer II) via the perforant path and forwards the signal to CA3 via the Mossy fibers. Pyramidal cells in CA3 synapse to CA1 neurons via the Schaffer collaterals which then close the loop by projections via the Subiculum (Sub) to the EC (layers IV-VI) or direct to the EC (layers IV-VI). Pyramidal cells in CA3 form a strong auto-associative synaptic network. Neurons in CA1, CA3, and the Subiculum also receive glutamatergic input from the EC. Image adapted from Wilson et al. (2006) and Brinton (2009). (**c**) GCs of the DG reside inside the granule cell layer (GCL) and receive glutamatergic input from the lateral entorhinal cortex via the lateral perforant path (LPP) in the outer molecular layer (OML), from the medial entorhinal cortex via the medial perforant path (MPP) in the middle molecular layer (MML), and from Mossy cell fibers in the inner molecular layer (IML). H, hilus; SGZ, subgranular zone.

3.2. Synaptic plasticity and electrophysiology in the hippocampus

The term synaptic plasticity describes the persistent, activity-driven changes in synaptic efficacy and is thought to be the basis of information storage in the brain. Long term potentiation (LTP) as a form of synaptic plasticity delineates the persistent strengthening of synapses based on preceding neuronal activity and is generally seen as the underlying mechanism for learning and memory (Escobar and Derrick, 2007; Bailey et al., 2015). On the other hand, long term depression (LTD) describes the reverse form of synaptic plasticity, namely the reduction of synaptic efficacy and may counteract or balance LTP (Escobar and Derrick, 2007; Bailey et al., 2015). LTP can be separated into an early and a late phase. Both phases are NMDA receptor-dependent, but the latter requires *de novo* protein synthesis, including the expression of immediate early genes (IEGs). IEGs are activated rapidly and transiently in response to a high variety of cellular stimuli (e.g. synaptic activation) and are classified into transcription factors (e.g. c-fos, zif268) and direct effector proteins (e.g. Arc). These transcription factors in turn, activate a second wave of genes, termed delayed early genes (Clayton, 2000; Loebrich and Nedivi, 2009). Changes in synaptic plasticity are the result of reorganization of the cytoskeleton, scaffolding proteins, membrane proteins, and receptors (Reymann and Frey, 2007).

The hippocampal formation is highly suited to study extracellular field potentials due to its laminated structure, densely packed neurons, parallel fibers, and synchronous firing of principal neurons. Electrophysiological properties of the perforant path-GC synapse has been intensively investigated during the past decades and fundamental studies were contributed by Bliss and Lomo (Lomo, 1971; Bliss and Lomo, 1973) who studied *in vivo* LTP by the recording of extracellular field potentials from the DG and stimulation of the perforant path in anesthetized animals. Synaptic activation of GCs evokes the depolarization of the postsynaptic membrane potential and gives rise to a field excitatory postsynaptic potential (fEPSP). The rising slope of the fEPSP is positively correlated to the synaptic strength and is uncontaminated from any induced network activation during the early phase. Stimulation above the spiking threshold synchronously discharges GCs, resulting in a population spike

that is superimposed on the fEPSP and positively correlated to the stimulus intensity. The GC-perforant path synapse features a high amount of plasticity and a variety of *in vivo* LTP- and LTD-inducing protocols were established over time to address questions regarding synaptic plasticity (Albensi et al., 2007) (**Fig. 2a, b**).
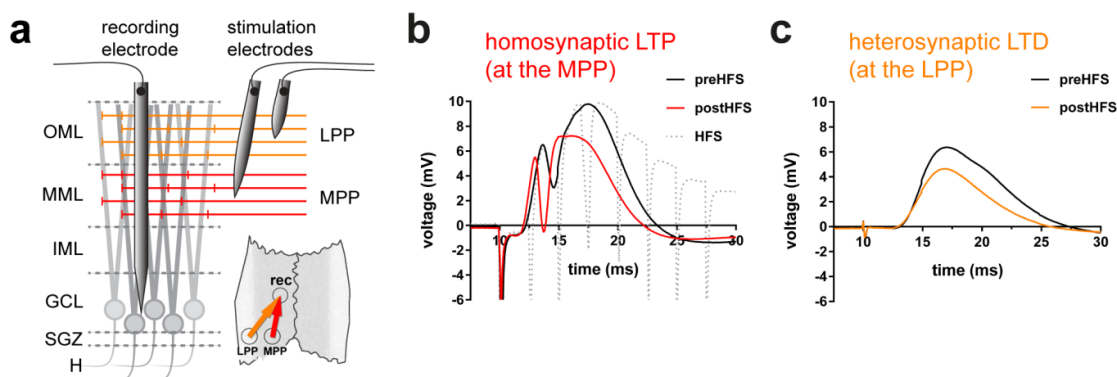
Figure 2. Electrophysiology of dentate gyrus granule cells. (**a**) Glutamatergic input to the DG is received from the medial and lateral entorhinal cortex via the medial (MPP) and lateral perforant path (LPP). Both pathways can be discriminated by characteristic electrophysiological and anatomical properties and consequently differentially stimulated. Inset: Schematic of rat brain with bipolar stimulation electrode in the MPP (red), and the LPP (orange) of the entorhinal cortex and a recording electrode in the DG of the hippocampus. (**b**) Sample traces of evoked local field potentials (fEPSP) of GCs by selective stimulation of the medial perforant path (MPP) before application of high frequency stimulation (HFS; 2 h, one train: 8 pulses at 400 Hz, 10 s inter-train-interval) at the MPP (black), during MPP HFS (gray dotted line) and following MPP HFS (red). The slope of the fEPSP is a measure of excitatory synaptic strength and the population spike is related to the strength of synchronized somatic action potentials evoked by stimulation. Note the increase of the slope and the strength of the population spike following HFS (red line): HFS of the MPP induced homosynaptic LTP at the MPP. (**c**) Sample traces of fEPSP by selective stimulation of the lateral perforant path (LPP) before application of HFS at the MPP (black) and following MPP HFS (orange). HFS of the MPP induced homosynaptic LTD at the LPP. (**b, c**) Images adapted from Jungenitz et al. (submitted manuscript). GCL, granule cell layer; H, hilus; IML, inner molecular layer; MML, middle molecular layer; OML, outer molecular layer; SGZ, subgranular zone.

LTP and LTD can be further classified into homosynaptic and heterosynaptic plasticity. Homosynaptic plasticity can be induced at synapses that are directly stimulated, while heterosynaptic plasticity takes place at inactive synapses neighboring stimulated synapses (Oh et al., 2015). In the DG, homosynaptic plasticity associated with concurrent heterosynaptic plasticity is a robust phenomenon (Christie and Abraham, 1992; Abraham et al., 1994, 2001; Jedlicka et al., 2015) and GCs have the intriguing ability to exhibit heterosynaptic plasticity when studied *in vivo* (Abraham et al., 2001). Stimulation of the perforant path is a classic *in vivo* model to study homosynaptic (Bliss and Lomo, 1973; Lomo, 2003) as well as heterosynaptic (Doyère et al., 1997; Abraham et al., 2007) long-term plasticity of synaptic connections in the DG. High frequency stimulation (HFS) elicits substantial LTP of the stimulated MPP input and, concurrently, LTD of the non-stimulated LPP input (Abraham et al., 2007; Bowden et al., 2012). Strengthening of one group of synapses is associated with concurrent weakening of another group of synapses and is hypothesized as a mechanism to enhance the hippocampal transfer of specific information. In addition, heterosynaptic LTD might be an important homeostatic mechanism to keep the overall input connection strength constant, to prevent runaway synaptic dynamics, to maintain synaptic competition (Chen et al., 2013; Chistiakova et al., 2015) (**Fig. 2a, b**).

3.3. Hippocampal adult neurogenesis

The long-held concept of an adult mammalian central nervous system that lacks the ability for regeneration at the cellular level was corrected by pioneering work from Joseph Altman and Gopal D. Das. They provided the first evidence for an ongoing neurogenesis in the hippocampus and shortly later, in the olfactory bulb of adult mammals (Altman and Das, 1965; Altman, 1969). These findings were debated with disbelief and slow progress was made during the following years until Nottebohm and colleagues found evidence for neurogenesis in the tectum (vocal control center) of adult singing birds associated with seasonal song learning (Goldman and Nottebohm, 1983; Paton and Nottebohm, 1984; Alvarez-Buylla and Nottebohm, 1988; Alvarez-Buylla et

al., 1988; Wilbrecht and Nottebohm, 2004). Since then, adult newborn neurons were found and intensively studied in many mammals (Gould, 2007; Amrein and Lipp, 2009; Amrein et al., 2011; Bonfanti and Peretto, 2011; Lipp and Bonfanti, 2016), including the human hippocampus (Eriksson et al., 1998; Spalding et al., 2013; Bergmann et al., 2015). According to the current state of knowledge, it is hypothesized that adult newborn hippocampal neurons are critically involved in cognitive processes, including learning and memory. Disturbances in the process of neurogenesis, for example neurodegenerative diseases or aging, are associated with abnormal network properties that manifest in deficits at the behavioral level (Shors et al., 2001, 2002; Snyder et al., 2005; Saxe et al., 2006; Winocur et al., 2006; Wojtowicz et al., 2008; Clelland et al., 2009; Kheirbek et al., 2012). Vice versa, external factors, such as stress or an enriched environment, are known to modulate differentiation, survival and integration of adult newborn neurons (Mirescu and Gould, 2006; Wojtowicz et al., 2008; Bednarczyk et al., 2011; Fitzsimons et al., 2012; Bergami et al., 2015; Lucassen et al., 2015; Dostes et al., 2016; Vivar et al., 2016). Although the majority of studies were conducted in rodents, there is little, but growing evidence, signifying the existence of adult neurogenesis in the human hippocampus (Eriksson et al., 1998; Spalding et al., 2013; Bergmann et al., 2015). Despite the steadily increasing number of scientific publications in this research field, there is a plethora of unanswered questions concerning the underlying molecular and cellular mechanisms, regulatory factors, and implications for cognitive processes. Fundamental insights and prerequisites for synaptic integration of new neurons into pre-existing neuronal networks and self-repair holds promising and stimulating potential for the development of clinical approaches targeting neurodegenerative brain diseases and injuries (for recent reviews see Zhao et al., 2008; Ming and Song, 2011; Piatti et al., 2013; Cameron and Glover, 2015; Kempermann et al., 2015).
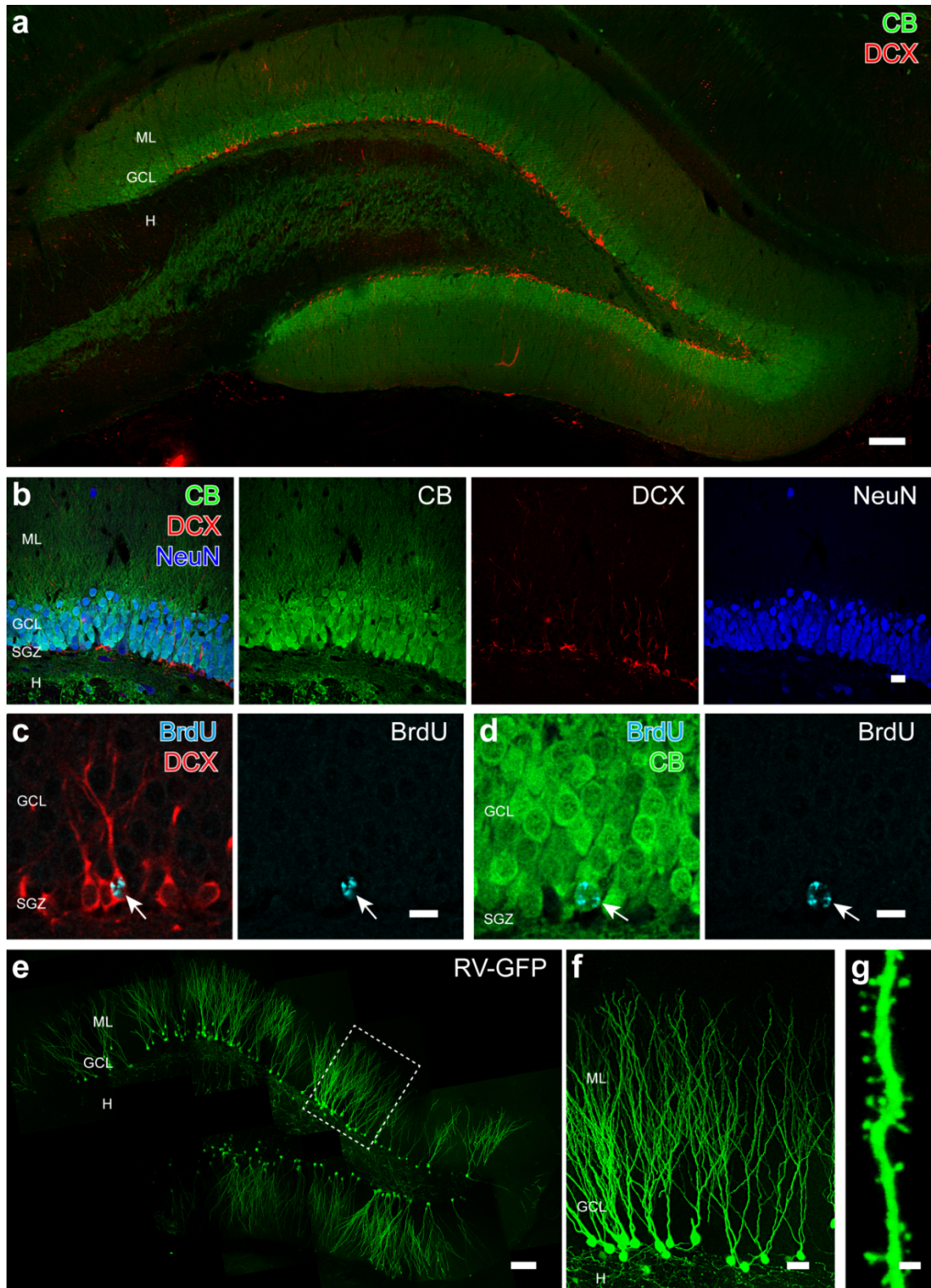
◄ **Figure 3. Adult newborn dentate gyrus granule cells.** (**a**) Expression of Calbindin (CB) in mature granule cells (mGCs) and Doublecortin (DCX) in immature adult newborn granule cells (abGCs). (**b**) Neuronal Nuclei (NeuN) is a neuron specific immunohistochemical marker. CB is present in almost all mGCs located in the granule cell layer (GCL). DCX is expressed in the somata and dendrites of abGCs which are located in the subgranular zone (SGZ). (**c, d**) Bromodeoxyuridine (BrdU) is an analog of thymidine and is incorporated into newly synthesized DNA of proliferating cells. Subsequent immunohistochemical staining can be used to detect abGCs at a specific age, and in combination with other markers, their stage of maturation can also be further identified. Illustrated are: an immature, DCX-positive granule cell (GC, **c**) and mature, CB-positive GC (**d**). (**e, f**) Labeling of abGCs by retroviral vectors derived from the Moloney murine leukemia virus (MLV) is another established technique to study adult neurogenesis. This recombinant virus is specific for mitotically active cells only and expression of green fluorescent protein (GFP) allows structural analysis of dendrites, axons, and spines of newly formed cells. (**g**) High-magnification of GFP-labeled dendritic segment with spines exhibiting a remarkable diversity of sizes and shapes. Scale bars: (**a, e**) 100 µm, (**b**) 10 µm, (**c, d**) 5 µm, (**f**) 25 µm, (**g**) 1 µm. H, hilus.

3.3.1. The adult hippocampal neurogenic niche

Hippocampal neural stem cells (NSCs) reside inside the subgranular zone (SGZ) of the DG which forms a specialized microenvironment with specific factors that are permissive for neurogenesis, called the neurogenic niche (Moore and Lemischka, 2006; Nicola et al., 2015). Adult newborn hippocampal neurons originate from radial glia-like precursor cells, so called type 1 cells (stem cells) (Seri et al., 2001; Filippov et al., 2003) and give rise to highly proliferative, lineage-determined type 2 intermediate progenitor cells (Filippov et al., 2003; Kronenberg et al., 2003). Type 2 cells can be further divided into glia-like type 2a and neuronally determined type 2b cells (Brandt et al., 2003; Brown et al., 2003; Filippov et al., 2003; Kronenberg et al., 2003). This phase is followed by type 3 cells (neuroblasts), which are still proliferative, but show more morphological changes (Brandt et al., 2003). Each of these early developmental stages can be identified by unique expression patterns of markers: Type 1 cells exhibit GFAP, Nestin, BLBP, and Sox2; Type 2a cells exhibit GFAP, Nestin, BLBP, and Sox2; Type 2b cells exhibit Nestin,

Doublecortin (DCX), PSA-NCAM, NeuroD, and Prox1; and Type 3 cells exhibit DCX, PSA-NCAM, NeuroD, and Prox1 (Seri et al., 2001; Brandt et al., 2003; Brown et al., 2003; Filippov et al., 2003; Kronenberg et al., 2003) (for review, see: Kempermann et al., 2004).

Dividing cells can be labeled either by Bromodeoxyuridine (**Fig. 3c, d**), which is an analog of thymidine and gets incorporated into newly synthesized DNA of proliferating cells (Taupin, 2006), or by fluorescent retroviral vectors that are derived from the Moloney murine leukemia virus (van Praag et al., 2002) (**Fig. 3e**). Retroviral vectors offer the advantage of GFP-labeling of complete cells and the subsequent structural analysis of dendrites, axons, and spines of newly formed cells (**Fig. 3f, g**).

3.3.2. **Structural maturation**

The axons of GCs, called mossy fibers, pass the hilar subfield and terminate at dendrites of CA3 pyramidal neurons (Claiborne et al., 1986; Frotscher et al., 1991). Mossy fiber terminals can be morphologically discriminated into three subtypes: large mossy terminals, filopodial extensions that project from the large mossy terminals, and small en passant varicosities (Amaral, 1979; Claiborne et al., 1986; Frotscher et al., 1991; Acsády et al., 1998). Large mossy terminals form synaptic contacts with CA3 pyramidal neurons and with mossy cells in the hilus. The small filopodial and en passant terminals selectively innervate only inhibitory interneurons (Acsády et al., 1998).

Within the first week, abGCs exhibit a rapid axonal growth towards CA3 (Hastings and Gould, 1999) and at about 2 weeks they start to form mossy fiber boutons at pyramidal cells. Axonal maturation is completed at 3 weeks when mossy fiber boutons possess mature morphological characteristics and a maximum density (Zhao et al., 2006; Sun et al., 2013). Strong anatomical connections with CA3 interneurons via en passant boutons and filopodia extensions from large mossy terminals peak at about 4 weeks, and by using channelrhodopsin mediated optical stimulation and contextual fear conditioning, it was demonstrated that abGCs at 4 weeks (but not at later time points) can

robustly activate CA3 interneurons (Restivo et al., 2015). This transient increase in connectivity to inhibitory circuits could be a mechanism modulating the excitation/inhibition balance during the process of synaptic integration (see 3.3.3).

The dendritic tree is the anatomical part of a neuron that receives the main afferent synaptic input from other neurons and thus defines the function via the amount and specificity of inputs (Lefebvre et al., 2015), shaping input-output behavior (Mainen and Sejnowski, 1996), performing local computations (Sidiropoulou et al., 2006; Branco and Häusser, 2010), integrating synaptic responses, and modulating the electric state of the soma, including the initial segment of the axon. GCs have a characteristic cone-shaped tree of dendrites that, under physiological conditions, are all located in the molecular layer and most of them terminate close to the hippocampal fissure (Claiborne et al., 1990; Vuksic et al., 2008). GCs receive synaptic inputs from multiple sources. The molecular layer can be roughly divided into three subdivisions according to the source of glutamatergic synaptic inputs. Dendritic compartments located inside the inner third receive input from mossy cells (via associational and commissural fibers), the middle third receives input from axons of the medial entorhinal cortex, and the outer third receives input from the lateral entorhinal cortex (see 3.1).

Rudimentary dendritic processes are already observable in abGCs within the first 12 h after neuronal differentiation and apical dendrites can already extend to the molecular layer by 48 h (van Praag et al., 2002; Zhao et al., 2006; Shapiro et al., 2007). Axonal growth precedes the extension of dendrites by about 3 days (Sun et al., 2013) and the major dendritic development is completed at 4 weeks of age (Zhao et al., 2006; Sun et al., 2013). Dendritic growth can be roughly divided into two phases. The first phase is characterized by a rapid outgrowth, which decelerates drastically in the second phase after 3 weeks when only minor dendritic changes take place (Sun et al., 2013). As a result of technical limitations, structural characterization studies of neurite development were conducted in fixed tissue in the past. These approaches have the disadvantage of lacking detailed information about structural

dynamics. Considerable progress has been made recently in using acute and organotypic hippocampal slice cultures with preserved synaptic organization and *in vivo* two-photon imaging for time lapse imaging of abGCs (Kamada et al., 2004; Raineteau et al., 2004; Kleine Borgmann et al., 2013; Gonçalves et al., 2016). These modern techniques allow the analysis of dynamic processes with a high temporal resolution in combination with pharmacological manipulations or behavior-associated responses at the cellular level. Application of *in vivo* time lapse imaging revealed over-branching followed by pruning during the first 3 weeks of dendrite development controlled by a homeostatic regulation in order to maintain similar dendritic structures of GCs (Gonçalves et al., 2016).

Dendritic spines are the major sites of excitatory glutamatergic synapses in the brain. The morphology is highly variable and spines are typical classified into three types: the mushroom, thin, and stubby spines. Thin spines have a long neck with a small bulbous head, stubby spines lack a neck, and mushroom spines contain a large head in comparison to the neck and represents the majority of mature spines (Bosch and Hayashi, 2012; Rochefort and Konnerth, 2012). Mushroom spines are the most stable type and associated with LTP. Spine morphology is of continuous nature, activity-dependent, and correlated with changes in synaptic strength (Alvarez and Sabatini, 2007). Spine size has been reported to match the size of the postsynaptic density (PSD), the amount of glutamate receptors, and therefore can be directly correlated with synaptic strength (Matsuzaki et al., 2001; Reymann and Frey, 2007). Furthermore, it was demonstrated that the spine head to spine neck ratio determines calcium-signaling (Matsuzaki et al., 2004), induction of LTP is associated with spine enlargement (Matsuzaki et al., 2004), and conversely, LTD is associated with shrinkage (Zhou et al., 2004). Thus, changes in spine size can be seen as structural equivalent of LTP and LTD.

Spine formation in abGCs starts around 16 dpi (Zhao et al., 2006; Ohkawa et al., 2012) with a sharp increase in spine density between 16-18 dpi in rats (Ohkawa et al., 2012) and about one week later in mice (Zhao et al., 2006; Toni et al., 2007), supporting the general idea that abGCs mature slightly faster in rats than in mice (Snyder et al., 2009). This early phase is followed by a

continuous increase during the following 8 weeks until spine density reaches a plateau at about 70 dpi. The time course of spine development underlies modulation by various stimuli and can show a prolonged structural maturation (Zhao et al., 2006; Toni et al., 2007, 2008). At ultrastructural level, the first developing synapses were observed during the third week in retrovirally labeled abGCs (Toni et al., 2007) and even in Doublecortin-positive immature neurons (Shapiro et al., 2007). The high incidence of so called multi synaptic boutons seen in ultrastructural analyses, supports the hypothesis that developing spines of newly formed neurons preferentially target preexisting axonal boutons, but with ongoing maturation, multi synaptic boutons are modified to single synaptic boutons (Toni et al., 2007).

3.3.3. Synaptic Integration

Synaptic integration of abGCs is guided by the major excitatory and inhibitory neurotransmitters glutamate and GABA. During early development, abGCs express ionotropic GABA receptors (GABA$_A$) and are responsive to tonic GABA activation by local interneurons (Tozuka et al., 2005; Wang et al., 2005; Ge et al., 2006). Initially, abGCs express NKCC1, a chloride (Cl$^-$) importer, which results in a high intracellular Cl$^-$ concentration and depolarization by GABA. Within the first 2-3 weeks, NKCC1 is gradually replaced by KCC2, a Cl$^-$ exporter, and the initial depolarization by GABA becomes converted into hyperpolarization. Tonic depolarization by GABA during that period is required for synapse formation and dendritic development. It has been hypothesized that the concentration of ambient GABA, released by interneurons, may serve as a general indicator of neuronal network activity (Ge et al., 2006). Electrophysiological studies imply that the development of synaptic connectivity is sequentially orchestrated in discrete stages, phasic GABAergic inputs at dendrites with slow responses are established first, and once glutamatergic terminals are formed, perisomatic GABAergic inputs with fast responses emerge (Espósito et al., 2005). Depolarizing GABAergic signaling also plays an important role during embryonal and neonatal development of the nervous system (Owens et al., 1996; Ben-Ari, 2002; Wang and Kriegstein, 2009).

Together with other shared similarities, it was hypothesized that adult neurogenesis recapitulates some features of embryonic development while possessing additional mechanisms (Espósito et al., 2005; Götz et al., 2016).

Electrophysiological analysis of abGCs has shown the expression of glutamate receptors (Ambrogini et al., 2004), and immunohistochemistry revealed the presence of the NMDA receptor subunit NR1 as well as the developmentally related receptor subunit NR2B from early developmental stages on (Nacher et al., 2007). Knock-out studies demonstrated that absence of NR1 negatively affects cell survival of abGCs, whereas deletion of NR2B leads to impairment in abGC-dependent forms of hippocampal learning (Cull-Candy and Leszkiewicz, 2004; Kheirbek et al., 2012). Studies on NR2B revealed greater abundance in NMDA receptors in ratio to NR2A during embryonic and early postnatal development of the brain (Jin et al., 1997; Wenzel et al., 1997; Wang et al., 2011), activation of unique molecular pathways, and a different form of synaptic plasticity (Liu et al., 2004; Barria and Malinow, 2005; Kim et al., 2005; Wang et al., 2011).

AbGCs feature a unique electrophysiological identity defined by a distinct composition of ion channels: a high input membrane resistance that declines during maturation (about 4.5 GΩ in abGCs versus 0.2 GΩ in mGCs), but a resting membrane potential that is similar between abGCs and mGCs (about 80 mV in abGCs versus 75 mV in mGCs) (Schmidt-Hieber et al., 2004; Mongiat et al., 2009; Dieni et al., 2013). Although glutamatergic synaptic input via perforant path afferents onto abGCs is weak during the early phase of development (Mongiat et al., 2009; Dieni et al., 2012, 2016), a lower stimulation intensity is required to elicit spiking and produce a similar spiking probability across all developmental stages (Mongiat et al., 2009). Spiking behavior was reported to depend on an increasing expression of inward rectifier potassium channels (Kir). Over-expression of Kir channels in abGCs induced mature-like firing properties, and conversely, blockade of Kir channels in mGCs resulted in a high excitability of young neurons (Mongiat et al., 2009). Further electrophysiological characterization identified a transient period of enhanced LTP during 4-6 weeks of age, when abGCs exhibit a reduced LTP induction

threshold and an increased amplitude following LTP stimulation protocols (Schmidt-Hieber et al., 2004; Ge et al., 2007). This period of enhanced plasticity was associated with the expression of NMDA receptor subunit NR2B (Ge et al., 2007).

Calcium-based synapse-to-nucleus communication is important to regulate the expression of plasticity genes (Bading, 2013). It was demonstrated that the amplitude of action-potential evoked dendritic Ca^{2+} transients is similar between abGCs and mGCs, but the decay time constant is much higher in abGCs compared to mGCs, resulting in a broader temporal summation of Ca^{2+} signals during repetitive activation (Stocca et al., 2008). Although the activity of Na^+/Ca^{2+} exchanger (NCX) remain relatively equal during maturation and plasma membrane Ca^{2+}-ATPase (PMCA) activity is not increased, the contribution of mitochondria and sarco-endoplasmic reticulum Ca^{2+}-ATPase (SERCA) to Ca^{2+} clearance is enhanced (Lee et al., 2009). High somatic Ca^{2+} levels might contribute to the activation of Ca^{2+}-dependent enzymes (e.g. CREB, CREST) regulating cellular developmental processes and synaptic integration.

The balance between neuronal excitation and inhibition is controlled by the relative contribution of excitatory and inhibitory synaptic inputs and determines the activity of a neuron. GCs receive the main excitatory input from the entorhinal cortex and inhibitory input from local interneurons (e.g. basket cells) (see 3.1). GC spiking behavior is constrained through feedforward (monosynaptic via perforant path) and feedback inhibition (disynaptic via GCs). Although 4-week-old abGCs show the ability to efficiently drive distal target cells in CA3, they only poorly activate proximal interneurons which are responsible for feedback inhibition. With ongoing maturation, recruitment of inhibitory feedback loops by abGCs is increased, and spiking of other GCs is restricted. In turn, abGCs are only weakly innervated by inhibitory interneurons at 4 weeks (Temprana et al., 2015). These data were complemented by reports about 4-week-old abGCs, which are less responsive to GABAergic inhibition, while activation via entorhinal input was more likely, producing more spikes per train, and responding to a wider range of stimulus frequencies in comparison to

mGCs (Marín-Burgin and Schinder, 2012; Pardi et al., 2015). Altogether, this suggests distinct coding strategies of immature and mGCs. While abGCs are highly responsive, integrative, and less specific, mGCs exhibit sparse activity and high input specificity.

Recently, a dual-virus approach combining monosynaptic rabies virus-mediated retrograde tracing and retroviral labeling was developed and applied to identify pre-synaptic partners and analyze the changes of connectivity patterns during the development of abGCs (Vivar et al., 2012). This study reported long range projections from the entorhinal cortex via the perforant path in a rapidly increasing quantity from 21 dpi on, substantial connectivity from mGCs to abGCs during the first month, and synaptic input from mossy cells at all observed time points (21-90 dpi). Input from the entorhinal cortex was restricted to the lateral part. Another study further enhanced this technique and verified findings of early input provided by mossy cells starting between 5-10 days post differentiation, together with increasing innervation by the entorhinal cortex from 21 dpi on (Deshpande et al., 2013). These authors further described synaptic input from modulatory cholinergic neurons in the medial septum, the nucleus of the diagonal band of Broca, and interneurons during the second week. However, a selective input to abGCs from the lateral entorhinal cortex could not be verified by this publication. In follow-up studies experience-dependent changes in the connectivity pattern of abGCs were investigated. In response to enriched environment exposure during 2-6 weeks post differentiation, innervation by local interneurons and long-distance input by cortical neurons increased significantly (Bergami, 2015; Bergami et al., 2015). Changes in intra-hippocampal connectivity appeared to be transient, whereas cortical input remained increased after animals were returned to standard housing conditions. These results provide strong evidence for experience-dependent structural plasticity within a specific time window during abGCs integration. Nevertheless, since the exact mechanisms of virus mediated retrograde tracing and its temporal and spatial specificity are not fully understood yet, further functional and anatomical research has to be carried out in order to clarify the development and dynamics of synaptic connectivity of abGCs. Further evidence for an early synaptic input by mossy cells was

provided by Chancey et al. (2014), who, by using pharmacology and optogenetics, demonstrated that mossy cells translate intra- and extrahippocampal synaptic activity to abGCs during the second postmitotic week.

In regard to synaptic integration, the term "critical phase" was coined to describe a developmental period taking place approximately between 4-6 weeks following neuronal differentiation, when abGCs exhibit enhanced synaptic plasticity with a lowered threshold for LTP induction, reduced perisomatic GABAergic inhibition, and preferred recruitment to the hippocampal network (Schmidt-Hieber et al., 2004; Ge et al., 2007, 2008). These transient characteristics may provide abGCs with a competitive advantage over integrated mGCs in order to facilitate and stabilize synaptic connectivity. Computational differences might also contribute to selective information processing, resulting in enhanced pattern separation of highly similar inputs (Aimone et al., 2010; Deng et al., 2010).

3.3.4. Regulation of adult neurogenesis

Adult neurogenesis is a complex process orchestrated by multiple intrinsic and extrinsic factors at the level of proliferation, differentiation, survival, and integration. Neurogenesis continuously generates neuronal precursor cells, but the majority get eliminated within the first two weeks, and only a very small population survives and becomes finally integrated into the hippocampal circuitry (Kempermann et al., 2003; Snyder et al., 2009). Numerous studies reported that maintenance, activation, and fate choice of neural precursor cells residing in the neurogenic niche is mediated by Notch-, sonic hedgehog (Shh)-, Wnt-, and bone morphogenetic proteins (BMP)-signaling pathways (Song et al., 2002; Lie et al., 2005; Han et al., 2008; Ming and Song, 2011; Pierfelice et al., 2011). Further extracellular players are growth factors, neurotrophins, cytokines, and hormones (Zhao et al., 2008). Diverse cell-cycle genes, transcription factors, and epigenetic factors act as intracellular regulators (Zhao et al., 2008).

Adult neurogenesis as a network activity-dependent process is regulated by excitatory and inhibitory transmitters. GABAergic signaling promotes dendritic growth, synapse formation, and survival of abGCs through CREB signaling (Jagasia et al., 2009) and Calcium-dependent expression of the neuronal differentiation factor NeuroD (Tozuka et al., 2005). LTP induction at the perforant path enhances proliferation and survival of abGCs (Bruel-Jungerman et al., 2006; Chun et al., 2006) and NMDA receptor-dependent activity is essential for survival of abGCs during a short, critical period after neuronal differentiation (Tashiro et al., 2006; Mu et al., 2015). More specifically, NMDA receptor subunit 2B is required for enhanced synaptic plasticity during the critical period (Ge et al., 2007; Kheirbek et al., 2012). Physical exercise like voluntary wheel running is positively correlated to cell proliferation (Martínez-Canabal, 2015), enriched environment during a critical period supports cell survival (Tashiro et al., 2007) and is likely to be mediated by BDNF and VEGF (Olson et al., 2006). Hippocampus-dependent learning tasks also contribute to survival of abGCs (Drapeau et al., 2007; Kee et al., 2007; Mouret et al., 2008). These positive regulators are opposed by negative effects of aging (Klempin and Kempermann, 2007) and stress (Mirescu and Gould, 2006). Pathological conditions such as temporal lobe epilepsy cause initial elevated proliferation of progenitors and neuroblasts that become fully integrated, but also abnormal morphology including hilar basal dendrites and ectopic migration (Jessberger et al., 2007; Walter et al., 2007). Focal or global ischemia induces cell proliferation and migration of abGCs to the infarct site, but on long term, the majority of cells fail to survive due to a lack of functional integration (Arvidsson et al., 2002; Thored et al., 2007).

3.3.5. Adult hippocampal neurogenesis and learning

Two major types of memory forming processes have been proposed to be mediated by the hippocampal formation. The first, called "declarative memory", can be divided into two categories: episodic and semantic memory which stores memories about factual information and events. The second type, "spatial memory", is involved in the formation of cognitive maps that are required for

spatial navigation. The hippocampus is further involved in multiple other brain functions such as behavioral inhibition and anxiety, sensorimotor function, and the hypothalamic-puitary axis (Andersen et al., 2006). A variety of interventional techniques were established and optimized to study the fundamental principles behind information processing in the hippocampus and the role of adult hippocampal neurogenesis. The most widely used approach to dissociate between a specific anatomical or physiological component and its functional role/associated behavior, is the lesion. Classically, lesions were performed by physical or pharmacological treatments. More modern and elegant approaches are based on pharmacogenetics or regionally confined irradiation. Each method has strengths and weaknesses, including the probability of nonspecificity. Lesion studies focused on the DG in general documented impairments in associative and spatial learning (Sutherland et al., 1983; Walsh et al., 1986; Nanry et al., 1989; Gilbert et al., 2001; Kesner et al., 2004; Hunsaker et al., 2007). On the contrary, reactivation of previously active GCs during fear conditioning evoked the stored memory and linked behavior (Liu et al., 2012, 2014; Ramirez et al., 2013). Studies designed on the basis of inhibiting adult neurogenesis reported impairments in various hippocampus-dependent tasks such as trace fear conditioning (Shors et al., 2001, 2002), deficits in investigation of novel objects (Denny et al., 2012; Kheirbek et al., 2012), contextual fear conditioning (Winocur et al., 2006; Wojtowicz et al., 2008; Snyder et al., 2009; Drew et al., 2010), spatial navigation using the Morris water maze (Snyder et al., 2005; Wojtowicz et al., 2008; Arruda-Carvalho et al., 2011; Ben Abdallah et al., 2013), and pattern separation (Aimone et al., 2010; Deng et al., 2010; Sahay et al., 2011a, 2011b; Groves et al., 2013; Agis-Balboa and Fischer, 2014).

Pattern separation is a computational process that disambiguates similar, overlapping neuronal representations and reduces interference between them in order to discriminate between similar events, places, or objects. This concept has recently gained attention and was discussed as a hallmark feature of episodic memory and a principle hippocampal function (Rolls and Kesner, 2006; Rolls, 2010, 2013; Yassa and Stark, 2011; Paleja et al., 2014). As already described, GCs in the DG outnumber their pre- and postsynaptic partners (see

3.1); as a result GCs receive diverging input from the entorhinal cortex and give rise to converging output to pyramidal cells in CA3 (Boss et al., 1987; Amaral et al., 1990; West et al., 1991; Mulders et al., 1997; Schmidt et al., 2012; van Dijk et al., 2016). Moreover, GCs receive feedforward and feedback inhibition from local interneurons (Freund and Buzsáki, 1998; Andersen et al., 2006; Amaral et al., 2007) and are more hyperpolarized (Mody et al., 1992; Spruston and Johnston, 1992; Staley et al., 1992). These characteristics results in sparsely active and finely tuned GCs, supporting the generation of orthogonalized information. Pattern separation is opposed to pattern completion which is a process that promotes generalization of previously stored representations by recalling information from a reduced number of inputs and is classically attributed to CA3. CA3 pyramidal neurons receive synaptic input from GCs via mossy fibers, the perforant path (layer 2), and recurrent collateral input from CA3 pyramidal neurons. This extensive recurrent collateral network is hypothesized to be an auto-associative network that promotes pattern completion (Leutgeb and Leutgeb, 2007; Yassa and Stark, 2011; Rolls, 2013; Neunuebel and Knierim, 2014; Kesner and Rolls, 2015).

There is growing evidence that abGCs are critically involved in facilitating pattern separation in the DG (Schmidt et al., 2012). Context discrimination studies revealed that rodents with inhibition of adult neurogenesis are impaired in discriminating between highly similar contexts (Clelland et al., 2009; Kheirbek et al., 2012; Nakashiba et al., 2012; Tronel et al., 2012; Clemenson et al., 2015). Furthermore, animals with increased neurogenesis showed an improved performance in discrimination (Creer et al., 2010; Sahay et al., 2011a). Based on these results, two descriptive models were recently proposed. The first model hypothesized, that abGCs act directly as pattern integrators. AbGCs are less selective in response to weak synaptic activity and broadly tuned during early development. With ongoing maturation, they acquire features of mGC, exhibiting sparse activity and therefore encoding new orthogonalized representations that contribute to pattern separation (Becker, 2005; Wiskott et al., 2006; Aimone et al., 2011; Johnston et al., 2016). The second model describes abGCs in a modulatory role, indirectly involved by maintaining the sparse activity of mGCs as a result of their low-threshold activity and strong

feedback inhibition onto mGCs (Sahay et al., 2011b). Although both models seem to be mutually exclusive, they share common ideas about the critical period of hyperexcitability, enhanced synaptic plasticity, and reduced GABAergic inhibition and abGCs as mediators for maximizing encoded information while minimizing interference (Johnston et al., 2016).

3.4. Questions

The growing amount in scientific publications about adult neurogenesis demonstrates the attractiveness and importance of this topic. Considerable effort in understanding the fundamental principles behind the development, synaptic integration and functional role of abGCs has been made in the past, but a number of questions remain unsolved. Although the process of histochemical marker expression, structural development and synaptic integration of abGCs has been studied each on its own, a comprehensive picture taking in account all of these aspects is still missing. The presented studies here will help to clarify the relationship between structural maturation and functional integration of abGCs.

The research was primarily focused on the morphological maturation and synaptic integration of abGCs into the adult hippocampal network under *in vivo* conditions in rat and mice, with the following questions addressed:

(**1**) DCX and calbindin are characteristic histochemical markers used to study adult neurogenesis. What is their exact time course of expression and is there a correlation between the time course of marker expression, structural maturation, and functional integration?

(**2**) What is the degree of histochemical and structural diversity among abGCs born within the same age cohort?

(**3**) What is the time course of synaptic integration into the adult hippocampal network? At which stage of maturation are abGCs responsive to synaptic stimulation and are able to contribute to hippocampal information processing?

(**4**) What is the course of dendritic and spine development and are there any structural prerequisites for a successful functional integration?

(**5**) At which time point and to what extent do abGCs exhibit the capacity of structural plasticity?

(**6**) Is there a critical phase of structural maturation and functional integration?

(**7**) Are there any differences at the level of structure and plasticity between abGCs and perinatally born mGCs?

In order to solve these questions, the following anatomical, histological and electrophysiological methods were used:

(**1**) Detection of abGCs and mGCs by application of histochemical stainings of DCX or CB, labeling of abGCs by BrdU administration, or intrahippocampal injections of retro- and adenoviral vectors for expression of GFP.

(**2**) LTP induction by electrophysiological HFS of the medial perforant path.

(**3**) Histochemical expression analysis of synaptic activity and plasticity marker following HFS.

(**4**) A detailed analysis of 3D computer reconstructed dendritic trees and dendritic spines including stimulation induced changes in GFP-labeled abGCs and mGCs.

4. Discussion

4.1. High-frequency stimulation induces gradual immediate early gene expression in maturing adult-generated hippocampal granule cells

(Jungenitz et al., 2014)

Electrophysiological stimulation of the perforant path is a well-established method to study synaptic plasticity at the GC-perforant path synapse in the hippocampus (Lomo, 1971; Bliss and Lomo, 1973). We applied *in vivo* high frequency stimulation (HFS) to the medial perforant path in urethane anaesthetized rats (Sprague Dawley) to induce a robust long term potentiation (LTP) that was verified by recordings of evoked field potentials (Steward et al., 1998). Animals were transcardially perfused and fixed with paraformaldehyde (PFA) right after the stimulation protocol was finished. Expression of immediate early genes (IEGs) is considered a prerequisite of protein biosynthesis-dependent late phase LTP (Clayton, 2000; Loebrich and Nedivi, 2009). IEGs are rapidly activated by synaptic activation and therefore a reliable marker of synaptic plasticity and activity (Jones et al., 2001; Fleischmann et al., 2003; Reymann and Frey, 2007; Bramham et al., 2010; Chen et al., 2010). We focused our immunohistochemical expression analysis on the following IEGs: Arc (Activity regulated cytoskeletal-associated protein), c-fos, pCREB133 (cAMP response element-binding protein, phosphorylated at serine 133), and zif268 (zinc finger protein clone 268; also known as EGR-1, early growth response protein 1).

Doublecortin (DCX) and calbindin (CB) are stage-specific markers of adult neurogenesis and used to differentiate between immature and mGCs (Snyder et al., 2009) (see 3.3.1). DCX is a microtubule-associated protein and is expressed in migrating and differentiating immature neurons (Francis et al., 1999; Gleeson et al., 1999; Kempermann et al., 2004, 2015; Couillard-despres et al., 2005). CB is a member of the calmodulin superfamily of Ca^{2+}-binding proteins, it functions as a Ca^{2+}-buffer and is considered as a Ca^{2+}-sensor (Baimbridge et al., 1992; Berggård et al., 2002). Expression of CB is a distinctive feature of mGCs (Kempermann et al., 2004, 2015). 2 h HFS of the

medial perforant path induced robust LTP and strong expression of c-fos and Arc in almost all mature CB-positive GCs, but failed to elicit expression in immature DCX-positive GCs. In order to exclude unphysiological side effects as response to the massive stimulation, we performed mild perforant path theta burst stimulation in anesthetized animals that led to c-fos and Arc expression in a sub-fraction of CB-positive GCs. In addition, an open-field exposure to a novel environment in awake animals that elevated home-cage activity induced expression of c-fos and Arc in CB-positive GCs (Marrone et al., 2008), but failed to activate DCX-positive GCs.

AbGCs transiently express DCX approximately during the first 3 weeks of development (Snyder et al., 2009). In order to birthdate and identify abGCs at later cell ages, we used bromodeoxyuridine (BrdU) as a marker of cell mitosis (Taupin, 2006). The applied administration protocol (one intraperitoneal injection of 200 mg/kg body weight) is widely used and known for maximum labeling of mitotic cells while maintaining a low toxicity risk (Cameron and Mckay, 2001; Mandyam et al., 2007; Snyder et al., 2009). This protocol targets dividing cells within a range of approximately 4 days (Dayer et al., 2003). BrdU labeling was performed to study the age-dependent expression of DCX and CB. DCX was present in most BrdU-labeled cells at 7 dpi and declined to low levels at 21 dpi. CB was already present in a minor sub-fraction at 7 and 14 dpi, but increased strongly at 21 dpi and represented the major population of BrdU-labeled abGCs. Double-labeling revealed a subpopulation of DCX- and CB-positive cells that most likely represent early CB-positive cells. Our results conform closely to results of comparable BrdU-studies performed in Sprague-Dawley and Long-Evans rats (Snyder et al., 2009). HFS was applied at 21, 28, 35, 49, 63, or 77 dpi following BrdU application. Stimulation-induced expression of c-fos and Arc was observed earliest at 21 dpi in about 10 % of BrdU-labeled abGCs. The percentage of c-fos and Arc-positive cells increased rapidly during the following 2 weeks and reached a plateau with about 80 % c-fos/Arc-positive BrdU-labeled GCs at 35 dpi. There was no further increase in the number of activated cells and notably 20 % of BrdU-labeled abGCs failed to elicited c-fos/Arc expression at 77 dpi.

Immunohistochemical labeling of pCREB133 and zif268 revealed that both markers were already endogenously expressed under non-stimulated, baseline conditions in a subpopulation of DCX-positive abGCs, as described earlier. However, there was no further increase of pCREB133/zif268 expression in DCX-positive cells following HFS. DCX-positive abGCs exhibited a high morphological diversity at the dendritic level which we used to categorize abGCs into distinct developmental stages. In order to investigate whether expression of pCREB133 or zif268 can be correlated to the structural developmental stage, we introduced a classification system based on dendritic arborization and defined six different stages: stage 1 - no process, 2 - principle dendrite in the subgranular zone, 3 - leading dendrite in the inner half of the granule cell layer (GCL), 4 - leading dendrite in the outer half of the GCL, 5 - leading dendrite in the IML, and 6 - leading dendrite in the MML and OML. According to this classification, cells at a specific stage are anatomically limited to a specific set of synaptic partners. Stage 1-4 cells exhibit no dendrites at all or short dendrites within the GCL, limiting their synaptic connections to local interneurons. Stage 5 cells have dendrites reaching the IML and therefore are capable to establish glutamatergic synaptic contacts with associational/commissural fibers of mossy cells that originate either from the ipsi- or contralateral hemisphere. Finally, stage 6 cells have established dendrites within the MML/OML and therefore receive main afferent synaptic input from perforant path fibers. We confirmed our classification system by co-labeling with NeuN (neuronal nuclei), a marker of postmitotic neurons (Lind et al., 2005; Gusel'nikova and Korzhevskiy, 2015) and found a positive correlation between an increasing dendritic complexity and the expression of NeuN in the nucleus of BrdU-labeled abGCs. Furthermore, we analyzed BrdU-labeled abGCs at 7 dpi and 14 dpi and found significant differences in the distribution of DCX-stages. The majority of DCX-positive abGCs at 7 dpi were classified as stages 1-4, only a minor subpopulation was attributed to stage 5-6. While the majority of cells was characterized as stage 5 or 6 at 14 dpi, we found some cells at stages 2-4. These findings indicate a certain degree of structural variability among cells of a similar age population: a minority of abGCs may undergo an accelerated maturation and might establish synaptic contacts to

entorhinal afferents within 14 dpi, while other abGCs would mature with some delay. The application of this classification system revealed a strong positive correlation between pCREB133 expression and the degree of structural maturation. Increase pf pCREB133 was detected during maturation within few pCREB133-positive cells at stage 2, but almost all cells labeled at stage 6. Zif268 was restricted to stage 5-6 cells. In consistence with our data regarding c-fos/Arc expression in DCX-positive abGCs, we found no further increase of pCREB133 and zif268 in DCX-positive cells at any stage following HFS.

The immunohistochemical expression intensity of zif268 showed a considerable variation among GCs and therefore demanded the measurement of the fluorescence-intensity in the cell nucleus. The expression intensity of BrdU-labeled abGCs was set in relation to neighboring CB-positive GCs. The time course of zif268 expression was similar to the expression of c-fos and Arc following HFS. The relative fluorescence-intensity increased from 21 dpi on and reached a maximum of about 70 % at 35 dpi. Yet again, the population of 77-days-old abGCs showed a weaker response to synaptic activation in comparison to mGCs.

This study revealed correlations between structural maturation, histochemical marker expression, age of abGCs, and their capability to express various IEGs following stimulation of the medial perforant path, as an indication of functional integration in the adult hippocampal network under *in vivo* conditions.

4.2. Differential structural development of adult-born septal hippocampal granule cells in the Thy1-GFP mouse, nuclear size as a new index of maturation

(Radic et al., 2015)

The previously described DCX-classification system (Jungenitz et al., 2014) (see 4.1) was used for the analysis of abGCs maturation in a widely used transgenic model, the Thy1-EGFP mouse (Feng et al., 2000). In this animal model, a low percentage of principal neurons including hippocampal GCs express green fluorescent protein (GFP) under the thymocyte differentiation

antigen 1 (thy1)-promotor, thus enabling complete dendritic reconstructions of neurons. This study included the dendritic structure, cell age, cell nucleus position within the SGZ/GCL, and nuclear size of abGCs. Intraperitoneal BrdU injections were performed to birth-date abGCs, animals were transcardially perfused with PFA at defined time points and the tissue was further processed for immunohistochemistry of the classical neurogenesis marker DCX. BrdU-labeling was combined with Prox1, a marker specific for GCs throughout all developmental stages in the adult hippocampus (Lavado and Oliver, 2007; Iwano et al., 2012). The number of BrdU-labeled abGCs was analyzed and revealed a decline of approximately 80 % within the first 5 weeks. These results are consistent with previous studies (Cameron et al., 1993; Dayer et al., 2003; Kempermann et al., 2003; Snyder et al., 2009) and support the critical importance of the first weeks for survival and further development of abGCs. This elimination process is presumably apoptotic, controlled by pro-apoptotic genes such as Bax (Biebl et al., 2000; Sun et al., 2004; Kuhn et al., 2005; Sahay et al., 2011a) and various other intrinsic and extrinsic survival factors (Tozuka et al., 2005; Ge et al., 2006; Tashiro et al., 2006; Imielski et al., 2012; Cancino et al., 2013; Ramírez-Rodríguez et al., 2013).

The number of DCX-positive BrdU-labeled abGCs declined steadily during the first 4 weeks and DCX expression disappeared completely after 5 weeks. Our DCX staging system revealed structural maturation of abGCs in general, but again with some considerable variability. Although the majority of DCX-positive cells reached stages 5-6 between 14 dpi and 21 dpi, we still observed cells of earlier stages at 28 dpi. Despite this high variability, the DCX stage can be used to approximately estimate a given DCX cell age. About 70 % of abGCs within stages 1-3 were found to belong to the group of 7 dpi cells, whereas about 90 % within stages 4-6 belonged to groups 14 dpi, 21 dpi, and 28 dpi. This degree of structural variability may reflect a different pace of maturation and a critical period of cell survival, depending on growth/survival factors (e.g. Brain-derived neurotrophic factor (BDNF)), and progress in synaptic integration (e.g. GABAergic signaling). The observed time course of abGC development resembles our findings in rats (Jungenitz et al., 2014) but reveals a small difference, namely that the development of abGCs is prolonged in mice by

about 1-2 weeks. This diversity was also described in a comparative study of adult neurogenesis in mice and rats published by Snyder et al., 2009. These authors describe the switch between immature and mature immunohistochemical markers and activity-induced IEG expression as an indication of synaptic plasticity 1-2 weeks earlier in rats than in mice. Furthermore, they could demonstrate that newborn neurons in rats are more likely to survive apoptosis-mediated cell death and to contribute to learning and memory processes.

Prox1 is a transcription factor that is involved in embryonal development of the nervous system, is postnatally expressed specifically only in GCs, and thought to be required as a factor to maintain the identity of GCs (Galeeva et al., 2007; Lavado et al., 2010; Iwano et al., 2012). Prox1 expression was found in all GCs and DCX-positive abGCs. Immunohistochemical labeling was restricted to the cell nucleus and was therefore used by us to determine the size (area) of the nucleus. We observed a positive correlation between nuclear size, structural maturation, and cell age. Based on the found distribution, we calculated the probability to predict the structural stage and cell age based on the nuclear size and found a 70 % reliability to discriminate between early (DCX-stage 1-3, 7-14 dpi) and late (DCX-stage 4-6, 21-77 dpi) developmental stages. If more improved, this approach could be used in the future as a novel and simple indicator of cell maturity.

The neurogenic niche is located in the SGZ of the DG. The GCL is organized in an outside-in layering which emerges from continuous neurogenesis throughout the embryonic and early postnatal development, and adulthood. Early-born cells are preferentially located within the outer layers and late-born cells are located within inner layers (Muramatsu et al., 2007; Mathews et al., 2010). We investigated the position of BrdU-labeled cells within the GCL in relation to cell structure and age, but could not find any correlation. Almost all abGCs were located either in the SGZ or the inner third of the GCL. However, abGCs in DCX stages 5-6 appeared to be more dispersed. This indicates that migration and localization might be determined very early during development.

This study provides a detailed understanding of structural maturation of abGCs. Our method of nuclear size measurement offers a novel toolset to simply estimate the developmental stage of abGCs that can be used in combination with functional or behavioral techniques to further illuminate the complex process of adult neurogenesis.

4.3. Adult-born hippocampal granule cells exhibit a critical period of dendritic reorganization and remain structurally distinct from perinatally-born granule cells

(Beining et al., 2016)

We performed *in vivo* intra-hippocampal injections of viral vectors to label abGCs and mGCs in the hippocampus of adult Sprague Dawley rats. The retroviral vector used for this study is derived from the Moloney murine leukemia retrovirus which is specific for mitotically active cells and is an established technique to study adult neurogenesis (RV-GFP) (van Praag et al., 2002). When successfully transduced, newborn cells are labeled with GFP under the CAG promotor (a synthetic promotor constructed from the cytomegalovirus enhancer element, the promotor of the chicken beta-actin gene, and the splice acceptor of the rabbit beta-globin gene) (Miyazaki et al., 1989; Niwa et al., 1991). For labeling of mature and presumably perinatally born GCs, we used an adeno-associated virus expressing GFP controlled by a synapsin promotor (AAV-GFP) (Fornasiero et al., 2010; Valtorta et al., 2011). This technique was combined with *in vivo* HFS of the medial perforant path to induce LTP and synaptically activate abGCs and mGCs (Jungenitz et al., 2014) (see 4.1). Stimulation effects were restricted to the ipsilateral hemisphere as expression of Arc and evoked field potentials at the contralateral side remained at baseline levels following HFS. Animals were transcardially perfused and fixed with PFA right after the stimulation was finished. To preferentially obtain entirely preserved dendritic trees, brains were cut to 300 µm thick sections with a vibratome. GFP expression was enhanced by immunohistochemistry and cells were imaged with a two-photon microscope (MaiTai HP Ti-sapphire laser). Dendritic trees were reconstructed in 3D (240 cells in total) using the TREES

toolbox (Cuntz et al., 2011) and analyzed comprehensively addressing the various morphological parameters on the complete cell- or molecular layer-specific level, e.g. dendritic length, number of branch and termination points, small terminal segments (defined as terminal segments smaller than one fifth of the tree's maximum path length), branching angle, curvature of dendritic segments, Sholl distribution, convex hull volume, and spatial density. In order to increase the likelihood of analyzing perinatally born AAV-GFP-labeled GCs, we collected only cells located in a defined distance (20 µm) to the subgranular zone, as perinatally born GCs are preferentially located within the outer part of the GCL (Mathews et al., 2010; Radic et al., 2015). RV-GFP-labeled abGCs were studied at 21 dpi, 28 dpi, 35 dpi, and 77 dpi.

Even though we performed a very detailed structural analysis, we could not find significant differences of abGCs between 21 dpi and 77 dpi, except for a slightly larger dendritic length in the IML at 35 dpi and a reduction of small terminal segments from 21 dpi to 28 dpi. Distal short terminal segments have been described as a phenotype associated with immature neurons (Emoto, 2011). Our findings illustrate that structural development of abGCs is typically completed between the third and the fourth week. On the contrary, when compared to RV-GFP-labeled abGCs, AAV-GFP-labeled mGCs featured significant structural differences. These included a reduced number of small terminal segments in conjunction with a greater number of dendrites terminating in the OML. Furthermore, we found that dendrites were less curved and a distinct distribution of branch points in mGCs, which were more located in the MML and less found in the IML and OML. Total dendritic length and number of branch points were comparable between both groups. Our findings demonstrate that abGCs and perinatally born mGCs represent structurally distinct groups.

To further elucidate the functional implications of the observed differences between abGCs and mGCs, a morphological model derived from the optimal wiring principles of dendritic trees (Cuntz et al., 2007, 2008, 2010) was established. This model is based on the minimum spanning tree algorithm which generates realistic dendritic morphologies by connecting target points (which can be interpreted as abstractions of synapses) while minimizing the

length and conduction times of the dendritic tree (Cuntz et al., 2010), and on the following assumptions during perinatal development: the GCL and ML expand from 80 µm in size at P4 (postnatal day), to 300 µm at P60 (Loy et al., 1977; Claiborne et al., 1990; Rihn and Claiborne, 1990); the number and density of commissural axons in the IML increases, and the number of Cajal-Retzius cells (guidance of dendritic arborization) at the hippocampal fissure decreases (Förster et al., 2006; Frotscher, 2010; D'Arcangelo, 2014). In our morphological model, target points for synthetic mGCs were distributed mainly in the OML and in a reduced DG volume. To simulate the expansion during hippocampal growth, the synthetic dendritic trees were subsequently stretched to fit the size of an adult DG. Synthetic abGCs were grown in the adult DG, with decreased target points in the OML and increased target points in the IML, while keeping all the other parameters constant. Remarkably, our model was sufficient to generate realistic GC-morphologies and reproduced the observed structural similarities and differences between 77 dpi abGCs and mGCs. These results suggest that distinct structural characteristics of abGCs and mGCs might emerge from changes of environmental conditions during early hippocampal development.

A comparison between GCs located at the ipsilateral, stimulated and the contralateral, unstimulated hemisphere revealed no differences; therefore stimulation had no effect on the dendritic structure in general. In the process of further examination, we resliced 300 µm sections (used for the reconstruction of dendritic trees) to 50 µm at the vibratome and performed immunohistochemical labeling of Arc. As stated above, applied HFS induced LTP and thus expression of Arc in the major population of GCs as well as in abGCs between 21 dpi and 35 dpi (Jungenitz et al., 2014) (see 4.1). Arc expression was correlated with all available structural properties, reconstructed GCs were classified into Arc-positive and -negative cells, and Arc-positive abGCs at 28 dpi and 35 dpi featured a significant reduced number of small terminal segments in the OML. The dendritic morphology can substantially influence a neuron's information processing and excitability (Rall and Rinzel, 1973) and studies have linked expression of key proteins to dendritic morphology and neuronal excitability (Duan et al., 2007; Fitzsimons et al., 2013; Šišková et al., 2014; Norkett et al.,

2016). However, reduction in total dendritic length was limited to about 5 % and therefore the change of input resistance and thus excitability seems to be very limited. In contrast, dendritic trees of abGCs at 77 dpi and mGCs were not altered. These results implicate an activity-induced dendritic remodeling of dendrites during a critical phase between 28 dpi and 35 dpi of maturation.

In this study we present a detailed structural characterization of abGCs and mGCs based on complete 3D-reconstructions of virally labeled dendritic trees. Our data provide convincing evidence that abGCs stay morphologically distinct from mGCs and that their dendritic arbor can be shaped by afferent activity during a narrow time window.

4.4. Structural homo- and heterosynaptic plasticity in adult newborn rat hippocampal granule cells

(Jungenitz et al., submitted manuscript)

This study was conducted in strong interrelation to our publication presented in 4.3 and is consequently based on the same source materials and methods. Here, the research focus was drawn to the structural evidence for synaptic plasticity of abGCs and mGCs. The anatomical structure receiving the main excitatory glutamatergic input is the dendritic spine. Spine morphology is highly variable, can undergo activity-dependent changes (Bosch and Hayashi, 2012; Rochefort and Konnerth, 2012). Spine size can be correlated with synaptic strength (Reymann and Frey, 2007) and therefore examination of spines can reveal important information about the extent of functional integration.

LTP is the activity-dependent persistent strengthening of synapses and is opposed by LTD, a long-lasting decrease of synaptic strength. Electrophysiological studies of the medial and lateral perforant paths reported a concurrent heterosynaptic LTD at synapses that were not active during the induction of homosynaptic LTP (Abraham et al., 1985, 2007). Selective stimulation of either the MPP or LPP has been demonstrated to result in the induction of homosynaptic LTP (Steward et al., 1998) and concurrent heterosynaptic LTD (Christie and Abraham, 1992; Abraham et al., 1994, 2001;

Jedlicka et al., 2015) in the respective MML or OML. Heterosynaptic LTD is discussed as a homeostatic mechanism for normalizing the overall synaptic weights, maintaining synaptic competition, and preventing runaway synaptic dynamics (Chen et al., 2013; Chistiakova et al., 2015). Furthermore, computational modelling showed that homosynaptically induced LTP would strengthen heterosynaptic LTD at neighboring dendritic segments (Jedlicka et al., 2015) and thus could lead to effective and long-lasting changes of synaptic weights as a requisite for learning and memory (see 3.2). However, the emergence of heterosynaptic plasticity during the maturation and synaptic integration of abGCs is not well studied and its impact to hippocampal network function is not fully understood yet.

Fukazawa and colleagues (2003) showed that *in vivo* LTP induction caused by stimulation of the perforant path leads to a long-lasting NMDA receptor-dependent reorganization of F-actin and a layer-specific increase of several other marker proteins involved in synaptic plasticity, including synaptopodin (Fukazawa et al., 2003). We verified the occurrence of heterosynaptic LTD by recording local field potentials of the lateral perforant path during LTP induction of the medial perforant path and analyzed the F-actin and synaptopodin distribution in the molecular layer by immunohistochemistry. Both proteins showed a notable accumulation in the MML (i.e. the lamina of MPP fiber projection) in response to HFS restricted to the ipsilateral side. Distribution of F-actin in the IML, MML, and OML was measured along the GCL-hippocampal fissure axis, starting from the border between GCL and IML up to the hippocampal fissure and was significantly elevated in the stimulated MML, while reduced in the unstimulated IML and OML. Synaptopodin is an actin-binding protein, which is functionally linked to the formation of the spine apparatus, while a synaptopodin deficiency leads to impaired LTP (Deller et al., 2003; Jedlicka et al., 2009). F-actin is a component of the cytoskeleton, associated with the plasma membrane and the organization of the postsynaptic density (PSD) in dendritic spines (Bosch and Hayashi, 2012). Polymerization of actin filaments is required for stable LTP (Kim and Lisman, 1999; Matsuzaki et al., 2004), whereas LTD is accompanied by depolymerization of F-actin (Okamoto et al., 2004). Our results indicate a high specificity of our applied stimulation

protocol in targeting fibers of the medial perforant path and a stimulation-induced homosynaptic LTP accompanied by a concurrent heterosynaptic LTD in the adjacent layers. We also provide first experimental evidence for heterosynaptic plasticity at commissural/associational IML synapses as it has been predicted by computational modeling (Benuskova and Jedlicka, 2012).

Dendritic segments of GFP-labeled GCs were imaged with a confocal microscope (60x objective, 5x field zoom) and a step distance set to 0.5 µm to obtain a good z-resolution while ensuring photostability at the same time. Segments were acquired from the IML, MML, and OML only when traceable back to the cell soma to guarantee investigation of layer-specific changes within individual dendritic trees. Filopodia and stubby spines were excluded from analysis and mushroom-like dendritic spines with a bigger head diameter than shaft diameter were exclusively counted. (for definitions see: Bosch and Hayashi, 2012; Rochefort and Konnerth, 2012). Small spines exhibit the ability to potentiate, whereas large spines are more stable and associated with larger synapses. Large spines with bulbous heads and head diameters > 0.6 µm are typically referred to as mushroom-spines (Sorra and Harris, 2000). Accordingly, spines were classified into small and large spines applying a grid overlay with a grid element size set to 0.2 µm² (square diagonal ~0.6 µm). The number of spines was normalized to the length of the dendritic segment. These data were complemented by direct measurement of spine size via obtaining the largest cross-sectional area of spine heads in confocal z-stacks. RV-GFP-labeled abGCs were analyzed at 21 dpi, 28 dpi, 35 dpi, 77 dpi, and compared to AAV-GFP-labeled mGCs.

The contralateral DG is connected to the ipsilateral hemisphere via direct commissural and indirect multi-synaptic (mossy cell fibers) projections. The commissural pathway is known for only a sparse activation of GCs and lacking the capacity of LTP induction under normal physiological conditions (Wilson et al., 1979, 1981; Wilson, 1981; Alvarez-Salvado et al., 2014). Although our applied stimulation protocol resulted in a robust LTP that was accompanied by strong ipsilateral IEG expression, the effects were restricted to the ipsilateral hemisphere. The contralateral DG exhibited no changes in evoked local field

potentials, expression of IEGs, or changes in the distribution of F-actin and synaptopodin, respectively. We therefore used GFP-labeled cells located at the contralateral side as controls. Small and large spines were already detectable at 21 dpi, increased in a parallel time course, and reached a mature state at 77 dpi. Large spines comprised about 15 % of the total number of spines. Spine formation of abGCs was reported to start at about 16 dpi in rats, followed by a rapid increase between 16-18 dpi (Ohkawa et al., 2012), and is somewhat delayed in mice (Zhao et al., 2006; Toni et al., 2007). Spines gain a mature state in quality and quantity at about 70 dpi, but can show prolonged structural maturation, modulated by a variety of stimuli (Zhao et al., 2006; Toni et al., 2007, 2008).

In our study, we found an enlargement of spines located in the stimulated MML in abGCs from 28 dpi on and in mGCs following 2 h HFS of the medial perforant path. In contrast, in the non-stimulated adjacent IML and OML 2 h HFS leads to spine shrinkage in abGCs from 35 dpi on and in mGCs. All analyzed dendritic segments featured a direct connection to the cell soma, thus enabling the investigation of layer-specific changes within individual dendritic trees. In the literature, the size of spines is correlated to the size of the postsynaptic density (PSD), the number of glutamate receptors, and thus to the strength of synaptic connectivity (Reymann and Frey, 2007). Furthermore, it was demonstrated that LTP induction is associated with spine enlargement (Matsuzaki et al., 2004), and LTD with spine shrinkage (Zhou et al., 2004). Thus, we found strong indication for the manifestation of homosynaptic structural LTP and concurrent heterosynaptic structural LTD in abGCs and mGCs. Furthermore, this is the first demonstration of concurrent homo- and heterosynaptic plasticity on the level of individual neurons. The total spine density remained unchanged throughout all layers following stimulation, indicating a homeostatic regulation (Chen et al., 2013; Chistiakova et al., 2014, 2015). It remains open if LTP or LTD is associated with *de novo* formation of spines or only morphological changes of pre-existing spines (Popov et al., 2004; Wosiski-Kuhn and Stranahan, 2012). We found stimulation-induced layer-specific homo- and heterosynaptic structural plasticity within the same dendritic tree in about 20 % of abGCs at 21 dpi and 28 dpi. A strong and significant

increase in the number of abGCs appeared at 35 dpi, when abGCs reached the state of mGCs (~60 %). Interestingly, there was no net change in spine size along the dendritic tree in comparison to unstimulated control GCs of the contralateral hemisphere. Therefore, we conclude that homosynaptic induced enlargement of spines in the MML was counteracted by heterosynaptic induced shrinkage of spines in the IML and OML. These findings support the idea of heterosynaptic plasticity as a homeostatic mechanism for normalization of synaptic weights and maintainance of synaptic competition (Chen et al., 2013; Chistiakova et al., 2014, 2015).

These results provide not only the first evidence for heterosynaptic structural plasticity in abGCs at the single cell level, but also the first experimental evidence for heterosynaptic plasticity at commissural/associational IML synapses, as it has been predicted by computational modeling (Benuskova and Jedlicka, 2012). In addition, our findings strengthen the idea of heterosynaptic plasticity as a homeostatic mechanism for normalization of synaptic weights (Chistiakova et al., 2015) taking place in abGCs from 21 dpi on.

4.5. Summary and conclusion

In the presented studies we focused on the structural maturation and functional integration of hippocampal abGCs in comparison to perinatally born mGCs. Newborn neurons were identified either by immunohistochemical markers, BrdU application, or retroviral *in vivo* labelling. Homosynaptic LTP and heterosynaptic LTD on GC-perforant path synapses were induced by *in vivo* HFS of the medial perforant path. The time course of neurochemical marker and IEGs expression was characterized and detailed morphological analyses of dendritic trees and spines of more than 240 GFP-labeled cells was conducted. The following key findings were summarized from these studies:

(**1**) Switch in expression between doublecortin to calbindin around 21 dpi and 28 dpi.

(**2**) Considerable variations in the time course of structural and histochemical development between individual abGCs during early development (< 21 dpi).

(**3**) Structural features, such as dendritic arborization and nuclear size, can be used to roughly determine a given cell age during early development (< 35 dpi).

(**4**) Positive correlation between endogenously expressed pCREB133, zif268, and NeuN and structural maturation of DCX-positive abGCs.

(**5**) Delayed onset of stimulation induced IEG expression in abGCs indicating delayed functional integration. No induction of IEGs expression in DCX-positive abGCs in response to HFS. Earliest HFS induced IEG expression from 21 dpi on and in the majority of abGCs from 35 dpi on. Less responsive population of abGCs at 77 dpi in comparison to mGCs.

(**6**) Mostly complete dendritic development at 21 dpi, indicating that structural maturation precedes functional integration.

(**7**) Structural differences between dendritic trees of maturated abGCs and mGCs.

(**8**) Medial perforant path stimulation induced remodeling of dendrites, i.e. dendritic structural plasticity between 28 dpi and 35 dpi.

(**9**) Stimulation induced homo- and heterosynaptic structural plasticity of spines from 28 dpi and 35 dpi on, respectively.

(**10**) Homosynaptically induced enlargement of spines was counteracted by heterosynaptic induced shrinkage of spines on individual neurons.

(**11**) No differences in the amount of structural plasticity between abGCs at 77 dpi and mGCs.

We conclude from our data that during their course of maturation, abGCs pass through distinct developmental phases that can roughly be grouped in an early phase of structural dendritic maturation and a late phase of functional and synaptic integration. AbGCs exhibit rapid dendritic outgrowth that is almost completed within the first 3 weeks followed by a gradual integration into the hippocampal network between 4-5 weeks of age. Dendritic trees have to first

extend through the GCL, and then sequentially enter the IML, MML, and OML (see 4.1). According to this development, cells at a specific stage are anatomically limited to a specific set of synaptic partners. Although, in average, the population of abGCs progress quite homogenously, there is considerable variability in the pace of maturation between individual cells. Dendrites of some cells exhibit a fast rate of extension and already arrive in the OML within the first week, whereas others need at least 3 weeks (see 4.1, 4.2). It was reported from observations in rats that dendritic spines first appear around 16 dpi with a sharp increase between 16-18 dpi (Zhao et al., 2006; Ohkawa et al., 2012). Our own results illustrate a gradual increase of spines from 21 dpi on, reaching a maximum density at 77 dpi. The first indication of a successful synaptic integration into the hippocampal network was observed at 21 dpi. Around that time, only a small minority of abGCs exhibited expression of IEGs and structural plasticity of dendritic spines in response to stimulation of the perforant path (see 4.1, 4.4). **Based on this sequence of events, we conclude that structural maturation of abGCs precedes their functional integration.**

Our data revealed a rapid increase in the degree of dendritic and synaptic plasticity between 21 dpi and 35 dpi. During this age, the population of abGCs exhibited an increasing capability to express synaptic plasticity-related IEGs (e.g. c-fos and Arc expression from ~15 % at 21 dpi to ~80 % at 35 dpi), structural plasticity of spines (change from primarily homosynaptic structural LTP at 28 dpi to homo- and heterosynaptic structural LTP and LTD at 35 dpi), and dendrites (dendritic pruning in Arc-positive abGCs at 28 dpi and 35 dpi) following HFS (see 4.1, 4.4). This time frame corresponds closely to the term "critical phase" which has been defined in previous studies and describes a developmental period when abGCs exhibit enhanced synaptic plasticity with a lowered threshold for LTP induction, reduced perisomatic GABAergic inhibition, and a preferential recruitment to the hippocampal network (Schmidt-Hieber et al., 2004; Ge et al., 2007, 2008). **The gradual appearance of homo- and heterosynaptic plasticity during the phase of integration may provide abGCs with a competitive acquisition over integrated mGCs in order to facilitate and stabilize synaptic connectivity.**

In the literature, comparative studies of abGCs and mGCs implied that the two groups represent structurally and functionally distinct cell populations and so far, it still remains insufficiently answered if abGCs converge fully to perinatally born mGCs during their late phase of maturation or if they persist as a distinct subpopulation (Espósito et al., 2005; Laplagne et al., 2006; Stone et al., 2011; Lemaire et al., 2012; Brunner et al., 2014; Tronel et al., 2015). Our data revealed that abGCs exhibit a continuous age-related increase in quantity and size of dendritic spines until reaching a mature state at 11 weeks. Homo- and heterosynaptic structural plasticity was present in about 60 % of the total population of abGCs at 77 dpi and mGCs following stimulation. There was evidently no difference in the amount of stimulation-induced structural spine plasticity between abGCs at 77 dpi and mGCs (see 4.1, 4.3, 4.4). **Our extensive characterization of dendritic trees revealed small but significant structural differences between maturated abGCs and mGCs indicating the existence of two distinct populations of GCs.**

Taken together, our results implicate a continuous synaptic integration of abGCs into the hippocampal network. Although our data provides strong evidence for a phase of dendritic plasticity and rapid increase in synaptic plasticity between the fourth and the fifth week, we cannot confirm the existence of a transient critical phase of enhanced synaptic plasticity. Structural differences between dendritic trees of maturated abGCs and mGCs suggest that abGCs form a morphologically distinct subpopulation. Hence, further investigations are necessary to elucidate the impact of our findings on the unique role of abGCs in hippocampal information processing.
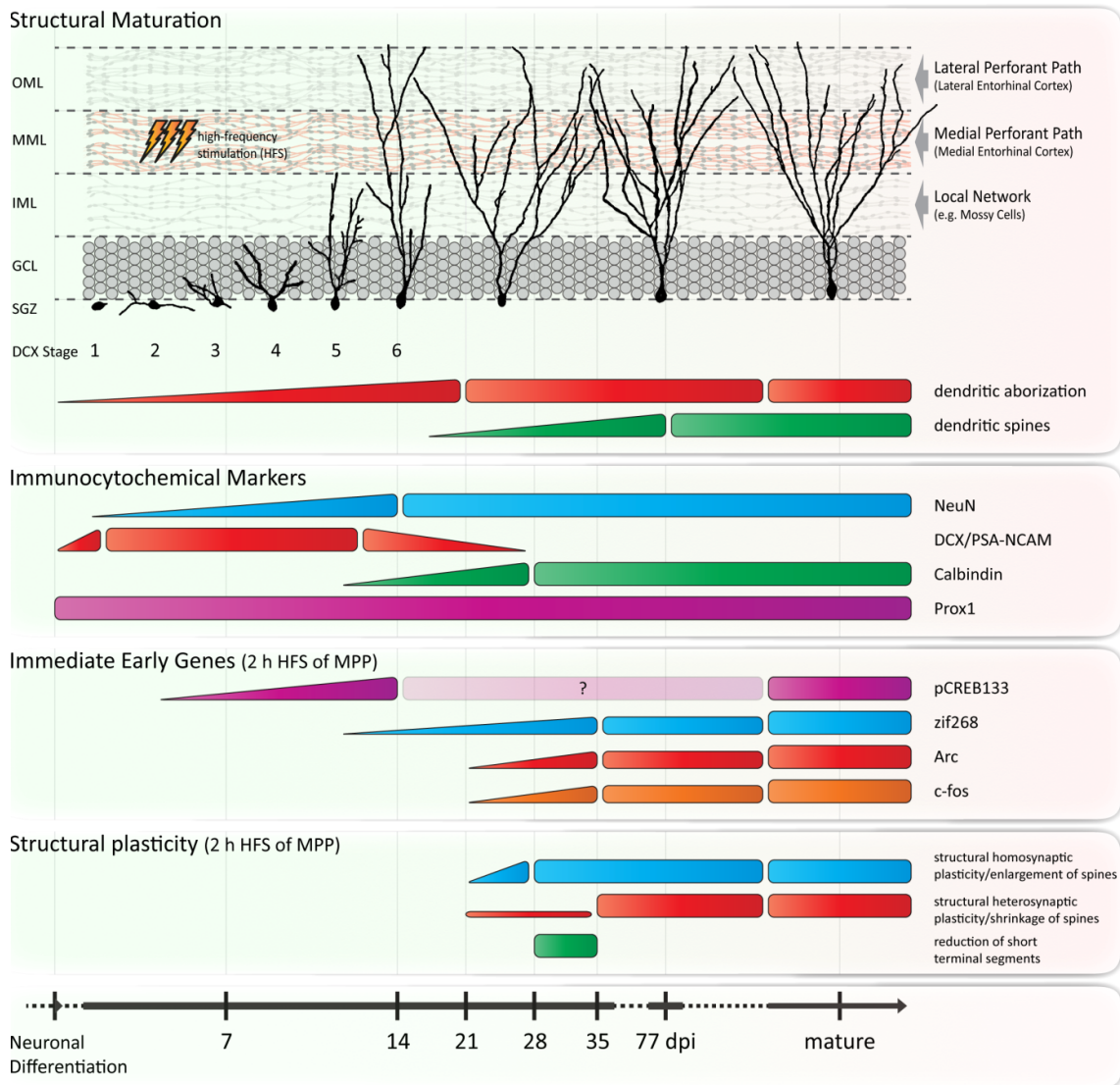
Figure 4. Schematic summary of the structural, chemical, and functional maturation of abGCs in the adult hippocampus. (**Structural maturation**) Dendritic development of immature Doublecortin-positive (DCX) cells showed rapid increase in complexity and was classified in 6 stages according to outgrowth. Maturation of dendritic trees was completed before 21 dpi and preceded functional integration. Dendritic trees of abGCs exhibited differences in some features compared to perinatally born GCs, implying, that abGCs are a structurally distinct population. Spine density increased with time and reached the level of a mature state at 77 dpi. (**Immunocytochemical markers**) NeuN expression increased with structural maturation of DCX-positive cells. Calbindin expression started in more mature DCX-positive cells and was increasingly present in older GCs. Prox1 was detectable at all stages during abGC development. (**Immediate early genes**) Expression of IEGs as sign of synaptic activity/plasticity following high frequency stimulation (HFS) of the

65

medial perforant path (MPP) increased with age and was present in about 75 % of maturing GCs between 35 dpi and 77 dpi. (**Structural plasticity**) Homosynaptic LTP-associated increase of spine size was observed from 28 dpi on and heterosynaptic LTD-associated decrease of spine size from 35 dpi on. At individual dendritic trees LTD-associated spine shrinkage counteracted LTP-associated spine enlargement which suggests a homeostatic mechanism for normalization of total synaptic weights. AbGCs at 28 dpi and 35 dpi were responsive to stimulation with remodeling of their dendritic arbor. Besides a general close correspondence between structural maturation, chemical marker expression, functional integration, and age, some variability in the time course of individual cell development has to be taken into account. GCL, granule cell layer; IML, inner molecular layer; MML, middle molecular layer; OML, outer molecular layer; SGZ, subgranular zone.

4.6. Outlook

We demonstrated layer-specific homo- and heterosynaptic structural plasticity of dendritic spines at the level of individual neurons. Following LTP induction of the medial perforant path spine sizes were increased in the MML while the accompanied induction of LTD in the lateral perforant path resulted in spine size reduction in the OML. It was shown earlier that the reverse phenomenon can be reproduced by stimulating the lateral perforant path, indicating its input specificity but pathway independency (Abraham and Goddard, 1983; Fukazawa et al., 2003). It would be interesting to establish a robust *in vivo* stimulation protocol that can be used to induce LTP via the lateral perforant path resulting in homosynaptic spine changes in the OML and heterosynaptic spine changes in the MML.

Our data provides new insights and broadens the understanding of the relation between structure and function during development of abGCs and supports the concept that abGCs need at least between 4-6 weeks for complete structural maturation and functional integration into the network until they are able to fully contribute to hippocampal forms of learning and memory. We successfully established techniques to differentially stimulate the main afferent inputs of GCs *in vivo* and to obtain highly detailed structural information by viral labeling. The applied methods were based on the processing of fixed tissue and therefore the obtained results were limited to snapshots of chosen time points after viral transduction or BrdU administration without any useful information in regard to cellular dynamics.

Considerable progress has been made in using *in vivo* two-photon time lapse imaging of hippocampal neurons with high temporal resolution (Niesner et al., 2007; Velasco and Levene, 2014; Gonçalves et al., 2016). This modern technique was recently used in combination with retroviral labeling of abGCs and revealed dynamic processes shaping dendritic trees during maturation (Gonçalves et al., 2016). Organotypic hippocampal slice cultures (OTCs) offer further possibilities to study the dynamics of neurons, dendrites and spines in the context of a preserved neuronal network (Stoppini et al., 1991) and a variety

of different conditions including pharmacological manipulations, denervation, and reinnervation by co-cultures of additional entorhinal cortices or hippocampi (Del Turco and Deller, 2007). Studies have shown a principal success in using OTCs to perform research on postnatal neurogenesis *in vitro* (Kamada et al., 2004; Raineteau et al., 2004). Another study combined retroviral *in vivo* labeling and a variation of acute hippocampal slice cultures of adult mice for confocal imaging of neurite growth and dynamics (Kleine Borgmann et al., 2013). These techniques commonly provide the methodological potential to observe dynamics of neuronal development and the requirement to answer a couple of follow-up questions: What are the dynamics of dendritic growth and spine formation? Does stabilization of dendritic compartments depend on synapse formation and are synaptically activated dendrites more stable than others? Is there a homeostatic mechanism involved that shapes structural complexity in relation to neuronal activity? Which effects can be mediated by application of extrinsic stimuli such as growth factors (e.g. BDNF), synaptic transmitters, or other pharmacological agents (e.g. Tetrodotoxin)?

Channelrhodopsins and halorhodopsins are light-gated ion channels and can be expressed in neurons to elicit light-stimulated depolarization or hyperpolarization with a high temporal resolution supporting high frequency trains. The discovery of these light-responsive proteins and consequent development of optogenetic applications had a revolutionary impact on modern neuroscience (Nagel et al., 2002; Sineshchekov et al., 2002). Optogenetics can be used to probe neuronal networks and map synaptic connections of specific subpopulations of neurons (Zhang et al., 2007, 2014; Liu et al., 2012; Tonegawa et al., 2015). Toni and colleagues (2008) adopted this system for restricted expression of Channelrhodopsin-2 in a subpopulation of abGCs. Light-evoked neurotransmitter release was sufficient to prove the existence of glutamatergic synapses from abGCs at mature stages onto target cells (e.g. mossy cells, hilar interneurons, and CA3 pyramidal cells) (Toni et al., 2008). This concept could be used in different ways. Direct transduction of abGCs could help to identify synaptic targets at various developmental stages and their impact on hippocampal information processing. A second option would be to target potential presynaptic partners and light-evoked stimulation of a specific

synaptic subpopulation could reveal its influence on structural dynamics and maturation, locally and globally.

A dual-virus approach combining monosynaptic rabies virus-mediated retrograde tracing and retroviral labeling was used by Vivar et al. (2012) and Deshpande et al. (2013) to identify pre-synaptic partners and connectivity dynamics of abGCs during their maturation. Briefly, the pseudotyped, recombinant rabies virus is retrogradelly transported and crosses just one synapse, therefore infecting only presynaptic partners of GCs. Using this method, presynaptic neurons in the entorhinal cortex and their axonal fibers to postsynaptic GCs can be visualized and analyzed. In addition to a fluorescence protein, the rabies virus can also encode channelrhodopsins, allowing for specific light-induced stimulation of retrogradely traced and monosynaptically connected axons of the MPP and/or the LPP. This highly cell-specific, and pathway-selective approach could be used to combine morphological analysis of dendrites, axons and spines with light-mediated and electrical stimulation to study spatial apposition of homo- and heterosynaptically altered spines with MPP and MPP boutons. This approach would allow the identification of stimulated axons and plastic spines, thereby characterizing heterosynaptic plasticity at the level of individual stimulated and unstimulated spines. This could clarify whether spine expansion is selectively induced at high frequency stimulated axon-spine connections and spine shrinkage at (neighboring or distant) unstimulated axon-spine connections, respectively.

The achieved experimental results could be combined with further available morphological and physiological data and finally integrated into *in silico* approaches creating a comprehensive and realistic model of the hippocampal neuronal network, including effects of abGCs on various computational processes such as pattern separation or completion. Single neurons or full networks could be simulated (Santhakumar, 2004; Schneider et al., 2012, 2014) in order to understand and to make valuable predictions about the importance of specific structural and functional properties of abGCs.

5. References

Abraham WC, Bliss TVP, Goddard G V (1985) Heterosynaptic changes accompany long-term but not short-term potentiation of the perforant path in the anaesthetized rat. J Physiol 363:335–349.

Abraham WC, Christie BR, Logan B, Lawlor P, Dragunow M (1994) Immediate early gene expression associated with the persistence of heterosynaptic long-term depression in the hippocampus. Proc Natl Acad Sci U S A 91:10049–10053.

Abraham WC, Goddard G V (1983) Asymmetric relationships between homosynaptic long-term potentiation and heterosynaptic long-term depression. Nature 305:717–719.

Abraham WC, Logan B, Wolff A, Benuskova L (2007) "Heterosynaptic" LTD in the dentate gyrus of anesthetized rat requires homosynaptic activity. J Neurophysiol 98:1048–1051.

Abraham WC, Mason-Parker SE, Bear MF, Webb S, Tate WP (2001) Heterosynaptic metaplasticity in the hippocampus in vivo: a BCM-like modifiable threshold for LTP. Proc Natl Acad Sci U S A 98:10924–10929.

Acsády L, Kamondi A, Sík A, Freund T, Buzsáki G (1998) GABAergic cells are the major postsynaptic targets of mossy fibers in the rat hippocampus. J Neurosci 18:3386–3403.

Agis-Balboa RC, Fischer A (2014) Generating new neurons to circumvent your fears: the role of IGF signaling. Cell Mol Life Sci 71:21–42.

Aimone JB, Deng W, Gage FH (2010) Adult neurogenesis: integrating theories and separating functions. Trends Cog Sci:1–13.

Aimone JB, Deng W, Gage FH (2011) Resolving new memories: a critical look at the dentate gyrus, adult neurogenesis, and pattern separation. Neuron 70:589–596.

Albensi BC, Oliver DR, Toupin J, Odero G (2007) Electrical stimulation protocols for hippocampal synaptic plasticity and neuronal hyper-excitability: Are they effective or relevant? Exp Neurol 204:1–13.

Altman J (1969) Autoradiographic and histological studies of postnatal neurogenesis. IV. Cell proliferation and migration in the anterior forebrain, with special reference to persisting neurogenesis in the olfactory bulb. J Comp Neurol 137:433–457.

Altman J, Das GD (1965) Autoradiographic and histological evidence of postnatal hippocampal neurogenesis in rats. J Comp Neurol 124:319–335.

Alvarez V a, Sabatini BL (2007) Anatomical and physiological plasticity of dendritic spines. Annu Rev Neurosci 30:79–97.

Alvarez-Buylla A, Nottebohm F (1988) Migration of young neurons in adult avian brain. Nature 335:353–354.

Alvarez-Buylla A, Theelen M, Nottebohm F (1988) Birth of projection neurons in the higher vocal center of the canary forebrain before, during, and after song learning. Proc Natl Acad Sci U S A 85:8722–8726.

Alvarez-Salvado E, Pallarés V, Moreno A, Canals S (2014) Functional MRI of long-term potentiation: imaging network plasticity. Philos Trans R Soc Lond B Biol Sci 369:20130152.

Amaral DG (1979) Synaptic extensions from the mossy fibers of the fascia dentata. Anat Embryol (Berl) 155:241–251.

Amaral DG, Ishizuka N, Claiborne B (1990) Neurons, numbers and the hippocampal network. Prog Brain Res 83:1–11.

Amaral DG, Scharfman HE, Lavenex P, Amaral D, Scharfman HE, Lavenex P (2007) The dentate gyrus: fundamental neuroanatomical organization (dentate gyrus for dummies). Prog Brain Res 153:390–394.

Ambrogini P, Lattanzi D, Ciuffoli S, Agostini D, Bertini L, Stocchi V, Santi S, Cuppini R (2004) Morpho-functional characterization of neuronal cells at different stages of maturation in granule cell layer of adult rat dentate gyrus. Brain Res 1017:21–31.

Amrein I, Isler K, Lipp H-P (2011) Comparing adult hippocampal neurogenesis in mammalian species and orders: influence of chronological age and life history stage. Eur J Neurosci 34:978–987.

Amrein I, Lipp H-P (2009) Adult hippocampal neurogenesis of mammals: evolution and life history. Biol Lett 5:141–144.

Andersen P, Morris R, Amaral D, Bliss T, O' Keefe J (2006) The Hippocampus Book (Andersen P, Morris R, Amaral D, Bliss T, O'Keefe J, eds). Oxford University Press.

Arruda-Carvalho M, Sakaguchi M, Akers KG, Josselyn SA, Frankland PW (2011) Posttraining ablation of adult-generated neurons degrades previously acquired memories. J Neurosci 31:15113–15127.

Arvidsson A, Collin T, Kirik D, Kokaia Z, Lindvall O (2002) Neuronal replacement from endogenous precursors in the adult brain after stroke. Nat Med 8:963–970.

Bading H (2013) Nuclear calcium signalling in the regulation of brain function. Nat Rev Neurosci 14:593–608.

Bailey CH, Kandel ER, Harris KM (2015) Structural Components of Synaptic Plasticity and Memory Consolidation. Cold Spring Harb Perspect Biol 7:a021758.

Baimbridge KG, Celio MR, Rogers JH (1992) Calcium-binding proteins in the nervous system. Trends Neurosci 15:303–308.

Barria A, Malinow R (2005) NMDA receptor subunit composition controls synaptic plasticity by regulating binding to CaMKII. Neuron 48:289–301.

Becker S (2005) A computational principle for hippocampal learning and neurogenesis. Hippocampus 15:722–738.

Bednarczyk MR, Hacker LC, Fortin-Nunez S, Aumont A, Bergeron R, Fernandes KJL (2011) Distinct stages of adult hippocampal neurogenesis are regulated by running and the running environment. Hippocampus 21:1334–1347.

Beining M, Jungenitz T, Radic T, Deller T, Cuntz H, Jedlicka P, Schwarzacher SW (2016) Adult-born dentate granule cells show a critical period of dendritic reorganization and are distinct from developmentally born cells. Brain Struct Funct.

Ben Abdallah NM-B, Filipkowski RK, Pruschy M, Jaholkowski P, Winkler J, Kaczmarek L, Lipp H-P (2013) Impaired long-term memory retention: common denominator for acutely or genetically reduced hippocampal neurogenesis in adult mice. Behav Brain Res 252:275–286.

References

Ben-Ari Y (2002) Excitatory actions of gaba during development: the nature of the nurture. Nat Rev Neurosci 3:728–739.

Benuskova L, Jedlicka P (2012) Computational modeling of long-term depression of synaptic weights: Insights from stdp, metaplasticity and spontaneous activity. Neural Netw World 22:161–180.

Bergami M (2015) Experience-dependent plasticity of adult-born neuron connectivity. Commun Integr Biol 8:e1038444.

Bergami M, Masserdotti G, Temprana SG, Motori E, Eriksson TM, G??bel J, Yang SM, Conzelmann KK, Schinder AF, G??tz M, Berninger B (2015) A Critical Period for Experience-Dependent Remodeling of Adult-Born Neuron Connectivity. Neuron 85:710–717.

Berggård T, Miron S, Önnerfjord P, Thulin E, Akerfeldt KS, Enghild JJ, Akke M, Linse S (2002) Calbindin D28k exhibits properties characteristic of a Ca2+ sensor. J Biol Chem 277:16662–16672.

Bergmann O, Spalding KL, Frisén J (2015) Adult Neurogenesis in Humans. Cold Spring Harb Perspect Biol 7:1–12.

Biebl M, Cooper CM, Winkler J, Kuhn HG (2000) Analysis of neurogenesis and programmed cell death reveals a self-renewing capacity in the adult rat brain. Neurosci Lett 291:17–20.

Bliss T, Lomo T (1973) Long-lasting potentiation of synaptic transmission in the dentate area of the anaesthetized rabbit following stimulation of the perforant path. J Physiol 232:331–356.

Bonfanti L, Peretto P (2011) Adult neurogenesis in mammals - a theme with many variations. Eur J Neurosci 34:930–950.

Bosch M, Hayashi Y (2012) Structural plasticity of dendritic spines. Curr Opin Neurobiol 22:383–388.

Boss BD, Turlejski K, Stanfield BB, Cowan WM (1987) On the numbers of neurons on fields CA1 and CA3 of the hippocampus of Sprague-Dawley and Wistar rats. Brain Res 406:280–287.

Bowden JB, Abraham WC, Harris KM (2012) Differential effects of strain, circadian cycle, and stimulation pattern on LTP and concurrent LTD in the dentate gyrus of freely moving rats. Hippocampus 22:1363–1370.

Bramham CR, Alme MN, Bittins M, Kuipers SD, Nair RR, Pai B, Panja D, Schubert M, Soule J, Tiron A, Wibrand K (2010) The Arc of synaptic memory. Exp Brain Res 200:125–140.

Branco T, Häusser M (2010) The single dendritic branch as a fundamental functional unit in the nervous system. Curr Opin Neurobiol 20:494–502.

Brandt MD, Jessberger S, Steiner B, Kronenberg G, Reuter K, Bick-Sander A, Behrens W Von Der, Kempermann G (2003) Transient calretinin expression defines early postmitotic step of neuronal differentiation in adult hippocampal neurogenesis of mice. Mol Cell Neurosci 24:603–613.

Braun SMG, Jessberger S (2014) Review: Adult neurogenesis and its role in neuropsychiatric disease, brain repair and normal brain function. Neuropathol Appl Neurobiol 40:3–12.

Brinton RD (2009) Estrogen-induced plasticity from cells to circuits: predictions for cognitive function. Trends Pharmacol Sci 30:212–222.

Brown JP, Couillard-Després S, Cooper-Kuhn CM, Winkler J, Aigner L, Kuhn HG, Couillard-despres S (2003) Transient expression of doublecortin during adult neurogenesis. J Comp Neurol 467:1–10.

Bruel-Jungerman E, Davis S, Rampon C, Laroche S (2006) Long-term potentiation enhances neurogenesis in the adult dentate gyrus. Eur J Neurosci 26:5888–5893.

Brun VH, Leutgeb S, Wu H-Q, Schwarcz R, Witter MP, Moser EI, Moser M-B (2008) Impaired spatial representation in CA1 after lesion of direct input from entorhinal cortex. Neuron 57:290–302.

Brunner J, Neubrandt M, Van-Weert S, Andrási T, Kleine Borgmann FB, Jessberger S, Szabadics J (2014) Adult-born granule cells mature through two functionally distinct states. Elife:e03104.

Buzsáki G, Moser EI (2013) Memory, navigation and theta rhythm in the hippocampal-entorhinal system. Nat Neurosci 16:130–138.

References

Cameron HA, Glover LR (2015) Adult Neurogenesis: Beyond Learning and Memory. Annu Rev Psychol 66:53–81.

Cameron HA, Mckay RD (2001) Adult neurogenesis produces a large pool of new granule cells in the dentate gyrus. J Comp Neurol 435:406–417.

Cameron HA, Woolley CS, McEwen BS, Gould E (1993) Differentiation of newly born neurons and glia in the dentate gyrus of the adult rat. Neuroscience 56:337–344.

Cancino GI, Yiu AP, Fatt MP, Dugani CB, Flores ER, Frankland PW, Josselyn SA, Miller FD, Kaplan DR (2013) p63 Regulates adult neural precursor and newly born neuron survival to control hippocampal-dependent Behavior. J Neurosci 33:12569–12585.

Chancey JH, Poulsen DJ, Wadiche JI, Overstreet-Wadiche L (2014) Hilar Mossy Cells Provide the First Glutamatergic Synapses to Adult-Born Dentate Granule Cells. J Neurosci 34:2349–2354.

Chao OY, Huston JP, Li JS, Wang AL, de Souza Silva MA (2016) The medial prefrontal cortex-lateral entorhinal cortex circuit is essential for episodic-like memory and associative object-recognition. Hippocampus 26:633–645.

Chen G, Zou X, Watanabe H, van Deursen JM, Shen J (2010) CREB binding protein is required for both short-term and long-term memory formation. J Neurosci 30:13066–13077.

Chen J-Y, Lonjers P, Lee C, Chistiakova M, Volgushev M, Bazhenov M (2013) Heterosynaptic Plasticity Prevents Runaway Synaptic Dynamics. J Neurosci 33:15915–15929.

Chistiakova M, Bannon NM, Bazhenov M, Volgushev M (2014) Heterosynaptic Plasticity: Multiple Mechanisms and Multiple Roles. Neurosci 20:483–498.

Chistiakova M, Bannon NM, Chen J-Y, Bazhenov M, Volgushev M (2015) Homeostatic role of heterosynaptic plasticity: models and experiments. Front Comput Neurosci 9:1–22.

Christie BR, Abraham WC (1992) NMDA-Dependent Heterosynaptic Long-Term Depression in the Dentate Gyms of Anaesthetized Rats. 6:1–6.

Chun SK, Sun W, Park J-J, Jung MW (2006) Enhanced proliferation of progenitor cells following long-term potentiation induction in the rat dentate gyrus. Neurobiol Learn Mem 86:322–329.

Claiborne BJ, Amaral DG, Cowan WM (1986) A light and electron microscopic analysis of the mossy fibers of the rat dentate gyrus. J Comp Neurol 246:435–458.

Claiborne BJ, Amaral DG, Cowan WM (1990) Quantitative, three-dimensional analysis of granule cell dendrites in the rat dentate gyrus. J Comp Neurol 302:206–219.

Clayton DF (2000) The genomic action potential. Neurobiol Learn Mem 74:185–216.

Clelland CD, Choi M, Romberg C, Clemenson GD, Fragniere A, Tyers P, Jessberger S, Saksida LM, Barker R a, Gage FH, Bussey TJ (2009) A functional role for adult hippocampal neurogenesis in spatial pattern separation. Science 325:210–213.

Clemenson GD, Lee SW, Deng W, Barrera VR, Iwamoto KS, Fanselow MS, Gage FH (2015) Enrichment rescues contextual discrimination deficit associated with immediate shock. Hippocampus 25:385–392.

Couillard-despres S, Winner B, Schaubeck S, Aigner R, Vroemen M, Weidner N, Bogdahn U, Winkler J, Kuhn H-GG, Aigner L (2005) Doublecortin expression levels in adult brain reflect neurogenesis. Eur J Neurosci 21:1–14.

Creer DJ, Romberg C, Saksida LM, van Praag H, Bussey TJ (2010) Running enhances spatial pattern separation in mice. Proc Natl Acad Sci U S A 107:2367–2372.

Cull-Candy SG, Leszkiewicz DN (2004) Role of distinct NMDA receptor subtypes at central synapses. Sci STKE 2004:re16.

Cuntz H, Borst A, Segev I (2007) Optimization principles of dendritic structure. Theor Biol Med Model 4:21.

Cuntz H, Forstner F, Borst A, Häusser M (2010) One rule to grow them all: a general theory of neuronal branching and its practical application. PLoS Comput Biol 6.

Cuntz H, Forstner F, Borst A, Häusser M (2011) The TREES toolbox--probing the basis of axonal and dendritic branching. Neuroinformatics 9:91–96.

Cuntz H, Forstner F, Haag J, Borst A (2008) The morphological identity of insect dendrites. PLoS Comput Biol 4:e1000251.

References

D'Arcangelo G (2014) Reelin in the Years: Controlling Neuronal Migration and Maturation in the Mammalian Brain. Adv Neurosci 2014:1–19.

Dayer AG, Ford AA, Cleaver KM, Yassaee M, Cameron HA (2003) Short-term and long-term survival of new neurons in the rat dentate gyrus. J Comp Neurol 572:563–572.

Del Turco D, Deller T (2007) Organotypic entorhino-hippocampal slice cultures--a tool to study the molecular and cellular regulation of axonal regeneration and collateral sprouting in vitro. Methods Mol Biol 399:55–66.

Deller T, Korte M, Chabanis S, Drakew A, Schwegler H, Stefani GG, Zuniga A, Schwarz K, Bonhoeffer T, Zeller R, Frotscher M, Mundel P (2003) Synaptopodin-deficient mice lack a spine apparatus and show deficits in synaptic plasticity. Proc Natl Acad Sci U S A 100:10494–10499.

Deng W, Aimone JB, Gage FH (2010) New neurons and new memories: how does adult hippocampal neurogenesis affect learning and memory? Nat Rev Neurosci 11:339–350.

Denny CA, Burghardt NS, Schachter DM, Hen R, Drew MR (2012) 4- to 6-week-old adult-born hippocampal neurons influence novelty-evoked exploration and contextual fear conditioning. Hippocampus 22:1188–1201.

Derdikman D, Moser EI (2010) A manifold of spatial maps in the brain. Trends Cog Sci 14:561–569.

Deshpande A, Bergami M, Ghanem A, Conzelmann K-K, Lepier A, Götz M, Berninger B (2013) Retrograde monosynaptic tracing reveals the temporal evolution of inputs onto new neurons in the adult dentate gyrus and olfactory bulb. Proc Natl Acad Sci U S A 110:E1152-1161.

Dieni C V, Chancey JH, Overstreet-Wadiche LS (2012) Dynamic functions of GABA signaling during granule cell maturation. Front Neural Circuits 6:113.

Dieni C V, Nietz AK, Panichi R, Wadiche JI, Overstreet-Wadiche L (2013) Distinct determinants of sparse activation during granule cell maturation. J Neurosci 33:19131–19142.

Dieni C V, Panichi R, Aimone JB, Kuo CT, Wadiche JI, Overstreet-Wadiche L (2016) Low excitatory innervation balances high intrinsic excitability of immature dentate neurons. Nat Commun 7:11313.

Dostes S, Dubreucq S, Ladevèze E, Marsicano G, Abrous DN, Chaouloff F, Koehl M (2016) Running per se stimulates the dendritic arbor of newborn dentate granule cells in mouse hippocampus in a duration-dependent manner. Hippocampus 26:282–288.

Doyère V, Srebro B, Laroche S (1997) Heterosynaptic LTD and Depotentiation in the Medial Perforant Path of the Dentate Gyrus in the Freely Moving Rat. J Neurophysiol 77:571–578.

Drapeau E, Mayo W, Aurousseau C, Moal L, M. P, P.v, Abrous DN (2003) Spatial memory performances of aged rats in the water maze predict levels of hippocampal neurogenesis. Proc Natl Acad Sci USA 100:14385–14390.

Drapeau E, Montaron M-F, Aguerre S, Abrous DN (2007) Learning-induced survival of new neurons depends on the cognitive status of aged rats. J Neurosci 27:6037–6044.

Drew MR, Denny CA, Hen R (2010) Arrest of adult hippocampal neurogenesis in mice impairs single- but not multiple-trial contextual fear conditioning. Behav Neurosci 124:446–454.

Duan X, Chang JH, Ge S, Faulkner RL, Kim JY, Kitabatake Y, Liu X, Yang C-H, Jordan JD, Ma DK, Liu CY, Ganesan S, Cheng H-J, Ming G, Lu B, Song H (2007) Disrupted-In-Schizophrenia 1 regulates integration of newly generated neurons in the adult brain. Cell 130:1146–1158.

Eisch AJ, Cameron H a, Encinas JM, Meltzer L a, Ming G-L, Overstreet-Wadiche LS (2008) Adult neurogenesis, mental health, and mental illness: hope or hype? J Neurosci 28:11785–11791.

Eisch AJ, Petrik D (2012) Depression and hippocampal neurogenesis: a road to remission? Science 338:72–75.

Emoto K (2011) Dendrite remodeling in development and disease. Dev Growth Differ 53:277–286.

Eriksson PS, Perfilieva E, Björk-Eriksson T, Alborn a M, Nordborg C, Peterson D a, Gage FH (1998) Neurogenesis in the adult human hippocampus. Nat Med 4:1313–1317.

Escobar M, Derrick B (2007) Long-Term Potentiation and Depression as Putative Mechanisms for Memory Formation. In: Neural Plasticity and Memory: From Genes to Brain Imaging, pp 15–46.

Espósito MS, Piatti VC, Laplagne DA, Ferrari CC, Pitossi FJ, Schinder AF (2005) Neuronal differentiation in the adult hippocampus recapitulates embryonic development. Hippocampus 25:10074–10086.

Feng G, Mellor RH, Bernstein M, Keller-Peck C, Nguyen QT, Wallace M, Nerbonne JM, Lichtman JW, Sanes JR (2000) Imaging neuronal subsets in transgenic mice expressing multiple spectral variants of GFP. Neuron 28:41–51.

Filippov V, Kronenberg G, Pivneva T, Reuter K, Steiner B, Wang L-P, Yamaguchi M, Kettenmann H, Kempermann G (2003) Subpopulation of nestin-expressing progenitor cells in the adult murine hippocampus shows electrophysiological and morphological characteristics of astrocytes. Mol Cell Neurosci 23:373–382.

Fitzsimons CP, van Hooijdonk LW a, Schouten M, Zalachoras I, Brinks V, Zheng T, Schouten TG, Saaltink DJ, Dijkmans T, Steindler D a, Verhaagen J, Verbeek FJ, Lucassen PJ, de Kloet ER, Meijer OC, Karst H, Joels M, Oitzl MS, Vreugdenhil E (2012) Knockdown of the glucocorticoid receptor alters functional integration of newborn neurons in the adult hippocampus and impairs fear-motivated behavior. Mol Psychiatry 18:993–1005.

Fitzsimons CP, van Hooijdonk LWA, Schouten M, Zalachoras I, Brinks V, Zheng T, Schouten TG, Saaltink DJ, Dijkmans T, Steindler DA, Verhaagen J, Verbeek FJ, Lucassen PJ, de Kloet ER, Meijer OC, Karst H, Joels M, Oitzl MS, Vreugdenhil E (2013) Knockdown of the glucocorticoid receptor alters functional integration of newborn neurons in the adult hippocampus and impairs fear-motivated behavior. Mol Psychiatry 18:993–1005.

Fleischmann A, Hvalby O, Jensen V, Strekalova T, Zacher C, Layer LE, Kvello A, Reschke M, Spanagel R, Sprengel R, Wagner EF, Gass P (2003) Impaired long-term memory and NR2A-type NMDA receptor-dependent synaptic plasticity in mice lacking c-Fos in the CNS. J Neurosci 23:9116–9122.

Fornasiero EF, Bonanomi D, Benfenati F, Valtorta F (2010) The role of synapsins in neuronal development. Cell Mol Life Sci 67:1383–1396.

Förster E, Zhao S, Frotscher M (2006) Laminating the hippocampus. Nat Rev Neurosci 7:259–267.

Francis F, Koulakoff A, Boucher D, Chafey P, Schaar B, Vinet M, Mcdonnell N, Reiner O, Kahn A, Mcconnell SK, Berwald-netter Y, Denoulet P, Chelly J, Cellulaire LDB, Berthelot PM (1999) Doublecortin is a developmentally regulated, microtubule-associated protein expressed in migrating and differentiating neurons. Neuron 23:247–256.

Freund TF, Buzsáki G (1998) Interneurons of the hippocampus. Hippocampus 6:347–470.

Frotscher M (2010) Role for Reelin in stabilizing cortical architecture. Trends Neurosci 33:407–414.

Frotscher M, Seress L, Schwerdtfeger WK, Buhl E (1991) The mossy cells of the fascia dentata: a comparative study of their fine structure and synaptic connections in rodents and primates. J Comp Neurol 312:145–163.

Fukazawa Y, Saitoh Y, Ozawa F, Ohta Y, Mizuno K, Inokuchi K (2003) Hippocampal LTP is accompanied by enhanced F-actin content within the dendritic spine that is essential for late LTP maintenance in vivo. Neuron 38:447–460.

Fyhn M, Hafting T, Witter MP, Moser EI, Moser M-B (2008) Grid cells in mice. Hippocampus 18:1230–1238.

Galeeva a, Treuter E, Tomarev S, Pelto-Huikko M (2007) A prospero-related homeobox gene Prox-1 is expressed during postnatal brain development as well as in the adult rodent brain. Neuroscience 146:604–616.

Ge S, Goh ELK, Sailor KA, Kitabatake Y, Ming G, Song H (2006) GABA regulates synaptic integration of newly generated neurons in the adult brain. Nature 439:589–593.

Ge S, Sailor K a, Ming G, Song H (2008) Synaptic integration and plasticity of new neurons in the adult hippocampus. J Physiol 586:3759–3765.

Ge S, Yang C-H, Hsu K-S, Ming G-L, Song H (2007) A critical period for enhanced synaptic plasticity in newly generated neurons of the adult brain. Neuron 54:559–566.

Gilbert PE, Kesner RP, Lee I (2001) Dissociating hippocampal subregions: double dissociation between dentate gyrus and CA1. Hippocampus 11:626–636.

Gleeson JG, Lin PT, Flanagan LA, Walsh CA (1999) Doublecortin Is a microtubule-associated protein and Is expressed widely by migrating neurons. Neuron 23:257–271.

Goldman S, Nottebohm F (1983) Neuronal production, migration, and differentiation in a vocal control nucleus of the adult female canary brain. Proc Natl Acad Sci U S A 80:2390–2394.

Gonçalves JT, Bloyd CW, Shtrahman M, Johnston ST, Schafer ST, Parylak SL, Tran T, Chang T, Gage FH (2016) In vivo imaging of dendritic pruning in dentate granule cells. Nat Neurosci:5–10.

Götz M, Nakafuku M, Petrik D (2016) Neurogenesis in the Developing and Adult Brain-Similarities and Key Differences. Cold Spring Harb Perspect Biol 8.

Gould E (2007) How widespread is adult neurogenesis in mammals? Nat Rev Neursci 8:481–488.

Groves JO, Leslie I, Huang G-J, McHugh SB, Taylor A, Mott R, Munafò M, Bannerman DM, Flint J (2013) Ablating adult neurogenesis in the rat has no effect on spatial processing: evidence from a novel pharmacogenetic model. PLoS Genet 9:e1003718.

Gusel'nikova V V, Korzhevskiy DE (2015) NeuN As a Neuronal Nuclear Antigen and Neuron Differentiation Marker. Acta Naturae 7:42–47.

Han Y-G, Spassky N, Romaguera-Ros M, Garcia-Verdugo J-M, Aguilar A, Schneider-Maunoury S, Alvarez-Buylla A (2008) Hedgehog signaling and primary cilia are required for the formation of adult neural stem cells. Nat Neurosci 11:277–284.

Hastings NB, Gould E (1999) Rapid extension of axons into the CA3 region by adult-generated granule cells. J Comp Neurol 413:146–154.

Hunsaker MR, Mooy GG, Swift JS, Kesner RP (2007) Dissociations of the medial and lateral perforant path projections into dorsal DG, CA3, and CA1 for spatial and nonspatial (visual object) information processing. Behav Neurosci 121:742–750.

Igarashi KM (2016) The entorhinal map of space. Brain Res 1637:177–187.

Imielski Y, Schwamborn JC, Lüningschrör P, Heimann P, Holzberg M, Werner H, Leske O, Püschel AW, Memet S, Heumann R, Israel A, Kaltschmidt C, Kaltschmidt B (2012) Regrowing the adult brain: NF-κB controls functional circuit formation and tissue homeostasis in the dentate gyrus. PLoS One 7:e30838.

Iwano T, Masuda A, Kiyonari H, Enomoto H, Matsuzaki F (2012) Prox1 postmitotically defines dentate gyrus cells by specifying granule cell identity over CA3 pyramidal cell fate in the hippocampus. Development 139:3051–3062.

Jagasia R, Steib K, Englberger E, Herold S, Faus-Kessler T, Saxe M, Gage FH, Song H, Lie DC (2009) GABA-cAMP Response Element-Binding Protein Signaling Regulates Maturation and Survival of Newly Generated Neurons in the Adult Hippocampus. J Neurosci 29:7966–7977.

Jedlicka P, Benuskova L, Abraham WC (2015) A Voltage-Based STDP Rule Combined with Fast BCM-Like Metaplasticity Accounts for LTP and Concurrent "Heterosynaptic" LTD in the Dentate Gyrus In Vivo. PLOS Comput Biol 11:e1004588.

Jedlicka P, Schwarzacher SW, Winkels R, Kienzler F, Frotscher M, Bramham CR, Schultz C, Bas Orth C, Deller T (2009) Impairment of in vivo theta-burst long-term potentiation and network excitability in the dentate gyrus of synaptopodin-deficient mice lacking the spine apparatus and the cisternal organelle. Hippocampus 19:130–140.

Jessberger S, Parent JM (2015) Epilepsy and Adult Neurogenesis. Cold Spring Harb Perspect Biol 7.

Jessberger S, Zhao C, Toni N, Clemenson GD, Li Y, Gage FH (2007) Seizure-associated, aberrant neurogenesis in adult rats characterized with retrovirus-mediated cell labeling. J Neurosci 27:9400–9407.

Jin DH, Jung YW, Ham SH, Ko BH, Moon IS (1997) Developmental expression, subcellular localization, and tyrosine phosphorylation of NR2A and NR2B in the rat brain. Mol Cells 7:64–71.

Jinde S, Zsiros V, Nakazawa K (2013) Hilar mossy cell circuitry controlling dentate granule cell excitability. Front Neural Circuits 7:14.

Johnston ST, Shtrahman M, Parylak S, Gonçalves JT, Gage FH (2016) Paradox of pattern separation and adult neurogenesis: A dual role for new neurons balancing memory resolution and robustness. Neurobiol Learn Mem 129:60–68.

Jones MW, Errington ML, French PJ, Fine A, Bliss T V, Garel S, Charnay P, Bozon B, Laroche S, Davis S (2001) A requirement for the immediate early gene Zif268 in the expression of late LTP and long-term memories. Nat Neurosci 4:289–296.

Jungenitz T, Radic T, Jedlicka P, Schwarzacher SW (2014) High-Frequency Stimulation Induces Gradual Immediate Early Gene Expression in Maturing Adult-Generated Hippocampal Granule Cells. Cereb Cortex 24:1845–1857.

Jungenitz T, Bening M, Radic T, Deller T, Cuntz H, Jedlicka P, Schwarzacher SW (submitted manuscript) Structural homo- and heterosynaptic plasticity in adult newborn rat hippocampal granule cells.

Kamada M, Li R-Y, Hashimoto M, Kakuda M, Okada H, Koyanagi Y, Ishizuka T, Yawo H (2004) Intrinsic and spontaneous neurogenesis in the postnatal slice culture of rat hippocampus. Eur J Neurosci 20:2499–2508.

Karalay O, Doberauer K, Vadodaria KC, Knobloch M, Berti L, Miquelajauregui A, Schwark M, Jagasia R, Taketo MM, Tarabykin V, Lie DC, Jessberger S (2011) Prospero-related homeobox 1 gene (Prox1) is regulated by canonical Wnt signaling and has a stage-specific role in adult hippocampal neurogenesis. Proc Natl Acad Sci U S A 108:5807–5812.

Kee N, Teixeira CM, Wang AH, Frankland PW (2007) Preferential incorporation of adult-generated granule cells into spatial memory networks in the dentate gyrus. Nat Neurosci 10:355–362.

Kempermann G, Gast D, Kronenberg G, Yamaguchi M, Gage FH (2003) Early determination and long-term persistence of adult-generated new neurons in the hippocampus of mice. Development 130:391–399.

Kempermann G, Jessberger S, Steiner B (2004) Milestones of neuronal development in the adult hippocampus. Trends Neurosci 27:447–452.

Kempermann G, Song H, Gage FH (2015) Neurogenesis in the Adult Hippocampus. Cold Spring Harb Perspect Biol 7:a018812.

Kesner RP, Lee I, Gilbert P (2004) A behavioral assessment of hippocampal function based on a subregional analysis. Rev Neurosci 15:333–351.

Kesner RP, Rolls ET (2015) A computational theory of hippocampal function, and tests of the theory: New developments. Neurosci Biobehav Rev 48:92–147.

Kheirbek M a, Tannenholz L, Hen R (2012) NR2B-Dependent Plasticity of Adult-Born Granule Cells is Necessary for Context Discrimination. J Neurosci 32:8696–8702.

Kim CH, Lisman JE (1999) A role of actin filament in synaptic transmission and long-term potentiation. J Neurosci 19:4314–4324.

Kim MJ, Dunah AW, Wang YT, Sheng M (2005) Differential roles of NR2A- and NR2B-containing NMDA receptors in Ras-ERK signaling and AMPA receptor trafficking. Neuron 46:745–760.

Kleine Borgmann FB, Bracko O, Jessberger S (2013) Imaging neurite development of adult-born granule cells. Development 140:2823–2827.

Klempin F, Kempermann G (2007) Adult hippocampal neurogenesis and aging. Clin Neurosci 257:271–280.

Kronenberg G, Reuter K, Steiner B, Brandt MD, Jessberger S, Yamaguchi M, Kempermann G (2003) Subpopulations of proliferating cells of the adult hippocampus respond differently to physiologic neurogenic stimuli. J Comp Neurol 467:455–463.

Kuhn HG, Biebl M, Wilhelm D, Li M, Friedlander RM (2005) Increased generation of granule cells in adult Bcl-2- overexpressing mice : a role for cell death during continued hippocampal neurogenesis. Animals 22:1907–1915.

Langston RF, Ainge JA, Couey JJ, Canto CB, Bjerknes TL, Witter MP, Moser EI, Moser M-B (2010) Development of the spatial representation system in the rat. Science 328:1576–1580.

Laplagne DA, Espósito MS, Piatti VC, Morgenstern N a, Zhao C, van Praag H, Gage FH, Schinder AF (2006) Functional convergence of neurons generated in the developing and adult hippocampus. Macklis J, ed. PLoS Biol 4:e409.

Lavado A, Lagutin O V., Chow LML, Baker SJ, Oliver G (2010) Prox1 Is required for granule cell maturation and intermediate progenitor maintenance during brain neurogenesis. PLoS Biol 8:43–44.

Lavado A, Oliver G (2007) Prox1 expression patterns in the developing and adult murine brain. Dev Dyn 236:518–524.

Lee SH, Ho W-K, Lee S-H (2009) Characterization of somatic Ca2+ clearance mechanisms in young and mature hippocampal granule cells. Cell Calcium 45:465–473.

Lefebvre JL, Sanes JR, Kay JN (2015) Development of Dendritic Form and Function. Annu Rev Cell Dev Biol 31:741–777.

Lemaire V, Tronel S, Montaron M-F, Fabre A, Dugast E, Abrous DN (2012) Long-Lasting Plasticity of Hippocampal Adult-Born Neurons. J Neurosci 32:3101–3108.

Leutgeb S, Leutgeb JK (2007) Pattern separation, pattern completion, and new neuronal codes within a continuous CA3 map. Learn Mem 14:745–757.

Li Y, Luikart BW, Birnbaum S, Chen J, Kwon C, Kernie SG, Bassel-duby R, Parada LF (2008) TrkB Regulates Hippocampal Neurogenesis and Governs Sensitivity to Antidepressive Treatment. Neuron 59:399–412.

Lie D, Colamarino SA, Song H, Désiré L, Mira H, Consiglio A, Lein ES, Jessberger S, Lansford H, Dearie AR, Gage FH (2005) Wnt signalling regulates adult hippocampal neurogenesis. Nature 437:1370–1375.

Lind D, Franken S, Kappler J, Jankowski J, Schilling K (2005) Characterization of the neuronal marker NeuN as a multiply phosphorylated antigen with discrete subcellular localization. J Neurosci Res 79:295–302.

Lipp H-P, Bonfanti L (2016) Adult Neurogenesis in Mammals: Variations and Confusions. Brain Behav Evol 87:205–221.

Liu L, Wong TP, Pozza MF, Lingenhoehl K, Wang Y, Sheng M, Auberson YP, Wang YT (2004) Role of NMDA receptor subtypes in governing the direction of hippocampal synaptic plasticity. Science 304:1021–1024.

Liu X, Ramirez S, Pang PT, Puryear CB, Govindarajan A, Deisseroth K, Tonegawa S (2012) Optogenetic stimulation of a hippocampal engram activates fear memory recall. Nature 484:381–385.

Liu X, Ramirez S, Tonegawa S (2014) Inception of a false memory by optogenetic manipulation of a hippocampal memory engram. Philos Trans R Soc Lond B Biol Sci 369:20130142.

Loebrich S, Nedivi E (2009) The Function of Activity-Regulated Genes in the Nervous System. Physiol Rev 89:1079–1103.

Lomo T (1971) Potentiation of monosynaptic EPSPs in the perforant path-dentate granule cell synapse. Exp brain Res 12:46–63.

Lomo T (2003) The discovery of long-term potentiation. Philos Trans R Soc London, Ser B 358:617–620.

Loy R, Lynch G, Cotman CW (1977) Development of afferent lamination in the fascia dentata of the rat. Brain Res 121:229–243.

Lucassen PJ, Oomen CA, Naninck EFG, Fitzsimons CP, van Dam A-M, Czeh B, Korosi A (2015) Regulation of Adult Neurogenesis and Plasticity by (Early) Stress, Glucocorticoids, and Inflammation. Cold Spring Harb Perspect Biol 7.

Mainen ZF, Sejnowski TJ (1996) Influence of dendritic structure on firing pattern in model neocortical neurons. Nature 382:363–366.

Malberg JE, Eisch a J, Nestler EJ, Duman RS (2000) Chronic antidepressant treatment increases neurogenesis in adult rat hippocampus. J Neurosci 20:9104–9110.

Mandyam CD, Harburg GC, Eisch AJ (2007) Determination of key aspects of precursor cell proliferation, cell cycle length and kinetics in the adult mouse subgranular zone. Neuroscience 146:108–122.

Marín-Burgin A, Schinder AF (2012) Requirement of adult-born neurons for hippocampus-dependent learning. Behav Brain Res 227:391–399.

Marrone DF, Schaner MJ, McNaughton BL, Worley PF, Barnes CA (2008) Immediate-early gene expression at rest recapitulates recent experience. J Neurosci 28:1030–1033.

Martínez-Canabal A (2015) Rewiring, forgetting and learning. Commentary: A critical period for experience-dependent remodeling of adult-born neuron connectivity. Front Neurosci 9:266–270.

Mathews EA, Morgenstern NA, Piatti VC, Zhao C, Jessberger S, Schinder AF, Gage FH (2010) A distinctive layering pattern of mouse dentate granule cells is generated by developmental and adult neurogenesis. J Comp Neurol 518:4479–4490.

Matsuzaki M, Ellis-Davies GC, Nemoto T, Miyashita Y, Iino M, Kasai H (2001) Dendritic spine geometry is critical for AMPA receptor expression in hippocampal CA1 pyramidal neurons. Nat Neurosci 4:1086–1092.

Matsuzaki M, Honkura N, Ellis-Davies GCR, Kasai H (2004) Structural basis of long-term potentiation in single dendritic spines. Nature 429:761–766.

Merz K, Lie DC (2013) Evidence that Doublecortin Is Dispensable for the Development of Adult Born Neurons in Mice. PLoS One 8.

Miller BR, Hen R (2015) The current state of the neurogenic theory of depression and anxiety. Curr Opin Neurobiol 30:51–58.

Ming G-L, Song H (2011) Adult neurogenesis in the mammalian brain: significant answers and significant questions. Neuron 70:687–702.

Mirescu C, Gould E (2006) Stress and adult neurogenesis. Hippocampus 16:233–238.

Miyazaki J, Takaki S, Araki K, Tashiro F, Tominaga A, Takatsu K, Yamamura K (1989) Expression vector system based on the chicken beta-actin promoter directs efficient production of interleukin-5. Gene 79:269–277.

Mody I, Köhr G, Otis TS, Staley KJ (1992) The electrophysiology of dentate gyrus granule cells in whole-cell recordings. Epilepsy Res Suppl 7:159–168.

Mongiat LA, Espósito MS, Lombardi G, Schinder AF (2009) Reliable activation of immature neurons in the adult hippocampus. PLoS One 4:e5320.

Moore KA, Lemischka IR (2006) Stem cells and their niches. Science 311:1880–1885.

Moser EI, Kropff E, Moser M-B (2008) Place cells, grid cells, and the brain's spatial representation system. Annu Rev Neurosci 31:69–89.

Mouret A, Gheusi G, Gabellec M-M, de Chaumont F, Olivo-Marin J-C, Lledo P-M (2008) Learning and survival of newly generated neurons: when time matters. J Neurosci 28:11511–11516.

Mu Y, Zhao C, Toni N, Yao J, Gage FH (2015) Distinct roles of NMDA receptors at different stages of granule cell development in the adult brain. Elife 4:1–18.

Mulders WHAM, West MJ, Slomianka L (1997) Neuron numbers in the presubiculum, parasubiculum, and entorhinal area of the rat. J Comp Neurol 385:83–94.

Muramatsu R, Ikegaya Y, Matsuki N, Koyama R (2007) Neonatally born granule cells numerically dominate adult mice dentate gyrus. Neuroscience 148:593–598.

Nacher J, Varea E, Gómez-Climent MA, Miguel Blasco-Ibáñez J, Castillo-Gómez E, Crespo C, Martínez-Guijarro FJ, McEwen BS (2007) N-methyl-d-aspartate receptor expression during adult neurogenesis in the rat dentate gyrus. Neuroscience 144:855–864.

Nagel G, Ollig D, Fuhrmann M, Kateriya S, Musti AM, Bamberg E, Hegemann P (2002) Channelrhodopsin-1: a light-gated proton channel in green algae. Science 296:2395–2398.

Nakashiba T, Cushman JD, Pelkey K a, Renaudineau S, Buhl DL, McHugh TJ, Barrera VR, Chittajallu R, Iwamoto KS, McBain CJ, Fanselow MS, Tonegawa S (2012) Young dentate granule cells mediate pattern separation, whereas old granule cells facilitate pattern completion. Cell 149:188–201.

Nanry KP, Mundy WR, Tilson HA (1989) Colchicine-induced alterations of reference memory in rats: role of spatial versus non-spatial task components. Behav Brain Res 35:45–53.

Neunuebel JP, Knierim JJ (2014) CA3 Retrieves Coherent Representations from Degraded Input: Direct Evidence for CA3 Pattern Completion and Dentate Gyrus Pattern Separation. Neuron 81:416–427.

Nicola Z, Fabel K, Kempermann G (2015) Development of the adult neurogenic niche in the hippocampus of mice. Front Neuroanat 9:53.

Niesner R, Andresen V, Neumann J, Spiecker H, Gunzer M (2007) The power of single and multibeam two-photon microscopy for high-resolution and high-speed deep tissue and intravital imaging. Biophys J 93:2519–2529.

Niwa H, Yamamura K, Miyazaki J (1991) Efficient selection for high-expression transfectants with a novel eukaryotic vector. Gene 108:193–199.

Norkett R, Modi S, Birsa N, Atkin TA, Ivankovic D, Pathania M, Trossbach S V, Korth C, Hirst WD, Kittler JT (2016) DISC1-dependent Regulation of Mitochondrial Dynamics Controls the Morphogenesis of Complex Neuronal Dendrites. J Biol Chem 291:613–629.

Oh WC, Parajuli LK, Zito K (2015) Heterosynaptic Structural Plasticity on Local Dendritic Segments of Hippocampal CA1 Neurons. Cell Rep 10:162–169.

Ohkawa N, Saitoh Y, Tokunaga E, Nihonmatsu I, Ozawa F, Murayama A, Shibata F, Kitamura T, Inokuchi K (2012) Spine Formation Pattern of Adult-Born Neurons Is Differentially Modulated by the Induction Timing and Location of Hippocampal Plasticity. PLoS One 7:e45270.

Okamoto K-I, Nagai T, Miyawaki A, Hayashi Y (2004) Rapid and persistent modulation of actin dynamics regulates postsynaptic reorganization underlying bidirectional plasticity. Nat Neurosci 7:1104–1112.

Olson AK, Eadie BD, Ernst C, Christie BR (2006) Environmental Enrichment and Voluntary Exercise Massively Increase Neurogenesis in the Adult Hippocampus via Dissociable Pathways. Hippocampus 16:250–260.

Owens DF, Boyce LH, Davis MB, Kriegstein AR (1996) Excitatory GABA responses in embryonic and neonatal cortical slices demonstrated by gramicidin perforated-patch recordings and calcium imaging. J Neurosci 16:6414–6423.

Paleja M, Girard TA, Herdman KA, Christensen BK (2014) Two distinct neural networks functionally connected to the human hippocampus during pattern separation tasks. Brain Cogn 92:101–111.

Pardi MB, Ogando MB, Schinder AF, Marin-Burgin A (2015) Differential inhibition onto developing and mature granule cells generates high-frequency filters with variable gain. Elife 4:1–17.

Paton JA, Nottebohm FN (1984) Neurons generated in the adult brain are recruited into functional circuits. Science 225:1046–1048.

Piatti VC, Ewell LA, Leutgeb JK (2013) Neurogenesis in the dentate gyrus: carrying the message or dictating the tone. Front Neurosci 7:1–11.

Pierfelice T, Alberi L, Gaiano N (2011) Notch in the vertebrate nervous system: an old dog with new tricks. Neuron 69:840–855.

Popov VI, Davies H a., Rogachevsky V V., Patrushev I V., Errington ML, Gabbott PL a, Bliss TVP, Stewart MG (2004) Remodelling of synaptic morphology but unchanged synaptic density during late phase long-term potentiation (LTP): A serial section electron micrograph study in the dentate gyrus in the anaesthetised rat. Neuroscience 128:251–262.

Radic T, Al-Qaisi O, Jungenitz T, Beining M, Schwarzacher SW (2015) Differential structural development of adult-born septal hippocampal granule cells in the Thy1-GFP mouse, nuclear size as a new index of maturation. PLoS One 10:e0135493.

Raineteau O, Rietschin L, Gradwohl G, Guillemot F, Gähwiler BH (2004) Neurogenesis in hippocampal slice cultures. Mol Cell Neurosci 26:241–250.

Rall W, Rinzel J (1973) Branch input resistance and steady attenuation for input to one branch of a dendritic neuron model. Biophys J 13:648–687.

Ramirez S, Liu X, Lin P-A, Suh J, Pignatelli M, Redondo RL, Ryan TJ, Tonegawa S (2013) Creating a false memory in the hippocampus. Science 341:387–391.

Ramírez-Rodríguez G, Babu H, Klempin F, Krylyshkina O, Baekelandt V, Gijsbers R, Debyser Z, Overall RW, Nicola Z, Fabel K, Kempermann G (2013) The α crystallin domain of small heat shock protein b8 (Hspb8) acts as survival and differentiation factor in adult hippocampal neurogenesis. J Neurosci 33:5785–5796.

Restivo L, Niibori Y, Mercaldo V, Josselyn SA, Frankland PW (2015) Development of Adult-Generated Cell Connectivity with Excitatory and Inhibitory Cell Populations in the Hippocampus. J Neurosci 35:10600–10612.

Reymann KG, Frey JU (2007) The late maintenance of hippocampal LTP: requirements, phases, "synaptic tagging", "late-associativity" and implications. Neuropharmacology 52:24–40.

Rihn LL, Claiborne BJ (1990) Dendritic growth and regression in rat dentate granule cells during late postnatal development. Dev Brain Res 54:115–124.

Rochefort NL, Konnerth A (2012) Dendritic spines: from structure to in vivo function. EMBO Rep 13:699–708.

Rolls ET (2010) A computational theory of episodic memory formation in the hippocampus. Behav Brain Res 215:180–196.

Rolls ET (2013) The mechanisms for pattern completion and pattern separation in the hippocampus. Front Syst Neurosci 7:74.

Rolls ET, Kesner RP (2006) A computational theory of hippocampal function, and empirical tests of the theory. Prog Neurobiol 79:1–48.

Sahay A, Scobie KN, Hill AS, O'Carroll CM, Kheirbek MA, Burghardt NS, Fenton AA, Dranovsky A, Hen R (2011a) Increasing adult hippocampal neurogenesis is sufficient to improve pattern separation. Nature 472:466–470.

Sahay A, Wilson DA, Hen R (2011b) Pattern separation: a common function for new neurons in hippocampus and olfactory bulb. Neuron 70:582–588.

Santhakumar V (2004) Role of Mossy Fiber Sprouting and Mossy Cell Loss in Hyperexcitability: A Network Model of the Dentate Gyrus Incorporating Cell Types and Axonal Topography. J Neurophysiol 93:437–453.

Saxe MD, Battaglia F, Wang JW, Malleret G, David DJ, Monckton JE, Garcia AD, Sofroniew M V, Kandel ER, Santarelli L (2006) Ablation of hippocampal neurogenesis impairs contextual fear conditioning and synaptic plasticity in the dentate gyrus. P Natl Acad Sci USA 103:17501–17506.

Scharfman HE, Myers CE (2012) Hilar mossy cells of the dentate gyrus: a historical perspective. Front Neural Circuits 6:106.

Schmidt B, Marrone DF, Markus EJ (2012) Disambiguating the similar: the dentate gyrus and pattern separation. Behav Brain Res 226:56–65.

Schmidt-Hieber C, Jonas P, Bischofberger J (2004) Enhanced synaptic plasticity in newly generated granule cells of the adult hippocampus. Nature 429:184–187.

Schneider CJ, Bezaire M, Soltesz I (2012) Toward a full-scale computational model of the rat dentate gyrus. Front Neural Circuits 6:83.

Schneider CJ, Cuntz H, Soltesz I (2014) Linking Macroscopic with Microscopic Neuroanatomy Using Synthetic Neuronal Populations. PLoS Comput Biol 10:e1003921.

Seri B, Garcia-Verdugo JM, McEwen BS, Alvarez-Buylla A (2001) Astrocytes give rise to new neurons in the adult mammalian hippocampus. J Neurosci 21:7153–7160.

Shapiro LA, Upadhyaya P, Ribak CE (2007) Spatiotemporal profile of dendritic outgrowth from newly born granule cells in the adult rat dentate gyrus. Brain Res 1149:30–37.

Shors TJ, Miesegaes G, Beylin A, Zhao M, Rydel T, Gould E (2001) Neurogenesis in the adult is involved in the formation of trace memories. Nature 410:372–376.

Shors TJ, Townsend DA, Zhao M, Kozorovitskiy Y, Gould E (2002) Neurogenesis may relate to some but not all types of hippocampal-dependent learning. Hippocampus 584:578–584.

Shruster A, Melamed E, Offen D (2010) Neurogenesis in the aged and neurodegenerative brain. Apoptosis 15:1415–1421.

Sidiropoulou K, Pissadaki EK, Poirazi P (2006) Inside the brain of a neuron. EMBO Rep 7:886–892.

Sineshchekov OA, Jung K-H, Spudich JL (2002) Two rhodopsins mediate phototaxis to low- and high-intensity light in Chlamydomonas reinhardtii. Proc Natl Acad Sci U S A 99:8689–8694.

Šišková Z, Justus D, Kaneko H, Friedrichs D, Henneberg N, Beutel T, Pitsch J, Schoch S, Becker A, von der Kammer H, Remy S (2014) Dendritic structural degeneration is functionally linked to cellular hyperexcitability in a mouse model of Alzheimer's disease. Neuron 84:1023–1033.

Snyder JS, Choe JS, Clifford MA, Jeurling SI, Hurley P, Brown A, Kamhi JF, Cameron HA (2009) Adult-Born Hippocampal Neurons Are More Numerous, Faster Maturing, and More Involved in Behavior in Rats than in Mice. J Neurosci 29:14484–14495.

Snyder JS, Hong NS, McDonald RJ, Wojtowicz JM (2005) A role for adult neurogenesis in spatial long-term memory. Neuroscience 130:843–852.

Song H, Stevens CF, Gage FH (2002) Astroglia induce neurogenesis from adult neural stem cells. Nature 417:39–44.

Sorra KE, Harris KM (2000) Overview on the structure, composition, function, development, and plasticity of hippocampal dendritic spines. Hippocampus 10:501–511.

Spalding KL, Bergmann O, Alkass K, Bernard S, Salehpour M, Huttner HB, Boström E, Westerlund I, Vial C, Buchholz B a, Possnert G, Mash DC, Druid H, Frisén J (2013) Dynamics of hippocampal neurogenesis in adult humans. Cell 153:1219–1227.

Spruston N, Johnston D (1992) Perforated patch-clamp analysis of the passive membrane properties of three classes of hippocampal neurons. J Neurophysiol 67:508–529.

Staley KJ, Otis TS, Mody I (1992) Membrane properties of dentate gyrus granule cells: comparison of sharp microelectrode and whole-cell recordings. J Neurophysiol 67:1346–1358.

Steward O, Wallace CS, Lyford GL, Worley PF (1998) Synaptic activation causes the mRNA for the IEG Arc to localize selectively near activated postsynaptic sites on dendrites. Neuron 21:741–751.

Stocca G, Schmidt-Hieber C, Bischofberger J (2008) Differential dendritic Ca2+ signalling in young and mature hippocampal granule cells. J Physiol 586:3795–3811.

Stone SSD, Teixeira CM, Zaslavsky K, Wheeler AL, Martinez-Canabal A, Wang AH, Sakaguchi M, Lozano AM, Frankland PW (2011) Functional convergence of developmentally and adult-generated granule cells in dentate gyrus circuits supporting hippocampus-dependent memory. Hippocampus 21:1348–1362.

Stoppini L, Buchs PA, Muller D (1991) A simple method for organotypic cultures of nervous tissue. J Neurosci Methods 37:173–182.

Sun GJ, Sailor K a, Mahmood Q a, Chavali N, Christian KM, Song H, Ming G (2013) Seamless reconstruction of intact adult-born neurons by serial end-block imaging reveals complex axonal guidance and development in the adult hippocampus. J Neurosci 33:11400–11411.

Sun W, Winseck A, Vinsant S, Park O, Kim H, Oppenheim RW (2004) Programmed cell death of adult-generated hippocampal neurons is mediated by the proapoptotic gene Bax. J Neurosci 24:11205–11213.

Sutherland RJ, Whishaw IQ, Kolb B (1983) A behavioural analysis of spatial localization following electrolytic, kainate- or colchicine-induced damage to the hippocampal formation in the rat. Behav Brain Res 7:133–153.

Tashiro A, Makino H, Gage FH (2007) Experience-specific functional modification of the dentate gyrus through adult neurogenesis: a critical period during an immature stage. J Neurosci 27:3252–3259.

Tashiro A, Sandler VM, Toni N, Zhao C, Gage FH (2006) NMDA-receptor-mediated, cell-specific integration of new neurons in adult dentate gyrus. Nature 442:929–933.

Taupin P (2006) BrdU immunohistochemistry for studying adult neurogenesis: Paradigms, pitfalls, limitations, and validation. Brain Res Rev 53:198–214.

Temprana SG, Mongiat L a, Yang SM, Trinchero MF, Alvarez DD, Kropff E, Giacomini D, Beltramone N, Lanuza GM, Schinder AF (2015) Delayed Coupling to Feedback Inhibition during a Critical Period for the Integration of Adult-Born Granule Cells. Neuron 85:116–130.

Thored P, Wood J, Arvidsson A, Cammenga J, Kokaia Z, Lindvall O (2007) Long-term neuroblast migration along blood vessels in an area with transient angiogenesis and increased vascularization after stroke. Stroke 38:3032–3039.

Tonegawa S, Pignatelli M, Roy DS, Ryan TJ (2015) Memory engram storage and retrieval. Curr Opin Neurobiol 35:101–109.

Toni N, Laplagne DA, Zhao C, Lombardi G, Ribak CE, Gage FH, Schinder AF (2008) Neurons born in the adult dentate gyrus form functional synapses with target cells. Nat Neurosci 11:901–907.

Toni N, Teng EM, Bushong EA, Aimone JB, Zhao C, Consiglio A, van Praag H, Martone ME, Ellisman MH, Gage FH (2007) Synapse formation on neurons born in the adult hippocampus. Nat Neurosci 10:727–734.

Tozuka Y, Fukuda S, Namba T, Seki T, Hisatsune T (2005) GABAergic Excitation Promotes Neuronal Differentiation in Adult Hippocampal Progenitor Cells. Neuron 47:803–815.

Tronel S, Belnoue L, Grosjean N, Revest J-M, Piazza P-V, Koehl M, Abrous DN (2012) Adult-born neurons are necessary for extended contextual discrimination. Hippocampus 22:292–298.

Tronel S, Lemaire V, Charrier V, Montaron MF, Abrous DN (2015) Influence of ontogenetic age on the role of dentate granule neurons. Brain Struct Funct 220:645–661.

Valtorta F, Pozzi D, Benfenati F, Fornasiero EF (2011) The synapsins: Multitask modulators of neuronal development. Semin Cell Dev Biol 22:378–386.

van Dijk RM, Huang S-H, Slomianka L, Amrein I (2016) Taxonomic Separation of Hippocampal Networks: Principal Cell Populations and Adult Neurogenesis. Front Neuroanat 10.

van Praag H, Schinder AAF, Christie BR, Toni N, Palmer TD, Gage FH (2002) Functional neurogenesis in the adult hippocampus. Nature 415:1030–1034.

Velasco MGM, Levene MJ (2014) In vivo two-photon microscopy of the hippocampus using glass plugs. Biomed Opt Express 5:1700–1708.

Vivar C, Peterson BD, van Praag H (2016) Running rewires the neuronal network of adult-born dentate granule cells. Neuroimage 131:29–41.

Vivar C, Potter MC, Choi J, Lee J-Y, Stringer TP, Callaway EM, Gage FH, Suh H, van Praag H (2012) Monosynaptic inputs to new neurons in the dentate gyrus. Nat Commun 3:1107.

Vuksic M, Del Turco D, Bas Orth C, Burbach GJ, Feng G, Müller CM, Schwarzacher SW, Deller T (2008) 3D-reconstruction and functional properties of GFP-positive and GFP-negative granule cells in the fascia dentata of the Thy1-GFP mouse. Hippocampus 18:364–375.

Walsh TJ, Schulz DW, Tilson HA, Schmechel DE (1986) Colchicine-induced granule cell loss in rat hippocampus: selective behavioral and histological alterations. Brain Res 398:23–36.

Walter C, Murphy BL, Pun RYK, Spieles-Engemann AL, Danzer SC (2007) Pilocarpine-Induced Seizures Cause Selective Time- Dependent Changes to Adult-Generated Hippocampal Dentate Granule Cells. Microscopy 27:7541–7552.

Wang CC, Held RG, Chang SC, Yang L, Delpire E, Ghosh A, Hall BJ (2011) A critical role for gluN2B-containing NMDA receptors in cortical development and function. Neuron 72:789–805.

Wang DD, Kriegstein AR (2009) Defining the role of GABA in cortical development. J Physiol 587:1873–1879.

Wang L, Kempermann G, Kettenmann H (2005) A subpopulation of precursor cells in the mouse dentate gyrus receives synaptic GABAergic input. Mol Cell Neurosci 29:181–189.

Wenzel A, Fritschy JM, Mohler H, Benke D (1997) NMDA receptor heterogeneity during postnatal development of the rat brain: differential expression of the NR2A, NR2B, and NR2C subunit proteins. J Neurochem 68:469–478.

West MJ, Slomianka L, Gundersen HJG (1991) Unbiased Stereological Estimation of the Total Number of Neurons in the Subdivisions of the Rat Hippocampus Using the Optical Fractionator. Anat Rec 231:482–497.

Wilbrecht L, Nottebohm F (2004) Age and Experience Affect the Recruitment of New Neurons to the Song System of Zebra Finches during the Sensitive Period for Song Learning. Ann NY Acad Sci 1021:404–409.

Wilson IA, Gallagher M, Eichenbaum H, Tanila H (2006) Neurocognitive aging: prior memories hinder new hippocampal encoding. Trends Neurosci 29:662–670.

Wilson RC (1981) Changes in translation of synaptic excitation to dentate granule cell discharge accompanying long-term potentiation. I. Differences between normal and reinnervated dentate gyrus. J Neurophysiol 46:324–338.

Wilson RC, Levy WB, Steward O (1979) Functional Effects of Lesio-Induced Plasticity: Long Term Potentiation in Normal and Lesion-Induced Temporodentate Connections. Brain Res 176:65–78.

Wilson RC, Levy WB, Steward O (1981) Changes in translation of synaptic excitation to dentate granule cell discharge accompanying long-term potentiation. II. An evaluation of mechanisms utilizing dentate gyrus dually innervated by surviving ipsilateral and sprouted crossed temporodentate inp. J Neurophysiol 46:339–355.

Winocur G, Wojtowicz JM, Sekeres M, Snyder JS, Wang S (2006) Inhibition of Neurogenesis Interferes With Hippocampus-Dependent Memory Function. Neuroscientist 304:296–304.

Wiskott L, Rasch MJ, Kempermann G (2006) A Functional Hypothesis for Adult Hippocampal Neurogenesis: Avoidance of Catastrophic Interference in the Dentate Gyrus. Hippocampus 343:329–343.

Wojtowicz JM, Askew ML, Winocur G (2008) The effects of running and of inhibiting adult neurogenesis on learning and memory in rats. Eur J Neurosci 27:1494–1502.

Wosiski-Kuhn M, Stranahan AM (2012) Transient increases in dendritic spine density contribute to dentate gyrus long-term potentiation. Synapse 66:661–664.

Yassa MA, Stark CEL (2011) Pattern separation in the hippocampus. Trends Neurosci 34:515–525.

Yoganarasimha D, Rao G, Knierim JJ (2011) Lateral entorhinal neurons are not spatially selective in cue-rich environments. Hippocampus 21:1363–1374.

Zhang F, Aravanis AM, Adamantidis A, de Lecea L, Deisseroth K (2007) Circuit-breakers: optical technologies for probing neural signals and systems. Nat Rev Neurosci 8:577–581.

Zhang S-J, Ye J, Couey JJ, Witter M, Moser EI, Moser M-B (2014) Functional connectivity of the entorhinal-hippocampal space circuit. Philos Trans R Soc Lond B Biol Sci 369:20120516.

Zhao C, Deng W, Gage FH (2008) Mechanisms and functional implications of adult neurogenesis. Cell 132:645–660.

Zhao C, Teng EM, Summers RG, Ming G-L, Gage FH (2006) Distinct morphological stages of dentate granule neuron maturation in the adult mouse hippocampus. J Neurosci 26:3–11.

Zhou Q, Homma KJ, Poo MM (2004) Shrinkage of dendritic spines associated with long-term depression of hippocampal synapses. Neuron 44:749–757.

6. High-frequency stimulation induces gradual immediate early gene expression in maturing adult-generated hippocampal granule cells

Tassilo Jungenitz[1], Tijana Radic[1], Peter Jedlicka[1], Stephan W. Schwarzacher[#1]

[1]Institute of Clinical Neuroanatomy, Goethe-University Frankfurt, NeuroScience Center, D-60590 Frankfurt am Main, Germany

[#]Author for correspondence: Stephan W. Schwarzacher, Institute of Clinical Neuroanatomy, Goethe-University, Theodor-Stern-Kai 7, D-60590 Frankfurt am Main, Phone: +49 (0)69 6301 6914, Fax: +49 (0)69 6301 6425, E-mail: schwarzacher@em.uni-frankfurt.de

6.1. Acknowledgments

6.2. Abstract

Increasing evidence shows that adult neurogenesis of hippocampal granule cells is advantageous for learning and memory. We examined at which stage of structural maturation and age new granule cells can be activated by strong synaptic stimulation. High-frequency stimulation of the perforant pathway in urethane-anesthetized rats elicited expression of the immediate early genes c-fos, Arc, zif268 and pCREB133 in almost 100 % of mature, calbindin-positive granule cells. In contrast, it failed to induce immediate early gene expression in immature doublecortin-positive granule cells. Furthermore, doublecortin-positive neurons did not react with c-fos or Arc expression to mild theta-burst stimulation or novel environment exposure. Endogenous expression of pCREB133 was increasingly present in young cells with more elaborated dendrites, revealing a close correlation to structural maturation. Labeling with bromodeoxyuridine revealed cell age dependence of stimulation-induced c-fos, Arc and zif268 expression, with only a few cells reacting at 21 days, but with up to 75 % of cells activated at 35 - 77 days of cell age. Our results indicate an increasing synaptic integration of maturing granule cells, starting at 21 days of cell age, but suggest a lack of ability to respond to activation with synaptic potentiation on the transcriptional level as long as immature cells express doublecortin.

6.3. Introduction

New hippocampal granule cells (GCs) are continuously generated from neural stem and progenitor cells throughout life in the mammalian dentate gyrus (Altman and Das 1965; Gage 2010). Neurogenesis within the adult hippocampus contributes to learning and memory, although the precise function is only beginning to be understood (Drapeau and Abrous 2008; Zhao et al. 2008). Increasing evidence indicates that newly generated GCs play a crucial role in spatial and episodic memory, particularly in pattern separation (Clelland et al. 2009; Alme et al. 2010; Nakashiba et al. 2012). Furthermore, suppression of granule cell neurogenesis in mice leads to deficits in various learning tasks that are related to hippocampus specific forms of spatial memory (Clelland et al. 2009; Jessberger et al. 2009).

The survival of maturing GCs depends on their functional integration into the existing network and can be increased by behavioral stimuli, such as exposure to an enriched environment (van Praag et al. 1999; Tashiro et al. 2007), hippocampus-dependent learning paradigms (Gould et al. 1999; Dupret et al. 2007; Kee et al. 2007) and acute stimulation of the entorhinal cortex (Stone et al. 2011). About 50 % of postmitotic GCs in the adult dentate gyrus die within the first four weeks after their birth (Dayer et al. 2003; Snyder et al. 2009). Surviving GCs become synaptically integrated into the neuronal network by spreading axons with synapses to hilar neurons and CA3 pyramidal cells, as well as extending dendrites with spines into the molecular layer, and receiving excitatory input from perforant path afferents (van Praag et al. 2002; Espósito et al. 2005; Kee et al. 2007; Zhao et al. 2007; Toni et al. 2008). However, it has remained an open issue at which stage of structural maturation newly generated GCs become functionally integrated, and at which time-point new neurons start to contribute to hippocampal learning and memory (Snyder et al. 2009, 2012). Whereas facilitated induction of associative long-term potentiation has been demonstrated for young maturing GCs (Schmidt-Hieber et al. 2004; Ge et al. 2007), new GCs are increasingly likely to be incorporated into circuits

supporting spatial memory at a more mature state of 6 to 12 weeks (Kee et al. 2007).

There is ample evidence that induction of effective synaptic plasticity associated with learning and memory requires de novo transcription in the cell nucleus (Sanes and Lichtman 1999). This process is initiated by immediate early genes (IEGs), which serve as reliable markers for synaptic activity and plasticity (Jones et al. 2001; Fleischmann et al. 2003; Reymann and Frey 2007; Bramham et al. 2010; Chen et al. 2010). Thus, it should be expected that newborn GCs respond to afferent stimulation with IEG expression during their critical period of dendritic arborization, spinogenesis, and enhanced synaptic excitability and plasticity (Schmidt-Hieber et al. 2004; Espósito et al. 2005; Ge et al. 2007; Zhao et al. 2008; Häussler et al. 2012). However, previous studies using behavioural tests or electrical stimulation with LTP-induction protocols have failed to induce IEGs in immature GCs (Kuipers et al. 2009; Sandoval et al. 2011). Here, we performed extensive high frequency stimulation (HFS) of the perforant path in adult rats under *in vivo* conditions (Steward et al. 1998) in order to induce maximal expression of IEGs in hippocampal GCs as a precondition to analyze the potential transcriptional response in maturing GCs.

Importantly, we found that young GCs are only synaptically activated on the transcriptional level after the phase of doublecortin (DCX) expression. Thereafter they become gradually activated with increasing age, but do not reach the activation state of the mature population.

6.4. Results

Mature dentate granule cells express c-fos and Arc following high frequency stimulation of the perforant path

In order to maximally stimulate GCs, we applied a strong HFS paradigm developed by Steward et al. (1998). 2 h HFS induced a robust LTP of the slope and population spike (data not shown). Following 2 h HFS, expression of a marker of synaptic activity, c-fos, and a marker of synaptic plasticity, activity

related cytoprotein (Arc), was significantly enhanced in the great majority of calbindin (CB)$^+$ GCs in the ipsilateral dentate gyrus (DG) (97.57 ± 1.72 %, n = 27, for c-fos; 95.57 ± 4.42 %, n = 29, for Arc; **Fig. 1A-D, G-H**) compared to control animals, in which c-fos and Arc expression was restricted to a few GCs, all of them being CB$^+$ (0.38 ± 0.11 % for c-fos, 1.03 ± 0.1 % for Arc **Fig. 1C-D, G-H**). A similar ipsilateral activation of GCs was observed following 30 min of HFS (data not shown). In the hippocampus, both, c-fos and Arc stainings were restricted to the ipsilateral DG, indicating a selective synaptic activation of ipsilateral GCs. In the contralateral DG no increase of c-fos or Arc expression over control levels could be detected after HFS. Triple-stainings with CB, the neuronal marker NeuN and the cell nuclei marker TO-PRO-3 revealed a co-expression of NeuN in 100 ± 0.0 % of CB$^+$ cells (n = 3), and a co-expression of CB in 95.61 ± 0.74 % of NeuN$^+$ cells (n = 3), indicating an almost complete CB-staining of mature GCs. TO-PRO3-staining served for delineation of the granule cell layer (GCL). CB$^-$/NeuN$^+$ cells of the GCL likely represented immature GCs (e.g. DCX$^+$ cells, see later) and interneurons that are sparsely located within the GCL (Woodson et al. 1989).

Immature dentate granule cells do not express c-fos and Arc following high frequency stimulation of the perforant path

Next, we analyzed if immature GCs could be activated by HFS. A variety of chemical markers can be used to label the different maturation stages of adult newborn GCs (Zhao et al. 2008; von Bohlen Und Halbach 2011). Pre- and young postmitotic maturing GCs of neuronal fate can be labeled in the adult DG with doublecortin (DCX) and polysialic acid neural cell adhesion molecule (PSA-NCAM) (Zhao et al. 2008). Both markers produced robust somato-dendritic staining. 100 % of PSA-NCAM cells were co-stained with DCX, whereas some additional cells were only DCX$^+$ (2.7 ± 0.23 % of all DCX$^+$-cells, n = 3). Therefore, DCX was preferred for labeling of immature GCs in this study. Whereas the majority of DCX$^+$ GCs were CB$^-$, a small subpopulation of DCX$^+$ GCs showed co-staining with CB (7.43 ± 2.42 %, n = 3, data not shown, for a cell age-related analysis see later).

Surprisingly, and in contrast to DCX⁻/CB⁺ cells, DCX⁺ cells did in no case exhibit immunoreactivity for c-fos and/or Arc following 2 h HFS **(Fig. 1E-H)**. Thus, young maturing DCX⁺ cells appeared not to be responsive for synaptic activation via HFS.

Young maturing adult newborn granule cells cannot be activated by mild stimulation or novel environment exposure

As the HFS protocol represents a massive stimulation that could possibly block physiological responses in immature neurons, we also performed a mild perforant path theta burst stimulation (TBS) for LTP-induction with a total of 216 pulses (Jones et al. 2001) that elicited c-fos and Arc immunoreactivity in ipsilateral mature CB+ GCs, but failed to activate any DCX⁺ cells (data not shown). In addition, we conducted an open field exposure to novel environment in awake animals which elicited c-fos and Arc expression in a subfraction of mature CB⁺ GCs **(Fig. 2B, D)**, but again, neither c-fos nor Arc labeling was detected in any DCX⁺ cell. In summary, unlike mature CB⁺ GCs, young maturing DCX⁺ GCs did not react with expression of markers of synaptic activity and plasticity to various forms of synaptic activation in conscious and anaesthetized adult rats.

Increasing synaptic activation of maturing dentate granule cells with cell age

Next, we wanted to analyze at which postmitotic age newborn cells become responsive to HFS. We performed intraperitoneal injections of the mitosis marker bromodeoxyuridine (BrdU) and studied the age-dependent expression of the two maturation markers DCX and CB. DCX was present in most BrdU⁺ cells 7 days post BrdU injection (dpi) and declined to low levels at 21 dpi **(Fig. 3)**. CB was already present in some BrdU⁺ cells at 7 dpi and 14 dpi and almost all of these cells were CB⁺/DCX⁺. CB⁺/DCX⁻ cells represented the major population of BrdU+ cells from 21 dpi on. Following 2 h HFS, expression of c-fos and Arc in BrdU⁺ cells was observed earliest at 21 dpi (15.39 ± 6.25 % of BrdU⁺ cells for c-fos (n = 3) and 7.18 ± 3.59 % of BrdU⁺ cells for Arc (n = 3).

The percentage of c-fos$^+$ and Arc$^+$/BrdU$^+$ cells after 2 h HFS increased with cell age and reached approximately 75 % at 35 dpi (83.96 ± 5.29. % of BrdU$^+$ cells for c-fos (n = 5) and 74.18 ± 4.93 % of BrdU$^+$ cells for Arc (n = 4) with no further increase until 77 dpi (77.12 ± 10.07 % of BrdU$^+$ cells for c-fos (n = 3) and 80.04 ± 6.28 % of BrdU$^+$ cells for Arc (n = 3). Statistical analysis revealed a significant difference between the amount of activated BrdU$^-$/CB$^+$ cells (i.e. the total population of mature and maturing CB$^+$ GCs except the BrdU$^+$ cells) and the subpopulations of BrdU-tagged GCs (for c-fos: BrdU$_{21 - 28 \, dpi}$ = 33.06 ± 8.61 %, n = 8; BrdU$_{35 - 77 \, dpi}$ = 78.07 ± 2.79 %, n = 16; BrdU$^-$ = 95.02 ± 0.4 %, n = 24; for Arc: BrdU$_{21 - 28 \, dpi}$ = 25.65 ± 6.32 %, n = 8; BrdU$_{35 - 77 \, dpi}$ = 73.87 ± 3 %, n = 15; BrdU$^-$ = 96.6 ± 0.28 %, n = 23; two-tailed Wilcoxon rank-sum test, p < 0.05, for c-fos and Arc). Based on these findings we concluded that even after 77 days of cell development, functional maturation and integration was not completed in all adult newborn dentate GCs.

pCREB133 expression does not increase in young dentate granule cells following high frequency perforant path stimulation

Next, we wanted to examine whether young maturing DCX$^+$ cells exhibited a detectable general reactivity to HFS. We took advantage of the fact that the transcription factor cAMP response element binding protein (CREB) is a rapidly responding intracellular effector of neurotransmitter signaling and is endogenously activated in non-stimulated young maturing granule neurons (Nakagawa et al. 2002; Fujioka et al. 2004). 2 h HFS elicited pCREB133 expression bilaterally in principal cells of the DG, CA1 and CA3 hippocampal regions **(Fig. 4A)**. Whereas virtually all CB$^+$ GCs in the ipsilateral (99.85 ± 0.07 %, n = 3) and contralateral (99.73 ± 0.05 %, n = 3) GCL of the DG were pCREB133$^+$, only a very few cells showed weak pCREB133 immunoreactivity in the control group (8.05 ± 3.6 %, n = 3; **Fig. 4C, D**). In contrast, about 40 % (39.66 ± 1.76 %, n = 3) of young maturing DCX$^+$ GCs partly expressed pCREB133 endogenously in control animals, but the expression could not be further enhanced following 2 h HFS (35.78 ± 4.36 %, n = 3; **Fig. 4E, F**).

We subsequently investigated if HFS could have an effect on pCREB133-expression of DCX-positive cells depending on their structural maturation. This concerned in particular the subpopulation of maturing DCX[+] GCs which already showed elaborated dendrites towards the outer molecular layer, the zone of perforant path afferent input, and thus might be responsive to HFS. DCX, as a microtubule-associated protein, is expressed throughout the somata and dendrites of GCs during the phase of structural maturation (Francis et al. 1999; Gleeson et al. 1999). We introduced a classification of DCX[+] GCs into 6 different stages, according to orientation and outgrowth of dendritic processes in the subgranular zone (stage 1, no processes; stage 2, processes in the subgranular zone), the granule cell layer (stage 3, inner half of the granule cell layer; and stage 4, outer half of the granule cell layer), inner molecular layer (stage 5) and outer molecular layer (stage 6; **Fig. 5A**, see also Methods). The 6 DCX[+] maturation stages correlated with cell age. At the age of 7 days, most DCX^{+} cells represented stage 1 - 4 neurons (≥ 85 %), and only a few cells exhibited dendrites that reached the IML (stage 5) and OML (stage 6). At the age of 14 days, a few stage 1 - 4 DCX[+] were left, whereas the majority of DCX^{+} cells (≥ 85 %) represented stage 5 - 6 **(Fig. 5C, D)**. Furthermore, DCX^{+} cells exhibited the marker Neuronal Nuclei (NeuN), an indicator for postmitotic neurons (Kempermann et al. 2003) with increasing numbers in later DCX[+] cell stages **(Fig. 5E, F)**. Therefore, DCX[+] cell staging appeared to be a useful classification system for structural maturation of young GCs.

Endogenous expression of pCREB133 closely correlated to structural maturation, with only a few pCREB133^{+} cells in stage 1 DCX^{+} cells, and more than 90 % pCREB133^{+} cells in stage 5 and 6 DCX^{+} cells **(Fig. 5G)**. Following 2 h HFS, there was no indication of an increased number of activated pCREB133^{+} cells at any structural stage **(Fig. 5H)**. Therefore, endogenous pCREB133 expression appears to be closely correlated to structural maturation of young GCs, but cannot be further enhanced through synaptic activation.

zif268 expression increases in maturing dentate granule cells following high frequency perforant path stimulation

Similar to pCREB133, zinc finger binding protein clone 268 (zif268) is a transcription factor that can be enhanced by increased neuronal activity (Bozon et al. 2002) and is required for long-term synaptic plasticity (Jones et al. 2001). 2 h HFS strongly increased zif268 expression in the ipsilateral GCL **(Fig. 6A)**. 97.12 ± 2.3 % (n = 3) of CB^+ GCs in the ipsilateral DG exhibited strong zif268 expression following HFS, whereas GCs only exhibited weak zif268 immunoreactivity in the contralateral GCL and in the control condition **(Fig. 6B, C, D)**. In addition, endogenous zif268 expression was found in some DCX^+-cells, but was restricted to the more mature stages 5 (≤ 2 % of DCX^+) and 6 (≥ 20 % of DCX^+). Application of 2 h HFS led to no significant increase of zif268 expression in stage 5 and 6 DCX^+ cells (Two-sided Wilcoxon rank-sum test: stage 5 p = 0.74, stage 6 p = 0.08, $n_{2\,h\,HFS} = 6$, $n_{control} = 8$; **Fig. 6E, F**).

To study the time course of zif268 expression in maturing GCs beyond the phase of DCX expression, we measured the zif268 immunofluorescence-intensities of BrdU-tagged cells at various dpi, and compared them to non-BrdU-tagged, but CB^+ cells within the proximity of the ipsilateral GCL. A stimulation-induced increase of zif268 immunoreactivity in CB^+ cells was first observed at 21 dpi (32.06 ± 3.8 %, n = 3), and then strongly increased to 67.97 ± 5.2 % of the total CB^+ cell population at 35 dpi (n = 3). Thenceforth, no further increase in zif268 immunofluorescence-intensity was observed. Younger (21 - 28 dpi) and older (35 - 77 dpi) $BrdU^+/CB^+$ GCs showed significantly weaker intensities compared to the $BrdU^-/CB^+$ GCs population ($BrdU^+_{21 - 28\,dpi} = 44.48 \pm 5.1$ %, n = 8; $BrdU^+_{35 - 77\,dpi} = 69.01 \pm 2.25$ %, n = 16; $BrdU^- = 100$ %, n = 24; two-sided Wilcoxon signed-rank test, p < 0.05; **Fig. 6G, H**). Therefore, young maturing CB^+ cells appear to be responsive to synaptic activation starting at 3 weeks of cell age, but show considerable less IEG expression following HFS than the total population of mature and maturing CB^+ cells.

6.5. Discussion

In this study, we examined correlations between the structural maturation, chemical marker expression and age of newly born GCs with their capability to express various IEGs following strong synaptic stimulation, as an indication of successful functional integration in the adult network under *in vivo* conditions. The applied HFS protocol led to c-fos and Arc expression in nearly all mature GCs, but failed to induce c-fos and Arc expression in young maturing DCX[+] GCs. Individual young GCs varied considerably in their time-course of structural maturation. Once maturing GCs started to express CB and lost DCX expression, they gradually became responsive to HFS from 21 days on and showed IEG expression in about 75 % of the maturing GCs at 35 - 77 days of cell age **(Fig. 7)**. We conclude, that structural and functional integration varies between individual young GCs and needs 3 weeks for the earliest maturated GCs, but requires at least 5 weeks until the majority of new GCs are able to respond to synaptic activation with signs of synaptic plasticity, and thus may contribute to processes of learning and memory formation.

Delayed onset of synaptic activation and IEG expression in young GCs

2 h HFS induced LTP with robust c-fos and Arc expression in practically all mature CB[+] GCs in the ipsilateral DG. Only a few CB[+] GCs could not be activated, but those likely represent young CB[+] GCs. Importantly, neither c-fos nor Arc expression was observed in young maturing DCX[+] GCs after HFS. In addition, shorter HFS (30 min) or a TBS-LTP protocol, and novel environment exposure in awake animals failed to elicit c-fos and Arc in DCX[+] GCs, whereas CB[+] GCs were activated in all tests. Furthermore, some CB[+] GCs in control animals expressed c-fos or Arc, attributed to home-cage activity (Marrone et al. 2008), but no spontaneously activated DCX[+] GCs were found. Thus, the lack of activated immature DCX[+] GCs is probably not due to an un-physiological or inadequate stimulation. In line with these findings, Kuipers et al. (2009) reported resistance to Arc activation in 1 - 28 days old GCs with a TBS-LTP protocol. Similarly, spatial exploration induced Arc expression in GCs only from 30 days on (Sandoval et al. 2011).

Following HFS, we observed a gradual increase of c-fos, Arc and zif268 expression in BrdU$^+$/CB$^+$ GCs starting at 21 days of cell age. Interestingly, Snyder et al. (2009) found earliest c-fos expression in newborn GCs at 2 weeks and in all BrdU$^+$ GCs at 4 weeks following seizure induction by intraperitoneal kainate injection, demonstrating that immature neurons have the capability to express IEGs under patho-physiological conditions. The time course of stimulation-induced zif268 expression preceded c-fos and Arc expression. An early onset of zif268 expression in 2 - 4 week old GCs was reported following a TBS-LTP protocol (Bruel-Jungerman et al. 2006; Kuipers et al. 2009) or physiological stimulation by water maze training as well as by kainate-induced seizures (Snyder et al. 2009, 2012). In our study, basal zif268 expression was endogenously present in CB$^+$ GCs and also in some DCX$^+$ GCs with elaborated dendrites. In some contrast to Snyder et al. (2009), who found a peak of stimulation-induced zif268 expression in 3 week old GCs, we observed a continuous increase of inducible zif268 expression until the 5th week of cell age. From this we conclude, that young GCs become gradually integrated in the existing adult network **(Fig. 7)**.

Gradual structural and functional integration of maturing GCs

Expression of IEGs such as c-fos, Arc and zif268 are considered as a prerequisite for a successful synaptic activation and biosynthesis dependent late phase of LTP (Guzowski et al. 2001; Jones et al. 2001; Davis 2003; Fleischmann et al. 2003). Numerous studies have shown that Arc plays an essential role in this process that requires up-regulation and trafficking of Arc mRNA to GC dendrites and local Arc translation at sites of synaptic activity, as well as sustained Arc synthesis for LTP consolidation and silencing of inactive synapses (Steward et al. 1998; Steward and Worley 2001; Messaoudi et al. 2007; Bramham et al. 2008; Jedlicka et al. 2008; Okuno et al. 2012). Therefore, maturing GCs that are involved in synaptic plasticity and learning should be responsive to LTP induction protocols and react with nuclear IEG expression. However, the lack of stimulation-induced c-fos, Arc and zif268 expression in young maturing GCs does not exclude forms of synaptic plasticity that do not

require IEG expression (Bramham 2010). We observed HFS induced c-fos and Arc expression in some maturing CB^{+} cells already at 3 weeks. On the other hand, c-fos and Arc expression as well as zif268 immunofluorescence-intensity increased gradually and reached only 75 % of the values for CB[+] GCs even after 11 weeks. Consistent with this delayed responsivity, Zhao et al., (2006) provided evidence for a sustained time course of 4 - 18 weeks for spinogenesis, especially of mature mushroom spines in new GCs. Furthermore, functional glutamatergic perforant path-GC synapses were detected from 3 weeks on (Espósito et al. 2005; Zhao et al. 2008). Several studies in adult rats have suggested that new GCs contribute to hippocampal function as early as 2 - 3 weeks of age (Shors et al. 2001, 2002; Madsen et al. 2003; Snyder et al. 2005). In contrast, in adult mice, electrophysiological studies (van Praag et al. 2002; Espósito et al. 2005; Ge et al. 2006, 2007), as well as morphological (Zhao et al. 2006; Jessberger et al. 2007) and behavioral (Jessberger and Kempermann 2003; Kee et al. 2007) reports, suggest that new neurons are minimally functional, and would be unlikely to contribute to behavior until at least 6 - 8 weeks of age. However, a direct comparison of adult neurogenesis in mice and rat (Snyder et al. 2009) revealed that newborn GCs in rats show faster maturation and signs of earlier and stronger activation than mice (Snyder et al. 2009). In summary, the gradual reactivity of newborn GCs to HFS observed in our study indicates that any network function attributed to very young GCs would likely be performed by a small number of early mature GCs. As the total number of new GCs represents only a subfraction of the mature GC population, the actual number of young GCs responsive to functional activity appears to be limited.

Correlation of chemical and structural GC maturation with age

In general, chemical and structural development of new GCs corresponded to cell age. Our data from Sprague-Dawley rats closely correlate to similar labelings in Long-Evans rats (Snyder et al. 2009). We found a change from DCX to CB expression in new GCs within 3 - 4 weeks. Double-labeling revealed a subpopulation of DCX[+]/CB^{+} cells that probably represented early CB^{+} cells.

Remarkably, these cells showed no enhancement of IEGs following HFS. Although structural development of DCX$^+$ cells increased with age, some neurons showed dendrites in the inner and outer molecular layer (stage 5 and 6) already at 1 week, whereas other neurons remained in early structural stages (stage 3 - 4) at 4 weeks. Thus, the individual structural development of young maturing GCs is subject to considerable variation.

Young GCs endogenously expressed pCREB133, as was described previously (Nakagawa et al. 2002). Interestingly, pCREB133 expression correlated with structural staging, being expressed in about 10 % of stage 2, but in 100 % of stage 6 DCX$^+$ GCs. This is in line with the role of CREB-signalling as an important factor for survival and dendritic development of GCs (Fujioka et al. 2004). However, we could not detect any enhancement of pCREB133 expression in DCX$^+$ GCs following HFS, although GABA-mediated activation of pCREB133 has been shown in maturing GCs (Nakagawa et al. 2002; Ge et al. 2006; Merz et al. 2011). In contrast to DCX$^+$ GCs, endogenous pCREB133 expression was hardly detectable in mature CB$^+$ GCs, but was strongly activated following HFS. Thus, the role of pCREB133 signaling appears to change from a growth-related function in maturing GCs to an excitation-related function in mature GCs.

The role of adult newborn GCs

The functional significance of adult newborn GCs remains a highly discussed topic (Ming and Song 2011; Bergami and Berninger 2012). Increasing evidence suggests that newly formed GCs contribute to hippocampus specific forms of learning and memory, which might be different to the function of mature (or permanent) GCs (Clelland et al. 2009; Aimone et al. 2011). Recent studies suggested a model of DG function, in which young GCs may support pattern separation, whereas old GCs contribute to rapid pattern completion (Nakashiba et al. 2012) or even may retire to a silent population (Alme et al. 2010). We found no indication for a functional silencing of old GCs, as more than 95 % of the mature GC appeared to be highly responsive to synaptic activation. On the other hand, a small number of young CB$^+$ GCs exhibited signs of structural and

functional maturation already as early as 3 weeks of cell age, but at least 5 weeks seem to be necessary, until the majority of newly generated GCs are responsive to successful synaptic activation and synaptic plasticity including late LTP, that requires de novo transcription. Therefore, young granule cells appear to be gradually integrated into the existing neuronal network, in order to contribute to different forms of hippocampal learning.

6.6. Materials and Methods

Animals

Adult male Sprague-Dawley rats (8 - 13 weeks, 220 - 450 g; Charles River, Sulzfeld, Germany) were housed under standard laboratory conditions in large rat cages (30 cm x 40 cm) with selected objects to assemble an enriched environment. All animal experiments were performed in conformance with German guidelines for the use of laboratory animals.

BrdU injections

To analyze newborn cells of a specific age (7, 14, 21, 28, 35, 49, 63 and 77 days), 5-bromo-2'-deoxyuridine (BrdU, AppliChem) was injected intraperitoneally (i.p.) at 200 mg/kg body weight at a single time point.

Surgical procedures, perforant path stimulation

All surgical procedures were performed under deep urethane anesthesia (1.25 g/kg body weight s. c. initially and additional injections as needed; 250 mg urethane/ml 0.9 % saline), in agreement with the German law on the use of laboratory animals. Surgery and stimulation procedures were performed as previously described (Schwarzacher et al. 2006; Jedlicka et al. 2009). In short, animals were placed in a Kopf stereotaxic device (Kopf instruments, Tujunga, CA, U.S.A.). Rectal temperature was maintained at 37.0 ± 0.5 °C. Two small holes (1.5 - 2.0 mm diameter) were drilled in the skull and a bipolar stainless steel stimulating electrode (NE-200; Rhodes Medical, Woodland Hills, CA,

U.S.A.) was placed in the angular bundle of the perforant path (coordinates from lambda: L: 4.5 mm; AP: +0.5 mm; V: -3.5 mm measured from the surface of the brain). Glass microelectrodes (1.5 mm outer diameter) were pulled on a Zeitz (München, Germany) electrode puller, filled with 0.9 % saline, and placed in the dorsal blade of the granule cell layer (coordinates from bregma: L: 2.0 mm, AP: -3.5 mm, V: -3.5 mm). The vertical tip position was optimized under perforant path control stimulation using the characteristic shape of the evoked potentials.

High frequency stimulation (HFS) was used to maximally evoke population spikes and induce robust long term potentiation (LTP) as has been described in detail (Steward, Wallace, Lyford, & Worley, 1998). HFS was applied for 30 min or for 2 h. One HFS train consisted of 8 pulses (500 µA, 0.1 ms pulse duration) of 400 Hz once per 10 s. A baseline fEPSP slope was calculated from the average of responses over the 10 min prior to the theta-burst stimulation (TBS). Baseline stimulus intensity was set to evoke a population spike of approximately 1 mV before LTP induction. The potentiation of the fEPSP slope was expressed as percentage change relative to baseline.

TBS for LTP-induction consisted of 6 series of 6 trains of 6 stimuli at 400 Hz, 200 ms between trains, 20 s between series (Jones et al. 2001). Pulse width and stimulus intensity was doubled during the TBS in comparison to baseline recordings.

In sham operated rats, stimulation and recording electrodes were placed with the aid of small voltage stimulation pulses and left in place for 2 h without stimulation. All animals were perfused 2 h after the start of stimulation or sham procedure.

Open field exposure

For novelty-induced activation, rats were conditioned to fearless handling several days in advance. Rats were exposed to a novel environment in a large

box (70 cm x 40 cm) for 1 h and were then transferred back into the cage and perfused after 2 h.

Immunohistochemistry

Rats were deeply anesthetized with an overdose of pentobarbital (300 mg/kg body weight) and transcardially perfused with a fixative containing 4 % paraformaldehyde in 0.1 M phosphate buffered saline (PBS), pH 7.4. Brains were removed and postfixed up to 18 h in 4 % paraformaldehyde in 0.1 M PBS. Serial frontal sections of the hippocampus (50 µm) were cut with a vibratome, washed in PBS, and stored at –20 °C in cryo-protection solution (30 % ethylene glycol, 25 % glycerin in PBS). After a blocking step to reduce non-specific staining (5 % bovine serum albumin), free-floating sections were incubated for 24 - 48 h at 4 °C in primary antibody solution, containing 2 % bovine serum albumin, 0.25 % Triton X-100, 0.1 % NaN_3 in 0.1 M PBS. The following primary antibodies were used: Anti-Arc (rabbit, polyclonal, 1:1000, Synaptic Systems, Ctl. 156002), calbindin D29k (CB, mouse, monoclonal, 1:500, SWANT, Ctl. 300), c-fos (rabbit, polyclonal, 1:1000, Santa Cruz, Ctl. Sc-52-G), doublecortin (DCX, goat, polyclonal, 1:500, Santa Cruz, Ctl. Sc-8066), zif268 (rabbit, monoclonal, 1:500, Cell Signaling, Ctl. 4153), NeuN (mouse, monoclonal, 1:1000, Chemicon, Ctl. MAB377) and pCREB Ser133 (rabbit, polyclonal, 1:500, Cell Signaling, Ctl. 9198S). For fluorescence-immunohistochemical detection, sections were incubated with secondary fluorescence-labeled antibodies (1:1000; Alexa 488, 568 and 633, Vector Labs., Burlingame, CA, U.S.A.) for 24 h at room temperature.

Following immunohistological staining of Arc, CB, c-fos, DCX or zif268, some sections were further processed for BrdU detection. Free-floating sections were incubated in 2 N HCl at 37 °C for 30 min and 0.1 M boracic acid (pH 8.5) at room temperature for 10 min, followed by incubation with anti-BrdU (rat, monoclonal, 1:200, Abcam, Ctl. 6326-250 or mouse, monoclonal, 1:200, Dako, Ctl. M0744) for 24 h at room temperature. Fluorescence-immunohistological detection of BrdU was performed with secondary fluorescence-labeled antibodies (1:1000; Alexa 488 and 568; Vector Labs., Burlingame, CA, U.S.A.)

for 24 h at room temperature. For staining of cell nuclei TO-PRO-3 (Invitrogen, Ctl. T3605) was used at a concentration of 1:30,000 at room temperature for 10 min.

Histological quantification and statistical analysis

All statistic evaluations were performed with 3 or more animals (n ≥ 3) per group. For each animal, images of z-stacks were acquired from frontal sections of the dorsal dentate gyrus (3 - 5 non-overlapping stacks along the suprapyramidal and infrapyramidal blade, the x-axis of the frames set perpendicular to the medio-lateral axis of the granule cell layer) using a confocal microscope (Nikon Eclipse 80i) and a 40x oil immersion objective (N.A. 1.3). Each Z-stack consisted of 20 - 30 frames (40 µm x 40 µm) separated by 1 µm in the z-axis. Non-BrdU histological evaluations were performed in 3 or more randomly selected sections per case (animal).

Structural maturation of DCX$^+$ cells was evaluated with a staging system based on the degree of elaboration of dendritic processes **(see Fig. 5)**, as follows: - Stage 1: the DCX$^+$ cell soma is positioned in the subgranular zone, and no processes are visible. - Stage 2: the DCX$^+$ cell has 1 - 2 small short processes that stay within the subgranular zone. - Stage 3: the principal dendrite of the DCX$^+$ cell extends into the inner half of the granule cell layer. - Stage 4: The leading dendrite reaches the outer half of the granule cell layer. - Stage 5: the leading dendrite reaches the inner molecular layer. - Stage 6: the leading dendrite reaches the outer molecular layer.

The expression of DCX, CB, c-fos, Arc or zif268 in BrdU-tagged cells was analyzed in ≥ 20 cells per animal. To study the graded immunofluorescence of zif268, the grey level values of the zif268 immunofluorescence-intensity of a given cell soma were measured in the confocal plane with the biggest largest cell nucleus diameter. Zif268 immunofluorescence-intensity of BrdU$^+$/CB$^+$ cells were compared to BrdU$^-$/CB$^+$ reference cells throughout the granule cell layer within the same z-stack. In order to take the background immunofluorescence-intensity into account, samples within the same z-stack were obtained from

three different randomly selected regions in the molecular layer and/or hilus, using a predefined rectangular selection box that did not contain any CB^+ somata. The averaged background value was subtracted from the cell values.

Data management and graphs were done with GraphPad Prism 5. Statistical comparisons were calculated with the two-sided Wilcoxon signed-rank test (in case of zif268 fluorescence intensity-analysis of $BrdU^+$ cells, **Fig. 6H**) or the Wilcoxon rank-sum test (Mann-Whitney-U test; in all other cases) using R 2.14.0 for Windows. Significance level was set at $p < 0.05$. Group values are reported as means ± SEM.

6.7. References

Aimone JB, Deng W, Gage FH. 2011. Resolving new memories: a critical look at the dentate gyrus, adult neurogenesis, and pattern separation. Neuron. 70:589–596.

Alme CBB, Buzzetti R a. a, Marrone DFF, Leutgeb JKK, Chawla MKK, Schaner MJJ, Bohanick JDD, Khoboko T, Leutgeb S, Moser EII, Moser M-BM-B, McNaughton BLL, Barnes C a. a. 2010. Hippocampal granule cells opt for early retirement. Hippocampus. 20:1109–1123.

Altman J, Das GD. 1965. Autoradiographic and histological evidence of postnatal hippocampal neurogenesis in rats. J Comp Neurol. 124:319–335.

Bergami M, Berninger B. 2012. A fight for survival: The challenges faced by a newborn neuron integrating in the adult hippocampus. Dev Neurobiol. 72:1016–1031.

Bozon B, Davis S, Laroche S. 2002. Regulated transcription of the immediate-early gene Zif268: mechanisms and gene dosage-dependent function in synaptic plasticity and memory formation. Hippocampus. 12:570–577.

Bramham CR. 2010. LTP not equal Learning: Lessons from Short-Term Plasticity. Front Behav Neurosci. 4:1–2.

Bramham CR, Alme MN, Bittins M, Kuipers SD, Nair RR, Pai B, Panja D, Schubert M, Soule J, Tiron A, Wibrand K. 2010. The Arc of synaptic memory. Exp Brain Res. 200:125–140.

Bramham CR, Worley PF, Moore MJ, Guzowski JF. 2008. The immediate early gene arc/arg3.1: regulation, mechanisms, and function. J Neurosci. 28:11760 –11767.

Bruel-Jungerman E, Davis S, Rampon C, Laroche S. 2006. Long-term potentiation enhances neurogenesis in the adult dentate gyrus. Eur J Neurosci. 26:5888 –5893.

Chen G, Zou X, Watanabe H, van Deursen JM, Shen J. 2010. CREB binding protein is required for both short-term and long-term memory formation. J Neurosci. 30:13066–13077.

Clelland CD, Choi M, Romberg C, Clemenson GD, Fragniere A, Tyers P, Jessberger S, Saksida LM, Barker R a, Gage FH, Bussey TJ. 2009. A functional role for adult hippocampal neurogenesis in spatial pattern separation. Science. 325:210–213.

Davis S. 2003. How necessary is the activation of the immediate early gene zif268 in synaptic plasticity and learning? Behav Brain Res. 142:17–30.

Dayer AG, Ford AA, Cleaver KM, Yassaee M, Cameron HA. 2003. Short-term and long-term survival of new neurons in the rat dentate gyrus. J Comp Neurol. 572:563–572.

Drapeau E, Abrous DN. 2008. Stem Cell Review Series: Role of neurogenesis in age-related memory disorders. Aging Cell. 7:569–589.

Dupret D, Fabre A, Döbrössy MD, Panatier A, Rodríguez JJ, Lamarque S, Lemaire V, Oliet SHR, Piazza P-V, Abrous DN. 2007. Spatial learning depends on both the addition and removal of new hippocampal neurons. PLoS Biol. 5:1683–1694.

Espósito MS, Espo MS, Piatti VC, Laplagne DA, Ferrari CC, Pitossi FJ, Schinder AF. 2005. Neuronal differentiation in the adult hippocampus recapitulates embryonic development. Hippocampus. 25:10074 –10086.

Fleischmann A, Hvalby O, Jensen V, Strekalova T, Zacher C, Layer LE, Kvello A, Reschke M, Spanagel R, Sprengel R, Wagner EF, Gass P. 2003. Impaired long-term memory and NR2A-type NMDA receptor-dependent synaptic plasticity in mice lacking c-Fos in the CNS. J Neurosci. 23:9116–9122.

Francis F, Koulakoff A, Boucher D, Chafey P, Schaar B, Vinet M, Mcdonnell N, Reiner O, Kahn A, Mcconnell SK, Berwald-netter Y, Denoulet P, Chelly J, Cellulaire LDB, Berthelot PM. 1999. Doublecortin is a developmentally regulated, microtubule-associated protein expressed in migrating and differentiating neurons. Neuron. 23:247–256.

Fujioka T, Fujioka A, Duman RS. 2004. Activation of cAMP signaling facilitates the morphological maturation of newborn neurons in adult hippocampus. J Neurosci. 24:319 –328.

Gage FH. 2010. Mammalian neural stem cells. Science. 287:1433–1438.

Ge S, Goh ELK, Sailor KA, Kitabatake Y, Ming G, Song H. 2006. GABA regulates synaptic integration of newly generated neurons in the adult brain. Nature. 439:589–593.

Ge S, Yang C-H, Hsu K-S, Ming G-L, Song H. 2007. A critical period for enhanced synaptic plasticity in newly generated neurons of the adult brain. Neuron. 54:559–566.

Gleeson JG, Lin PT, Flanagan LA, Walsh CA. 1999. Doublecortin Is a microtubule-associated protein and Is expressed widely by migrating neurons. Neuron. 23:257–271.

Gould E, Beylin A, Tanapat P, Reeves A, Shors TJ. 1999. Learning enhances adult neurogenesis in the hippocampal formation. Nat Neurosci. 2:260–265.

Guzowski JF, Setlow B, Wagner EK, McGaugh JL. 2001. Experience-dependent gene expression in the rat hippocampus after spatial learning: a comparison of the immediate-early genes Arc, c-fos, and zif268. J Neurosci. 21:5089–5098.

Häussler U, Bielefeld L, Froriep UP, Wolfart J, Haas CA. 2012. Septotemporal position in the hippocampal formation determines epileptic and neurogenic activity in temporal lobe epilepsy. Cereb cortex. 22:26–36.

Jedlicka P, Schwarzacher SW, Winkels R, Kienzler F, Frotscher M, Bramham CR, Schultz C, Bas Orth C, Deller T. 2009. Impairment of *in vivo* theta-burst long-term potentiation and network excitability in the dentate gyrus of synaptopodin-deficient mice lacking the spine apparatus and the cisternal organelle. Hippocampus. 19:130–140.

Jedlicka P, Vlachos A, Schwarzacher SW, Deller T. 2008. A role for the spine apparatus in LTP and spatial learning. Behav Brain Res. 192:12–19.

Jessberger S, Clark RE, Broadbent NJ, Clemenson GD, Consiglio A, Lie DC, Squire LR, Gage FH. 2009. Dentate gyrus-specific knockdown of adult neurogenesis impairs spatial and object recognition memory in adult rats. Learn Memory. 16:147–154.

Jessberger S, Kempermann G. 2003. Adult-born hippocampal neurons mature into activity-dependent responsiveness. Eur J Neurosci. 18:2707–2712.

Jessberger S, Zhao C, Toni N, Clemenson GD, Li Y, Gage FH. 2007. Seizure-associated, aberrant neurogenesis in adult rats characterized with retrovirus-mediated cell labeling. J Neurosci. 27:9400–9407.

Jones MW, Errington ML, French PJ, Fine A, Bliss TV, Garel S, Charnay P, Bozon B, Laroche S, Davis S. 2001. A requirement for the immediate early gene Zif268 in the expression of late LTP and long-term memories. Nat Neurosci. 4:289–296.

Kee N, Teixeira CM, Wang AH, Frankland PW. 2007. Preferential incorporation of adult-generated granule cells into spatial memory networks in the dentate gyrus. Nat Neurosci. 10:355–362.

Kempermann G, Gast D, Kronenberg G, Yamaguchi M, Gage FH. 2003. Early determination and long-term persistence of adult-generated new neurons in the hippocampus of mice. Development. 130:391–399.

Kuipers SD, Tiron A, Soule J, Messaoudi E, Trentani A, Bramham CR. 2009. Selective survival and maturation of adult-born dentate granule cells expressing the immediate early gene Arc/Arg3.1. PLoS One. 4:e4885.

Madsen T, Kristjansen PEG, Bolwig TG, Wörtwein G. 2003. Arrested neuronal proliferation and impaired hippocampal function following fractionated brain irradiation in the adult rat. Neuroscience. 119:635–642.

Marrone DF, Schaner MJ, McNaughton BL, Worley PF, Barnes CA. 2008. Immediate-early gene expression at rest recapitulates recent experience. J Neurosci. 28:1030–1033.

Merz K, Herold S, Lie DC. 2011. CREB in adult neurogenesis - master and partner in the development of adult-born neurons? Eur J Neurosci. 33:1078–1086.

Messaoudi E, Kanhema T, Soulé J, Tiron A, Dagyte G, da Silva B, Bramham CR. 2007. Sustained Arc/Arg3.1 synthesis controls long-term potentiation consolidation through regulation of local actin polymerization in the dentate gyrus *in vivo*. J Neurosci. 27:10445–10455.

Ming G-L, Song H. 2011. Adult neurogenesis in the mammalian brain: significant answers and significant questions. Neuron. 70:687–702.

Nakagawa S, Kim J-E, Lee R, Malberg JE, Chen J, Steffen C, Zhang Y-J, Nestler EJ, Duman RS. 2002. Regulation of neurogenesis in adult mouse hippocampus by cAMP and the cAMP response element-binding protein. J Neurosci. 22:3673–3682.

Nakashiba T, Cushman JD, Pelkey K a, Renaudineau S, Buhl DL, McHugh TJ, Barrera VR, Chittajallu R, Iwamoto KS, McBain CJ, Fanselow MS, Tonegawa S. 2012. Young dentate granule cells mediate pattern separation, whereas old granule cells facilitate pattern completion. Cell. 149:188–201.

Okuno H, Akashi K, Ishii Y, Yagishita-Kyo N, Suzuki K, Nonaka M, Kawashima T, Fujii H, Takemoto-Kimura S, Abe M, Natsume R, Chowdhury S, Sakimura K, Worley PF, Bito H. 2012. Inverse synaptic tagging of inactive synapses via dynamic interaction of Arc/Arg3.1 with CaMKIIβ. Cell. 149:886–898.

Reymann KG, Frey JU. 2007. The late maintenance of hippocampal LTP: requirements, phases, "synaptic tagging", "late-associativity" and implications. Neuropharmacology. 52:24–40.

Sandoval CJ, Martínez-Claros M, Bello-Medina PC, Pérez O, Ramírez-Amaya V. 2011. When are new hippocampal neurons, born in the adult brain, integrated into the network that processes spatial information? PLoS One. 6:e17689.

Sanes JR, Lichtman JW. 1999. Can molecules explain long-term potentiation? Nat Neurosci. 2:597–604.

Schmidt-Hieber C, Jonas P, Bischofberger J. 2004. Enhanced synaptic plasticity in newly generated granule cells of the adult hippocampus. Nature. 429:184–187.

Schwarzacher SW, Vuksic M, Haas CA, Burbach GJ, Sloviter RS, Deller T. 2006. Neuronal hyperactivity induces astrocytic expression of neurocan in the adult rat hippocampus. Glia. 53:704–714.

Shors TJ, Miesegaes G, Beylin a, Zhao M, Rydel T, Gould E. 2001. Neurogenesis in the adult is involved in the formation of trace memories. Nature. 410:372–376.

Shors TJ, Townsend DA, Zhao M, Kozorovitskiy Y, Gould E. 2002. Neurogenesis may relate to some but not all types of hippocampal-dependent learning. Hippocampus. 584:578 –584.

Snyder JS, Choe JS, Clifford MA, Jeurling SI, Hurley P, Brown A, Kamhi JF, Cameron HA. 2009. Adult-born hippocampal neurons are more numerous, faster maturing, and more involved in behavior in rats than in mice. J Neurosci. 29:14484–14495.

Snyder JS, Clifford M a, Jeurling SI, Cameron H a. 2012. Complementary activation of hippocampal-cortical subregions and immature neurons following chronic training in single and multiple context versions of the water maze. Behav Brain Res. 227:330–339.

Snyder JS, Hong NS, McDonald RJ, Wojtowicz JM. 2005. A role for adult neurogenesis in spatial long-term memory. Neuroscience. 130:843–852.

Steward O, Wallace CS, Lyford GL, Worley PF. 1998. Synaptic activation causes the mRNA for the IEG Arc to localize selectively near activated postsynaptic sites on dendrites. Neuron. 21:741–751.

Steward O, Worley PF. 2001. Selective targeting of newly synthesized Arc mRNA to active synapses requires NMDA receptor activation. Neuron. 30:227–240.

Stone SSD, Teixeira CM, DeVito LM, Zaslavsky K, Josselyn SA, Lozano AM, Frankland PW. 2011. Stimulation of entorhinal cortex promotes adult neurogenesis and facilitates spatial memory. J Neurosci. 31:13469–13484.

Tashiro A, Makino H, Gage FH. 2007. Experience-specific functional modification of the dentate gyrus through adult neurogenesis: a critical period during an immature stage. J Neurosci. 27:3252–3259.

Toni N, Laplagne DA, Zhao C, Lombardi G, Ribak CE, Gage FH, Schinder AF. 2008. Neurons born in the adult dentate gyrus form functional synapses with target cells. Nat Neurosci. 11:901–907.

Woodson W, Nitecka L, Ben-Ari Y. 1989. Organization of the GABAergic system in the rat hippocampal formation: a quantitative immunocytochemical study. J Comp Neurol. 280:254–271.

Zhao C, Deng W, Gage FH. 2008. Mechanisms and functional implications of adult neurogenesis. Cell. 132:645–660.

Zhao C, Laplagne DA, Kamienkowski JE, Espo MS, Gage FH, Schinder AF. 2007. Similar GABAergic inputs in dentate granule cells born during embryonic and adult neurogenesis. Neuroscience. 25:2973–2981.

Zhao C, Teng EM, Summers RG, Jr. M, G.I, Gage FH. 2006. Distinct morphological stages of dentate granule neuron maturation in the adult mouse hippocampus. J Neurosci. 26:3–11.

van Praag H, Kempermann G, Gage FH. 1999. Running increases cell proliferation and neurogenesis in the adult mouse dentate gyrus. Nat Neurosci. 2:266–270.

van Praag H, Schinder A, Christie B, Toni N. 2002. Functional neurogenesis in the adult hippocampus. Nature. 415:1030–1034.

von Bohlen Und Halbach O. 2011. Immunohistological markers for proliferative events, gliogenesis, and neurogenesis within the adult hippocampus. Cell Tissue Res. 345:1–19.

6.8. Figures with legends
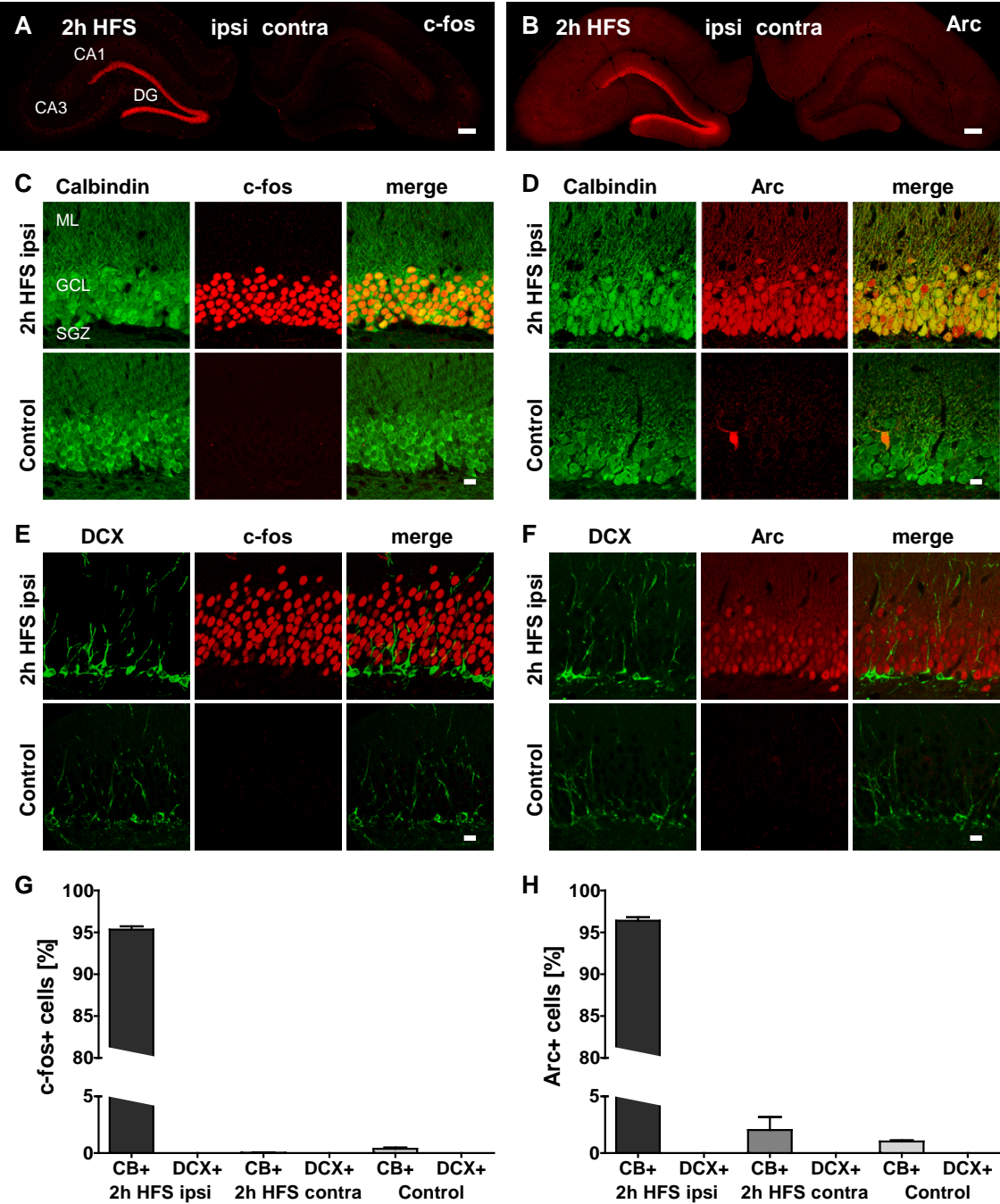
Figure 1 Expression of c-fos and Arc in hippocampal granule cells (GCs) following 2 h high frequency stimulation (HFS) of the perforant path. HFS induced the expression of markers for synaptic activity, c-fos **(A)** and synaptic plasticity, Arc **(B)** in the ipsilateral (ipsi) granule cell layer (GCL) of the dentate gyrus (DG). Co-labeling for calbindin (CB) a marker of mature GCs, revealed that most CB$^+$ cells were c-fos **(C, G)** and Arc **(D, H)** positive following 2 h HFS. Newly born GCs labeled with

124

doublecortin (DCX) did not exhibit c-fos **(E, G)** nor Arc **(F, H)**, neither in the control, nor ipsi- or contralateral (contra) sides following 2 h HFS. **G**, c-fos/CB 2 h HFS ipsi n = 27, contra n = 3, control n = 10; c-fos/DCX, 2 h HFS ipsi n = 3, contra n = 3, control n = 3. **H**, Arc/CB 2 h HFS ipsi n = 29, contra n = 6, control n = 8; Arc/DCX 2 h HFS ipsi n = 6, contra n = 6, control n = 3. Scale bars **A, B** 100 µm; **C, D, E, F** 10 µm. GCL, granule cell layer; ML, molecular layer; SGZ, subgranular zone.
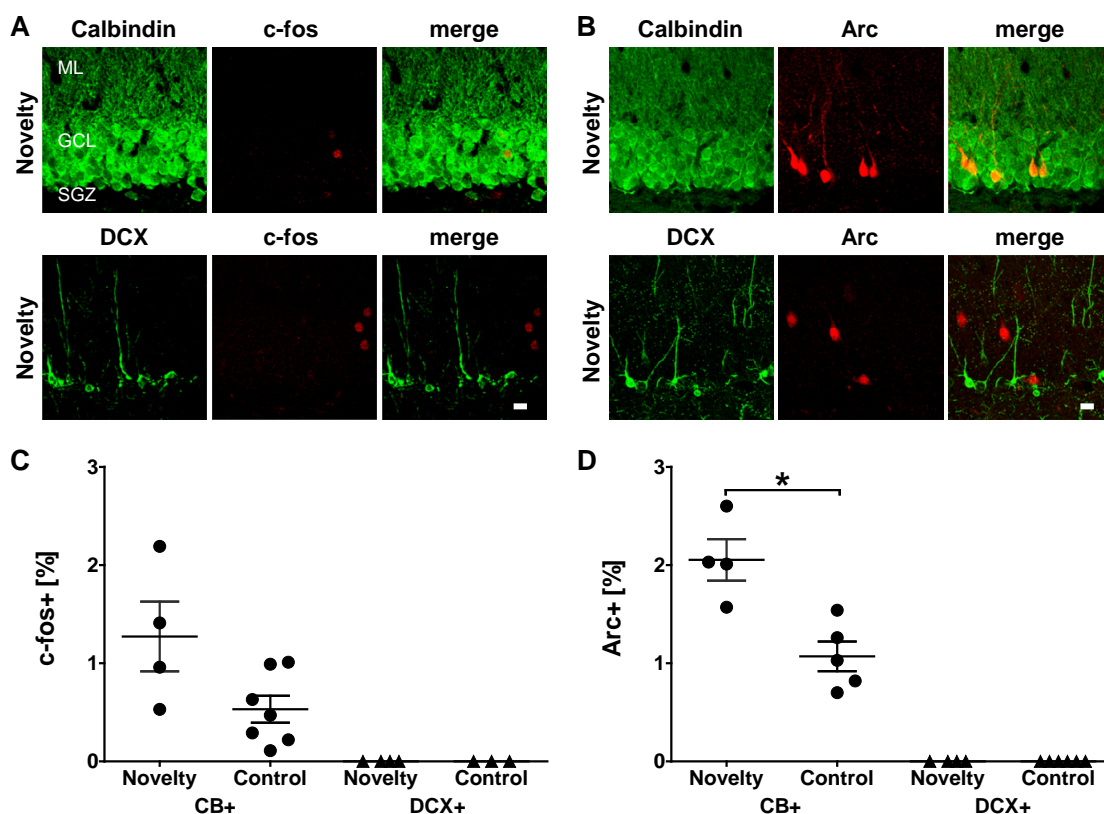
Figure 2 C-fos and Arc expression is not induced in young maturing GCs following novel environment exposure. Exposure to novel environment increased the number of c-fos⁺ **(A, C)** and Arc+ **(B, D)** mature calbindin (CB)⁺ GCs in awake rats, but failed to elicit any c-fos or Arc immunoreactivity in young maturing doublecortin (DCX)⁺ GCs of the subgranular zone (SGZ) and granule cell layer (GCL). **C**, c-fos/CB novelty n = 4, control n = 7; c-fos/DCX novelty n = 4, control n = 3. **D**, Arc/CB novelty n = 4, control n = 5; Arc/DCX novelty n = 4, control n = 6. Two-sided Wilcoxon rank-sum test: *$p < 0.05$. Scale bars 10 µm. GCL, granule cell layer; ML, molecular layer; SGZ, subgranular zone.
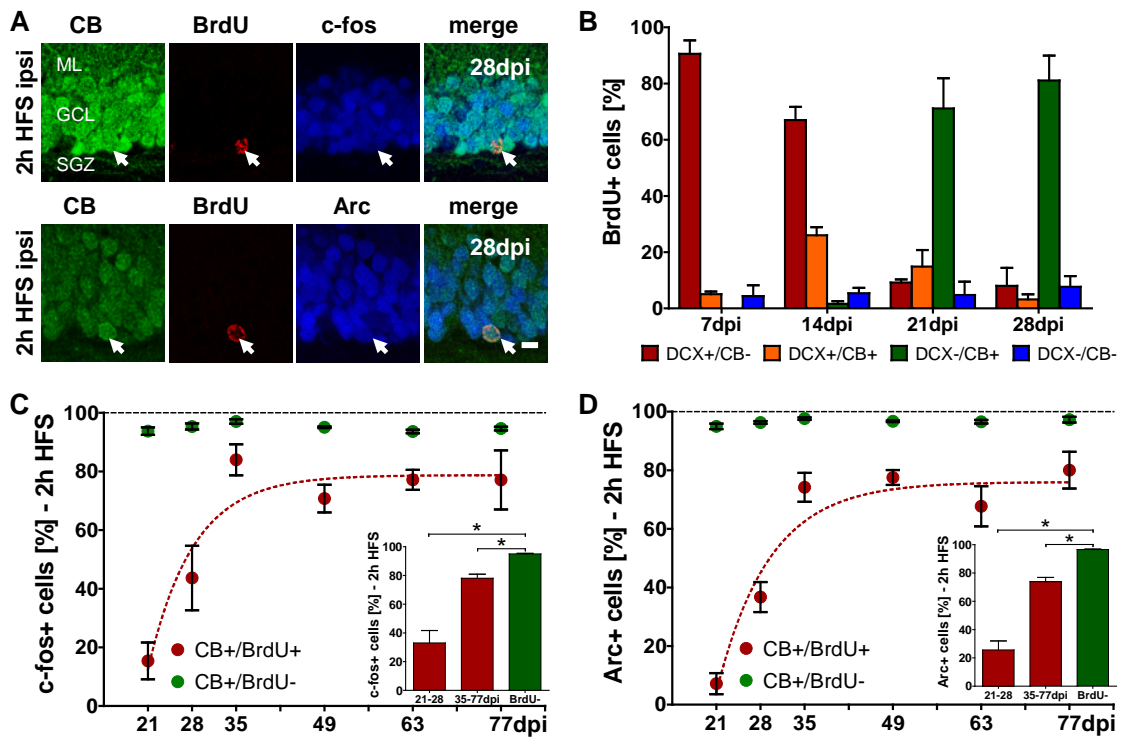
Figure 3 Increasing synaptic activation of maturing dentate GCs with age. Following 2 h HFS, c-fos and Arc immunoreactivity was detected in calbindin (CB)$^+$/BrdU$^+$ GCs 21 to 77 days post injection (dpi) of BrdU (**A**, 35 dpi). The expression of DCX and CB in maturing BrdU+-cells correlated strongly with cell age. During the first 14 days, the majority of cells were DCX$^+$, with an ongoing transition towards CB$^+$ cells and a decline of DCX$^+$ cells after 14 days **(B)**. 2 h HFS-induced expression of c-fos and Arc was present in BrdU$^+$/CB$^+$ GCs from 21 dpi on with increasing age and resulted in a plateau from 35 to 77 dpi **(C,D)**. Even at 77 dpi, only about 80 % of analyzed BrdU$^+$ cells exhibited c-fos **(C)** or Arc **(D)**. Younger (21 - 28 dpi) and older (35 - 77 dpi) BrdU$^+$ GCs expressed significantly less c-fos$^+$ and Arc$^+$ compared to the total population of BrdU$^-$ GCs following 2 h HFS **(insets in C and D)**. **B**, BrdU/CB/DCX, $n_{7\,dpi} = 3$, $n_{14\,dpi} = 3$, $n_{21\,dpi} = 3$, $n_{28\,dpi} = 5$; **C**, c-fos/BrdU/CB. $n_{21\,dpi} = 3$, $n_{28\,dpi} = 5$, $n_{35\,dpi} = 5$, $n_{49\,dpi} = 3$, $n_{63\,dpi} = 5$, $n_{77\,dpi} = 3$, $n_{21-28\,dpi} = 8$, $n_{35-77\,dpi} = 16$, $n_{BrdU-} = 24$; **D**, Arc/BrdU/CB, $n_{21\,dpi} = 3$, $n_{28\,dpi} = 5$, $n_{35\,dpi} = 4$, $n_{49\,dpi} = 3$, $n_{63\,dpi} = 5$, $n_{77\,dpi} = 3$, $n_{21-28\,dpi} = 8$, $n_{35-77\,dpi} = 15$, $n_{BrdU-} = 23$. Two-sided Wilcoxon rank-sum test: *p < 0.05. Scale bar 10 μm. GCL, granule cell layer; ML, molecular layer; SGZ, subgranular zone.
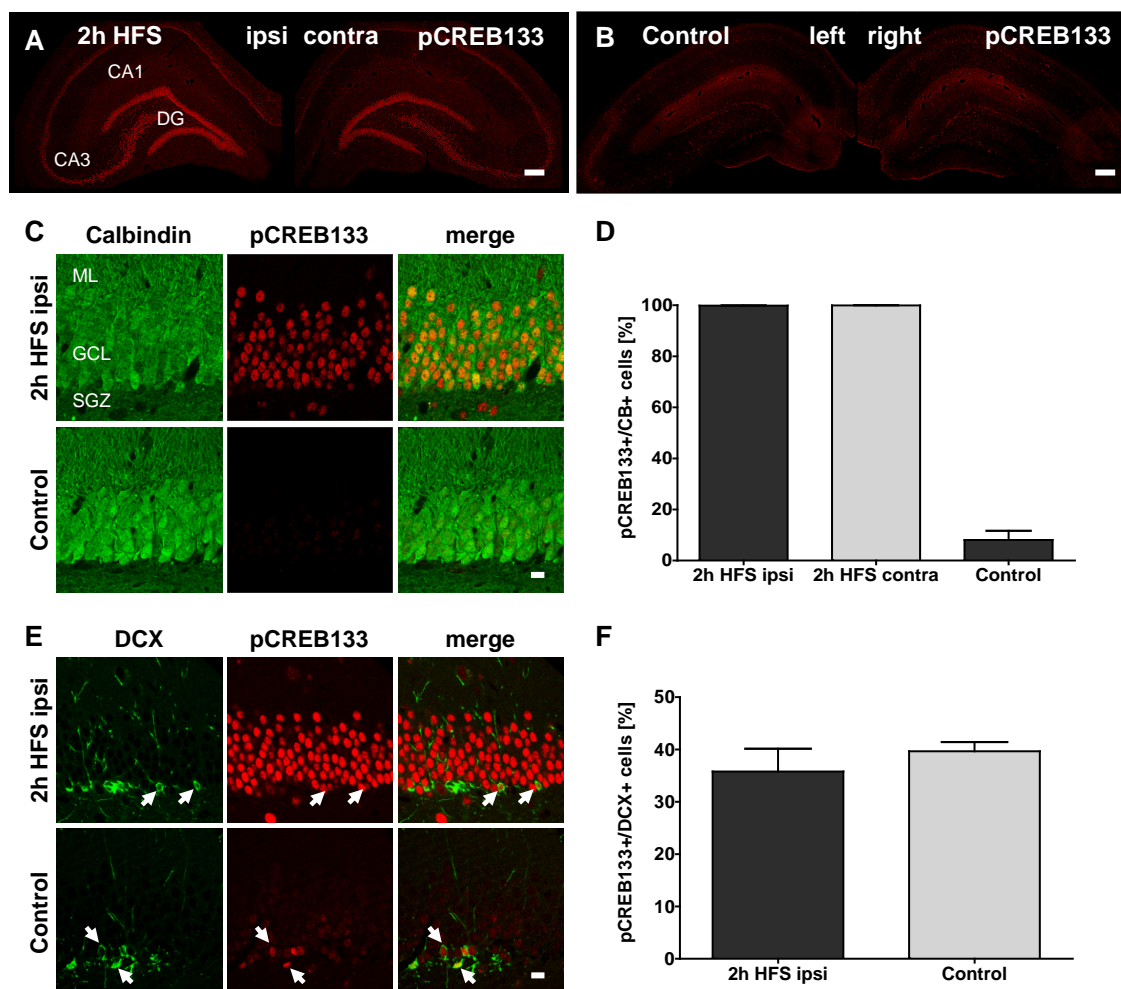
Figure 4 Increased pCREB133 expression in dentate GCs following HFS. 2 h HFS elicited bilateral pCREB133 expression in principal cells of the dentate gyrus (DG), and of the CA1 and CA3 hippocampal regions **(A, B)**. Whereas most CB[+] GCs in the ipsi- and contralateral granule cell layer (GCL) of the DG were pCREB133[+] following 2 h HFS, only a few cells showed weak pCREB133 immunoreactivity under control conditions **(C, D)**. pCREB133 was endogenously expressed in about 36 % of immature DCX^{+} cells of control animals, but was not further enhanced by 2 h HFS **(E, F)**. **D**, pCREB133/CB, n = 3; **F**, pCREB133/DCX, n = 3. Scale bars **A, B** 100 µm; **C, E** 10 µm. ML, molecular layer; SGZ, subgranular zone.
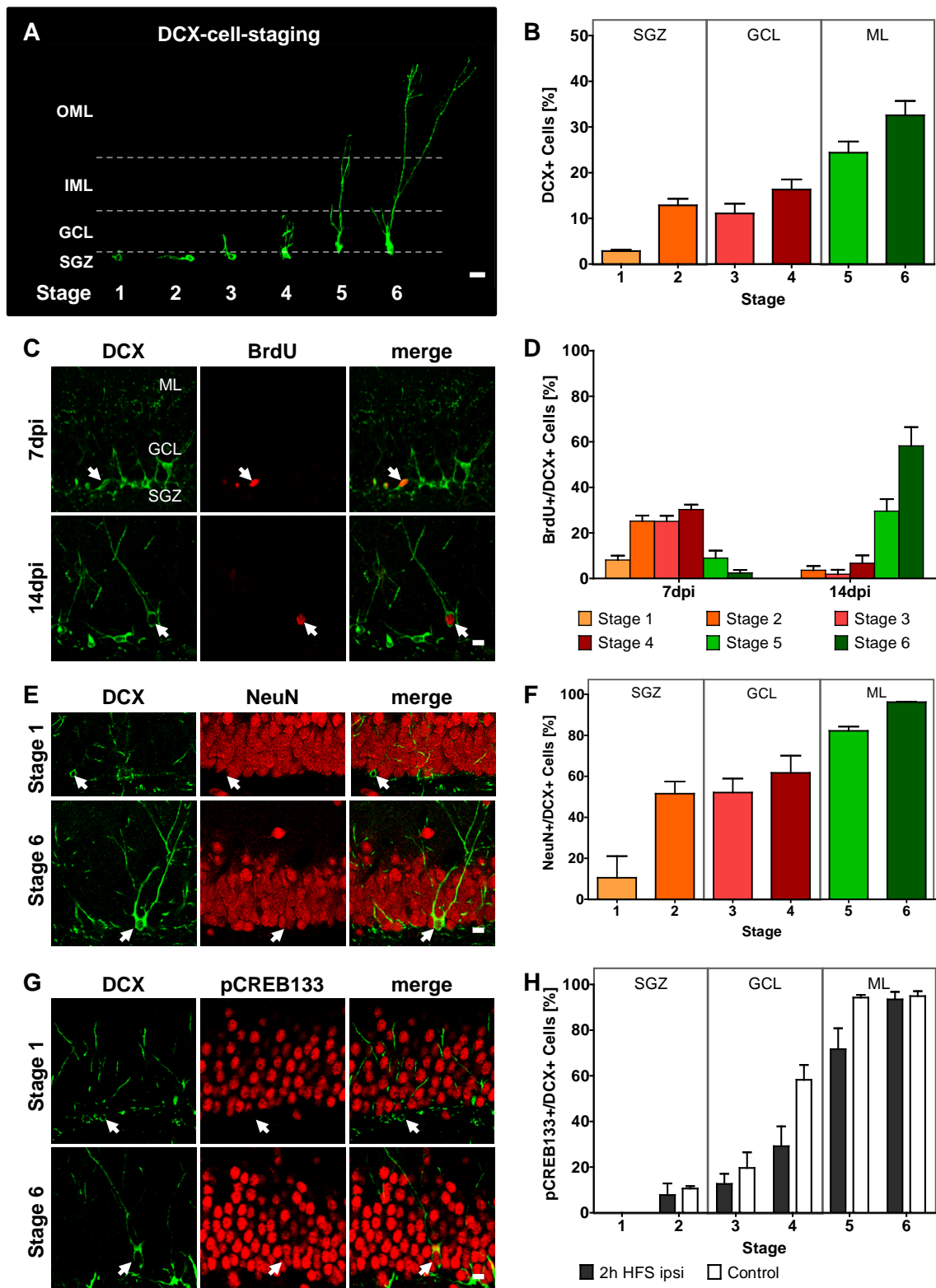
Figure 5 pCREB133 expression is not enhanced in maturing DCX+-cells following HFS. Young maturing adult newborn DCX[+] GCs were classified into 6 stages according to orientation and outgrowth of dendritic processes in the subgranular zone (SGZ; stage 1, no processes; stage 2, processes in the SGZ), the granule cell layer (GCL;

stage 3, inner half of the GCL; stage 4, outer half of the GCL), the inner molecular layer (IML, stage 5), and outer molecular layer (OML, stage 6; **A, B**). Classification of BrdU-tagged DCX$^+$ cells showed an age dependent progression of dendritic outgrowth within the first 14 days **(C, D)**. The neuronal marker Neuronal Nuclei (NeuN) was increasingly expressed with structural maturation and was expressed in all stage 6 DCX$^+$ cells **(E, F)**. pCREB133 expression in DCX$^+$ cells tightly correlated to structural maturation in unstimulated controls, but no indication of an enhancement of pCREB$^+$ following 2 h HFS was found at any DCX$^+$ stage **(G, H)**. **B, D, F, H,** n = 3 for all groups. Scale bars 10 µm. ML, molecular layer.
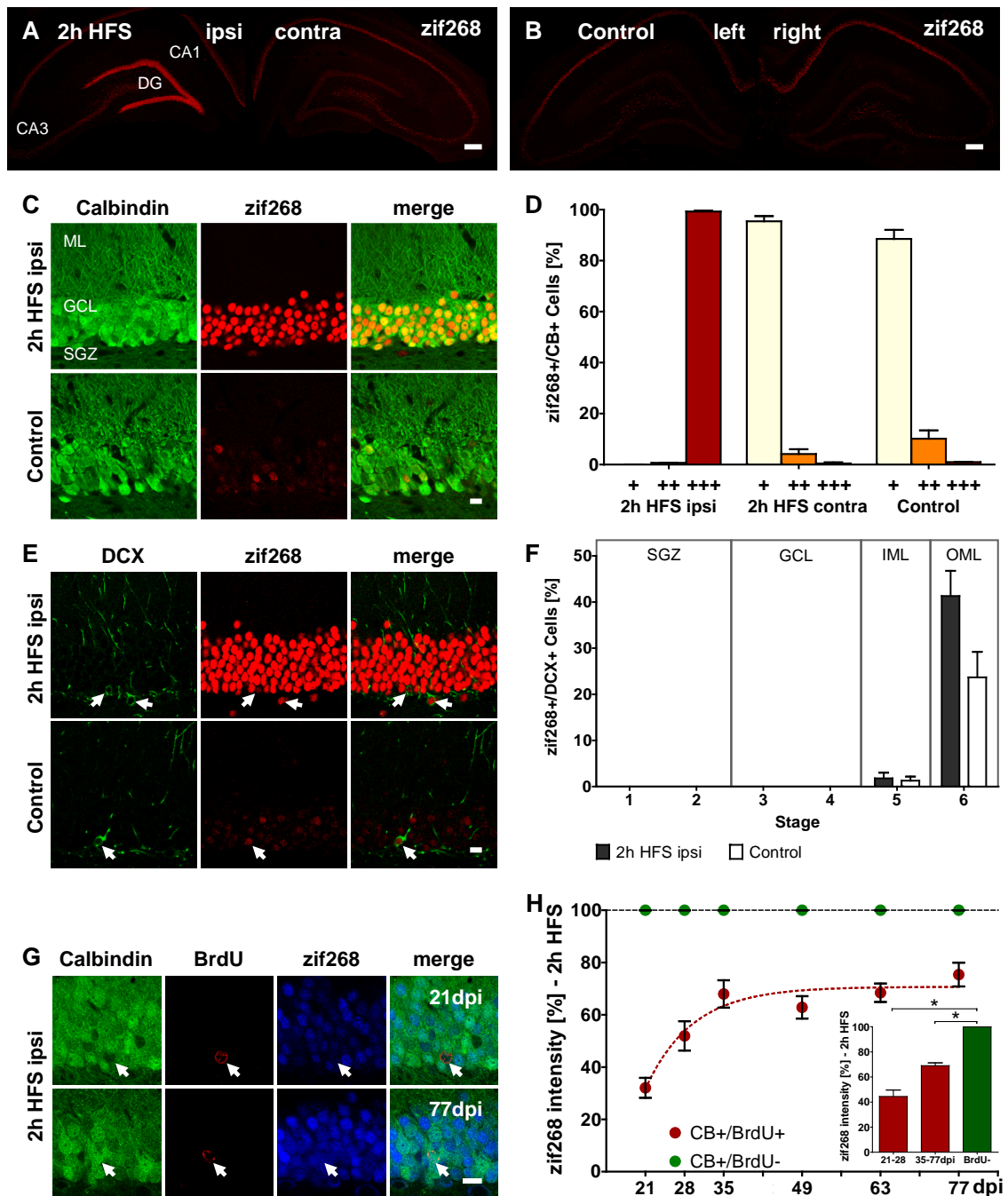
Figure 6 Increased zif268 expression in dentate GCs following HFS. 2 h HFS strongly increased ipsilateral zif268 expression in principal cells of the dentate gyrus (DG), and of the CA1 and CA3 hippocampal regions in comparison to a weak endogenous zif268 expression on the contralateral side, and in sham control sections **(A, B)**. After 2 h HFS, most CB⁺ GCs in the ipsilateral granule cell layer of the DG exhibited strong zif268 expression (+++), whereas contralateral and control GCs showed weak (+) or medium (++) zif268 immunoreactivity **(C, D)**. Endogenous zif268 expression was only present in stage 5 and stage 6 of young maturing DCX⁺ cells

(arrow-heads in E), and was not significantly enhanced following 2 h HFS (**E, F**; Two sample, two-sided Wilcoxon-test: stage 5 $p = 0.74$, stage 6 $p = 0.08$, $n_{2\,h\,HFS} = 6$, $n_{control} = 8$). Following 2 h HFS, a comparison between $CB^+/BrdU^+$ (**arrowheads in G**, 21 and 77 dpi BrdU), and $CB^+/BrdU^-$ cells revealed an age-correlated increase of zif268 immunofluorescence intensity in maturing CB+-cells reaching a plateau at 35 - 77 dpi (BrdU) with 70 % zif268 immunofluorescence intensity of the total population of $BrdU^-/CB^+$ cells **(G, H)**. Younger (21 - 28 dpi) and older (35 - 77 dpi) $BrdU^+$ GCs showed significantly less zif268 immunofluorescence intensity than $BrdU^-$ GCs **(inset in H)**. Zif268/BrdU/CB, $n_{21\,dpi} = 3$, $n_{28\,dpi} = 5$, $n_{35\,dpi} = 4$, $n_{49\,dpi} = 3$, $n_{63\,dpi} = 5$, $n_{77\,dpi} = 4$, $n_{21-28\,dpi} = 8$, $n_{35-77\,dpi} = 16$, $n_{BrdU-} = 24$. Two-sided Wilcoxon signed-rank test: *$p < 0.05$. Scale bars **A, B** 100 µm; **C, E, G** 10 µm. GCL, granule cell layer; IML, inner molecular layer; OML, outer molecular layer; SGZ, subgranular zone.
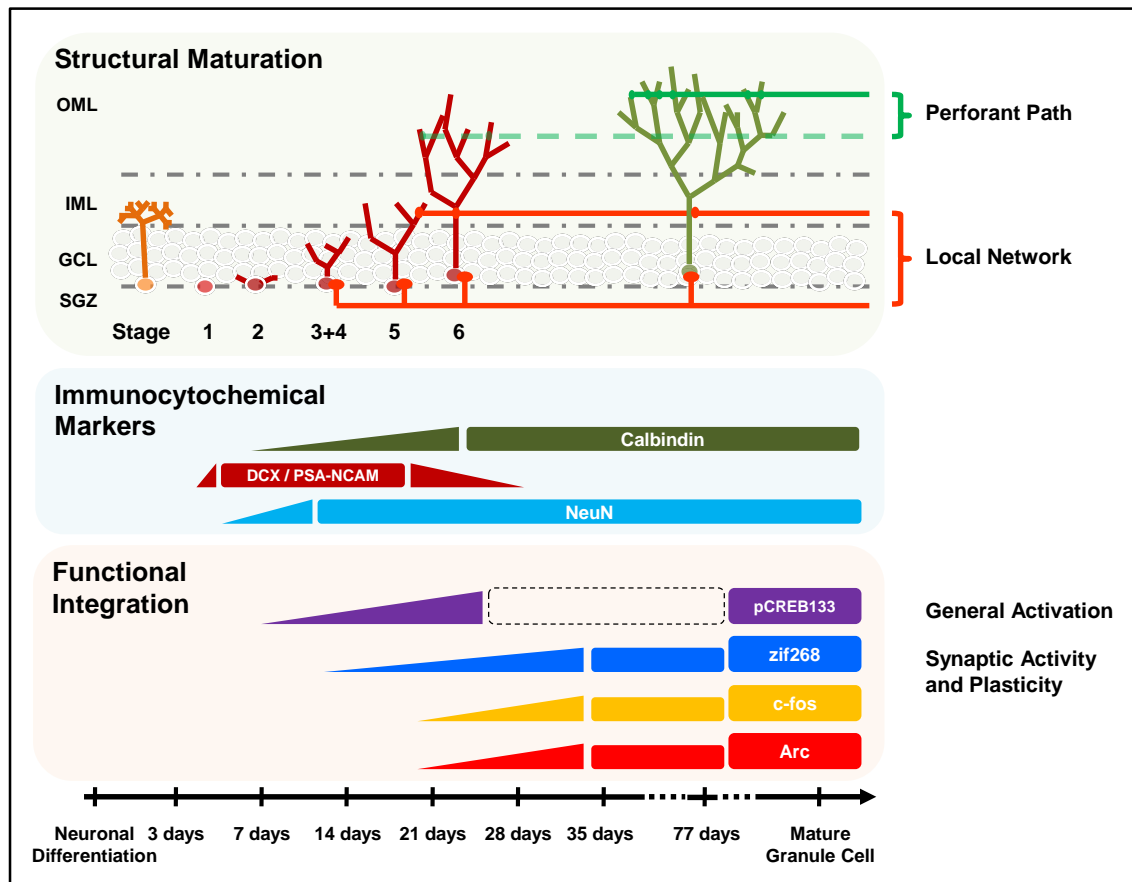
Figure 7 Schematic summary of the structural, chemical and functional maturation of newborn GCs in the adult hippocampus. Structural development of immature DCX$^+$ cells can be classified in 6 stages according to dendritic outgrowth. NeuN expression increases with structural maturation of DCX$^+$ cells. Calbindin expression starts in more mature DCX$^+$ cells and is increasingly present in older GCs. HFS-induced expression of immediate early genes as signs of synaptic activity and plasticity also increases with structural maturation and age and affects about 75 % of maturing GCs between 35 and 77 days. Besides a general close correspondence between structural maturation, chemical marker expression, functional integration, and age, some variability in the time course of individual cell development has to be taken into account. Morphological development, dendritic outgrowth into the DG, and synaptic connectivity **(top)**. Expression of characteristic immunocytochemical markers of immature and mature GCs **(middle)**. Expression of Immediate early genes (IEGs) following 2 h HFS **(bottom)**. GCL, granule cell layer; IML, inner molecular layer; OML, outer molecular layer; SGZ, subgranular zone.

7. Differential structural development of adult-born septal hippocampal granule cells in the Thy1-GFP mouse, nuclear size as a new index of maturation

Tijana Radic*[1], Omar Al-Qaisi*[1], **Tassilo Jungenitz*[1]**, Marcel Beining[1], Stephan W. Schwarzacher[#1]

[1]Institute of Clinical Neuroanatomy, NeuroScience Center, Goethe-University Frankfurt, Frankfurt am Main, Germany

*These Authors contributed equally to this work (joint-first coauthors)

[#]Author for correspondence: Stephan W. Schwarzacher, Institute of Clinical Neuroanatomy, Goethe-University, Theodor-Stern-Kai 7, D-60590 Frankfurt am Main, Phone: +49 (0)69 6301 6914, Fax: +49 (0)69 6301 6425, E-mail: schwarzacher@em.uni-frankfurt.de

7.1. Acknowledgements

7.2. Abstract

Adult neurogenesis is frequently studied in the mouse hippocampus. We examined the morphological development of adult-born, immature granule cells in the suprapyramidal blade of the septal dentate gyrus over the period of 7 - 77 days after mitosis with BrdU-labeling in 6-weeks-old male Thy1-GFP mice. As Thy1-GFP expression was restricted to maturated granule cells, it was combined with doublecortin-immunolabeling of immature granule cells. We developed a novel classification system that is easily applicable and enables objective and direct categorization of newborn granule cells based on the degree of dendritic development in relation to the layer specificity of the dentate gyrus. The structural development of adult-generated granule cells was correlated with age, albeit with notable differences in the time course of development between individual cells. In addition, the size of the nucleus, immunolabeled with the granule cell specific marker Prospero-related homeobox 1 gene, was a stable indicator of the degree of a cell's structural maturation and could be used as a straightforward parameter of granule cell development. Therefore, further studies could employ our doublecortin-staging system and nuclear size measurement to perform investigations of morphological development in combination with functional studies of adult-born granule cells. Furthermore, the Thy1-GFP transgenic mouse model can be used as an additional investigation tool because the reporter gene labels granule cells that are 4 weeks or older, while very young cells could be visualized through the immature marker doublecortin. This will enable comparison studies regarding the structure and function between young immature and older matured granule cells.

7.3. Introduction

Adult neurogenesis is a process in which new neurons are generated from neural stem cells (NSCs) in the adult brain. In the adult hippocampus of mammals, including humans, dentate granule cells (DGCs) are continually generated in the subgranular zone (SGZ) and settle within the granule cell layer (GCL) of the dentate gyrus (Altman and Das, 1967; Zhao et al., 2008; Ming and Song, 2011; Spalding et al., 2013). Although the majority of adult-born DGCs in rodents die within the first month (Dayer et al., 2003; Snyder et al., 2009a), the surviving cells become structurally and functionally integrated into the existing cellular network and thus contribute to hippocampus-dependent functions involving learning, memory, and emotion (Madsen et al., 2003; Clelland et al., 2009; Deng et al., 2010). More specifically, these neurons appear to play an essential part in spatial memory and pattern separation (Clelland et al., 2009; Jessberger et al., 2009; Creer et al., 2010; Nakashiba et al., 2012). Dysfunction of the adult neurogenesis process has been linked to neurological and psychiatric diseases, including epilepsy, Alzheimer's disease, and depression (Braun and Jessberger, 2014). Detailed understanding of developmental processes and mechanisms involved in adult neurogenesis is fundamental to enable therapeutic strategies for neuronal loss and brain repair (Lie et al., 2004; Braun and Jessberger, 2014).

Growth and maturation of newly born neurons in the adult hippocampus show much similarity to the embryonic development of DGCs (Espósito et al., 2005; Ming and Song, 2011). However, adult-born DGCs seem to mature at a slower pace (Overstreet-Wadiche et al., 2006; Zhao et al., 2006) and need several weeks or longer to become functionally integrated (van Praag et al., 2002; Vivar and van Praag, 2013; Jungenitz et al., 2014). There are still open questions in relation to the time course of development and functional activity of adult-generated DGCs, as some studies appear to generate contradicting results regarding the involvement of newborn DGCs in the existing cellular network (for review see Kim et al., 2011; Vivar and van Praag, 2013). This could be due to a high variability in the neuronal developmental course and the

regulating factors involved in it. In order to fully understand the developmental process and characteristics that are necessary for DGCs to become integrated into the hippocampal network, a more detailed examination of the cells' maturation process is essential.

Detailed structural information of neurons can be acquired in the transgenic Thy1-GFP mouse model in which the reporter gene GFP is expressed in approximately 10 % of all DGCs (Feng et al., 2000). It has been demonstrated that labeled cells do not differ in morphology or function compared to DGCs that do not express Thy1-GFP (Vuksic et al., 2008). In the present study, we show that the Thy1-GFP mouse model could be used to investigate the structure of DGCs beyond the maturation phase and thus enable comparative studies of mature and newly-generated DGCs.

Recently, we have demonstrated that the speed of structural development varies substantially between individual adult-born DGCs in the rat (Jungenitz et al., 2014). We introduced a 6-stage classification system of structural maturation based on morphological characteristics of cells that express the immature neuronal marker doublecortin (DCX). In the current study, we adapted the staging method to closely examine the structural development of adult-generated DGCs in mice and investigate the relationships between structural maturation and age, as well as cell position and nuclear size. Our results reveal a general correlation between structural development and age as well as a considerable variability in growth dynamics between individual cells.

In addition, we found that the size of a cell's nucleus is indicative of its age and degree of structural maturation and could therefore be used as an additional parameter for cell development. Hence, our detailed evaluation of granule cell morphological maturation provide a structural basis and novel techniques for future studies of adult-born DGC development and integration into the mature hippocampal network.

7.4. Results

Doublecortin-labeling in dentate granule cells does not co-localize with GFP expression in the Thy1-GFP mouse

In the present study, adult neurogenesis was investigated in the transgenic Thy1-GFP mouse model in which approximately 10 % of all dentate granule cells (DGCs) express GFP. These cells presumably do not differ in morphology or function compared to unlabeled DGCs (Vuksic et al., 2008). In order to evaluate to what extent Thy1-GFP might be present in maturing adult-born DGCs, we performed immunocytochemistry with doublecortin (DCX), a marker for immature neurons (Francis et al., 1999; von Bohlen Und Halbach, 2007) and Prox1, a specific granule cell marker that is expressed early on and throughout the development of DGCs (Galeeva et al., 2007; Lavado and Oliver, 2007; Iwano et al., 2012). Prox1 was present in all detectable granule cell nuclei throughout the entire granule cell layer (GCL) and in the DCX$^+$ cells. The somata of DCX$^+$ cells were concentrated in the subgranular zone (SGZ) with dendritic processes extending toward the molecular layer (ML). In addition, Thy1-GFP expression was observed in a subset of DGCs, but there was no co-localization of Thy1-GFP and DCX. All Thy1-GFP$^+$ cells of the GCL also expressed Prox1 **(Fig. 1)**. Even though Thy1-GFP and Prox1 are shown in the same color, the Thy1-GFP labeling was clearly distinguishable from the Prox1 staining, as Thy1-GFP intensely labeled the whole cell including the soma and dendritic processes as opposed to Prox1 which only labels the cell nuclei. The combination of these two markers in the same color channel did not pose any problems during analysis.

The first Thy1-GFP/BrdU$^+$ cell was detected at 28 dpi. Overall, we found that 4.86 % ± 2.48 (n = 15 animals) of BrdU-labeled cells between 28 and 77 dpi were Thy1-GFP positive. Taken together, our data indicate that, in the present mouse model, Thy1-GFP expression is only present in maturated DGCs. This offers the possibility to perform structural studies on two non-overlapping populations of immature DCX$^+$ DGCs and mature Thy1-GFP$^+$ DGCs in the same object simultaneously.

Adult-born dentate granule cells show limited survival rate

Next, we wanted to determine the proliferation and survival rates of newborn DGCs and, in particular, the population of DCX$^+$ cells. The mitotic marker BrdU was administered to adult Thy1-GFP mice in order to label newborn cells. Co-immunostainings against BrdU, as well as the granule cell marker Prox1, and the immature neuronal marker DCX were performed between 7 and 77 days following BrdU injection. **Figure 2A and B** shows examples of newborn DGCs labeled with BrdU at 7 and 77 dpi, respectively. We calculated the number of BrdU$^+$ DGCs as a percentage of the number of BrdU/Prox1$^+$ cells at 7 dpi **(Fig. 2C)**. Our results reveal that the number of newly born neurons continuously decreased until 35 dpi (14.36 % ± 6.04; **see Fig. 2C**). At 14 dpi there were 64.89 % ± 9.32; at 21 dpi, 56.91 % ± 10.15; and at 28 dpi, 39.36 % ± 5.07 BrdU$^+$ cells. After 35 dpi, the number of newborn DGCs remained constant until 77 dpi.

Similarly, there was a steady decline in the number of DCX$^+$ newborn DGCs between 7 dpi (91.32 ± 3.49 %) and 28 dpi (35.39 ± 1.06 %). From 35 dpi on, no BrdU/DCX$^+$ cells could be detected **(Fig. 2E)**. This suggests that during the first 5 weeks after birth only a fraction of newly generated DGCs are selected for survival and eventual functional integration. Those that do survive undergo a process of maturation beyond the phase of DCX-expression.

We did not find Thy1-GFP expression in BrdU$^+$ cells from 7 - 21 dpi. At later time points (28 - 77 dpi), co-labeled Thy1-GFP/BrdU$^+$ DGCs were occasionally found, at very limited numbers unsuitable for further analysis. This indicates that Thy1-GFP expression may be present from day 28 in aging DGCs.

Structural maturation of Doublecortin-expressing dentate granule cells increases with cell age

In order to analyze the degree and age dependency of structural maturation of newly formed DGCs, we further examined DCX/BrdU$^+$ newborn DGCs at different time points between 7 and 28 dpi, i.e. the phase of DCX-expression. We adapted a DCX staging system that was previously established in the rat (Jungenitz et al., 2014) to our mouse model. DCX$^+$ cells were categorized into

six different stages based on the extent of dendritic arborization and soma position. A DCX$^+$ granule neuron was classified as stage 1 when its soma was located in the SGZ and lacked dendritic processes. When a cell exhibited one or two short processes that were located within the SGZ, it was considered to be stage 2. Once the principle dendrite of a cell extended into the inner half of the GCL, the cell was categorized as stage 3. Stage 4 was determined when the leading dendrite of the cell reached the outer half of the GCL; stage 5 when the leading dendrite extended into the inner molecular layer (IML); and stage 6 when the leading dendrite extended into the outer molecular layer (OML; **see Fig. 3A**).

We found that the degree of structural maturation increased with cell age in the Thy1-GFP mouse model **(Fig. 3B and C)**. At 7 dpi, a substantial number of DCX$^+$ cells were grouped in stage 1 (29.21 ± 5.57 %) or stage 2 (30.56 ± 3.10 %), while only a small number of cells were in stage 5 (6.83 ± 2.57 %) or stage 6 (4.05 ± 2.12 %). In contrast, most DCX$^+$ granule neurons at 14 dpi were classified as stage 5 (60.20 ± 12.67 %) or stage 6 (20.17 ± 5.31 %). At 21 dpi, the vast majority of DCX$^+$ DGCs were at stage 5 (20.56 ± 12.03 %) or stage 6 (72.78 ± 13.62 %). By 28 dpi, 91.67 ± 14.43 % of the DCX$^+$ cells were at stage 6. However, at this time point, we also found cells at stage 3 (8.33 ± 8.33 %). The distribution of DCX$^+$ cell ages according to each stage demonstrated the prevalence of DCX stages 1 - 4 at 7 dpi (DCX stage 1: 84.02 %, stage 2: 76.09 %, stage 3: 58.71 % and stage 4: 62.06 %) and DCX stages 5 - 6 at 14 (DCX stage 5: 68.74 %, stage 6: 10.69 %), 21 (DCX stage 5: 23.47 %, stage 6: 38.58 %), and 28 dpi (DCX stage 6: 48.59 %; **Fig. 3D**). DCX stages 1 - 3 and 4 - 6 were pooled and revealed that 72.02 % of DCX$^+$ cells of stages 1 - 3 were at 7 dpi, whereas DCX$^+$ cells of stages 4 - 6 were essentially evenly distributed between 14 (28.96 %), 21 (32.19 %), and 28 dpi (30.88 %; **Fig 3E**). No DCX$^+$ cells were observed after 28 dpi.

Generally, the findings suggest that the degree of structural maturation of DCX$^+$ cells increases with cell age. However, since we identified cells of all structural maturation stages at 7, 14, and 21 dpi, there appeared to be marked

differences in the course of maturation between individual neurons within this time frame.

Nuclear size of newborn DGCs is positively correlated with structural maturation and cell age

To introduce an additional indicator of cell maturation, we examined the relationship between a cell's degree of maturation with the size of its nucleus. Since Prox1 is a specific marker for granule cell nuclei, the labeling was used to determine the nuclear sizes of DCX$^+$ DGCs of different stages according to the DCX staging system. **Figure 4A** depicts 21-days-old Prox1/DCX$^+$ cells at stage 1 (upper panel) and stage 6 (lower panel). Our results indicate that nuclear size increased with each consecutive stage **(Fig. 4B)**. DCX$^+$ DGCs that were classified as stage 1 had on average the smallest nuclei, while stage 6 cells had the largest (stage 1: 11.79 ± 1.06 µm², n = 5; stage 2: 17.23 ± 1.05 µm², n = 7; stage 3: 21.05 ± 1.49 µm², n = 4; stage 4: 24.15 ± 1.97 µm², n = 6; stage 5: 30.56 ± 2.75 µm², n = 9; stage 6: 42.08 ± 3.48 µm², n = 11). Statistical analysis revealed significant differences in nuclear size between stages 1 and 6 (Kruskal-Wallis Dunn's multiple comparison test, $P < 0.05$), as well as between stages 1 and 5 ($P < 0.05$); stages 2 and 6 ($P < 0.05$); and stages 3 and 6 ($P < 0.05$). Subsequently, we investigated whether the nuclear size of DGCs also related to cell age. We found that nuclear size was smallest at 7 dpi (18.75 ± 0.61 µm²) and continued to increase with age until 35 dpi (47.03 ± 1.54 µm²) when it reached a plateau **(Fig. 4C)**. Consequently, our data indicate that the size of a DGC nucleus could be used as a distinct marker of cell maturation and age.

Next, we wanted to know to what extent the nuclear size measurement of a given DGC can predict its structural (DCX) stage and cell age. Nuclear size data from all animals were pooled and are shown as a dot plot of single cells in **Fig. 5A and D** to highlight the variability of the nuclear size in DCX stages and across all cell ages. The data were further pooled into an early and a late structural phase and cell age **(Fig. 5B and E)**, considering DCX stage 1 - 3 and 7 - 14 dpi as an early phase and DCX stage 4 - 6 and 21 - 77 dpi as a late

phase. The mean nuclear sizes of each phase were determined (DCX stage early phase 16.16 ± 0.53 µm², late phase 33.00 ± 1.20 µm²; early cell age 20.95 ± 0.47 µm², late cell age 41.00 ± 0.84 µm²) and used to calculate the equidistance between early and late phases (DCX stage: 24.58 µm², cell age: 30.97 µm²), which was then used as a threshold to discriminate between early and late phases **(shown as red dashed lines in Fig. 5B and E)**. Based on that threshold, single cells were classified into 3 different types of predictive values: true positive, false negative and false positive **(Fig. 5C and F, see also methods for details)**. The amount of true positive classified cells and therefore the likelihood of a true prediction was about 70 % (DCX stage 1 - 3: 71.57 %, 4 - 6: 72.64 %; age 7 - 14 dpi: 71.43 %, 21 - 77 dpi: 70.11 %).

In order to validate the prediction efficiency, an additional blinded study was performed (data not shown) in which the cell age of single cells were manually predicted from measuring the nuclear size. Samples for the early phase were selected from 7 and 14 dpi (animals = 6, cells = 109) and for the late phase from 21, 35, 63 and 77 dpi (animals = 11, cells = 74). The assignment of cells was based on the threshold (cell age: 30.97 µm²) calculated from the full dataset **(Fig. 5)**. The prediction from this blinded study showed a reliability of 72.5 % for the early and 65.63 % for the late cell age (true positive assignments). In summary, our calculations show that nuclear size measurement can be used as a tool to discriminate between early and late structural stages and cell ages with an accuracy of about 70 %, indicating a new, valuable method to categorize developing DGCs.

Doublecortin-expressing adult newborn dentate granule cells are located in the inner part of the granule cell layer irrespective of maturation stage and age

Previous studies have shown that young granule cells are primarily located in the SGZ and the inner part of the GCL closer to the hilus, while older DGCs are typically situated in the outer layers of the GCL, closer to the ML (Muramatsu et al., 2007; Mathews et al., 2010). Therefore, we subsequently investigated the positions of DCX[+] somata within the GCL in relation to the cells' structural

maturation and age. Triple stainings with Prox1, BrdU, and DCX enabled the analysis of cell position, stage and age of DCX$^+$ granule cells. Cell position was defined as the shortest distance from the lower border of the Prox1$^+$ nucleus to the GCL/SGZ border normalized to the thickness of the GCL (i.e. distance from the SGZ to the IML). Our results revealed that the majority of DCX$^+$ newborn DGCs were located in the inner half of the GCL notwithstanding the current structural stage, although cells in stages 5 and 6 appeared to be more dispersed so that individual cells could be found in more distal parts of the GCL **(Fig. 4D)**. In addition, cell age did not appear to be correlated with the position of newborn DGCs between the ages 7 - 77 days. Most cells were located within the inner part of the GCL, close to the SGZ **(Fig. 4E)**. Hence, the relationship between age and cell position described previously (Muramatsu et al., 2007; Mathews et al., 2010) may only pertain to longer time courses or early (embryonic to early postnatal) developmental phases.

7.5. Discussion

In the current study we examined the structural development of newly born dentate granule cells with a focus on a specific region of the dentate gyrus, namely the suprapyramidal blade of the septal hippocampus in Thy1-GFP mice. However, various structural and functional differences have been described throughout the septotemporal axis of the DG as well as between the supra- and infrapyramidal blades (Snyder et al., 2009b, 2012; Fanselow and Dong, 2010; Piatti et al., 2011). It has been shown that the rate of adult neurogenesis is greater in the septal DG, and the adult-born DGCs in that region display faster morphological and electrophysiological maturation compared with the temporal DG (Snyder et al., 2009b, 2012; Piatti et al., 2011). In addition, adult-born DGCs in the suprapyramidal blade exhibit a greater rate of survival compared with those located in the infrapyramidal blade (Snyder et al., 2012). The greater survival may be due to greater neuronal activity in suprapyramidal neurons (Chawla et al., 2005). Additional studies would be necessary to investigate and

compare the course of structural maturation in the infrapyramidal blade and the temporal DG.

We demonstrated that Thy1-GFP does not co-localize with the immature neuronal marker DCX and hence labels only mature DGCs. This finding makes this mouse model interesting for studies concerning cell reconstruction and direct comparisons between immature and mature DGCs. Chemical markers such as BrdU, Prox1, and DCX were used to determine post-mitotic cell age, survival rates over time, and phase of neuronal development.

All animals were injected with BrdU at the age of six weeks, a time point when mice have reached fertility but may still be considered juvenile or adolescent until 2 months of age. Therefore, all analyzed cells were generated in relatively young animals. However, brain samples were harvested and examined at different time points while the animals were either adolescent (7 - 14 dpi) or young adult (21 - 77 dpi). As a result, there is a possibility that the transition between late adolescence and adulthood may have an effect on granule cell development. However, it is difficult to determine whether and how the degree of maturity of the animal past the age of six weeks might influence the course of development of individual newly born cells. By the age of six weeks, the brain development of the animals is completed and the hippocampal circuitry is established, but functional and behavioral studies showed differences in memory processing between juvenile (1 - 2 months) and early adult (2 - 6 months) mice (Martinez-Canabal et al., 2013).

We used DCX, which is expressed in cell somata as well as dendrites, to classify newborn DGCs into distinct structural maturation stages and thus examine relationships between structural maturation and cell age, nuclear size, and position within the GCL. While our results revealed a distinct correlation between the age and the structural development of newly born DCX$^+$ DGCs, we found that the time in which individual neurons reach different levels of maturation varied to a large extent. In addition, nuclear size was positively correlated with both cell age and degree of structural maturation, suggesting that the size of the nucleus could be used as an additional indicator of cell

development. Finally, we observed that cell position of DCX$^+$ DGCs did not vary with cell age nor maturation stage because the majority of those cells were located within the inner layer of the GCL close to the SGZ. Our findings reveal essential structural characteristics of newborn DGCs that ought to be considered in functional studies of adult neurogenesis in mice.

Survival of newly born dentate granule cells

To determine survival rates of newly born DGCs, we marked newborn cells by administering BrdU in a single injection of 200 mg/kg body weight. This particular administration protocol has been shown to yield maximal labeling of mitotic cells while posing a low toxicity risk in (Cameron and Mckay, 2001; Mandyam et al., 2007; Snyder et al., 2009a). We combined BrdU-labeling with the granule cell marker Prox1 to allow for specific evaluation of DGC neurogenesis (Lavado and Oliver, 2007; Iwano et al., 2012), excluding BrdU-labeling of newly generated interneurons, glial cells, or vascular tissue cells. Prox1 has been shown to be a specific marker for granule cells that is expressed throughout all developmental stages of DGCs including the phase of DCX expression. The transcription factor Prox1 plays an important role in granule cell differentiation and survival, particularly during the early stages of development (Lavado and Oliver, 2007; Lavado et al., 2010; Karalay et al., 2011).

Consistent with previous studies (Kuhn et al., 1996; Kempermann et al., 2003; Snyder et al., 2009a), we found that adult born DGC survival rate decreases steadily until 35 dpi and a constant number of surviving cells at 49, 63, and 77 dpi **(Fig. 2C)**. Our results are in line with previous findings that demonstrated a 70 % decrease in BrdU$^+$ cell number between 1 and 4 weeks following BrdU injection in mice. The number of surviving cells was not further reduced at 10 weeks following BrdU treatment (Snyder et al., 2009a). Snyder et al. (2009) have established the rate of newborn cell loss over time in the mouse based on stereological analyses, a method that takes hippocampal volume changes into account, and enables generation of absolute cell numbers (Snyder et al., 2009a). Nevertheless, our results based on relative cell numbers are

consistent with this work. This further supports the notion that the first 5 weeks after mitosis represent a critical period of newborn DGC survival and development.

Time course of adult-born dentate granule cell structural maturation varies between individual cells

The period of DCX expression encompasses the phases of development from neuronal progenitor to the phase when dendrites of maturing granule cells reach the OML and form functional synapses with entorhinal fibers, the main afferents to the granule cells (Espósito et al., 2005; Toni et al., 2007). DCX is expressed in the entire cell, including all neurites, and has been shown to be an accurate marker of newly born DGCs that acts as an indicator of adult neurogenesis and its modulation (Brown et al., 2003; Couillard-despres et al., 2005). We developed a novel staging system and classified individual cells into six stages of structural maturation.

Whereas stage 1 and 2 cells represent progenitors and early immature granule cells of the SGZ (Kempermann et al., 2004), stage 3 and 4 cells exhibit dendrites that reach the inner and outer part of the GCL, respectively. These stages represent the phase when newborn DGCs typically start to receive synaptic input from axons of GABAergic interneurons (Espósito et al., 2005). The GABAergic input leads to depolarization in these cells and has been shown to play an essential role in the survival and further maturation of granule cells (Bhattacharyya et al., 2008; Jagasia et al., 2009). Stage 5 cells are characterized by dendrites that extend into the IML where they can establish synaptic contacts with glutamatergic associational/commissural fibers of mossy cells that project from ipsi- and contralateral hilar regions (Espósito et al., 2005; Vivar et al., 2012; Chancey et al., 2014). Most DCX$^+$ newborn DGCs have reached stage 5 at 14 - 21 dpi which corresponds to the period of intense dendritic spine formation from day 16 post birth on (Espósito et al., 2005; Zhao et al., 2006; Toni et al., 2007; Ming and Song, 2011). However, we also still observed cells of stages 1 - 4 until 21 dpi, as well as cells of stage 3 at 28 dpi, which demonstrates individual differences in the time course of development

between cells. This may also be a crucial period in which cell death occurs if newborn cells do not establish a sufficient amount of synaptic contacts. Finally, stage 6 DCX cells exhibit an elaborate dendritic tree that extends into the OML, where the main afferent synaptic input is received from entorhinal fibers (Espósito et al., 2005; Vivar et al., 2012). Although the majority of stage 6 cells were discovered at 21 - 28 dpi, the first stage 6 cells could already be found at 7 dpi. This indicates that some DGCs develop very rapidly and may contact entorhinal fibers shortly after birth. Despite the high variability, some predictions can be estimated regarding the DCX cell age based on the DCX cell stage. For instance, about 70 % of the early DCX cell stages 1 - 3 were found to belong to the group of DCX^{+} cells at 7 dpi, whereas about 90 % of the late DCX cell stages 4 - 6 belonged to groups 14, 21, and 28 dpi.

Previous studies have presented temporal analyses of structural development of newborn DGCs (Espósito et al., 2005; Zhao et al., 2006). In these studies, adult generated cells were labeled with a retroviral vector and examined at different time points following virus injection. The findings show a general line of increasing dendritic trees and maturation of newborn DGCs over time (Espósito et al., 2005; Zhao et al., 2006). Zhao, et al. (2006) examined the morphological development of newborn neurons in postnatal and adult mouse brains. They analyzed the time course of dendritic and axonal outgrowth as well as spine formation and found that adult-generated DGCs show a slower developmental progression than cells born during an early postnatal period (P10). As a result, they defined four age-dependent stages of granule cell maturation: Stage A (0 - 3 dpi) during which polarization, migration and initial morphogenesis begins; Stage B (3 - 16 dpi) that represents major dendritic and axonal growth; Stage C (starting at 16 dpi) in which spines begin to be formed; and Stage D (starting shortly after spine formation during stage C) that is marked by synaptic modification and presence of mushroom spines (Zhao et al., 2006). In comparison, our results show that the level of structural maturation at any given time point is actually quite diverse. Consistent with our findings, Plümpe, et al. (2006) reported that structural maturation of DCX[+] newborn DGCs varied between 3 days and several weeks and was not altered by

regulators of cell proliferation (Plümpe et al., 2006). It should be taken into account that our results are based on DCX immunoreactivity and may therefore differ from retrovirally labeled cells. However, DCX expression overlaps extensively with cytoskeletal proteins such as β III tubulin and is particularly present in distal parts of dendritic processes starting in early immature neurons and persisting throughout the time period of DCX expression (Francis et al., 1999). Because our staging is based on how far the leading dendrite reaches into the GCL and ML, DCX labeling appears to be a practical fit for our analysis and thus any limitations regarding a nonhomogeneous distribution of the labeling in proximal dendrites would not distort our findings. Nevertheless, our results support the idea that the process of DGC maturation does not abide by a general temporal order but is influenced by more specific regulatory factors.

Our findings could have several implications in relation to the functional development of newly born DGCs, even though our DCX staging system is solely based on the structural extent of dendritic processes towards the different layers of the dentate gyrus, and does not specify functional stages. Recent studies revealed a number of differences in respect to the time period when newborn DGCs become integrated into the existing hippocampal network. While a few studies have shown that newborn DGCs received synaptic glutamatergic input at 2 - 3 weeks in the mouse (Espósito et al., 2005; Zhao et al., 2008) as well as in the rat (Shors et al., 2001, 2002; Madsen et al., 2003), others have suggested that adult-generated DGCs display connectivity and become involved in behavior from 4 - 8 weeks on (Jessberger and Kempermann, 2003; Ge et al., 2007; Kee et al., 2007; Marín-Burgin et al., 2012; Dieni et al., 2013). A recent study, in which the roles of both, young and old adult-born DGCs was examined, provided evidence that younger (3 - 4-week-old) adult-generated DGCs play an essential part in pattern separation between memories of very similar contexts and spaces, while older (> 6 weeks of age) adult-born and prenatally-generated DGCs are important for rapid pattern completion, i.e. the prompt retrieval of existent memories through the use of partial cues (Nakashiba et al., 2012). This implies a switch of function as newborn DGCs get older. In addition, it has been shown that ablation of DCX^{+} neurons in adult mice

leads to impairment in spatial learning acquisition but not in the recall of stored memories (Vukovic et al., 2013). This further suggests that young granule cells make contributions to learning while they are still in the DCX-expression phase of development. However, since DCX$^+$ cells exhibit variable stages of maturation, further investigations are needed to elucidate at which stage DCX$^+$ DGCs get involved in behavior.

In a recent rat study, we examined the expression of immediate early gene (IEG) expression in newborn DGCs following long term potentiation (LTP) induction via high frequency stimulation (Jungenitz et al., 2014). We found that basal pCREB133 and zif268 expression is positively correlated to DCX-cell morphology. While the DCX-staging is solely based on morphology, it might indicate possible functional associations which could be examined in further studies. Furthermore, the results indicated that synaptic activation and integration of newborn DGCs took place only gradually starting at about 3 weeks of cell age. In addition, IEG-expression in newly generated cells could only be activated after the phase of DCX-expression. On the other hand, the process of functional maturation follows a gradual course that starts as early as 7 dpi (Espósito et al., 2005). The variability in the time course of functional maturation may be associated with morphological growth as indicated by DCX staging. The time frame in which the staging system can be applied appears to be a crucial phase of continuous structural growth, possibly in order to establish relevant connections to other cells, which is thus followed by stabilization of structure and functional integration.

Granule cell nuclear size increases with each consecutive stage of structural maturation and cell age

Prox1 is a nuclear marker that is specifically expressed in granule cells (Lavado and Oliver, 2007; Iwano et al., 2012). Therefore it was used in combination with BrdU and DCX to selectively label and measure the nuclear size of newborn DGCs. We observed a direct correlation between nuclear size and structural maturation stage that revealed a steady increase of nuclear size with dendritic tree growth. Furthermore, nuclear size also increased with cell

age until 35 dpi after which it remained stable **(Fig. 4B and C)**. Interestingly, the nuclear size of DGCs becomes constant at the same time as the number of surviving adult-born DGCs begins to stabilize **(see Fig. 2C and D)**. Overall, our findings support the notion that at 5 weeks of age, DGCs possess the necessary qualities that allow them to survive and become fully mature and functional.

Our finding of a concrete association of the size of the nucleus with the stage of dendritic maturation and the age of newborn DGCs can be used as a simple way to determine the maturational stage or age of a new DGC. Despite the variability of the nuclear size across the different cell ages, the steady increase within the first five weeks allows a discrimination between an early (7 - 14 dpi) and a late phase (21 - 77 dpi), which can be used to predict a cell's age with a reliability of about 70%. Hence, the nuclear size measure shows a considerable reliability to predict the developmental stage and cell age of a newborn DGC **(Fig. 5)** and could be used as a useful novel indicator of cell maturity.

Adult-born granule cells remain located in the inner part of the granule cell layer

During the development of the dentate gyrus, granule cells migrate from the lateral ventricle and settle in the hippocampal area to form the GCL. The postnatally born cells are generated within the hippocampus, in what is to become the SGZ, and migrate a short distance to the inner part of the GCL, while the prenatally generated cells occupy the outer part of the GCL (Schlessinger et al., 1975; Altman and Bayer, 1990). A recent study demonstrated an outside-in layering of the GCL based on the time of cell birth (Mathews et al., 2010). In addition, it has been suggested that the position of newborn cells could have important functional implications relating to the type of information these cells process (see (Aimone et al., 2010) for review). Our results show that almost all of the adult-generated DGCs were located in the SGZ and inner part of the GCL. This indicates that age and degree of structural maturation did not affect migration and thus the position of the cells. Our

findings support the notion that newborn DGC localization is determined very early and remains stable throughout development (Kempermann et al., 2003).

Our findings portray a detailed structural characterization of newborn DGCs in the adult mouse brain during the DCX-expression phase using the novel techniques DCX staging, and nuclear size measurement. This provides structural groundwork to be considered in future studies in which our tools could be combined with functional and behavioral techniques to further elucidate the process of adult neurogenesis. Detailed examinations of neural stem cell development and integration in the adult brain are needed to ultimately enable advancement in therapies for learning and memory disorders, as well as certain neurological and psychiatric diseases.

7.6. Materials and Methods

Animals

Adult male Thy1-GFP transgenic mice (GFP-M line, see (Feng et al., 2000; Vuksic et al., 2008); 18 - 26 g) were bred on a C57BL/6 background and housed under standard conditions at the animal facility of Goethe University Frankfurt, Germany, in a 12 h light/dark cycle (lights on at 0600 hours), with food and water available ad libitum. Animal care and experimental procedures were performed in agreement with the German law on the use of laboratory animals (animal welfare act; TierSchG; §4 par 3) and approved by the animal welfare officer of Goethe-University, Faculty of medicine (reference number BB01/10/2011).

BrdU administration

In order to label newly born cells, 5-bromo-2´-deoxyuridine (BrdU; AppliChem) was administered to each animal with a single intraperitoneal injection (200 mg/kg body weight) at postnatal day 42 (P42). Animals were sacrificed at 7, 14, 21, 28, 35, 49, 63, and 77 days post BrdU injection (dpi) for evaluation of newborn neuron survival at these time points.

Immunohistochemistry

Animals were anesthetized with isoflourane and transcardially perfused with 0.9 % NaCl followed by 4 % paraformaldehyde (PFA) in 0.1 M phosphate buffered saline (PBS). Brains were removed, postfixed in 4 % PFA overnight at 4 °C, and serially sectioned in the frontal plane (75 µm) with a vibratome. Sections were washed in TRIS-buffered saline (TBS; pH 7.40), and stored in cryoprotectant solution containing 30 % ethylenglycol and 25 % glycerin in 0.1 M PBS at -20 °C. Free floating sections were washed in TBS and incubated in a blocking solution containing 5 % bovine serum albumin and 2.5 % Triton X-100 for 1 hour at room temperature. In stainings involving BrdU detection, sections were pre-treated with 2 N HCl for 30 minutes at 37 °C to denature DNA, followed by neutralization in 0.1 M boric acid (pH 8.5) for 10 minutes at room temperature, and three rinses in TBS prior to blocking. Subsequently, sections were incubated in the primary antibody solution containing 1 % Triton X-100 and 2 % BSA in 0.1 M TBS for 48 hours at room temperature. The following primary antibodies were used against: BrdU (rat, polyclonal, 1:250, Abcam, Ctl. A-2139), doublecortin (DCX, goat, polyclonal, 1:500, Santa Cruz, Ctl. SC-8066), and Prospero-related homeobox 1 gene (Prox1, rabbit, polyclonal, 1:1000, ReliaTech, Ctl. 102-PA30S). For visualization, sections were treated with secondary fluorescent dye conjugated antibodies (1:1000; Alexa 488, 568, and 633, Vector Labs., Burlingame, CA, USA) for 48 hours at room temperature.

Histological data analysis

All data were acquired from three animals per age group (n = 3; at 7, 14, 21, 28, 35, 49, 63, and 77 dpi) and 3 sections per animal. High resolution (1024 x 1024 pixel) confocal images of histological frontal sections were obtained with a confocal laser scanning microscope (Nikon Eclipse 80i) using a 40x oil immersion lens (N.A. 1.3). Serial frontal brain sections containing the dorsal part of the hippocampal formation were collected. Series were rostro-caudally standardized according to the atlas of Franklin and Paxinos (1997). The first section corresponded to the stereotaxic position -1.265 mm from

bregma and the last section corresponded to -3.065 mm from bregma (Franklin and Paxinos, 1997). For the Prox1, BrdU immunostaining, the 2nd, 11th and 20th serial sections were selected (corresponding to -1.34 mm, -2.015 mm, and 2.69 mm from bregma respectively), while the 7th, 16th and 25th sections (1.715, 2.39, and -3.065 mm from bregma, respectively (Franklin and Paxinos, 1997)) were used for triple immunostainings (DCX, Prox1, and BrdU).

In each section, three adjacent, non-overlapping regions of interest (medial, middle and lateral), were chosen for imaging along the suprapyramidal blade of the right dentate gyrus starting directly laterally from the crest where the supra- and infrapyramidal blades clearly separate. Image z-stacks (45 - 55 images per stack; z-axis interval between consecutive frames: 1 µm) were oriented perpendicular to the longitudinal axis of the granule cell layer (GCL). Each image frame had a width of 318.25 µm, i.e. the three frames together represented a total GCL length of 954.75 µm per section. Accordingly, cell counting in three sections per animal was always standardized against a total GCL length of 2864.25 µm. The GCL width, measured perpendicular to the longitudinal axes of the GCL, was found to be 53.363 ± 1.34 µm. Cell numbers for BrdU/Prox1$^+$ and DCX$^+$ cells were calculated per mm GCL length. DCX/BrdU/Prox1$^+$ cells were counted in the same manner and standardized against the total number of BrdU/Prox1$^+$ cells. The number of BrdU/Prox1$^+$ cells at each time point was also standardized against the number of BrdU/Prox1$^+$ cells at 1 week to determine the percentage of loss of newborn cells over time.

The degree of structural maturation of DCX$^+$ cells was determined by classifying cells into one of six stages based on dendrite morphology (see Jungenitz et al., 2014). Each stage was defined by the length and elaboration of the dendritic tree in the following manner: stage 1: the DCX$^+$ cell soma is positioned in the subgranular zone (SGZ) and no processes are visible; stage 2: the DCX$^+$ cell soma has one or two short processes that do not extend beyond the SGZ; stage 3: the principal dendrite of the DCX$^+$ cell extends into the inner half of the GCL; stage 4: The leading dendrite reaches the outer half of the GCL; stage 5: the leading dendrite extends into the inner molecular layer (IML); stage 6: the leading dendrite extends into the outer molecular layer (OML) of

the dentate gyrus. DCX$^+$ cells that showed cut dendritic branches, i.e. labeled branches that reached the surface of the section, were excluded from analysis.

Nuclear size was determined by measuring the largest cross-sectional area of each Prox1$^+$ cell nucleus using the polygon selection tab in ImageJ (Image Processing and Analysis in Java, version 1.43u). To determine predictive values of the nuclear size in relation to structural (DCX) stage and age of each granule cell, nuclear size data from different animals were pooled and categorized into an early and a late structural stage and cell age, considering DCX stage 1 - 3 and 7 - 14 dpi as an early phase and DCX stage 4 - 6 and 21 - 77 dpi as a late phase. The mean nuclear sizes of each phase were determined and used to calculate the equidistance between early and late phases, which was then used as a threshold to discriminate between early and late phases. Based on that threshold, single cells were classified into 3 different types of predictive values: true positive, false negative and false positive. The definitions for the different predictive values of the early phase were the following: true positive assigned cells belonged to the early phase and were below the threshold; false negative assigned cells belonged to the early phase, but were above the threshold and false positive assigned cells belonged to the late phase, but were below the threshold for the early phase and therefore assigned wrongly to the early phase. The conditions for the assignments of the late phase were defined as the opposite to the early phase.

The position of granule cell somata in relation to the SGZ and GCL was obtained by measuring the distance perpendicular to the medio-lateral axis of the GCL from the SGZ/GCL border to the lower border of the newly born granule cell's nucleus which was normalized to the total distance from the SGZ/GCL border to the border of the GCL toward the IML (representing GCL thickness) at the particular confocal plane.

All statistic evaluations were performed with ≥ 3 animals (n ≥ 3) per group. For the correlation evaluation between nuclear size and DCX stage, data of all animals from 7 dpi to 28 dpi were pooled for analysis. Statistical differences between groups (stage 1: n = 5; stage 2: n = 7; stage 3: n = 4; stage 4: n = 6;

stage 5: n = 9; stage 6: n = 11; n represents number of animals) were assessed with the non-parametric Kruskal-Wallis one-way analysis of variance (Dunn's multiple comparison) test. Statistical significance was set at $P < 0.05$. Results are expressed as means $\pm$ SEM. All statistical analyses and graphs were produced using GraphPad Prism 5.03.

7.7. References

Aimone JB, Deng W, Gage FH (2010) Adult neurogenesis: integrating theories and separating functions. Trends Cog Sci:1–13.

Altman J, Bayer S a (1990) Migration and distribution of two populations of hippocampal granule cell precursors during the perinatal and postnatal periods. J Comp Neurol 301:365–381.

Altman J, Das GD (1967) Postnatal Neurogenesis in the Guinea-Pig. Nature 214:1098–1101.

Bhattacharyya BJ, Banisadr G, Jung H, Ren D, Cronshaw DG, Zou Y, Miller RJ (2008) The chemokine stromal cell-derived factor-1 regulates GABAergic inputs to neural progenitors in the postnatal dentate gyrus. J Neurosci 28:6720–6730.

Braun SMG, Jessberger S (2014) Adult neurogenesis and its role in neuropsychiatric disease, brain repair and normal brain function. Neuropathol Appl Neurobiol 40:3–12.

Brown JP, Couillard-Després S, Cooper-Kuhn CM, Winkler J, Aigner L, Kuhn HG, Couillard-despres S (2003) Transient expression of doublecortin during adult neurogenesis. J Comp Neurol 467:1–10.

Cameron HA, Mckay RD (2001) Adult neurogenesis produces a large pool of new granule cells in the dentate gyrus. J Comp Neurol 435:406–417.

Chancey JH, Poulsen DJ, Wadiche JI, Overstreet-Wadiche L (2014) Hilar mossy cells provide the first glutamatergic synapses to adult-born dentate granule cells. J Neurosci 34:2349–2354.

Chawla MK, Guzowski JF, Ramirez-Amaya V, Lipa P, Hoffman KL, Marriott LK, Worley PF, McNaughton BL, Barnes CA (2005) Sparse, environmentally selective expression of Arc RNA in the upper blade of the rodent fascia dentata by brief spatial experience. Hippocampus 15:579–586.

Clelland CD, Choi M, Romberg C, Clemenson GD, Fragniere A, Tyers P, Jessberger S, Saksida LM, Barker R a, Gage FH, Bussey TJ (2009) A functional role for adult hippocampal neurogenesis in spatial pattern separation. Science (80-) 325:210–213.

Couillard-despres S, Winner B, Schaubeck S, Aigner R, Vroemen M, Weidner N, Bogdahn U, Winkler J, Kuhn H-GG, Aigner L (2005) Doublecortin expression levels in adult brain reflect neurogenesis. Eur J Neurosci 21:1–14.

Creer DJ, Romberg C, Saksida LM, van Praag H, Bussey TJ (2010) Running enhances spatial pattern separation in mice. Proc Natl Acad Sci U S A 107:2367–2372.

Dayer AG, Ford AA, Cleaver KM, Yassaee M, Cameron HA (2003) Short-term and long-term survival of new neurons in the rat dentate gyrus. J Comp Neurol 572:563–572.

Deng W, Aimone JB, Gage FH (2010) New neurons and new memories: how does adult hippocampal neurogenesis affect learning and memory? Nat Rev Neurosci 11:339–350.

Dieni C V, Nietz AK, Panichi R, Wadiche JI, Overstreet-Wadiche L (2013) Distinct determinants of sparse activation during granule cell maturation. J Neurosci 33:19131–19142.

Espósito MS, Piatti VC, Laplagne DA, Ferrari CC, Pitossi FJ, Schinder AF (2005) Neuronal differentiation in the adult hippocampus recapitulates embryonic development. Hippocampus 25:10074–10086.

Fanselow MS, Dong H-W (2010) Are the dorsal and ventral hippocampus functionally distinct structures? Neuron 65:7–19.

Feng G, Mellor RH, Bernstein M, Keller-Peck C, Nguyen QT, Wallace M, Nerbonne JM, Lichtman JW, Sanes JR (2000) Imaging neuronal subsets in transgenic mice expressing multiple spectral variants of GFP. Neuron 28:41–51.

Francis F, Koulakoff A, Boucher D, Chafey P, Schaar B, Vinet MC, Friocourt G, McDonnell N, Reiner O, Kahn A, McConnell SK, Berwald-Netter Y, Denoulet P, Chelly J (1999) Doublecortin is a developmentally regulated, microtubule-associated protein expressed in migrating and differentiating neurons. Neuron 23:247–256.

Franklin KBJ, Paxinos G (1997) The Mouse Brain in Stereotaxic Coordinates. San Diego: Academic Press.

Galeeva a, Treuter E, Tomarev S, Pelto-Huikko M (2007) A prospero-related homeobox gene Prox-1 is expressed during postnatal brain development as well as in the adult rodent brain. Neuroscience 146:604–616.

Ge S, Yang C-H, Hsu K-S, Ming G-L, Song H (2007) A critical period for enhanced synaptic plasticity in newly generated neurons of the adult brain. Neuron 54:559–566.

Iwano T, Masuda A, Kiyonari H, Enomoto H, Matsuzaki F (2012) Prox1 postmitotically defines dentate gyrus cells by specifying granule cell identity over CA3 pyramidal cell fate in the hippocampus. Development 139:3051–3062.

Jagasia R, Steib K, Englberger E, Herold S, Faus-Kessler T, Saxe M, Gage FH, Song H, Lie DC (2009) GABA-cAMP Response Element-Binding Protein Signaling Regulates Maturation and Survival of Newly Generated Neurons in the Adult Hippocampus. J Neurosci 29:7966–7977.

Jessberger S, Clark RE, Broadbent NJ, Clemenson GD, Consiglio A, Lie DC, Squire LR, Gage FH (2009) Dentate gyrus-specific knockdown of adult neurogenesis impairs spatial and object recognition memory in adult rats. Learn Mem 16:147–154.

Jessberger S, Kempermann G (2003) Adult-born hippocampal neurons mature into activity-dependent responsiveness. Eur J Neurosci 18:2707–2712.

Jungenitz T, Radic T, Jedlicka P, Schwarzacher SW (2014) High-frequency stimulation induces gradual immediate early gene expression in maturing adult-generated hippocampal granule cells. Cereb Cortex 24:1845–1857.

Karalay O, Doberauer K, Vadodaria KC, Knobloch M, Berti L, Miquelajauregui A, Schwark M, Jagasia R, Taketo MM, Tarabykin V, Lie DC, Jessberger S (2011) Prospero-related homeobox 1 gene (Prox1) is regulated by canonical Wnt signaling and has a stage-specific role in adult hippocampal neurogenesis. Proc Natl Acad Sci U S A 108:5807–5812.

Kee N, Teixeira CM, Wang AH, Frankland PW (2007) Preferential incorporation of adult-generated granule cells into spatial memory networks in the dentate gyrus. Nat Neurosci 10:355–362.

Kempermann G, Gast D, Kronenberg G, Yamaguchi M, Gage FH (2003) Early determination and long-term persistence of adult-generated new neurons in the hippocampus of mice. Development 130:391–399.

Kempermann G, Jessberger S, Steiner B (2004) Milestones of neuronal development in the adult hippocampus. Trends Neurosci 27:447–452.

Kim WR, Christian K, Ming G-L, Song H (2011) Time-dependent involvement of adult-born dentate granule cells in behavior. Behav Brain Res.

Kuhn HG, Dickinson-Anson H, Gage FH (1996) Neurogenesis in the Dentate Gyrus of the Adult Rat: Age-Related Decrease of Neuronal Progenitor Proliferation Rat. J Neurosci 16:2027–2033.

Lavado A, Lagutin O V., Chow LML, Baker SJ, Oliver G (2010) Prox1 Is required for granule cell maturation and intermediate progenitor maintenance during brain neurogenesis. PLoS Biol 8:43–44.

Lavado A, Oliver G (2007) Prox1 expression patterns in the developing and adult murine brain. Dev Dyn 236:518–524.

Lie DC, Song H, Colamarino SA, Ming G, Gage FH (2004) Neurogenesis in the adult brain: new strategies for central nervous system diseases. Annu Rev Pharmacol Toxicol 44:399–421.

Madsen T, Kristjansen PEG, Bolwig TG, Wörtwein G (2003) Arrested neuronal proliferation and impaired hippocampal function following fractionated brain irradiation in the adult rat. Neuroscience 119:635–642.

Mandyam CD, Harburg GC, Eisch AJ (2007) Determination of key aspects of precursor cell proliferation, cell cycle length and kinetics in the adult mouse subgranular zone. Neuroscience 146:108–122.

Marín-Burgin A, Mongiat L a, Pardi MB, Schinder AF (2012) Unique processing during a period of high excitation/inhibition balance in adult-born neurons. Science 335:1238–1242.

Martinez-Canabal A, Akers KG, Josselyn SA, Frankland PW (2013) Age-dependent effects of hippocampal neurogenesis suppression on spatial learning. Hippocampus 23:66–74.

Mathews E a, Morgenstern N a, Piatti VC, Zhao C, Jessberger S, Schinder AF, Gage FH (2010) A distinctive layering pattern of mouse dentate granule cells is generated by developmental and adult neurogenesis. J Comp Neurol 518:4479–4490.

Ming G-L, Song H (2011) Adult neurogenesis in the mammalian brain: significant answers and significant questions. Neuron 70:687–702.

Muramatsu R, Ikegaya Y, Matsuki N, Koyama R (2007) Neonatally born granule cells numerically dominate adult mice dentate gyrus. Neuroscience 148:593–598.

Nakashiba T, Cushman JD, Pelkey K a, Renaudineau S, Buhl DL, McHugh TJ, Barrera VR, Chittajallu R, Iwamoto KS, McBain CJ, Fanselow MS, Tonegawa S (2012) Young dentate granule cells mediate pattern separation, whereas old granule cells facilitate pattern completion. Cell 149:188–201.

Overstreet-Wadiche LS, Bensen AL, Westbrook GL (2006) Delayed development of adult-generated granule cells in dentate gyrus. J Neurosci 26:2326–2334.

Piatti VC, Davies-Sala MG, Espósito MS, Mongiat L a, Trinchero MF, Schinder AF (2011) The timing for neuronal maturation in the adult hippocampus is modulated by local network activity. J Neurosci 31:7715–7728.

Plümpe T, Ehninger D, Steiner B, Klempin F, Jessberger S, Brandt M, Römer B, Rodriguez GR, Kronenberg G, Kempermann G (2006) Variability of doublecortin-associated dendrite maturation in adult hippocampal neurogenesis is independent of the regulation of precursor cell proliferation. BMC Neurosci 14:1–14.

Schlessinger AR, Cowan WM, Gottlieb DI (1975) An autoradiographic study of the time of origin and the pattern of granule cell migration in the dentate gyrus of the rat. J Comp Neurol 159:149–175.

Shors TJ, Miesegaes G, Beylin A, Zhao M, Rydel T, Gould E (2001) Neurogenesis in the adult is involved in the formation of trace memories. Nature 410:372–376.

Shors TJ, Townsend DA, Zhao M, Kozorovitskiy Y, Gould E (2002) Neurogenesis may relate to some but not all types of hippocampal-dependent learning. Hippocampus 584:578–584.

Snyder JS, Choe JS, Clifford MA, Jeurling SI, Hurley P, Brown A, Kamhi JF, Cameron HA (2009a) Adult-Born Hippocampal Neurons Are More Numerous, Faster Maturing, and More Involved in Behavior in Rats than in Mice. J Neurosci 29:14484–14495.

Snyder JS, Ferrante SC, Cameron HA (2012) Late maturation of adult-born neurons in the temporal dentate gyrus. PLoS One 7:e48757.

Snyder JS, Radik R, Wojtowicz JM, Cameron HA (2009b) Anatomical gradients of adult neurogenesis and activity: young neurons in the ventral dentate gyrus are activated by water maze training. Hippocampus 19:360–370.

Spalding KL, Bergmann O, Alkass K, Bernard S, Salehpour M, Huttner HB, Boström E, Westerlund I, Vial C, Buchholz B a, Possnert G, Mash DC, Druid H, Frisén J (2013) Dynamics of hippocampal neurogenesis in adult humans. Cell 153:1219–1227.

Toni N, Teng EM, Bushong E a, Aimone JB, Zhao C, Consiglio A, van Praag H, Martone ME, Ellisman MH, Gage FH (2007) Synapse formation on neurons born in the adult hippocampus. Nat Neurosci 10:727–734.

van Praag H, Schinder A, Christie B, Toni N (2002) Functional neurogenesis in the adult hippocampus. Nature 415:1030–1034.

Vivar C, Potter MC, Choi J, Lee J-Y, Stringer TP, Callaway EM, Gage FH, Suh H, van Praag H (2012) Monosynaptic inputs to new neurons in the dentate gyrus. Nat Commun 3:1107.

Vivar C, van Praag H (2013) Functional circuits of new neurons in the dentate gyrus. Front Neural Circuits 7:15.

von Bohlen Und Halbach O (2007) Immunohistological markers for staging neurogenesis in adult hippocampus. Cell Tissue Res 329:409–420.

Vukovic J, Borlikova GG, Ruitenberg MJ, Robinson GJ, Sullivan RKP, Walker TL, Bartlett PF (2013) Immature doublecortin-positive hippocampal neurons are important for learning but not for remembering. J Neurosci 33:6603–6613.

Vuksic M, Del Turco D, Bas Orth C, Burbach GJ, Feng G, Müller CM, Schwarzacher SW, Deller T (2008) 3D-reconstruction and functional properties of GFP-positive and GFP-negative granule cells in the fascia dentata of the Thy1-GFP mouse. Hippocampus 18:364–375.

Zhao C, Deng W, Gage FH (2008) Mechanisms and functional implications of adult neurogenesis. Cell 132:645–660.

Zhao C, Teng EM, Summers RG, Jr. M, G.I, Gage FH (2006) Distinct morphological stages of dentate granule neuron maturation in the adult mouse hippocampus. J Neurosci 26:3–11.

7.8. Figures with legends
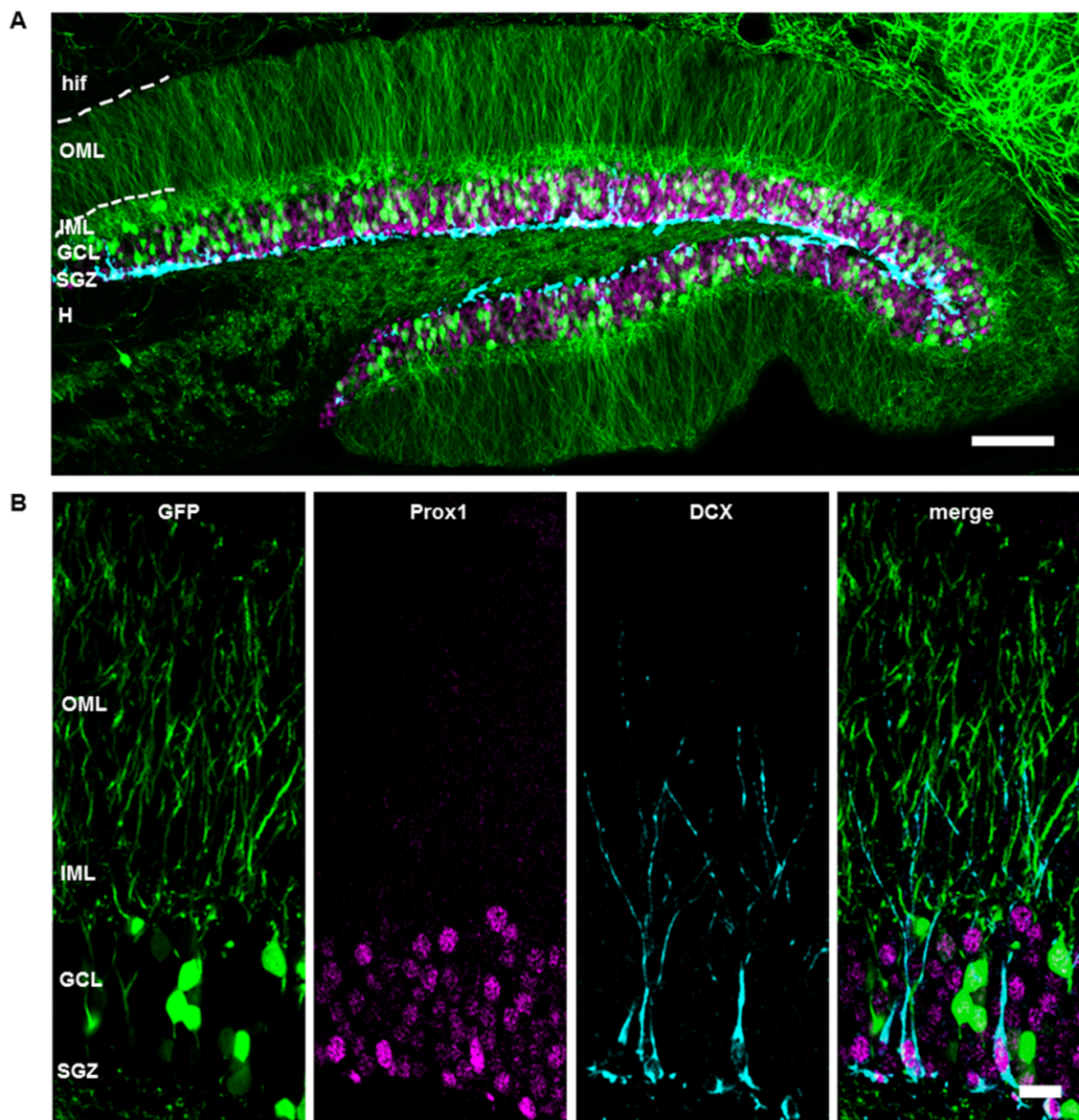
Figure 1. Doublecortin-labeling does not co-localize with Thy1-GFP expression. **(A)** Frontal section of the dorsal hippocampal formation from a Thy-1-GFP mouse. Thy1-GFP expression was observed in a subpopulation of dentate granule cells (DGCs) and was expressed throughout dendritic processes of DGCs which extend into the inner molecular layer (IML) and outer molecular layer (OML) toward the hippocampal fissure (hif). Prospero homeobox protein 1 (Prox1, magenta), a specific nuclear marker of granule cells, was confined to granule cell nuclei of the granule cell layer (GCL). Doublecortin (DCX, cyan) labeled young maturing cells that are positioned in the subgranular zone (SGZ). **(B)** There was no co-localization of DCX and Thy1-GFP which suggests that Thy1-GFP is generally expressed in more mature (DCX⁻)

164

DGCs. Both DCX$^+$ and Thy1-GFP$^+$ granule cells co-localized with Prox1 even during early stages of DCX expression (see small DCX$^+$ cells in the SGZ). Scale bars: **(A)** 100 µm; **(B)** 20 µm. CA1, Cornu Ammonis area 1; H, hilus.
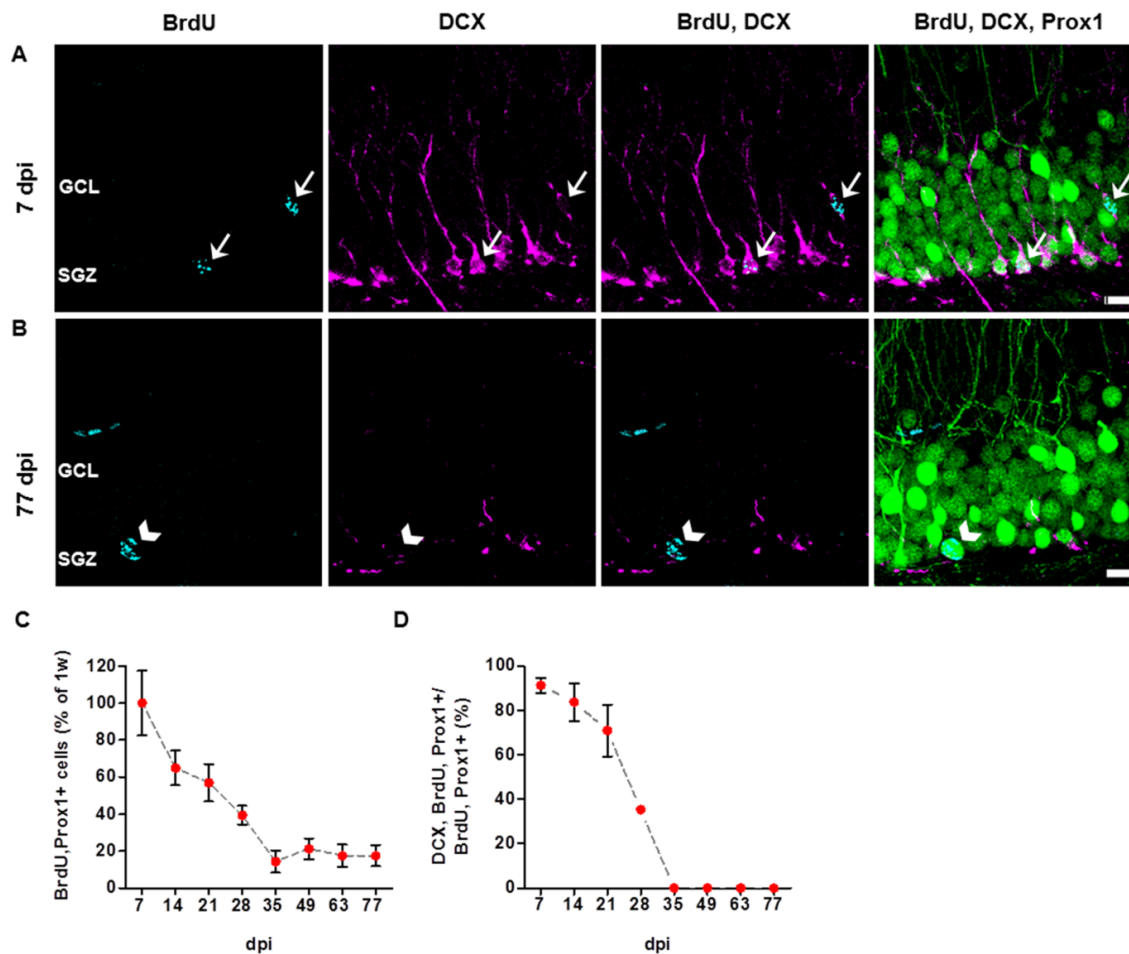
Figure 2. Survival rate of newborn dentate granule cells decreases over the first 4 weeks. (A, B) Newly born DGCs labeled with the mitosis marker BrdU (cyan) frequently displayed DCX-expression (magenta) at 7 days post BrdU injection (7 dpi; **A**), while there was no co-localization of BrdU and DCX at 77 dpi **(B)**. All of the counted BrdU^{+} cells were Prox1^{+} (green; **A, B**). Arrows in **(A)** point to BrdU/DCX/Prox1^{+} cells. Arrowheads in **(B)** point to a BrdU/Thy1-GFP[+] cell. Due to their intense somato-dendritic labeling, Thy1-GFP^{+} cells could be easily distinguished from the green nuclear Prox1 immunostaining. **(C)** Quantification of BrdU/Prox1^{+} cells revealed a decline in survival of newborn DGCs between 7 and 35 dpi, whereas the total number of BrdU^{+} cells did not change between 35 and 77 dpi. Compared to the first week post BrdU injection, 14 % of BrdU/Prox1^{+} cells were retained at 35 dpi, after which there was no further cell loss. **(D)** The number of BrdU/Prox1^{+} DGCs that expressed DCX also decreased between 7 and 35 dpi. No DCX/BrdU/Prox1^{+} cells could be detected between 35 and 77 dpi. All analyses were performed in the suprapyramidal blade of the right dorsal dentate gyrus (n = 3 animals for each group, 3 sections per animal). Error

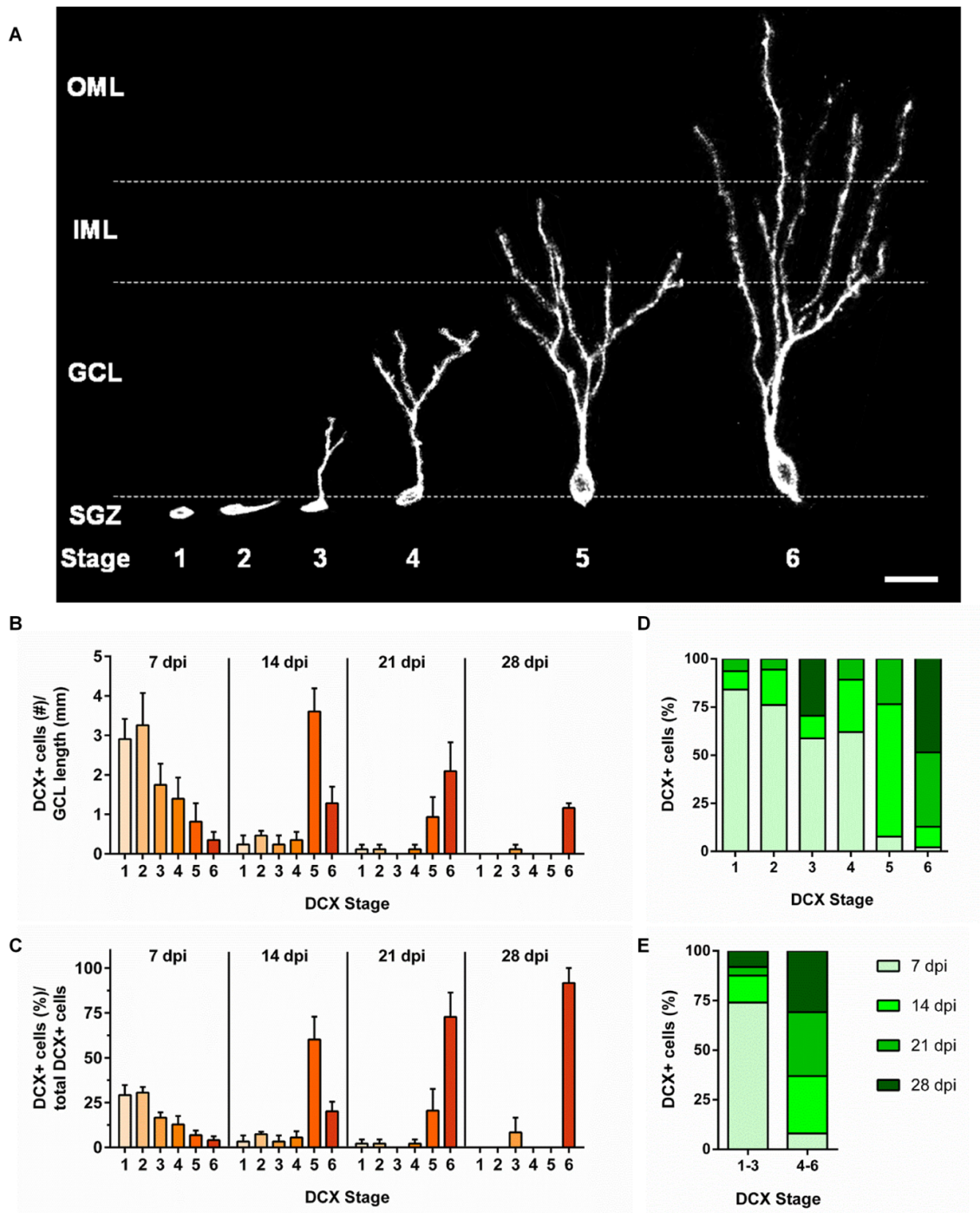bars represent SEM. Scale bars in **(A, B)**: 10 µm. GCL, granule cell layer; SGZ, subgranular zone.

Figure 3. Structural maturation of DCX-expressing newborn DGCs is correlated with cell age. (A) DCX^{+} cells were categorized into six stages according to the degree of their structural maturation. Cells were considered to be in stage 1 when the soma was positioned in the subgranular zone (SGZ) and no dendritic processes were visible; stage 2 when the cell displayed short processes that were located within the SGZ; stage 3 when the principal dendritic process projected into the inner half of the granule cell layer (GCL); stage 4 when the leading dendrite reached the outer half of the GCL;

stage 5 when the leading dendrite extended into the inner molecular layer (IML); and stage 6 when the leading dendrite reached the outer molecular layer (OML). **(B, C)** Staging of newborn DCX$^+$ DGCs at different time points revealed a marked shift in stage distribution according to cell age. At 7 dpi, the majority of newborn DCX$^+$ DGCs were classified as stage 1 or 2, while at 14 dpi, the majority of cells were classified as stage 5 or 6. At 28 dpi, about 92 % of the DCX$^+$ cells were classified as stage 6, but a small percentage of DCX$^+$ cells were classified as stage 3. **(D, E)** The distribution of DCX$^+$ cell ages according to each stage illustrates the prevalence of DCX stages 1 - 4 at 7 dpi and DCX stages 5 - 6 at 14 to 28 dpi. No BrdU/DCX$^+$ DGCs were observed after 28 dpi. Notably, DCX$^+$ cells of stages 1 - 6 co-existed at the same time points (7 - 21 dpi), suggesting a variability in the maturation time course of individual neurons. All data were obtained from 3 animals (n = 3) per group, and 3 sections per animal. Error bars represent SEM. Scale bar in **(A)**: 20 µm.
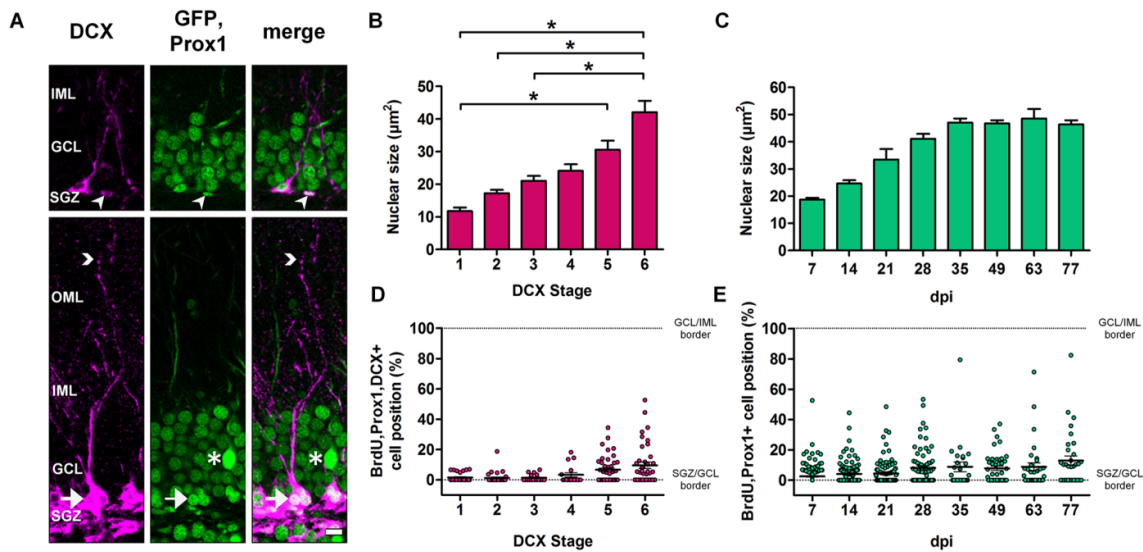
Figure 4. Nuclear size and soma position are positively correlated with structural maturation and age of newborn DGCs. (A) Examples of a 21-day-old stage 1 DCX/Prox1^{+} cell that is located in the subgranular zone (SGZ) and has no dendritic processes (arrowheads, upper panel) and a 21-day-old stage 6 DCX/Prox1^{+} cell (arrows, lower panel) with a dendrite extending into the outer molecular layer (OML; arrowheads, lower panel). Asterisk denotes the soma of an intensively labeled Thy1-GFP[+] cell. **(B)** Nuclear size (determined with the nuclear marker Prox1, green) increased with structural maturity. There were significant differences in nuclear size between stages 1 and 6, as well as between stages 1 and 5, stages 2 and 6, and stages 3 and 6 (Kruskal-Wallis Dunn's multiple comparison test between animals, *P < 0.05; stage 1: n = 5 animals, stage 2: n = 7, stage 3: n = 4, stage 4: n = 6, stage 5: n = 9, stage 6: n = 11). **(C)** In BrdU/Prox1^{+} DGCs, nuclear size increased gradually with age until it reached a plateau at 35 dpi (n = 3 per group). **(D, E)** The majority of newborn DGCs was positioned in the SGZ and the inner half of the granule cell layer (GCL), regardless of structural stage and age. Error bars represent SEM. Scale bars in **(A)**: 10µm. IML, inner molecular layer.
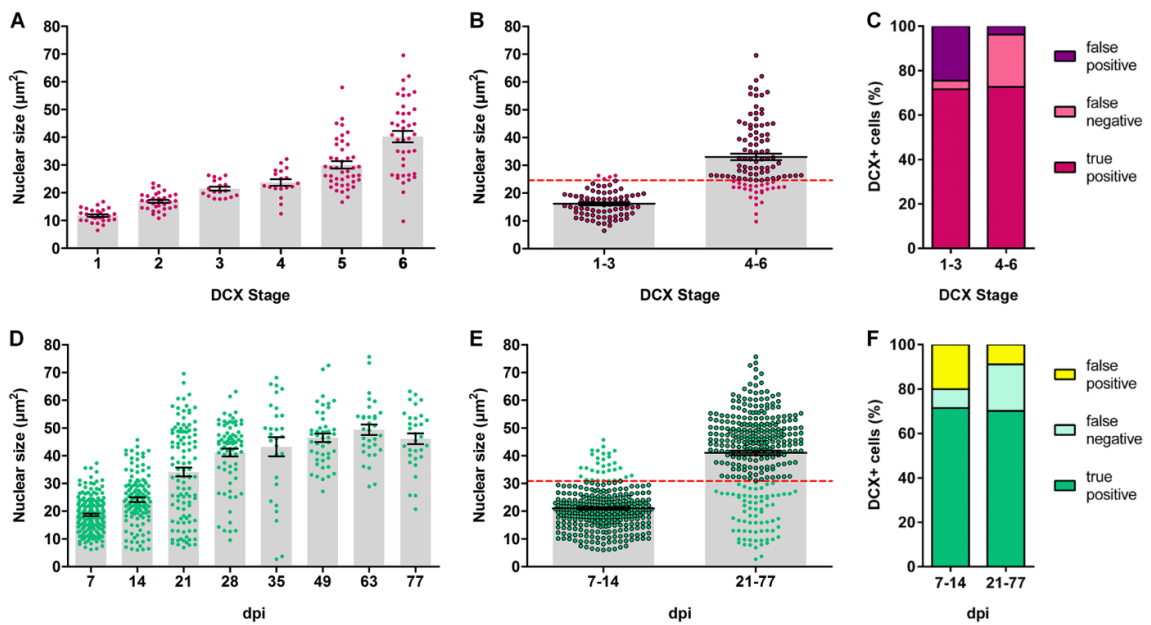
Figure 5. Nuclear size measurement as a valuable tool to discriminate between early and late stages in structural maturation and age of newborn DGCs. **(A, D)** The correlation of nuclear size with structural stage and cell age is illustrated as a dot plot (each dot represents a single cell, pooled from all animals per group) to highlight the variability. **(B, E)** Newborn DGCs were pooled in an early (DCX stage 1 - 3, cell age 7 - 14 dpi) and a late phase (DCX stage 4 - 6, cell age 21 - 77 dpi). The mean nuclear sizes of each group were determined and used to calculate the equidistance between early and late phases, which was then used as a threshold to discriminate and assign newborn DGCs to the early or the late phase of development (shown as red dashed line). **(C, F)**. Based on that threshold, cells were categorized into true positive, false positive and false negative predictive values. True positive classifications were found with a reliability of about 70 % across all stages. Number of animals: **(A, D)** DCX stage 1: n = 5, stage 2: n = 7, stage 3: n = 4, stage 4: n = 6, stage 5: n = 9, stage 6: n = 11; cell age: n = 3 per group. **(B, E)** DCX stage 1 - 3: n = 8, stage 4 - 6: n = 12; cell age 7 – 14 dpi: n = 6, age 21 - 77 dpi: n = 18. Error bars represent SEM.

8. Adult-born hippocampal granule cells exhibit a critical period of dendritic reorganization and remain structurally distinct from perinatally born granule cells

Beining M[*,1,2,3], **Jungenitz T**[*,1], Radic T[1], Deller T[1], Cuntz H[+,2,3], Jedlicka P[+,1], Schwarzacher SW[+,1]

[1]Institute of Clinical Neuroanatomy, Goethe University Frankfurt/Main, D-60528 Germany

[2]Ernst Strüngmann Institute (ESI) for Neuroscience in Cooperation with Max Planck Society, Frankfurt/Main, D-60528 Germany

[3]Frankfurt Institute for Advanced Studies (FIAS), Frankfurt/Main, D-60438 Germany

[*]Joint-first authors, [+]Joint-last authors

Corresponding author:

Marcel Beining,

Ernst-Strüngmann-Institute (ESI) for Neuroscience

Deutschordenstr. 46

D-60528 Frankfurt am Main

E-Mail: beining@fias.uni-frankfurt.de

8.1. Acknowledgement

8.2. Abstract

Adult-born dentate granule cells (abGCs) exhibit a critical developmental phase during function integration. The time window of this phase is debated and whether abGCs become indistinguishable from developmentally born mature granule cells (mGCs) is uncertain. We analyzed complete dendritic reconstructions from abGCs and mGCs using viral labeling. AbGCs from 21-77 days post intrahippocampal injection (dpi) exhibited comparable dendritic arbors, suggesting that structural maturation precedes functional integration. In contrast, significant structural differences were found compared to mGCs: AbGCs had more curved dendrites, more short terminal segments, a different branching pattern, and more proximal terminal branches. Morphological modeling attributed these differences to developmental dendritic pruning and postnatal growth of the dentate gyrus. We further correlated GC morphologies with the responsiveness to unilateral medial perforant path stimulation using the immediate-early-gene Arc as a marker of synaptic activation. Only abGCs at 28 and 35 dpi but neither old abGCs nor mGCs responded to stimulation with a remodeling of their dendritic arbor. Summarized, abGCs stay distinct from mGCs and their dendritic arbor can be shaped by afferent activity during a narrow critical time window.

8.3. Introduction

In the hippocampal dentate gyrus (DG), granule cells (GCs) are continuously born and integrated into the neural network (for recent reviews, see Bergmann et al., 2015; Kempermann, 2015). Studies suggest that adult-born granule cells (abGCs) are crucial for certain forms of hippocampus-dependent spatial learning, i.e. they facilitate pattern separation, whereas perinatally born matured granule cells (mGCs) facilitate pattern completion (Clelland et al., 2009; Nakashiba et al., 2012). Pattern separation might be promoted between 4-6 weeks after mitosis, when young abGCs exhibit distinct functional properties compared to mature abGCs or mGCs, such as less inhibitory input (Marín-Burgin et al., 2012; Temprana et al., 2014), high excitability (Mongiat et al., 2009), enhanced synaptic plasticity (Ge et al., 2007; Gu et al., 2012), preferential recruitment into spatial memory networks (Kee et al., 2007), specific connectivity (Restivo et al., 2015), and experience-dependent remodeling of connections (Bergami et al., 2015). This critical phase is also delineated on the synaptic level since spinogenesis increases gradually starting at week 3 (van Praag et al., 2002; Espósito et al., 2005; Zhao et al., 2006; Sun et al., 2013).

As abGCs are selectively recruited by the network (e.g. reviewed in Li and Pleasure, 2010), it is important to elucidate whether abGCs remain a functionally distinctive subgroup, or rather transiently provide new plastic neurons to a spatial memory circuit and converge with perinatally born mGCs thereafter. Evidence for convergence was found by comparing synaptic properties and firing behavior of abGCs and mGCs (Espósito et al., 2005; Laplagne et al., 2006) and by analyzing their functional integration during behavioral tasks (Stone et al., 2011). In contrast, it has been proposed that abGCs form a specialized population of GCs because they are more plastic and are recruited for distinct spatial tasks even when they have fully matured (Lemaire et al., 2012; Tronel et al., 2014). Adding another level of complexity, it was recently shown that abGCs divide into two functionally distinguishable populations with different input integration properties independent of cell age (Brunner et al., 2014), suggesting that abGCs might partly converge and partly stay distinct from mGCs.

175

Importantly, the existence of different GC populations has so far not been studied in detail at the structural level, even though the dendrites generate the basic frame defining amount and specificity of inputs (recently reviewed in Lefebvre et al., 2015), shaping input-output behavior (Mainen and Sejnowski, 1996), and performing local computations (reviewed in Sidiropoulou et al., 2006; Branco and Häusser, 2010), thus defining most functions of the neuron. Interestingly, in a recent in vivo study pruning of dendritic terminal segments was found in 3-4 week old mouse abGCs, a time point when most of the cell's specific input is defined (Gonçalves et al., 2016). Hence, abGCs may go through a critical time window during which dendrites are altered in response to afferent input (reviewed in Tavosanis, 2012), changing its functional fate. In this study, we analyzed the dendritic morphology of abGCs during and after network integration in order to elucidate 1) whether we can find differences in dendritic arborization between abGCs and mGCs that indicate different subpopulations, and 2) whether there is any evidence for a phase of dendritic reorganization in response to activation of specific afferents.

To address these questions we used bilateral retrovirus (RV) -mediated GFP expression to selectively label abGCs at different time points (van Praag et al., 2002) and an adeno-associated viral (AAV) GFP expression system to label mGCs (Kügler et al., 2001, 2003). Combining this approach with ipsilateral in vivo high-frequency stimulation of the medial perforant path yielded unstimulated and stimulated GC populations in the same brain which could be reconstructed and analyzed (240 in total). Our data reveal that the dendritic development of abGCs is essentially complete before functional integration. Furthermore, mature abGCs remained structurally distinct from perinatally born mGCs and thus form a distinct subgroup. Using a morphological computer model, we provided an ontogenetic explanation for the observed differences. Finally, we detected activity-dependent loss of short distal dendrites exclusively in young abGCs, providing new evidence for the existence of a critical phase during which activity can shape the dendritic arbor of abGCs.

8.4. Results

We utilized a retroviral vector (RV) expressing GFP under the CAG promoter
that enabled us to label abGCs at their time of birth (**Fig. 1A**; van Praag et al.,
2002). Young adult rats (8-13 weeks) were perfused at different time points
after injection (21, 28, 35, and 77 dpi) to obtain abGCs of different cell ages. In
order to keep the same definitions as other studies on adult neurogenesis, we
continue using the term 'adult-born' as we did before (Jungenitz et al., 2014),
even though new GCs at that animal age might be also called 'juvenile-born',
since a recent careful comparison between rat and human life cycles eventually
defined the beginning of adulthood in rat at the age of 6 months (Sengupta,
2013). For a structural analysis of perinatally born mGCs, we injected an adeno-
associated viral vector expressing GFP under the Synapsin1 promoter (referred
to as AAV, **Fig. 1B**), that labels synaptically maturated hippocampal neurons
(Fornasiero et al., 2010) and is strongly expressed in dentate GCs (Kuroda et
al., 2008).. In the first analysis, we assessed normal structural maturation of
abGCs; hence we focused on the non-activated, contralateral hemisphere.
Labeled dendritic trees of RV-labeled abGCs (21-77 dpi) and AAV-labeled
mGCs in the supra- and infrapyramidal blades were reconstructed in 3D with
the freely available TREES toolbox (Cuntz et al., 2010, 2011). Completeness of
the dendritic reconstruction was determined for each cell (see Material &
Methods) and complete dendritic trees were analyzed with respect to the inner,
middle, and outer molecular layer (IML, MML, OML) (**Fig. 1C-E**).

**Structural maturation of dendritic trees is completed between the third
and the fourth week of cell age in adult born granule cells**

We looked for cellular and layer-specific morphological differences between
all observed abGC cell ages (for exemplary reconstructions, see **Fig. 2A&B**).
When analyzing the distribution of terminal segment lengths we found that
segments could be divided in long and short terminal segments (STS), the latter
being smaller than 100 µm (**Fig. 2C inset and Fig. S1**). We recognized that
young abGCs (21 dpi) had many distal STS (**Fig. 2A** cyan segments), a
phenotype associated with immature neurons (Emoto, 2011). Interestingly,

these STS were substantially reduced one week later (28 dpi) and remained in low numbers until 77 dpi (**Fig. 2C**). In contrast, the total number of termination points and particularly their relative distribution in the molecular layer stayed rather constant over all investigated time points (**Fig. 2D**). Even though we performed extensive computer-aided morphological analyses on total and layer-specific dendritic lengths, branch points and angles, curvature, Sholl distribution, cone axes lengths, hull volumes, and spatial density (**Fig. 3 and Fig. S3**), we did not find any other significant differences between abGCs of different ages, except a higher dendritic length in the IML at 35 dpi compared to 28 dpi (607.3 ± 52.7 µm at 21 dpi, 565.2 ± 33.1 µm at 28 dpi, 724.1 ± 33.8 µm at 35 dpi, 597.7 ± 38.2 µm at 77 dpi, mean and SEM.; **Fig. 3C**). The latter finding might indicate some ongoing dendritic dynamics that decrease until 77 dpi. However, as this transient increase was limited to the IML and total dendritic length at 35 dpi was not significantly increased, dendritic growth appears to be very limited beyond 28 dpi. Together, these findings demonstrate that the structural maturation of dendritic trees is largely completed between the third and the fourth week of cell age and thus precedes the critical phase of functional maturation and synaptic integration which has been reported to occur from the 4th to the 6th week after cell birth (Ge et al., 2007; Mongiat et al., 2009; Marín-Burgin et al., 2012; Temprana et al., 2014; Bergami et al., 2015; Restivo et al., 2015, see also Introduction).

Aged adult-born GCs stay structurally distinct from perinatally born GCs

Next we analyzed whether mature abGCs converge structurally to the same cell population as perinatally born mGCs or whether they form a distinct subpopulation even after the critical phase of integration has ended. As abGCs appeared to be structurally fully mature from 4 weeks on (see previous section), we could be confident that the reconstructed old (77 dpi) RV-labeled abGCs represent old matured abGCs, and thus could be compared with AAV-labeled mGCs (Typical morphologies are shown in **Fig. 4 A and I**). AAV-labeled GCs were identified by their characteristic GC morphology and the location of the soma within the GCL. Due to the outside-in layering of the DG, the embryonically and perinatally born GCs occupy the upper parts of the GCL,

whereas younger adult-born GCs are located near the SGZ (Muramatsu et al., 2007; Mathews et al., 2010; Radic et al., 2015). Hence, in order to increase the likelihood of selecting perinatally born mGCs we avoided the reconstruction of AAV-labeled GCs with somata located near the SGZ (**Fig. 1B2&3**). We also did not reconstruct superficial GCs as they are known to have several morphological differences compared to GCs located in deep layers (Claiborne et al., 1990). Using these restrictions and, due to the much higher incidence of perinatally born mGCs in comparison to mature abGCs (Mathews et al., 2010), we assumed that the vast majority of AAV-labeled reconstructed mGCs were indeed generated perinatally.

The most prominent difference between abGCs and AAV-labeled mGCs was that nearly all dendrites of the latter ended in the OML, consistent with literature (Desmond and Levy, 1982), whereas in abGCs, a subset of dendrites terminated in the proximal layers (**Fig. 4B-D**). Interestingly, we also found much less STS in AAV-labeled mGCs compared to abGCs (**Fig. 4E**, AAV: 32.14 ± 15.90 µm vs. 77 dpi: 116.40 ± 30.80 µm summed length STS, $p < 0.05$). Furthermore, AAV-labeled mGCs exhibited less curved dendrites (**Fig. 4F and Fig. S4E**) and had a different arborization pattern with more branch points in the MML and less in the IML and the OML (**Fig. 4G**). However, the total and layer-specific dendritic lengths were similar in mGCs and abGCs ($p > 0.05$, **Fig. 4H**), indicating that the higher curvature and more proximal branch points in abGCs might compensate for the more proximally terminating dendrites. Summarized, these results show that mature abGCs form a subpopulation structurally distinct from mGCs.

A morphological model accounts for structural differences between abGCs and mGCs

To explain the observed structural differences between abGCs and mGCs, we utilized a morphological model based on optimal wiring principles (Cuntz et al., 2007, 2008, 2010; Schneider et al., 2014). The morphological model uses the minimum spanning tree (MST) algorithm which generates realistic dendritic morphologies by connecting target points in space while minimizing total

dendrite length and conduction times in the dendritic tree (Cuntz et al. 2010). **Fig. 5A** shows our hypothesis which is based on the observation that the DG changes in size and composition during development. Perinatally born mGCs developed in the young DG which has a much thinner GCL and ML than the matured DG (Rihn and Claiborne, 1990). Furthermore, during development, the area close to the hippocampal fissure contains numerous Cajal-Retzius cells (**Fig. 5A**, upper left tree) that express reelin, a protein that plays a crucial role in guiding dendritic arborization of GCs in the DG (Förster et al., 2006; Frotscher, 2010; D'Arcangelo, 2014). Accordingly, for synthetic perinatally born mGCs we distributed target points for the MST algorithm mainly within the OML and within a volume that corresponds to the smaller dimensions of a young DG. A pruning step with an absolute threshold to mimic maturational dendrite pruning (Schuldiner and Yaron, 2014) was applied subsequently (**Fig. 5A**, purple dendrites). During and after maturation of perinatally born GCs, the dendritic tree becomes significantly stretched since the ML broadens massively between birth and adulthood (about 275 % from P4 to P60) due to the ingrowth of afferent fibers and GC dendrites (Loy et al., 1977; Claiborne et al., 1990; Rihn and Claiborne, 1990). To mimic this process, we stretched the developmentally grown dendritic trees of mGCs to the size of the adult DG (**Fig. 5A**, upper half).

In contrast to mGCs, abGCs grow within the already mature adult DG (lower left tree in **Fig. 5A**). Accordingly, to model abGCs, we distributed the target points in a DG of adult size. Furthermore, in the adult DG, reelin-expressing cells in the OML are drastically reduced (Alcántara et al., 1998; Pesold et al., 1998), whereas commissural axons have populated the IML (Alcántara et al., 1998; Förster et al., 2006; Yu et al., 2014). Therefore, in our model, target points were reduced in the OML and increased in the IML while keeping all other parameters and steps the same. Surprisingly, implementing these two differences was sufficient to produce realistic morphologies (**Fig. 5B**) and to reproduce the observed morphological differences and analogies of 77 dpi abGCs and AAV-labeled mGCs in almost all parameters and layers (**Fig. 5C-H**). In conclusion, morphological modeling suggests that the structural differences

found between abGCs and mGCs originate from their particular environmental constraints during growth and maturation within the adult or perinatal DG.

Young adult-born GCs exhibit a critical phase of dendritic reorganization following HFS

Using Arc (activity-regulated cytoskeleton-associated protein) as a marker of synaptic activation (Lyford et al., 1995; Jungenitz et al., 2014), we were interested whether we can find activity-related structural differences in abGCs (21-77 dpi) or mGCs in the ipsi- compared to the contralateral hemisphere. Two hour unilateral HFS (scheme as inset in **Fig. 6A**) of the medial perforant path induced strong LTP only in ipsilateral GCs, indicated by bilateral local field potential recordings and subsequent F-actin staining (**Fig. 6A-C**). We further found a strong Arc-expression in more than 90 % of all GCs that was restricted to the ipsilateral GCL (Fig. 6D) consistent with literature (Steward et al., 1998; Jungenitz et al., 2014). Notably, we were unable to detect ipsilateral Arc-expression in RV-labeled abGCs at 21 dpi (n = 4 animals). This was expected because in our prior BrdU-study with identical stimulation conditions, the number of ipsilateral Arc-positive abGCs (21 dpi) after HFS was less than 10 % (Jungenitz et al., 2014). Thus, this group was excluded from comparison. At all other time-points, Arc-negative and Arc-positive RV- or AAV-labeled GCs on the ipsilateral side (see exemplary 35 dpi morphologies in **Fig. 6E**) were compared with RV- or AAV-labeled GCs on the contralateral side which served as the non-activated control. We found structural differences in ipsilateral Arc-positive abGCs at 28 and 35 dpi that proved to be a significant reduction of STS exclusively in the OML (**Fig. 6F-H**). This was not observed in Arc-negative abGCs of the same age (**Fig. 6F-H**), suggesting that Arc-negative ipsilateral GCs indeed had not been sufficiently activated during HFS. Importantly, old abGCs (77 dpi) and mGCs showed no stimulation- or Arc-correlated differences in STS length (**Fig. 6F-H**), thus revealing a critical time window for activity-induced dendritic reorganization at 28-35 dpi (**Fig. 6I**).

8.5. Discussion

Here we present a detailed structural study of young and old abGCs, as well as mGCs, based on complete 3D-reconstructions of RV-GFP- or AAV-GFP-labeled dendritic trees. Our analysis provides four major findings: First, dendritic maturation of abGCs is essentially complete by three weeks after birth. Second, abGCs form a subgroup that stays structurally distinct from mGCs even when fully matured (77 dpi). Third, the structural differences between abGCs and mGCs can be accounted for by different developmental conditions in the perinatal and adult dentate gyrus (DG), as indicated by our morphological model. Fourth, only young abGCs (28-35 dpi) but neither old abGCs nor mGCs responded to high-frequency perforant path stimulation (HFS) with a reduction of short distal dendrites. In sum, we conclude that abGCs stay distinct from mGCs and that their dendritic arbor can be shaped by afferent activity during a narrow critical phase/time window.

Complete reconstructions of abGCs and mGCs

As recently reviewed, detailed knowledge of the dendritic morphology of abGCs would be important for the understanding, prevention, and treatment of neuropathological alterations that emerge in conjunction with impaired adult hippocampal neurogenesis (Llorens-Martín et al., 2016). To our knowledge, this is the first report of 3D-reconstructed complete dendritic trees of rat abGCs. In earlier studies, rat abGCs had been reconstructed in 2D using flattened z-stacks of 40-50 µm thick slices (Rosenzweig and Wojtowicz, 2011; Teixeira et al., 2012; Lee et al., 2015). In our study the average total dendritic length of all reconstructed GCs was 2255 ± 45 µm supra- and 2137 ± 49 µm infrapyramidally (**SupplFig. 2C**, AAV-labeled mGCs only: 2347 ± 120 µm and 2437 ± 172 µm, mean ± SEM). Using iontophoretic HRP-filling of GCs in adult rat hippocampal slices, Clairbone et al. (1990) reported a considerably higher total dendritic length of 3.478 ± 88 µm and 2.793 ± 74 µm, respectively. Furthermore, when we compared the publicly available GCs (Rihn and Claiborne, 1990) to our AAV-labeled mGCs we found our GCs to have a lower number of branch points (data not shown). However, results from John (1997)

using biocytin-fillings of hippocampal GCs in adult rats, were comparable to our data. Interestingly, they also found a tissue swelling of 35 % by the glycerol clearing step used by many former studies which might explain the reported higher dendritic lengths (Desmond and Levy, 1982; Claiborne et al., 1990; Rihn and Claiborne, 1990). A further explanation for discrepancies between different studies might be that GCs from the middle third (i.e. 30 to 70 % along HC) of the septotemporal axis were reconstructed in these studies, whereas we used only slices from the septal HC (i.e. 20 to 40 % along HC). It would be interesting to analyze if GCs generally become larger from septal to temporal HC.

Structural maturation of abGCs precedes the critical phase of functional integration

We found that maturation of the dendritic tree is largely completed at 21 dpi in RV-labeled rat abGCs, followed by only marginal structural changes identified as a reduction in number of short terminal segments (STS) between 21 and 28 dpi, and a transient increase of dendritic length that is restricted to week 5 (35 dpi) and to the IML. The end of major structural changes in abGCs at 4 weeks of age has also been shown in mouse (Zhao et al., 2006; Sun et al., 2013) arguing for a similar rate of maturation in mouse and rat. Interestingly, the reduction of STS in our study falls into the same phase when young mouse abGCs showed growth and pruning of terminal segments in a recent in vivo study (Gonçalves et al., 2016), suggesting similar dynamic processes in both species. Furthermore, in postnatal rat GCs, rapid dendritic growth followed by a reduction in distal primarily small segments was reported, arguing for a general intrinsic process in developing GCs (Rihn and Claiborne, 1990; Rahimi and Claiborne, 2007).

The critical phase of functional integration in abGCs has been determined to occur between the 4th and 6th week in mice (Ge et al., 2007; Mongiat et al., 2009; Restivo et al., 2015) which suggests that structural maturation of abGCs follows an endogenous program and might be mostly independent of specific functional synaptic input.

Structurally distinct populations of GCs in the dentate gyrus

Whether abGCs exhibit different functions as mGCs is currently a subject of strong debate. Whereas many studies indicate that after the critical time window, old abGCs and mGCs are functionally indistinguishable (Espósito et al., 2005; Laplagne et al., 2006; Nakashiba et al., 2012), others show that old abGCs still exert structural plasticity upon learning and are recruited during different learning tasks than mGCs (Lemaire et al., 2012; Tronel et al., 2014). However, until now, the structural divergence of old abGCs and old mGCs has not been analyzed in detail. Total dendritic length and number of branch points were reported to be similar (Vuksic et al., 2008; Sun et al., 2013) but postnatal GCs initially show multipolar morphologies compared to uni- or bipolar dendritic trees in immature abGCs (reviewed in Ribak and Shapiro, 2007). In the current study, we extended this knowledge and observed that abGCs have more dendrites ending in proximal regions, a higher amount of STS, and a higher curvature than mGCs. We proposed a morphological model explaining these differences by a stagnating growth of the ML, combined with a change of dendritic targets (a lower reelin-gradient, and more ingrown axonal fibers) of the adult compared to the postnatal DG. Similar to our model, pruning might occur prior to tissue growth in real perinatally born GCs, too, as they seem to maintain their total dendritic length despite massive DG expansion (Rihn and Claiborne, 1990), meaning that dendrites, most probably the shortest ones, must undergo pruning. However, another plausible explanation could be competition and space restriction: mGCs grow in a nearly unoccupied ML but subsequently lose their shorter branches to vacate space for newly ingrowing dendrites of abGCs, whereas the latter would not be able to fully extend their dendrites to the OML due to occupied space and only few free synaptic targets.

To estimate the functional impact of the structural disparities of abGCs and mGCs, combining both morphologies with a detailed biophysical model would be the next straight-forward step.

A novel form of dendritic reorganization in abGCs during the critical phase of synaptic integration

Following HFS of the medial perforant path, we found a reduction of distal STS exclusively in young abGCs (28-35 dpi) that responded with Arc expression (**Fig. 6H**). Notably, this cell age coincides with the steepest increase in HFS-induced Arc-positive cell numbers found in our earlier BrdU study (Jungenitz et al., 2014). Dendritic alterations following in vivo stimulation had been reported previously in neocortical layers 3 and 5 (Ivanco et al., 2000; Monfils and Teskey, 2004; Teskey et al., 2006), however this is the first report of activity-induced dendritic reorganization in the DG. Since short dendrites are often related to immature morphologies (Emoto, 2011), our observation could suggest that one population of abGCs was more mature than their Arc-negative counterparts and were therefore capable to exhibit IEG responsiveness. We argue that our findings rather indicate an activity-induced and Arc-correlated dendritic reorganization due to two reasons. First, whereas in mGCs the vast majority of STS was observed in the OML (**Fig. 4E**), this layer was nearly void of STS in Arc-positive young abGCs following HFS (**Fig. 6E, H**), indicating that the reduced STS cannot originate from intrinsic developmental pruning as in mGCs. Second, old abGCs (77 dpi) showed Arc expression without reduced STS, arguing against decreased STS being an indicator for maturity in abGCs. Interestingly, a recent in vivo time-lapse study reported accelerated pruning of young abGC dendrites in mice exposed to an enriched environment (Gonçalves et al., 2016) supporting the idea of young abGCs being amenable to activity-induced dendritic reorganization (illustrated in **Fig. 6I**).

We chose a study design where GCs of the contralateral unstimulated hemisphere served as the non-activated control in each animal which offers the advantage of direct comparison of stimulated and unstimulated cells within the same animal. However, contralateral GCs receive limited ipsilateral input via commissural entorhinal cortex or mossy cells axons. On the other side, the crossed temporo-dentate pathway from the ipsilateral entorhinal cortex to the contralateral DG was shown to be unable to evoke LTP under normal conditions (Wilson et al., 1979; Wilson, 1981; Reeves and Steward, 1986), To exclude

significant activation via commissural pathways, we performed contralateral LFP recordings during ipsilateral HFS and found no contralateral induction of LTP at the electrophysiological level or with the LTP marker F-actin (**Fig. 6B, C**). Furthermore, immediate-early-gene markers such as Arc (**Fig. 6D**), c-fos and zif-268 were expressed solely in the ipsilateral DG following HFS (Jungenitz et al., 2014) arguing against significant activation of the contralateral control GCs, that could lead to structural changes. In line with this, a recent study showed that activation of the hilar commissural pathway resulted in increased inhibition in contralateral GCs compared to increased excitation with perforant path stimulation from the same hemisphere (Hsu et al., 2015).

We used Arc to label GCs that had been synaptically activated during HFS. Could Arc also be mechanistically involved in the loss of STS in young abGCs? Arc had been shown to be involved in synaptic plasticity (reviewed in Bramham et al., 2010) and particularly in heterosynaptic LTD with a reduction of big mushroom, and formation of thin instable spines in unstimulated layers (Waung et al., 2008; Peebles et al., 2010; Okuno et al., 2012). Thus, one could speculate that destabilization of spines might lead to destabilization of the occupied dendrite, since dendritic and spine stability are tightly correlated (reviewed in Koleske, 2013). Spinogenesis in abGCs is starting during week 3 (van Praag et al., 2002; Espósito et al., 2005; Zhao et al., 2006; Ohkawa et al., 2012; Sun et al., 2013), thus dendrites in young abGCs, especially short ones, might be less stable and more amenable to reorganization, explaining the observed time window of 28-35 dpi (**Fig. 6H**). Interestingly, we previously showed that after entorhinal cortex lesion GCs not only lose spines but also dendrites located in denervated layers (Vuksic et al., 2011), suggesting that even old GCs show dendritic reorganization when a critical number of spines is lost.

What might be the functional consequence of such subtle changes as the loss of short distal dendrites in abGCs, whether developmentally- or activity-driven? Generally, dendritic morphology can substantially influence a neuron's information processing and excitability (Rall and Rinzel, 1973). Numerous studies have examined genetic deletions of key proteins and found aberrant

dendritic morphology together with substantial alterations of neuronal excitability (Duan et al., 2007; Fitzsimons et al., 2012; Šišková et al., 2014; Norkett et al., 2016). However, reduction in total dendritic length in our study was limited to ~5 %, which would result in very limited changes of input resistance, and thus excitability. Alternatively, reduction of distal STS might help abGCs in their suggested role in pattern separation (Myers and Scharfman, 2011; Nakashiba et al., 2012; Deng et al., 2013; Johnston et al., 2015): When GCs prune dendritic segments in the OML, they receive less contextual input from the lateral entorhinal cortex and thereby might sharpen the group of context features that they are responding to, which is a key requirement for pattern separation. However, even though granule cells are electrotonically compact neurons and signal propagation from somata to dendrites is quite fast and efficient (Schmidt-Hieber et al., 2007), the impact of single synaptic inputs (that would be reduced distally through loss of short dendrites) was reported to be rather weak (Krueppel et al., 2011). Hence, further investigations are necessary to elucidate the putative functional impact of reduced short distal dendrites.

8.6. Material and Methods

Animals

Young adult male Sprague-Dawley rats (8-13 weeks, 220-450 g; Charles River, Sulzfeld, Germany) were housed under standard laboratory conditions in large rat cages (30 cm x 40 cm). All animal experiments conformed to the German guidelines for the use of laboratory animals. A total of 24 animals (4 RV-21 dpi, 5 RV-28 dpi, 5 RV-35 dpi, 5 RV-77 dpi and 5 AAV, for details **see Tab. 1**) were used.

Retrovirus production

We used Calcium-Phosphate precipitation to co-transfect HEK293T cells with pCAG-GFP, pCMV-GP and pCMV-VSV-G (3:2:1) helper plasmids that together reconstitute the full viral vector (van Praag et al., 2002). Retrovirus-containing supernatant was collected 48 h after transfection. Supernatant was cleared from

cell debris by centrifugation at 3200 x g for 10 min, filtered through a 0.22 µm filter, concentrated by ultra-centrifugation at 65000 x g for 2 h, and resuspended in 200 µl phosphate buffered saline (PBS). Viral titer was 105 colony forming units. Aliquots were stored at 80°C.

Adeno-associated virus production

We used Calcium-Phosphate precipitation to co-transfect HEK293T cells with pDP1rs, pDG and GFP-vector helper plasmids (6:4:1) necessary for reproduction of the full viral vector (Kügler et al., 2001, 2003). Transfected HEK293T cells were collected 48 h after transfection. Cells were washed twice by centrifugation at 1500 x g for 5 min and resuspended in PBS. Multiple freeze thaw cycles (4×) were applied to set free the viral particles inside the cells. The supernatant was washed by centrifugation at 10000 rpm for 10 min. Aliquots were stored at 80°C.

Intra-hippocampal viral injection in vivo

Surgical procedures were performed under deep anesthesia (150 µg Medetomidin, 2 mg Midazolam, 5 µg Fentanyl per kg body weight i.m. initially, additional injections as needed). Rats were placed in a Kopf stereotaxic device (Kopf instruments, Tujunga, CA, U.S.A.) and two small holes (1.5-2.0 mm diameter) were drilled in the skull at -3.8 mm from Bregma and 2.2 mm laterally at both hemispheres. RV- or AAV-containing solution (0.75 µl per hemisphere) was slowly injected bilaterally within the dentate gyrus (DG, 3.2 mm and 3.7 mm below the brain surface) using a NanoFil syringe (World Precision Instruments, Inc., Sarasota, FL, U.S.A.) with a 35 gauge beveled needle (NF35BV-2; World Precision Instruments, Inc., Sarasota, FL, U.S.A.). Animals were perfused 14 days post injection (dpi) in the case of AAV and 21, 28, 35 or 77 dpi in the case of RV injection.

Perforant path stimulation

Animals were anesthetized with Urethane (1.25 g/kg body weight s. c. initially and additional injections as needed; 250 mg urethane/ml 0.9 % saline). Surgery and stimulation procedures were performed as previously described

(Schwarzacher et al., 2006; Jedlicka et al., 2009, 2015; Jungenitz et al., 2014). In short, a bipolar stainless steel stimulating electrode was placed in the angular bundle of the medial perforant path (coordinates from lambda: L: 4.5 mm; AP: +0.5 mm; V: -3.5 mm). Glass microelectrodes (1.5 mm outer diameter, filled with 0.9 % saline) were placed in the dorsal blade of the granule cell layer (coordinates from bregma: L: 2.0 mm, AP: -3.5 mm, V: -3.5 mm). 2 hours of high frequency stimulation (HFS) were performed that maximally evoked population spikes and induced robust LTP on the stimulated hemisphere (**see Fig. 6A, C**; Steward et al., 1998; Jungenitz et al., 2014). In three control animals, we put an additional stimulation and recording electrode on the opposite, contralateral hemisphere in order to estimate the effects of HFS of the medial perforant path on the contralateral DG (**Fig. 6C**). Only the early slope component of the evoked field potential was measured to avoid contamination by the population spike. Rats were transcardially perfused with a fixative containing 4 % paraformaldehyde in 0.1 M PBS (PFA), pH 7.4 immediately after stimulation was finished. F-actin (**Fig. 6B**) and Arc (**Fig. 6D1/2**) staining was used to further evaluate the selectivity of our medial perforant path stimulation and the LTP induction (Fukazawa et al., 2003; Jungenitz et al., 2014).

Tissue preparation

Brains were postfixed up to 18 h in 4 % PFA. Serial frontal sections of the hippocampus (300 µm) were cut with a vibratome, washed in 0.1 M TRIS-buffered saline (TBS), and stored at -20°C in cryoprotectant-solution (30 % ethylene glycol, 25 % glycerin in PBS).

Immunohistochemistry

300 µm sections were washed in TBS, blocked with 5 % bovine serum albumin (BSA, 1 h, room temperature), and incubated with an anti-GFP488 (mouse, 1:500, fluorescence-labeled Alexa 488, Sigma) primary antibody for 5 d at 4°C. To further increase the signal-to-noise ratio, a secondary fluorescence-labeled Alexa 488 antibody (1:1000, Vector Labs., Burlingame, CA, U.S.A.) was applied for 3 d at 4°C.

Image acquisition

Imaging of GFP-labeled GCs on both hemispheres was done with a custom-built two photon microscope based on Sutter Instruments Movable Objective Microscope (Sutter Instruments, Novato, CA, U.S.A.) and a 20 x water immersion objective (Olympus XLUMPlan FI, NA 0.95). The excitation source was a MaiTai HP Ti-sapphire mode-locked laser (Spectra-Physics, Darmstadt, Germany) tuned to a wavelength of 890 nm to excite GFP. ScanImage 3.8.1 (Pologruto et al. 2003) was used for image acquisition. Multiple image stack tiles were imaged to fully cover areas with GFP-labeled cells in the DG. The obtained image stacks were further processed using Matlab (MathWorks, Natick, MA, U.S.A.) and ImageJ (e.g. for contrast normalization) and subsequently stitched together using XuvStitch 1.8.0 in order to obtain an image stack of the complete DG area comprising all GFP-labeled cells (composite stack, **see Fig. 1A, B**).

Cell ID Assignment

In order to re-identify one cell in all images and sections, each cell located in the composite stack was assigned a unique cell ID marker in the cell's soma using ImageJ (National Institutes of Health). Cells were re-identified in the Arc-immunostained thin sections based on their location, morphology, and neighboring cells (reidentification success of > 85 %).

Dendritic reconstruction and post-processing

Reconstruction of complete GC dendritic trees was done with a customized version of the TREES Toolbox (Cuntz et al., 2010, 2011) in Matlab (MathWorks, Natick, MA, U.S.A.). Dendritic trees of the supra- and infrapyramidal blades and of the contra- (unstimulated) and ipsilateral (stimulated) hemispheres were reconstructed. Since dendritic morphologies of GCs can vary along the pyramidal blade, we attempted not to reconstruct cells at the hilar crest and to choose equal numbers of medially and laterally localized cells in order to obtain a general and unbiased picture of GC morphologies in the DG. We identified granule cells in the AAV-labeled population by their morphology and location of

the cell body within the GCL. Furthermore, since GCs localized superficially within the GCL can be different to deeply localized cells (Green and Juraska, 1985; Claiborne et al., 1990), we did not reconstruct AAV-labeled GCs from the two most superficial cell layers (for further criteria, see Results). RV-labeled GCs were always localized near to the hilar GCL border (**see Fig. S3C**). Even though we used 300 µm thick sections dendrites of GFP-labeled GCs were occasionally cut off. Therefore, cells with dendrites cut off in the proximal region (inner molecular layer (IML) or below) or cells with generally too many incomplete dendrites were excluded from reconstruction. The resulting numbers of reconstructed complete dendritic trees are summarized in **Tab. 1**.

Reconstruction was done by tracing the cell's dendrites to their end point, thereby placing nodes along the current dendrite section in 3D. Dendrites cut by the slicing process at the top or bottom of the stack were marked in order to rate completeness of the reconstructed tree post hoc. After reconstruction, all trees were resampled to an internode distance of 1 µm. Dendritic diameter and soma thickness was adjusted semi-automatically to fit the image counterpart, while ignoring the fluorescence halo around the branches of the tree. Dendritic completeness was rated by considering the amount and location of cut or faint dendrites.

For a layer-specific analysis of dendritic trees, the anatomical borders of the DG were reconstructed in each composite stack (**see example in Fig. 1C**) using a self-written program in Matlab (MathWorks, Natick, MA, U.S.A.). Borders between the outer, middle, and inner ML (OML, MML, and IML respectively) were automatically calculated by dividing the area between the fissure and the GCL into three equal parts. This rough estimation was chosen because of its simplicity and to make the reconstruction of a large number of GCs feasible. Immunostainings of the real molecular sublayers in rats (e.g. defining the IML with VGlut2, data not shown) confirmed this approximation. Nodes of all reconstructed trees were then automatically assigned to one of the following regions according to the layer contours: subgranular zone (SGZ), GCL, IML, MML, or OML (**Fig. 1D**).

Reslicing and immunohistochemistry in imaged tissue sections

In a subsequent step, the 300 μm frontal sections of the hippocampus were resliced to 50 μm frontal sections with a vibratome, and stored at -20°C in cryoprotectant solution (see above). Resliced sections were washed in TBS and blocked with 5 % bovine serum albumin (BSA, 1 h, room temperature) to reduce non-specific staining. To stain for the immediate-early-gene Arc (activity-regulated cytoskeleton-associated protein) as a marker of synaptic activation (Lyford et al., 1995), free floating sections were incubated with anti-Arc (rabbit, polyclonal, 1:1000, Synaptic Systems, Ctl. 156002) primary antibody for 48 h at room temperature and secondary fluorescence-labeled Alexa 568 antibodies (1:1000, Vector Labs., Burlingame, CA, U.S.A.) for 24 h at room temperature.

Image acquisition of Arc-stained sections

For expression analysis of Arc, all GFP-labeled granule cells located on a resliced section (ipsilateral and contralateral) were imaged using a confocal microscope (Nikon Eclipse 80i) and a 40 x oil immersion objective (N.A. 1.3). The general Arc staining pattern confirmed complete stimulation on the ipsilateral side (**Fig. 6B1**) whereas the lack of Arc expression on the contralateral hemisphere confirmed the absence of stimulation (**Fig. 6B2**). However, it was hard to obtain sufficient numbers of 77 dpi Arc-negative abGCs because the percentage of Arc-positive cells is already very high at this age (Jungenitz et al., 2014). We also found no Arc-negative AAV-GFP-labeled mGC in all 5 animals examined indicating that mGCs are fully functionally integrated into the DG.

Morphological analysis

Calculation of morphological parameters was done with Matlab (MathWorks, Natick, MA, U.S.A.), TREES Toolbox (Cuntz et al., 2010, 2011) and self-written algorithms. Only dendritic trees with a rated completeness of more than 70 % were further analyzed. For visualization purposes and cone fitting, dendritic trees were rotated and aligned automatically using principal component analysis. In detail, the somata centers were aligned first, followed by rotating the

dendritic centers of mass onto the x-axis. Finally, the tree was rotated around the x-axis to have the tree's maximum variation within the xy-plane. Dendritic parameters (e.g. number of branch and termination points, dendritic length, and branching angle) were additionally analyzed in each anatomical layer separately (see above for reconstruction and assignment of layers).

The soma thickness was directly taken from the diameter information of the soma reconstruction. The relative soma position (depth) within the GCL was calculated using the reconstructed anatomical borders of each DG, where 0 µm denotes the hilar GCL border and negative values denote somata located in the hilus. Similarly, the relative location of termination points was calculated with 0 % denoting the GCL-ML border and 100 % the hippocampal fissure. Terminal segments were assigned to the region where most of its length was located. Cut and thus incomplete segments were excluded from analysis. According to the terminal segment length histograms (**Fig. S1**) revealing two overlapping groups of segments with different average lengths, segments shorter than 100 µm were defined as short terminal segments (STS). Terminal segment length histograms were not tested for significant differences.

We assumed that the dendritic tree of GCs has a cone-like shape, which is in line with literature (Desmond and Levy, 1982; Amaral et al., 2007). To obtain the cone shape the tree's nodes were projected to the cone's base and the soma was defined as the cone end. Subsequently, a 2D Gaussian distribution was fitted to the projected nodes. The distance of 6 σ (i.e. ≈ 99 % of all nodes were enclosed by the cone) then represented the major and minor axes of the cone's base, respectively.

The 3D convex hull volume of each tree was calculated using the qhull algorithm in Matlab. Spatial density was calculated by subsampling the fitted cone into voxels (10 × 10 × 10 µm³) and calculating the Euclidian distance to the nearest dendrite. Spatial density in μm^{-1} was the inverse of this distance averaged over all voxels in the cone. The curvature was calculated as the mean of the second derivative of the unit direction vectors along all dendrites of the tree.

We analyzed the morphological differences between the supra- and the infrapyramidal blade and found only marginal differences in the Sholl distribution and the thickness of the molecular layer while the number of branching and termination points, STS length, mean location of topological points, total dendritic length, convex hull volume, curvature, soma position, soma thickness, branching angle, spatial density and length of the cone axis remained unchanged (**Fig. S2**). Since the differences found were negligible and the cell numbers in each blade were similar, cells were pooled together.

Statistical analysis of dendritic morphology

Data management, statistical analysis and visualization were done with Matlab. To test for statistical significance, we used an unpaired, two-tailed Student's t-test or one-way ANOVA (if more than two groups were compared) with Tukey's honestly significant difference criterion to correct for multiple comparisons. Since we reconstructed equal numbers of GCs in each animal of one group/condition (3-5) we assumed that between-animal variations average out in each group. Significance levels were set at $P < 0.05$ (*), $P < 0.01$ (**) and $P < 0.001$ (***). Group values are reported as means ± SEM.

Morphological Modeling

The morphological models of abGCs and mGCs were developed in Matlab (MathWorks, Natick, MA, U.S.A.) using a customized version of the TREES toolbox (Cuntz et al., 2010). Synthetic granule cell dendrite morphologies were generated by connecting target points using a minimum spanning tree (MST) algorithm based on wiring optimization principles as described previously (Cuntz et al., 2007, 2010). For the mGC model, first a postnatal (i.e. small) cubic DG volume was defined comprising the hilar region and GCL with a thickness of 45 µm each, as well as the inner, middle and outer molecular layer (IML, MML, OML) with a thickness of 50 µm each. The total ML thickness was therefore 150 µm. A cone shape was created by using fixed transverse and longitudinal angles of 33° and 22° starting at the hilar GCL border and reaching to the fissure. Target points were distributed in a cone-shaped volume with a relative distribution of 0 : 20 : 80 % (IML : MML : OML) that approximated

194

dendritic targets such as reelin-gradients mainly established by Cajal-Retzius cells in the postnatal DG (Alcántara et al., 1998; Pesold et al., 1998). GC growth is always directed, which means a dendrite growing to the right will never turn to reach a distant point to the left. In order to consider this directed growth, the random target points in IML, MML and OML were complemented by directed target points that were placed at random depths between the soma and clusters of random target points with a ratio of 60 % random to 40 % directed target points. All target points were subsequently connected by the MST algorithm satisfying two wiring costs: (1) the total amount of wiring should be minimal and (2) the path length from any target point to the soma should be minimal. (Cuntz et al., 2007) These two constraints were applied using a balancing factor of 0.9, which weighted the second cost against the first cost. Resampling to 1 µm internode distance and node jittering (two times with length constants 10 and 4 µm and standard deviations of 0.4 and 0.23 µm, respectively, but see function jitter_tree in TREES toolbox) was applied to mimic the curving of real dendrites during growth. At last, a soma was added. We then applied a pruning step that deleted all terminal segments smaller than an absolute threshold of 35 µm mimicking developmental pruning (**Fig. 5A, purple dendrites**). The resulting morphology represented mGCs in the young postnatal DG. To mimic the growth of DG, the DG and the tree was than stretched in z by a factor of 1.8 to obtain a final adult ML thickness of 270 µm, which approximates the average of the DG thickness in our slices from young adult rat (273.69 ± 1.82 µm, SEM, n = 240). Furthermore, both structures were also stretched in x and y by a factor of 2.25 and 2 to simulate DG expansion in the transverse and longitudinal direction. This resulted in the final mGC morphology. In contrast, abGCs grow in the adult DG. Hence, for the abGC model we stretched the DG volume first with the mentioned x, y and z factors before creating the cone volume and target points. The random target point distribution here was 25 : 20 : 55 % (IML : MML : OML) in order to mimic reduction of reelin-expressing cells in the adult OML (Alcántara et al., 1998; Pesold et al., 1998) and appearance of commissural axons as targets in the adult IML (Alcántara et al., 1998; Förster et al., 2006; Yu et al., 2014). The other parameters as well as the post-processing (resampling, jittering, adding soma and a pruning threshold of 35 µm) were exactly the same

as for the mGC model. With this method 10 abGC and 16 mGC morphologies were created to correspond to the numbers of contralateral reconstructions of 77 dpi abGCs and AAV-labeled mGCs, which the models should mimic. The subsequent morphological analysis and comparison of synthetic abGC and mGC morphologies was done in the same way as with the real morphologies.

8.7. References

Alcántara S, Ruiz M, Arcangelo GD, Ezan F, Lecea L De, Curran T, Sotelo C, Soriano E (1998) Regional and cellular patterns of reelin mRNA expression in the forebrain of the developing and adult mouse. J Neurosci 18:7779–7799.

Ascoli G a., Donohue DE, Halavi M (2007) NeuroMorpho.Org: A Central Resource for Neuronal Morphologies. J Neurosci 27:9247–9251.

Bergami M, Masserdotti G, Temprana SG, Motori E, Eriksson TM, Göbel J, Yang SM, Conzelmann KK, Schinder AF, Götz M, Berninger B (2015) A critical period for experience-dependent remodeling of adult-born neuron connectivity. Neuron 85:710–717.

Bergmann O, Spalding KL, Frisén J (2015) Adult Neurogenesis in Humans. Cold Spring Harb Perspect Biol 7:1–12.

Bramham CR, Alme MN, Bittins M, Kuipers SD, Nair RR, Pai B, Panja D, Schubert M, Soule J, Tiron A, Wibrand K (2010) The Arc of synaptic memory. Exp Brain Res 200:125–140.

Branco T, Häusser M (2010) The single dendritic branch as a fundamental functional unit in the nervous system. Curr Opin Neurobiol 20:494–502.

Brunner J, Neubrandt M, Van-Weert S, Andrási T, Kleine Borgmann FB, Jessberger S, Szabadics J (2014) Adult-born granule cells mature through two functionally distinct states. Elife:e03104.

Claiborne BJ, Amaral DG, Cowan WM (1990) Quantitative, three-dimensional analysis of granule cell dendrites in the rat dentate gyrus. J Comp Neurol 302:206–219.

Clelland CD, Choi M, Romberg C, Clemenson GD, Fragniere A, Tyers P, Jessberger S, Saksida LM, Barker R a, Gage FH, Bussey TJ (2009) A functional role for adult hippocampal neurogenesis in spatial pattern separation. Science (80-) 325:210–213.

Cuntz H, Borst A, Segev I (2007) Optimization principles of dendritic structure. Theor Biol Med Model 4:21.

Cuntz H, Forstner F, Borst A, Häusser M (2010) One rule to grow them all: a general theory of neuronal branching and its practical application. PLoS Comput Biol 6.

Cuntz H, Forstner F, Borst A, Häusser M (2011) The TREES Toolbox — Probing the Basis of Axonal and Dendritic Branching. Neuroinformatics 9:91–96.

Cuntz H, Forstner F, Haag J, Borst A (2008) The morphological identity of insect dendrites. PLoS Comput Biol 4:e1000251.

D'Arcangelo G (2014) Reelin in the Years: Controlling Neuronal Migration and Maturation in the Mammalian Brain. Adv Neurosci 2014:1–19.

Deng W, Mayford M, Gage FH (2013) Selection of distinct populations of dentate granule cells in response to inputs as a mechanism for pattern separation in mice. Elife 2:e00312.

Desmond NL, Levy WB (1982) A quantitative anatomical study of the granule cell dendritic fields of the rat dentate gyrus using a novel probabilistic method. J Comp Neurol 212:131–145.

Emoto K (2011) Dendrite remodeling in development and disease. Dev Growth Differ 53:277–286.

Espósito MS, Piatti VC, Laplagne DA, Morgenstern NA, Ferrari CC, Pitossi FJ, Schinder AF (2005) Neuronal differentiation in the adult hippocampus recapitulates embryonic development. J Neurosci 25:10074–10086.

Förster E, Zhao S, Frotscher M (2006) Laminating the hippocampus. Nat Rev Neurosci 7:259–267.

Frotscher M (2010) Role for Reelin in stabilizing cortical architecture. Trends Neurosci 33:407–414.

Fukazawa Y, Saitoh Y, Ozawa F, Ohta Y, Mizuno K, Inokuchi K (2003) Hippocampal LTP is accompanied by enhanced F-actin content within the dendritic spine that is essential for late LTP maintenance in vivo. Neuron 38:447–460.

Ge S, Yang C-H, Hsu K-S, Ming G-L, Song H (2007) A critical period for enhanced synaptic plasticity in newly generated neurons of the adult brain. Neuron 54:559–566.

Gonçalves JT, Bloyd CW, Shtrahman M, Johnston ST, Schafer ST, Parylak SL, Tran T, Chang T, Gage FH (2016) In vivo imaging of dendritic pruning in dentate granule cells. Nat Neurosci:5–10.

Gu Y, Arruda-Carvalho M, Wang J, Janoschka SR, Josselyn SA, Frankland PW, Ge S (2012) Optical controlling reveals time-dependent roles for adult-born dentate granule cells. Nat Neurosci 15:1700–1706.

Hsu T-T, Lee C-T, Tai M-H, Lien C-C (2015) Differential Recruitment of Dentate Gyrus Interneuron Types by Commissural Versus Perforant Pathways. Cereb Cortex:bhv127 – .

Ivanco TL, Racine RJ, Kolb B (2000) Morphology of layer III pyramidal neurons is altered following induction of LTP in sensorimotor cortex of the freely moving rat. Synapse 37:16–22.

Jedlicka P, Schwarzacher SW, Winkels R, Kienzler F, Frotscher M, Bramham CR, Schultz C, Bas Orth C, Deller T (2009) Impairment of in vivo theta-burst long-term potentiation and network excitability in the dentate gyrus of synaptopodin-deficient mice lacking the spine apparatus and the cisternal organelle. Hippocampus 19:130–140.

Jedlicka P, Vnencak M, Krueger DD, Jungenitz T, Brose N, Schwarzacher SW (2015) Neuroligin-1 regulates excitatory synaptic transmission, LTP and EPSP-spike coupling in the dentate gyrus in vivo. Brain Struct Funct 220:47–58.

Johnston ST, Shtrahman M, Parylak S, Gonçalves JT, Gage FH (2015) Paradox of Pattern Separation and Adult Neurogenesis: A Dual Role for New Neurons Balancing Memory Resolution and Robustness. Neurobiol Learn Mem.

Jungenitz T, Radic T, Jedlicka P, Schwarzacher SW (2014) High-frequency stimulation induces gradual immediate early gene expression in maturing adult-generated hippocampal granule cells. Cereb Cortex 24:1845–1857.

Kee N, Teixeira CM, Wang AH, Frankland PW (2007) Preferential incorporation of adult-generated granule cells into spatial memory networks in the dentate gyrus. Nat Neurosci 10:355–362.

Kempermann G (2015) Activity Dependency and Aging in the Regulation of Adult Neurogenesis. Cold Spring Harb Perspect Biol 7:a018929.

Koleske AJ (2013) Molecular mechanisms of dendrite stability. Nat Rev Neurosci 14:536–550.

Kügler S, Kilic E, Bähr M (2003) Human synapsin 1 gene promoter confers highly neuron-specific long-term transgene expression from an adenoviral vector in the adult rat brain depending on the transduced area. Gene Ther 10:337–347.

Kügler S, Meyn L, Holzmüller H, Gerhardt E, Isenmann S, Schulz JB, Bähr M (2001) Neuron-specific expression of therapeutic proteins: evaluation of different cellular promoters in recombinant adenoviral vectors. Mol Cell Neurosci 17:78–96.

Laplagne DA, Espósito MS, Piatti VC, Morgenstern NA, Zhao C, van Praag H, Gage FH, Schinder AF (2006) Functional convergence of neurons generated in the developing and adult hippocampus. PLoS Biol 4:e409.

Lee H, Kang E, Goodsmith D, Yoon DY, Song H, Knierim JJ, Ming G, Christian KM (2015) DISC1-mediated dysregulation of adult hippocampal neurogenesis in rats. Front Syst Neurosci 9:1–8.

Lefebvre JL, Sanes JR, Kay JN (2015) Development of Dendritic Form and Function. Annu Rev Cell Dev Biol 31:741–777.

Lemaire V, Tronel S, Montaron M-F, Fabre A, Dugast E, Abrous DN (2012) Long-Lasting Plasticity of Hippocampal Adult-Born Neurons. J Neurosci 32:3101–3108.

Li G, Pleasure SJ (2010) Ongoing interplay between the neural network and neurogenesis in the adult hippocampus. Curr Opin Neurobiol 20:126–133.

Loy R, Lynch G, Cotman CW (1977) Development of afferent lamination in the fascia dentata of the rat. Brain Res 121:229–243.

Lyford GL, Yamagata K, Kaufmann WE, Barnes CA, Sanders LK, Copeland NG, Gilbert DJ, Jenkins NA, Lanahan AA, Worley PF (1995) Arc, a growth factor and activity-regulated gene, encodes a novel cytoskeleton-associated protein that is enriched in neuronal dendrites. Neuron 14:433–445.

Mainen ZF, Sejnowski TJ (1996) Influence of dendritic structure on firing pattern in model neocortical neurons. Nature 382:363–366.

Marín-Burgin A, Mongiat L a, Pardi MB, Schinder AF (2012) Unique processing during a period of high excitation/inhibition balance in adult-born neurons. Science 335:1238–1242.

Mathews EA, Morgenstern NA, Piatti VC, Zhao C, Jessberger S, Schinder AF, Gage FH (2010) A distinctive layering pattern of mouse dentate granule cells is generated by developmental and adult neurogenesis. J Comp Neurol 518:4479–4490.

Monfils M-H, Teskey GC (2004) Induction of long-term depression is associated with decreased dendritic length and spine density in layers III and V of sensorimotor neocortex. Synapse 53:114–121.

Mongiat L a, Espósito MS, Lombardi G, Schinder AF (2009) Reliable activation of immature neurons in the adult hippocampus. PLoS One 4:e5320.

Muramatsu R, Ikegaya Y, Matsuki N, Koyama R (2007) Neonatally born granule cells numerically dominate adult mice dentate gyrus. Neuroscience 148:593–598.

Myers CEC, Scharfman HE (2011) Pattern separation in the dentate gyrus: A role for the CA3 backprojection. Hippocampus 21:1190–1215.

Nakashiba T, Cushman JD, Pelkey K a, Renaudineau S, Buhl DL, McHugh TJ, Barrera VR, Chittajallu R, Iwamoto KS, McBain CJ, Fanselow MS, Tonegawa S (2012) Young Dentate Granule Cells Mediate Pattern Separation, whereas Old Granule Cells Facilitate Pattern Completion. Cell 149:188–201.

Ohkawa N, Saitoh Y, Tokunaga E, Nihonmatsu I, Ozawa F, Murayama A, Shibata F, Kitamura T, Inokuchi K (2012) Spine formation pattern of adult-born neurons is differentially modulated by the induction timing and location of hippocampal plasticity. PLoS One 7:e45270.

Okuno H, Akashi K, Ishii Y, Yagishita-Kyo N, Suzuki K, Nonaka M, Kawashima T, Fujii H, Takemoto-Kimura S, Abe M, Natsume R, Chowdhury S, Sakimura K, Worley PF, Bito H (2012) Inverse Synaptic Tagging of Inactive Synapses via Dynamic Interaction of Arc/Arg3.1 with CaMKIIβ. Cell 149:886–898.

Peebles CL, Yoo J, Thwin MT, Palop JJ, Noebels JL, Finkbeiner S (2010) Arc regulates spine morphology and maintains network stability in vivo. Proc Natl Acad Sci U S A 107:18173–18178.

Pesold C, Impagnatiello F, Pisu MG, Uzunov DP, Costa E, Guidotti A, Caruncho HJ (1998) Reelin is preferentially expressed in neurons synthesizing gamma-aminobutyric acid in cortex and hippocampus of adult rats. Proc Natl Acad Sci U S A 95:3221–3226.

Radic T, Al-Qaisi O, Jungenitz T, Beining M, Schwarzacher SW (2015) Differential Structural Development of Adult-Born Septal Hippocampal Granule Cells in the Thy1-GFP Mouse, Nuclear Size as a New Index of Maturation. PLoS One 10:e0135493.

Rahimi O, Claiborne BJ (2007) Morphological development and maturation of granule neuron dendrites in the rat dentate gyrus. Prog Brain Res 163:167–181.

Reeves TM, Steward O (1986) Emergence of the capacity for LTP during reinnervation of the dentate gyrus: evidence that abnormally shaped spines can mediate LTP. Exp Brain Res 65:167–175.

Restivo L, Niibori Y, Mercaldo V, Josselyn SA, Frankland PW (2015) Development of Adult-Generated Cell Connectivity with Excitatory and Inhibitory Cell Populations in the Hippocampus. J Neurosci 35:10600–10612.

Ribak CE, Shapiro L a (2007) Dendritic development of newly generated neurons in the adult brain. Brain Res Rev 55:390–394.

Rihn LL, Claiborne BJ (1990) Dendritic growth and regression in rat dentate granule cells during late postnatal development. Dev Brain Res 54:115–124.

Rosenzweig S, Wojtowicz JM (2011) Analyzing dendritic growth in a population of immature neurons in the adult dentate gyrus using laminar quantification of disjointed dendrites. Front Neurosci 5:34.

Schneider CJ, Cuntz H, Soltesz I (2014) Linking Macroscopic with Microscopic Neuroanatomy Using Synthetic Neuronal Populations. PLoS Comput Biol 10:e1003921.

Schuldiner O, Yaron A (2014) Mechanisms of developmental neurite pruning. Cell Mol Life Sci 72:101–119.

Schwarzacher S, Vuksic M, Haas C, Burbach G, Sloviter RS, Deller T (2006) Neuronal hyperactivity induces astrocytic expression of neurocan in the adult rat hippocampus. Glia 714:704–714.

Sengupta P (2013) The Laboratory Rat: Relating Its Age With Human's. Int J Prev Med 4:624–630.

Sidiropoulou K, Pissadaki EK, Poirazi P (2006) Inside the brain of a neuron. EMBO Rep 7:886–892.

Steward O, Wallace CS, Lyford GL, Worley PF (1998) Synaptic activation causes the mRNA for the IEG Arc to localize selectively near activated postsynaptic sites on dendrites. Neuron 21:741–751.

Stone SSD, Teixeira CM, Zaslavsky K, Wheeler AL, Martinez-Canabal A, Wang AH, Sakaguchi M, Lozano AM, Frankland PW (2011) Functional convergence of developmentally and adult-generated granule cells in dentate gyrus circuits supporting hippocampus-dependent memory. Hippocampus 21:1348–1362.

Sun GJ, Sailor KA, Mahmood QA, Chavali N, Christian KM, Song H, Ming G (2013) Seamless reconstruction of intact adult-born neurons by serial end-block imaging reveals complex axonal guidance and development in the adult hippocampus. J Neurosci 33:11400–11411.

Tavosanis G (2012) Dendritic structural plasticity. Dev Neurobiol 72:73–86.

Teixeira CM, Kron MM, Masachs N, Zhang H, Lagace DC, Martinez A, Reillo I, Duan X, Bosch C, Pujadas L, Brunso L, Song H, Eisch AJ, Borrell V, Howell BW, Parent JM, Soriano E (2012) Cell-Autonomous Inactivation of the Reelin Pathway Impairs Adult Neurogenesis in the Hippocampus. J Neurosci 32:12051–12065.

Temprana SG, Mongiat LA, Yang SM, Trinchero MF, Alvarez DD, Kropff E, Giacomini D, Beltramone N, Lanuza GM, Schinder AF (2014) Delayed Coupling to Feedback Inhibition during a Critical Period for the Integration of Adult-Born Granule Cells. Neuron:1–15.

Teskey GC, Monfils M-HH, Silasi G, Kolb B, Young NA, Van Rooyen F, Larson SEM, Flynn C, Monfils M-HH, Kleim JA, Henry LC, Goertzen CD, Silasi G, Kolb B (2006) Neocortical kindling is associated with opposing alterations in dendritic morphology in neocortical layer V and striatum from neocortical layer III. Synapse 59:1–9.

Tronel S, Lemaire V, Charrier V, Montaron M-F, Abrous DN (2014) Influence of ontogenetic age on the role of dentate granule neurons. Brain Struct Funct:1–17.

van Praag H, Schinder AF, Christie BR, Toni N, Palmer TD, Gage FH (2002) Functional neurogenesis in the adult hippocampus. Nature 415:1030–1034.

Vuksic M, Del Turco D, Bas Orth C, Burbach GJ, Feng G, Müller CM, Schwarzacher SW, Deller T (2008) 3D-reconstruction and functional properties of GFP-positive and GFP-negative granule cells in the fascia dentata of the Thy1-GFP mouse. Hippocampus 18:364–375.

Vuksic M, Del Turco D, Vlachos A, Schuldt G, Müller CM, Schneider G, Deller T (2011) Unilateral entorhinal denervation leads to long-lasting dendritic alterations of mouse hippocampal granule cells. Exp Neurol 230:176–185.

Waung MW, Pfeiffer BE, Nosyreva ED, Ronesi JA, Huber KM (2008) Rapid Translation of Arc/Arg3.1 Selectively Mediates mGluR-Dependent LTD through Persistent Increases in AMPAR Endocytosis Rate. Neuron 59:84–97.

Wilson RC (1981) Changes in translation of synaptic excitation to dentate granule cell discharge accompanying long-term potentiation. I. Differences between normal and reinnervated dentate gyrus. J Neurophysiol 46:324–338.

Wilson RC, Levy WB, Steward O (1979) Functional effects of lesion-induced plasticity: long term potentiation in formal and lesion-induced temporodentate connections. Brain Res 176:65–78.

Yu D, Fan W, Wu P, Deng J, Liu J, Niu Y, Li M, Deng J (2014) Characterization of hippocampal Cajal-Retzius cells during development in a mouse model of Alzheimer's disease (Tg2576). Neural Regen Res 9:394.

Zhao C, Teng EM, Summers RG, Ming G-L, Gage FH (2006) Distinct morphological stages of dentate granule neuron maturation in the adult mouse hippocampus. J Neurosci 26:3–11.

8.8. Tables with legend

Table 1 Summary of cell and animal numbers

Groups	Cells			Animals		
	Arc^+(ipsi)	Arc^- (ipsi)	contra	Arc^+ (ipsi)	Arc^- (ipsi)	contra
abGC (21 dpi)	$-$ [a]	23	9	$-$ [a]	4	3
abGC (28 dpi)	21	25	21	5	5	5
abGC (35 dpi)	24	22	20	5	5	5
abGC (77 dpi)	17	15	10	5	4	3
mGC (AAV)	17	$-$ [a]	16	5	$-$ [a]	5
Total	79	85	76	20	18	21

[a] No corresponding cells could be found (see Material & Methods).

8.9. Figures with legends
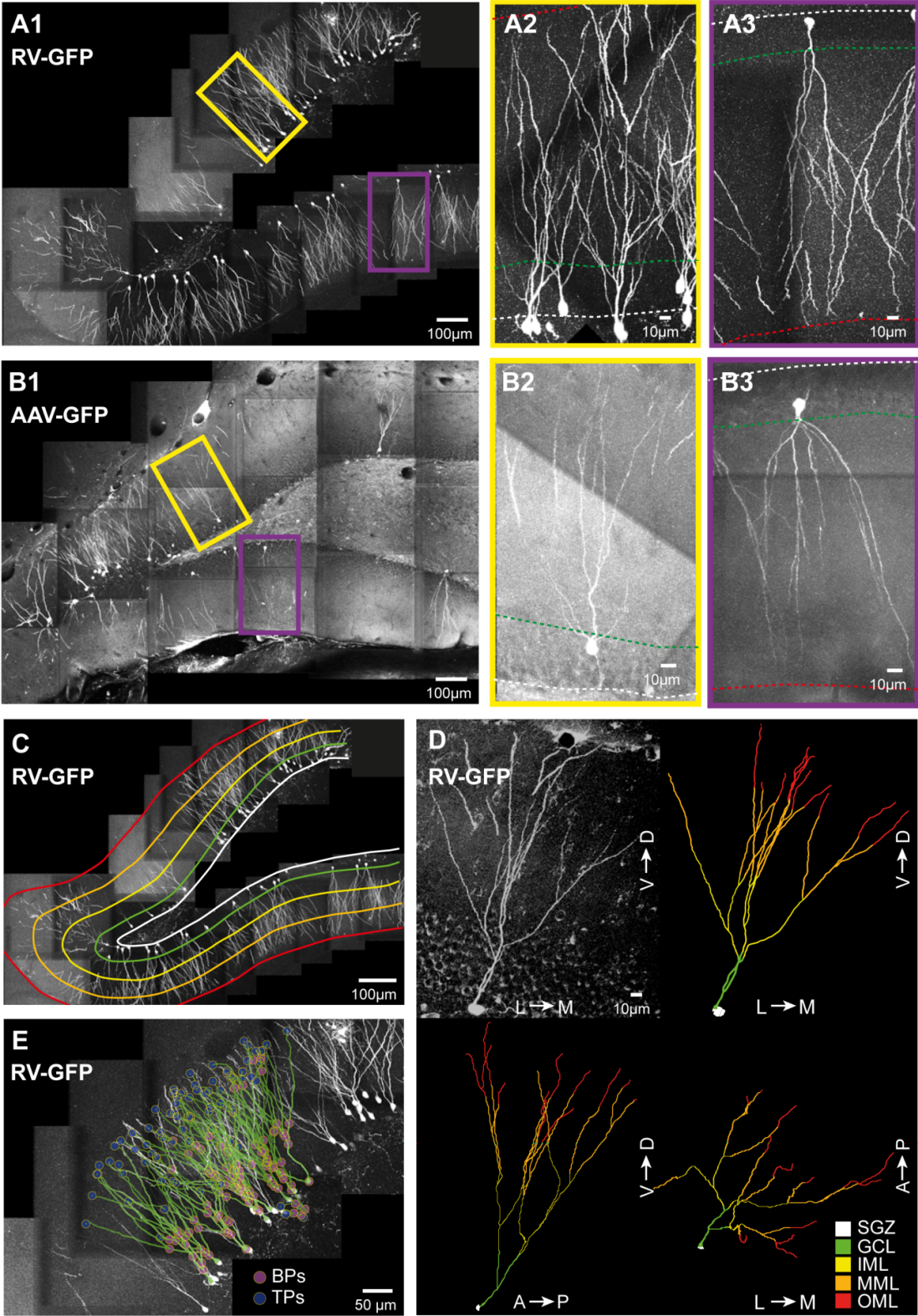
◄ **Figure 1. Obtaining morphologies of RV-labeled adult-born granule cells (abGCs) and AAV-labeled mature granule cells (mGCs) in the dentate gyrus (DG).** **A**, abGCs (28 dpi) labeled with the RV-CAG-GFP vector. **A1**, Maximum intensity projection in z of a stitched composite stack imaged with two-photon microscopy showing the pattern of GFP-positive abGCs. **A2–3**, High magnification of **A1** showing suprapyramidal (yellow frame, **A2**) and infrapyramidal (violet frame, **A3**) abGCs. Borders of the GCL to the hilus (white) and to the IML (green) as well as the fissure (red) are illustrated as dashed lines. **B**, mGCs labeled with the AAV-Syn1-GFP vector. Same layout as in **A. C**, Reconstructed DG layers from **A1** (border colors: white: hilus-GCL, green: GCL-ML, yellow: IML-MML, orange: MML-OML, red: hippocampal fissure). **D**, Representative fluorescence image of an abGC (28 dpi, upper left panel) with a corresponding 3D-reconstruction (3 different views: combinations of L → M lateral-medial, V → D ventral-dorsal, A → P anterior-posterior). The reconstructed DG layers were mapped onto the 3D-reconstruction of GCs to assign the respective layers (see legend). **E**, Overlay of dendritic reconstructions (green) and the fluorescence image of suprapyramidal abGCs from **A1** with automatically marked branching (magenta, BPs) and termination (blue, TPs) points. Abbreviations: subgranular zone (SGZ); granule cell layer (GCL); inner, middle and outer molecular layer (IML, MML, and OML).
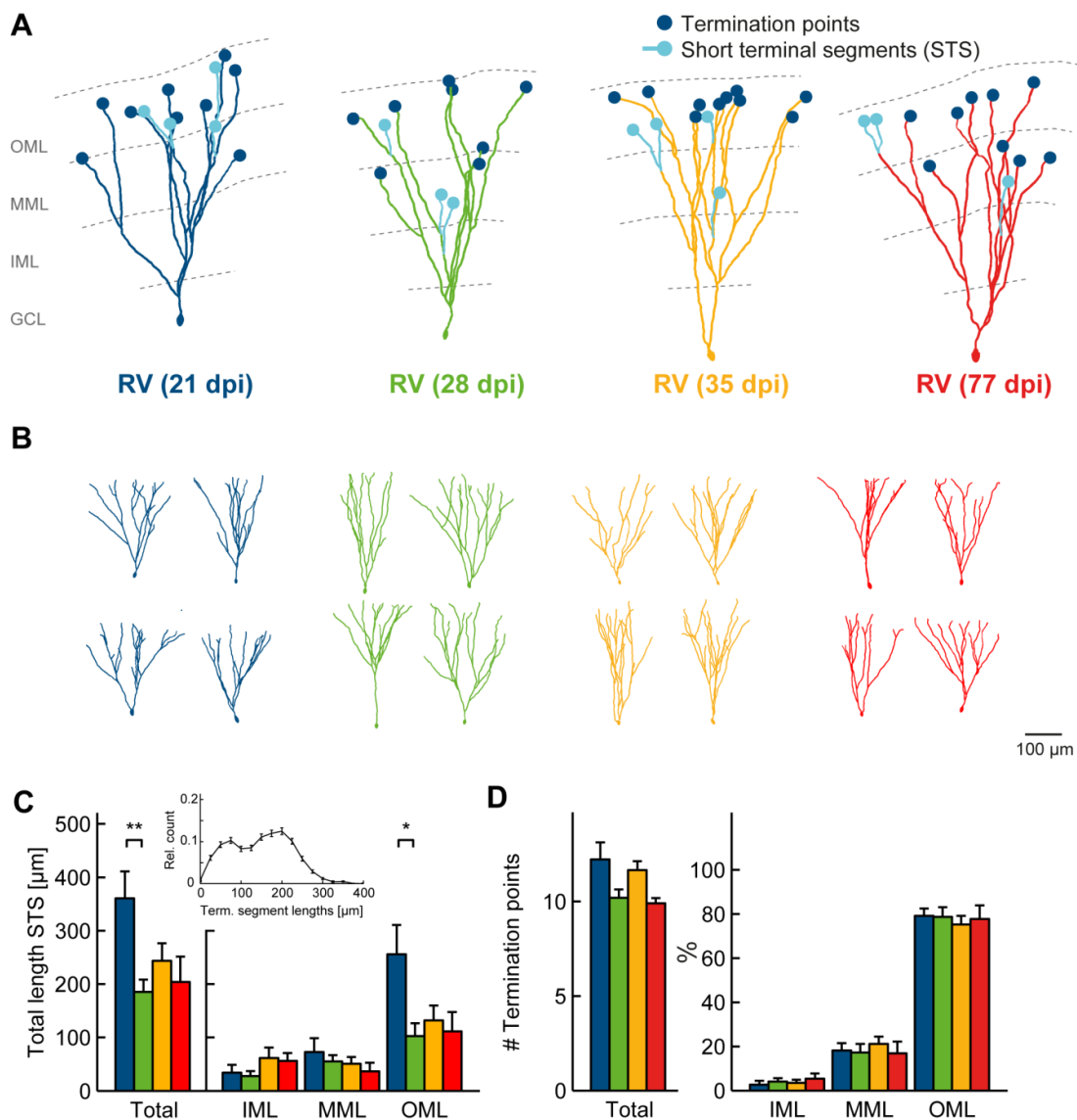
Figure 2. Pruning of short terminal segments (STS) in the dendrites of abGCs 3-4 weeks after cell birth. A, Representative examples of abGC reconstructions (21 - 77 dpi) with marked termination points (blue) and short terminal segments (STS, cyan). **B**, More examples illustrating the variation in dendritic morphology. **C**, Mean summed length of STS showing dendritic pruning in the OML between 21 and 28 dpi. **D**, The number of termination points and their relative distribution in the molecular layer stays constant over all time points investigated. Abbreviations: IML, inner molecular layer; MML, middle molecular layer; OML, outer molecular layer. Error bars represent mean ± SEM. P values are $P < 0.05$ (*) and $P < 0.01$ (**). Cell (and animal) numbers: 21 dpi: 9 (3); 28 dpi: 21 (5); 35 dpi: 20 (5); 77 dpi: 10 (3).
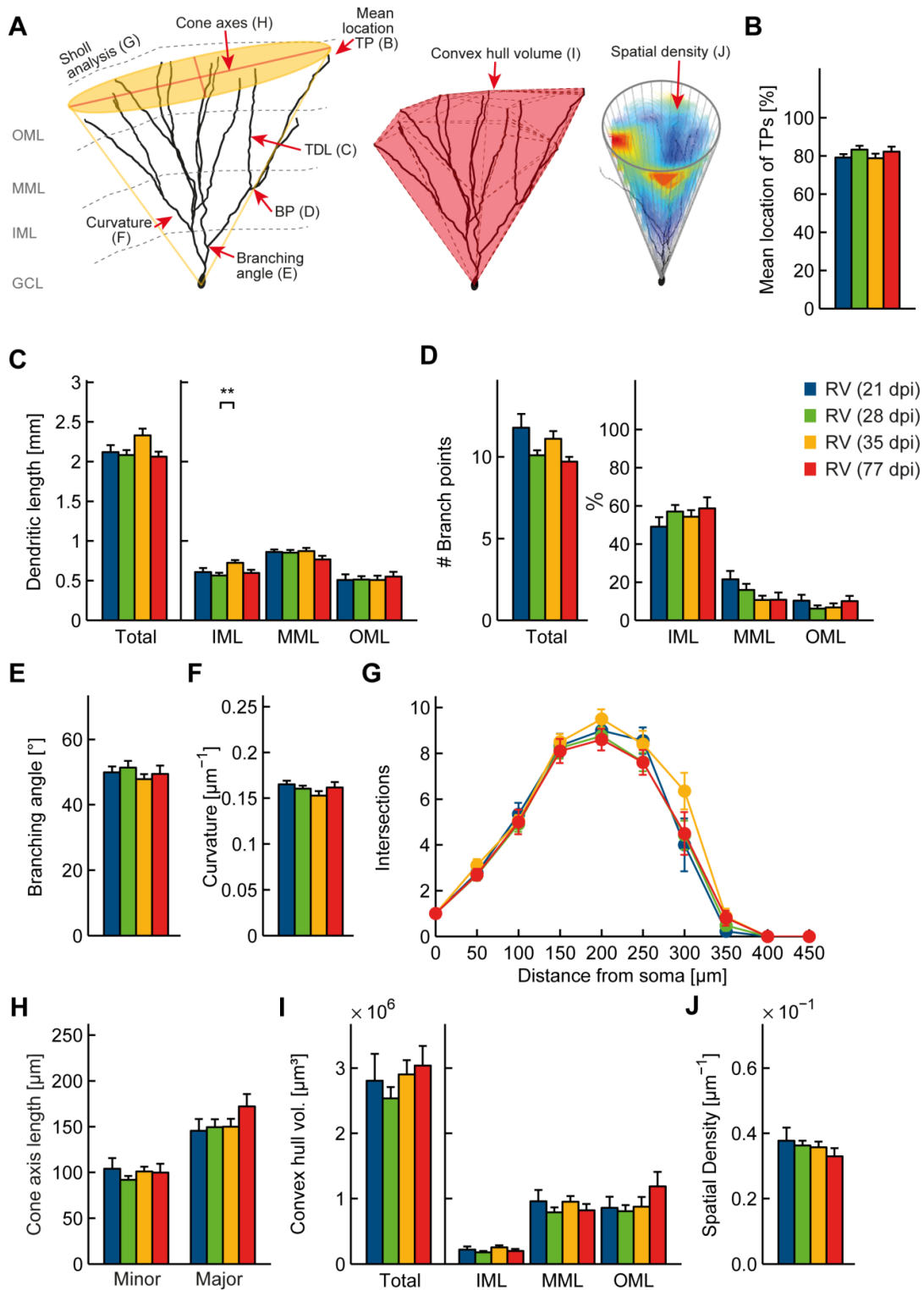
Figure 3. Detailed morphological analysis reveals that structural maturation of developing abGCs is completed by 3 weeks after cell birth. A, Schematic illustrating morphological parameters analyzed in **B–J** using the TREES toolbox and custom software in Matlab. **B**, Mean location of termination points. **C**, Dendritic length. **D**, Branch points and their relative distribution in the molecular layer. **E**, Branching

209

angle. **F**, Curvature. **G**, Sholl intersections. **H**, Length of major and minor axis of the fitted Gaussian cone. **I**, Volume of the tree's convex hull. **J**, Spatial density of the tree within its cone-shaped space. See text and Methods for a detailed description of each dendritic parameter. Error bars represent mean ± SEM. P values are $P < 0.01$ (**). Cell (and animal) numbers: 21 dpi: 9 (3); 28 dpi: 21 (5); 35 dpi: 20 (5); 77 dpi: 10 (3). Abbreviations: branch point (BP), termination point (TP), total dendritic length (TDL), inner molecular layer (IML), middle molecular layer (MML), outer molecular layer (OML).
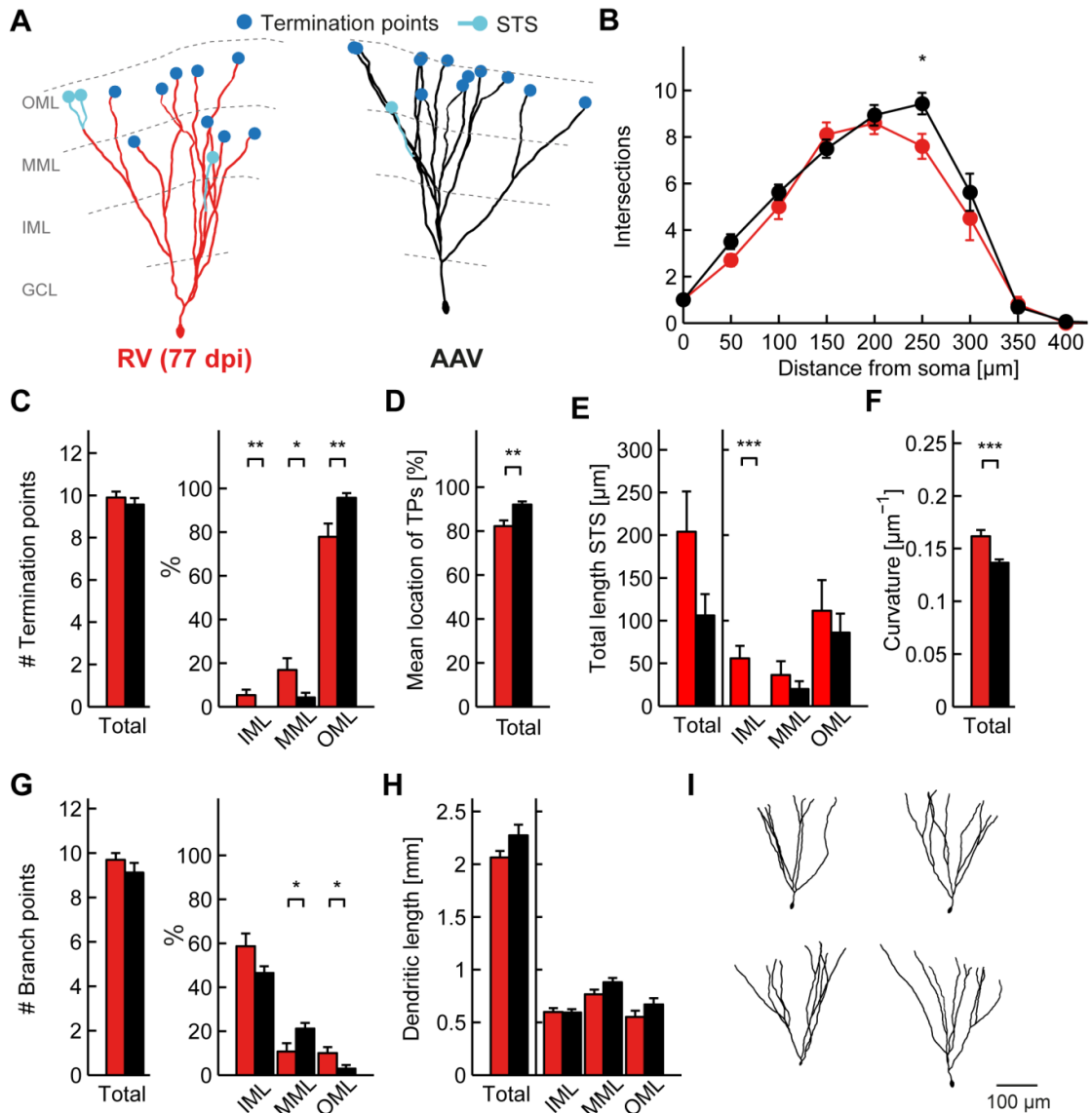
Figure 4. Old abGCs remain structurally distinct from mGCs. A, Representative reconstruction of an 77 dpi old abGCs (red) and a AAV-labeled mGC (black) with marked termination points (blue) and STS (cyan). **B**, More examples of AAV-labeled mGCs illustrating the variation in dendritic morphology **C**, Mean summed length of STS. **D**, Termination points and their relative distribution in the molecular layer. **E**, Mean location of termination points. **F**, Curvature. **G**, Branch points and their relative distribution in ML. **H**, Dendritic length. Error bars are mean ± SEM. P values are $P < 0.05$ (*), $P < 0.01$ (**) and $P < 0.005$ (***). Cell (and animal) numbers: 77 dpi: 10 (3); AAV: 16 (5).
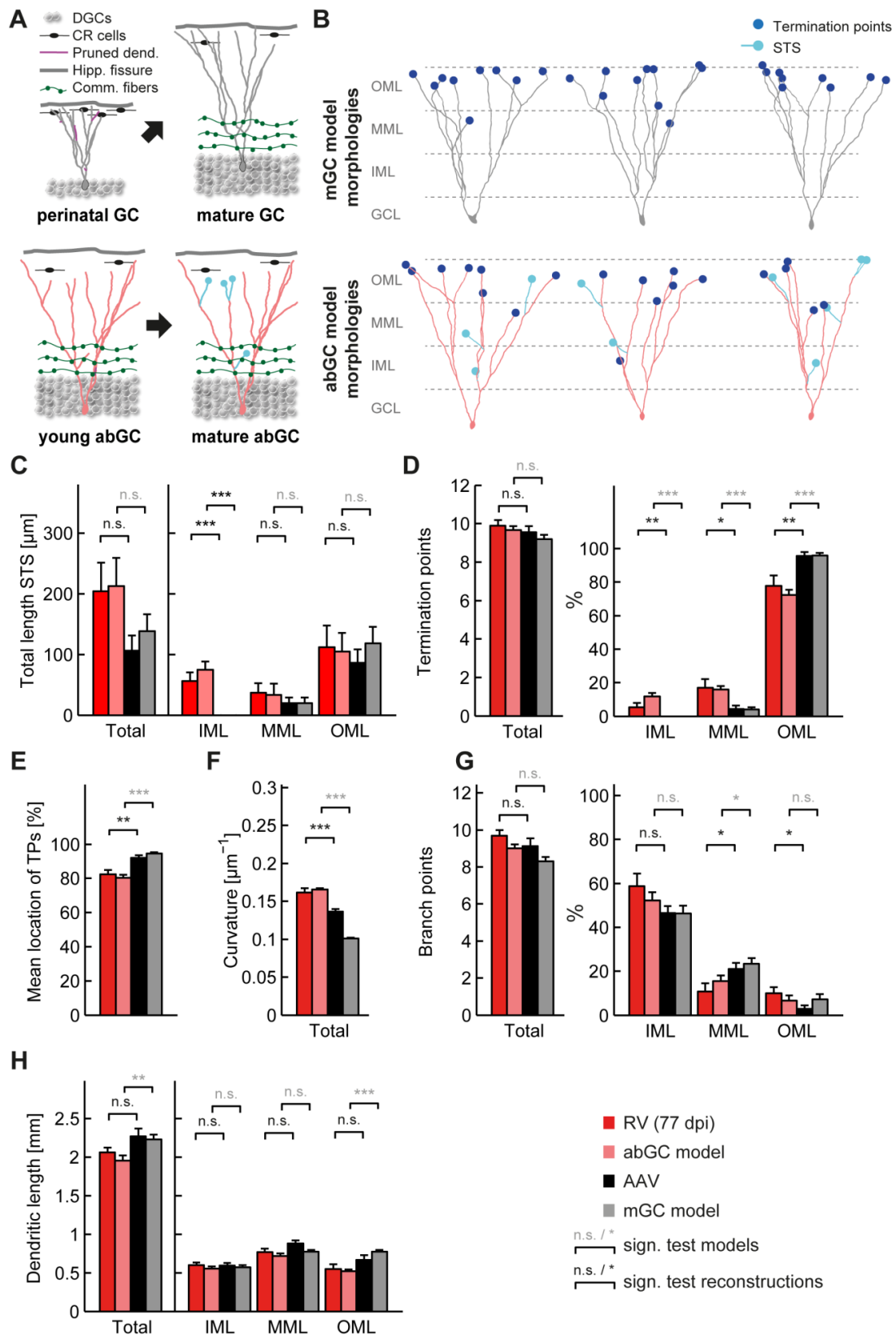
◄ **Figure 5. Morphological model shows that dendritic pruning and developmental growth of the dentate gyrus (DG) accounts for experimental data. A**, Schematic explaining the difference between the morphological model of abGCs and mGCs. AAV-positive mGCs grow in the young small DG with a high reelin gradient produced by Cajal-Retzius (CR) and other cells (upper left panel), and are stretched subsequently when the DG matures (upper right panel). RV-positive abGCs grow in the already stretched, mature DG with a lower reelin gradient but commissural fibers as targets in the IML (lower panels). Short dendritic segments that are pruned during maturation are depicted in purple. STS are depicted in cyan. **B**, Representative examples of synthetic morphologies for both RV-labeled abGCs and AAV-labeled mGCs created using a minimum spanning tree algorithm of the TREES toolbox (see Methods for details). **C–H**, Morphological comparison of synthetic and reconstructed morphologies (AAV: black, mGC model: gray, RV 77 dpi: red, abGC model bright red). Test for significance was only done between RV (77 dpi) and AAV (lower row, black text) as well as between the abGC and mGC model (upper row, gray text) in order to illustrate where experimental and model data are comparable. No differences in both cases imply consensus between experiment and model, too. Note that consensus was found in all parameters except for the number of branch points in the OML (**G**), and the total dendritic length and dendritic length in the OML (**H**). Error bars are mean ± SEM. Cell (and animal) numbers: 77 dpi: 10 (3); RV model: 10 (-); AAV: 16 (5); AAV model: 16 (-).
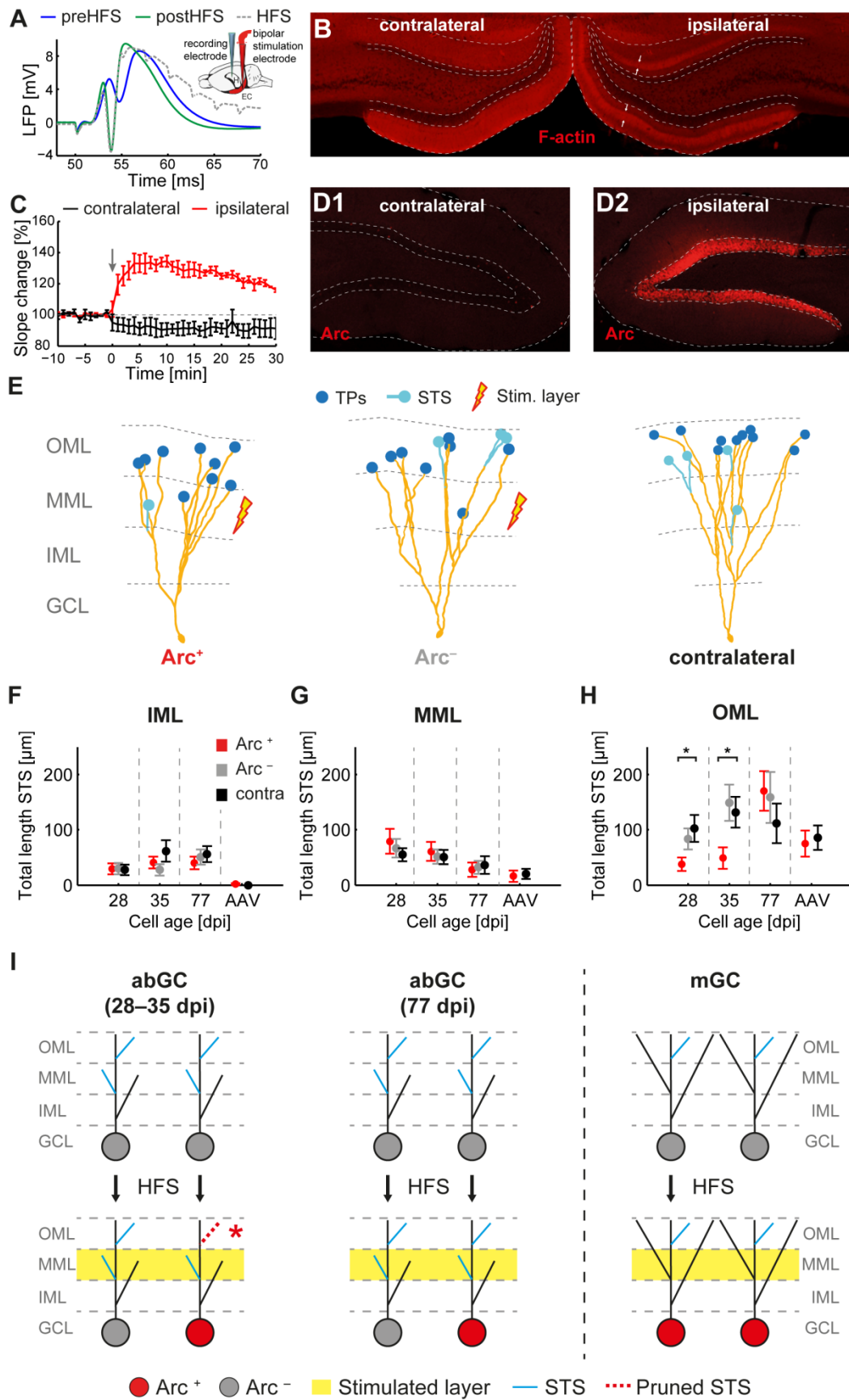
◄ **Figure 6. Arc expression correlates with reduced short terminal segments in the OML of young abGCs following HFS. A**, Local field potentials recorded in the ipsilateral DG before (blue) and after (green) 2 h HFS (test pulse to the ipsilateral medial perforant path, 5 traces averaged). Inset: Schematic of rat brain with bipolar stimulation electrode (red) in the medial perforant path of the entorhinal cortex (EC) and a recording electrode (blue) in the DG of the hippocampus (H). **B**, Epifluorescence images of a 50 µm frontal section showing enrichment of F-actin in the ipsilateral MML (white arrows) compared to homogenous F-actin distribution in the contralateral ML. **C**, Change of the early local field potential slope following a test pulse (500 µA) to the corresponding medial perforant path (red: ipsilateral, black: contralateral, n = 3). The start of the HFS protocol is indicated (gray arrow). **D**, Confocal images (maximum intensity z projection) of a 50 µm frontal section showing absence of Arc expression in the contralateral hemisphere (**D1**) compared to robust Arc expression in the granule cell layer of the ipsilateral side (**D2**). **E**, Representative dendritic reconstructions of an Arc-positive (left tree) and Arc-negative (middle tree) ipsilateral abGC (35 dpi) compared to a contralateral (right tree) abGC (35 dpi). **F-G**, Mean summed lengths of STS in the MML (**F**) and OML (**G**) after 2 h of medial perforant path stimulation (HFS) are shown for the RV-labeled abGC (28-77 dpi) groups and the AAV-labeled mGCs. Gray values denote Arc-negative cells, red values denote Arc-positive cells, and black values denote the contralateral side as the unstimulated control. Note that in the stimulated hemisphere, there were no Arc-negative mGCs as all mGCs were Arc-positive (see Methods). **H**, Schematic illustrating that abGCs exhibit a critical phase (28-35 dpi) when medial perforant path stimulation of the middle molecular layer (yellow band, lower row) can induce dendritic reorganization in the OML as observed by the loss of STS (dashed red segment and asterisk). STS in other layers or cells of different ages (cyan segments) were not affected by the stimulation. Error bars are mean + SEM. P values are $P < 0.05$ (*) and $P < 0.01$ (**). Abbreviations: short terminal segment (STS), inner molecular layer (IML), middle molecular layer (MML), outer molecular layer (OML).
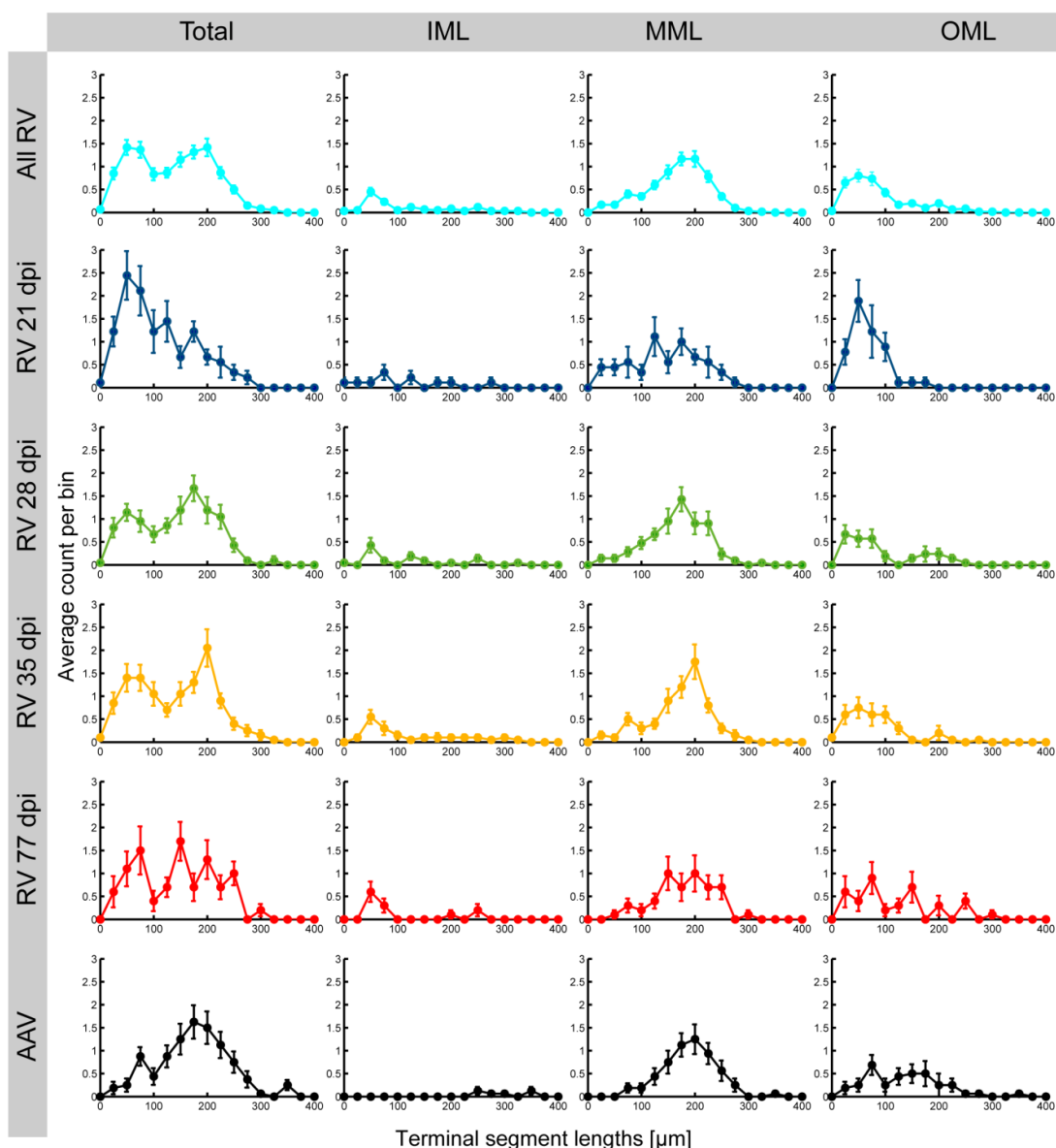
Supplementary Figure 1: Terminal segments change in length at different ages.
Absolute histograms of terminal dendritic segments in abGCs (RV 21-77 dpi) and mGCs (AAV) of the complete dendritic arbor ("Total", left column) or in the inner, middle and outer molecular layer (IML, MML, OML), respectively. Note the bimodal distribution of shorter and larger terminal segments and the shift from mainly short terminal segments (STS, < 100 µm) at 21 dpi to mainly large terminal segments in AAV-labeled mGCs in the left column. The few STS which are left in mGCs are located in the OML. Since the binning dilutes the differences (which can affect as much as 10 % of the total dendritic length as from RV 21 to 28 dpi), we summed the length of STS for the main figures.
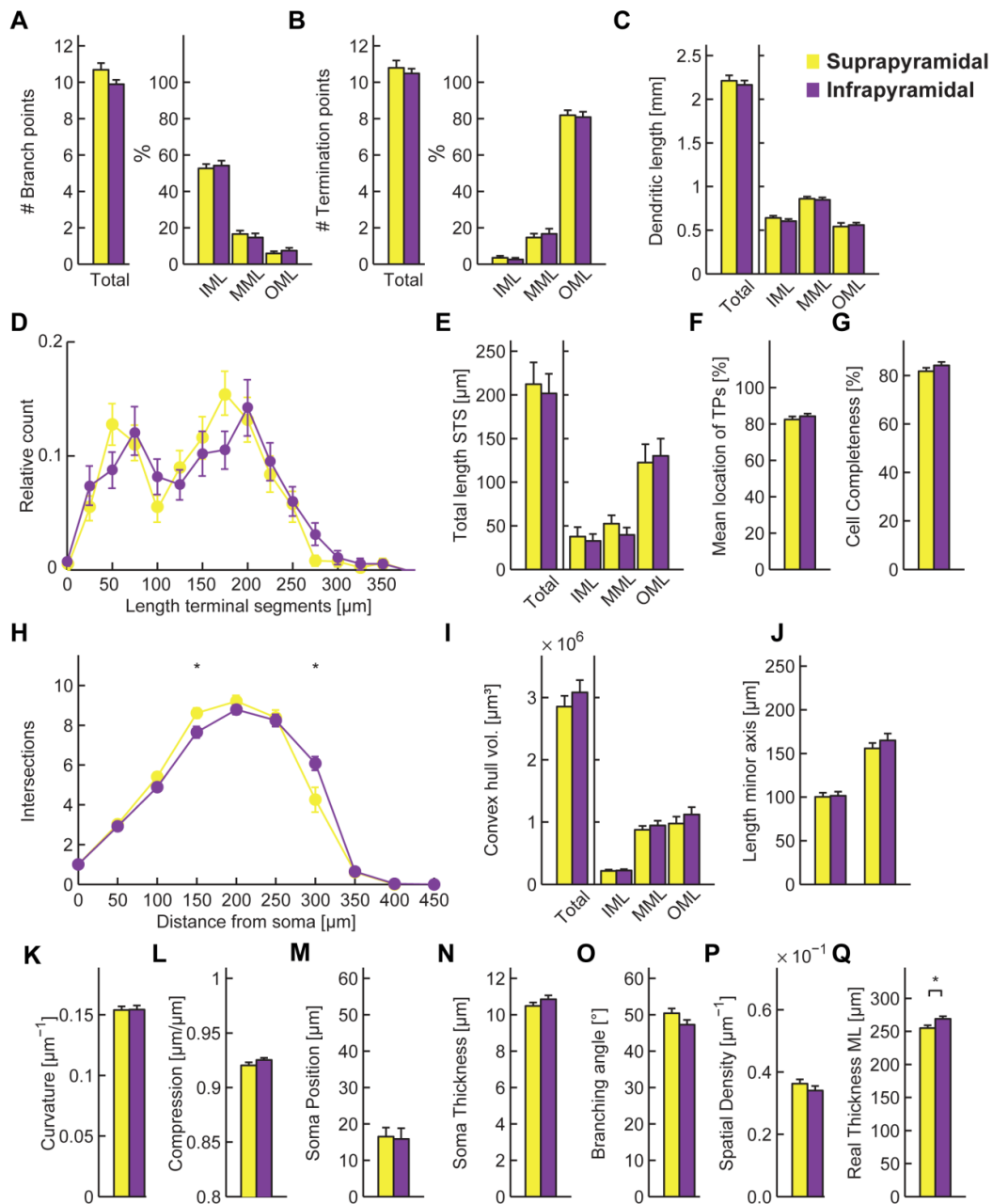
Supplementary Figure 2: Supra- and infrapyramidal GCs are structurally similar and thus were pooled. All reconstructed cells were pooled according to their supra- or infrapyramidal location to analyze difference arising only from location on the pyramidal blade **A-P,** Same morphological analyses as in **Figures 2-6** and **Suppl. Fig. 2-4** showing only small differences in the Sholl distribution (H) and the thickness of the ML (Q) which might both be correlated due to different GCL and ML thicknesses. Hence results of those two parameters should be valued less strong in the other sections of this paper.
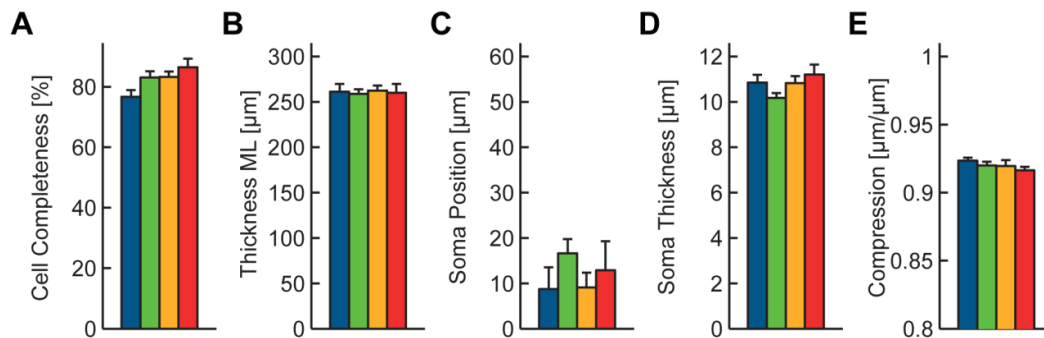
Supplementary Figure 3: Remaining morphological comparisons in the developing abGC groups (21-77 dpi). A, Rated cell completeness (see Material & Methods). **B,** Thickness of molecular layer (ML). **C,** Vertical position of somata. **D,** Thickness of somata. **E,** Compression (euclidean length of each dendritic segment endings divided by path length along the segment) as another measure of dendritic curvature.
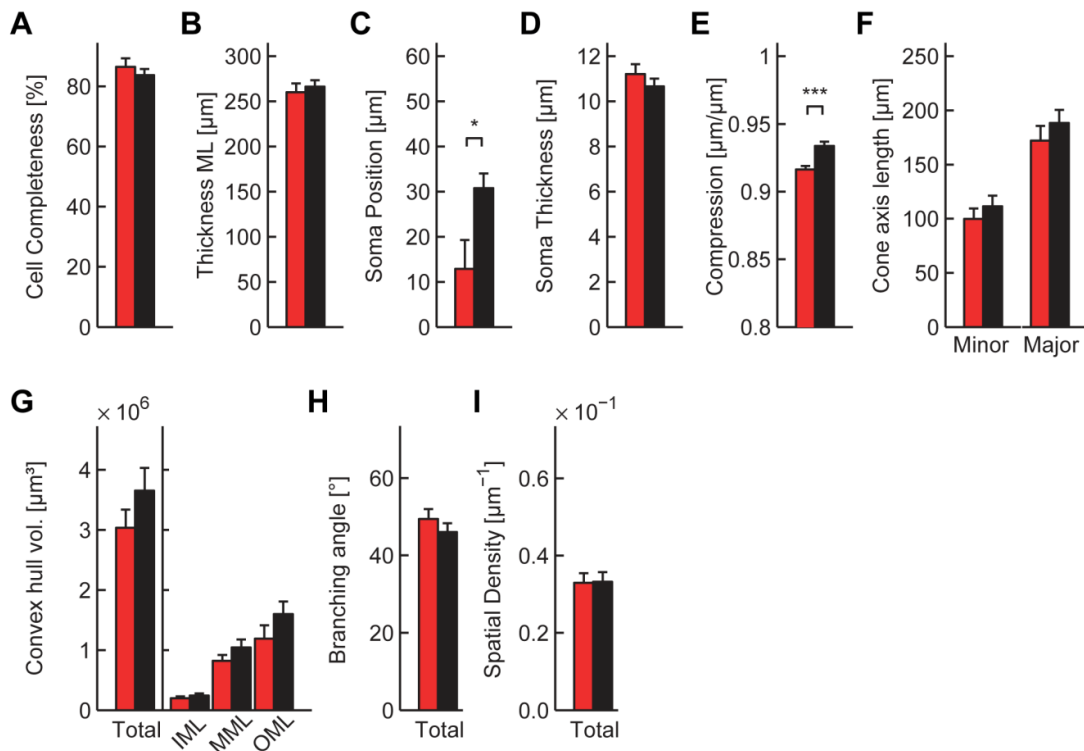
Supplementary Figure 4: Remaining morpholoical comparisons between abGCs (77 dpi) and AAV-labeded mGCs. A, Rated cell completeness (see Material & Methods). **B,** Thickness of molecular layer (ML). **C,** Vertical position of somata showing abGCs are located near to the hilus even at 77 dpi. **D,** Thickness of somata. **E,** Compression (euclidean length of each dendritic segment endings divided by path length along the segment) shows same result as curvature. **F,** Length of major and minor axis of the fitted Gaussian cone. **G,** Volume of the dendritic arbor's convex hull. **H,** Branching angle. **I,** Spatial dendity of the dendritic arbor within its cone-shaped space. Error bars are mean ± SEM.

9. Structural homo- and heterosynaptic plasticity in adult newborn rat hippocampal granule cells

Submitted research article

Tassilo Jungenitz[*#1,2], Marcel Beining[*1,2,3,4], Tijana Radic[1,2], Thomas Deller[1], Hermann Cuntz[3,4], Peter Jedlicka[1], Stephan W. Schwarzacher[1]

[1]Institute of Clinical Neuroanatomy, Goethe-University Frankfurt, Frankfurt am Main, Germany

[2]Faculty of biosciences, Goethe-University Frankfurt, Frankfurt am Main, Germany

[3]Ernst Strüngmann Institute (ESI) for Neuroscience in Cooperation with Max Planck Society, Frankfurt/Main, Germany

[4]Frankfurt Institute for Advanced Studies (FIAS), Frankfurt/Main, Germany

[*]These Authors contributed equally to this work (joint-first coauthors)

[#]Author for correspondence: Tassilo Jungenitz, Institute of Clinical Neuroanatomy, Goethe-University, Theodor-Stern-Kai 7, D-60590 Frankfurt am Main, Phone: +49 (0)69 6301 6914, Fax: +49 (0)69 6301 6425, E-mail: tassilo.j@gmx.de

9.1. Acknowledgments

9.2. Abstract

Adult newborn hippocampal granule cells (abGCs) contribute to spatial learning and memory. AbGCs are thought to play a specific role in pattern separation, distinct from developmentally born mature GCs (mGCs) that enable completion of stored patterns. During the time course of synaptic integration in the adult network abGCs undergo a critical phase of enhanced synaptic activity. Here we examine on the level of individual structurally analyzed cells at which exact cell age abGCs are synaptically integrated in the adult network and which forms of synaptic plasticity are expressed. We used virus-mediated labeling of abGCs and mGCs to analyze changes in spine morphology as indicator of plasticity in rats in vivo. High-frequency stimulation of the medial perforant path induced LTP in the middle molecular layer (MML) and LTD in the non-stimulated outer molecular layer (OML). Stimulation elicited homosynaptic spine enlargement in the MML and heterosynaptic spine shrinkage in the inner and OML. Both processes were concurrently present on individual dendritic trees of mGCs and abGCs. Spine shrinkage counteracted spine enlargement and thus could play a homeostatic role, normalizing synaptic weights. Spine plasticity appeared gradually from 21 dpi on, with a sharp increase at 28-35 dpi. This is the first demonstration of structural homo- and heterosynaptic plasticity in mGCs and abGCs and defines the critical phase for abGC integration between 21-35 dpi.

9.3. Statement of significance

The lifelong genesis of hippocampal granule cells (abGCs) enables specific forms of spatial learning. Learning and memory are mediated by LTP and LTD of synaptic strength, called synaptic plasticity. Following LTP and LTD induction, three week old abGCs show spine enlargement in stimulated dendritic segments and spine shrinkage in non-stimulated segments of the same cell. This concurrent structural homo- and heterosynaptic plasticity increases at 4-5 weeks of cell age, defining a critical phase of abGCs integration. Structural homo- and heterosynaptic plasticity is also present in mature granule cells, confirming a general form of synaptic plasticity and homeostasis. The presence of increasing structural plasticity on abGCs provides novel evidence on their direct involvement in synaptic plasticity underlying learning.

9.4. Introduction

Hippocampal granule cells (GCs) are generated throughout life in the mammalian dentate gyrus (DG) (Gage, 2010) and are considered to be important for spatial learning and memory (Cameron and Glover, 2015). AbGCs are thought to play a distinct role in separation and identification of new patterns, whereas mature GCs (mGCs), born during development, enable completion of stored patterns upon partial activation (Clelland et al., 2009; Nakashiba et al., 2012). Generation and maturation of GCs follows a course of differentiation, structural growth, and functional integration (Kempermann et al., 2015). Within 3-11 weeks of age, adult newborn granule cells (abGCs) become increasingly integrated into the hippocampal network (Deshpande et al., 2013; Denny et al., 2014). This particular function of abGCs might depend on a critical time window at 3-6 weeks when abGCs exhibit enhanced synaptic plasticity (Schmidt-Hieber et al., 2004; Ge et al., 2007), an increased excitation to inhibition balance (Marin-Burgin et al., 2012; Temprana et al., 2015), and the capability for experience-dependent remodeling of their connectivity (Martínez-Canabal, 2015).

Dendritic spines of abGCs appear during the third week (Zhao et al., 2006), forming first glutamatergic contacts at perforant path synapses (Toni et al., 2007; Toni and Sultan, 2011). Spine morphology is activity-dependent, and correlated with changes in synaptic strength (Alvarez and Sabatini, 2007). Spine size has been reported to match the size of the postsynaptic density (PSD) and number of glutamate receptors, and therefore is directly correlated with synaptic strength (Reymann and Frey, 2007). Numerous studies demonstrated that induction of LTP is associated with spine enlargement (Huber and Menzel, 2004), and conversely, LTD is associated with shrinkage (Zhou et al., 2004). Thus, change in spine size can be seen as structural equivalent of LTP and LTD. These two opposing types of synaptic plasticity (Oh et al., 2015) can be further classified into homosynaptic and heterosynaptic plasticity. Homosynaptic plasticity can be induced at synapses that are directly stimulated, while heterosynaptic plasticity takes place at inactive synapses neighboring stimulated synapses (Oh et al., 2015).

Excitatory synaptic contacts impinge on GC dendrites in the molecular layer (ML) of the DG. The ML is highly laminated and receives inputs via the medial perforant path (MPP) in the middle molecular layer (MML), inputs via the lateral perforant path (LPP) in the outer molecular layer (OML) and inputs from associated and commissural fibers of mossy cells in the inner molecular layer (IML) (David G. Amaral et al., 2007).

In previous studies, selective stimulation of either the MPP or LPP revealed homosynaptic LTP (Steward et al., 1998) and heterosynaptic LTD (Abraham et al., 2007) in the respective MML or OML. Heterosynaptic LTD has been discussed recently as a homeostatic mechanism for normalizing the overall synaptic weights and maintaining synaptic competition (Chistiakova et al., 2015). Furthermore, computational modelling showed that homosynaptically induced LTP would strengthen heterosynaptic LTD at neighboring dendritic segments (Jedlicka et al., 2015) and thus could lead to effective and long-lasting changes of synaptic weights as a requisite for learning and memory. How and when heterosynaptic plasticity emerges during development and

contributes to integration of abGCs into the hippocampal network is currently not known.

We performed intra-hippocampal injections of viral vectors for GFP-labeling of abGCs and mGCs to study the time course of development and structural plasticity of dendritic spines. In vivo high-frequency stimulation (HFS) of the MPP revealed enlargement of spines located in the MML in abGCs from 21 dpi on. Furthermore, neighboring spines in the unstimulated IML and OML of the same dendritic tree exhibited shrinkage. Thus, we could demonstrate for the first time the occurrence of homo- and heterosynaptic structural plasticity in abGCs.

9.5. Results

High-frequency stimulation of the perforant path induced expression of Arc in newborn and mature dentate granule cells

The population of abGCs was transduced with a GFP-expressing murine leukemia retroviral vector (RV-GFP) by an intra-hippocampal injection followed by HFS of the MPP at distinct time points between 21-77 dpi, in order to analyze the time course of development and structural plasticity of spines (**Fig. 1a, f-i**). Furthermore, we used intra-hippocampal injections of an adeno-associated viral vector to express GFP under the control of a synapsin promotor in order to study developmentally born mGCs (**Fig. 1a, j, k**). We refer to RV-GFP and AAV-GFP labeled cells as abGCs and mGCs respectively in the remaining text, although it is worth noting that AAV-GFP labeling does not exclude mature adult-born GCs (see Methods). We then performed 2 h HFS of the MPP with a protocol that induced robust LTP as well as a strong expression of immediate early genes (IEGs) in more than 90 % of all granule cells (**Fig. 1b, d**; Steward et al., 1998; Jungenitz et al., 2014). In addition, 2 h HFS resulted in enhanced expression of the LTP-markers F-actin and synaptopodin (Fukazawa et al., 2003) in the ipsilateral MML, i.e. the lamina of MPP fiber projection (see later, **Fig. 3**). Following 2 h HFS, expression of the synaptic plasticity-related IEG Arc was detected in the vast majority of GCs in the ipsilateral DG, including

abGCs and mGCs (**Fig. 1g, i, k**). LTP induction at the MPP is known to generate a concurrent heterosynaptic LTD of the LPP input (Abraham et al., 1985, 2007). In order to evaluate the occurrence of heterosynaptic LTD following HFS of the MPP we placed a second stimulation electrode in the LPP in control experiments. Stimulation of the LPP was discriminated from the concurrent MPP stimulation by characteristic differences in the shape of the evoked local GC field potentials and in the latency of the population spike (**Fig. 1b**, Abraham et. al. 2007, Petersen et al. 2013). Furthermore, low intensity paired pulse stimulation typically exhibited paired pulse facilitation at 20 ms interpulse-interval following LPP but not MPP stimulation, as has been described earlier (**Fig. 1c**, Petersen et al. 2013). Following 2 h HFS, homosynaptic LTP at the MPP was accompanied by heterosynaptic LTD at the LPP following 2 h HFS (**Fig. 1d**). The contralateral, non-stimulated DG showed no LTP induction following HFS in control recordings, and no enhancement of Arc-expression in the GCL as well as no enhancement of the LTP-marker F-actin and synaptopodin in all stimulation experiments. The contralateral DG therefore served as a control and was used to study the general time course of spine development in abGCs (**Fig. 1e, f, h, j**).

Time course of spine development in adult newborn granule cells

Dendritic segments of abGCs (**Fig. 2a, top**) and mGCs (**Fig. 2a, bottom**) were sampled from the IML, MML, and OML of the contralateral, unstimulated dentate gyrus (**Fig. 2c**). Only segments with a direct traceable connection to the soma were used. Time points for the analysis of abGC spines were chosen based on previous findings from rat in vivo(Jungenitz et al., 2014), starting at 21 dpi (n = 3 animals), with additional time points at 28 (n = 6), 35 (n = 5), and 77 dpi (n = 4) and compared to mGCs (n = 5). Dendritic segments in GCs showed a high diversity of spine sizes and shapes. Spines were classified into small (< 0.2 µm²) and large spines (> 0.2 µm²) using a grid based approach (**Fig. 2b**, for details see Methods). The density of spines, irrespective of size, increased gradually in all layers (IML, MML, and OML) between 21-77 dpi: starting at 21 dpi with 0.84 ± 0.02 µm^{-1} in the IML, 0.99 ± 0.01 µm^{-1} in the MML, 0.95 ± 0.18 µm^{-1} in the OML and reaching mature levels with 1.41 ± 0.09 µm^{-1} in

the IML, 1.58 ± 0.04 μm^{-1} in the MML and 1.77 ± 0.13 μm^{-1} in the OML at 77 dpi (**Fig. 2d$_1$**). At 77 dpi, spine density in abGCs showed no significant differences to mGCs in all layers (IML: 1.29 ± 0.20 μm^{-1}, MML: 1.49 ± 0.16 μm^{-1}, OML: 1.56 ± 0.17 μm^{-1}). Both small (**Fig. 2e$_1$**) and large spines (**Fig. 2f$_1$**) exhibited a similar gradual age-dependent increase in density throughout all MLs, reaching the density of mGCs at 77 dpi. The density of small spines in abGCs increased from 0.81 ± 0.04 μm^{-1} at 21 dpi to 1.35 ± 0.07 μm^{-1} at 77 dpi with no significant difference to mGCs with 1.18 ± 0.11 μm^{-1}. Large spine density in mGCs increased from 0.10 ± 0.02 μm^{-1} (21 dpi) to 0.22 ± 0.03 μm^{-1} (77 dpi) with large spine density in mGCs being 0.18 ± 0.03 μm^{-1}. Thus, large spines formed about 15 % of the spine density, and there was no significant change in the percentage of large spines over the entire time period that we analyzed (**Fig. 2g$_1$**). Data from all analyzed animals were pooled to perform a layer-specific, cell age-independent comparison. The spine density (including small and large spines) found in the MML and OML was significantly higher than in the IML (**Fig. 2d$_2$, f$_2$**). However, the MML showed a higher percentage of large spines in contrast to the IML and the OML (**Fig. 2g$_2$**).

We conclude from these results that a gradual development of spines occurs in abGCs between 21 dpi and 77 dpi, when spine size and density reach the levels found in mGCs.

High-frequency stimulation of the perforant path induced a layer specific expression of F-actin and synaptopodin

F-actin and synaptopodin are located in dendritic spines and are involved in processes regulating structural modifications of spines related to changes in synaptic plasticity (Deller et al., 2003; Fukazawa et al., 2003). F-actin and synaptopodin expression has been described as a valuable tool to measure layer-specific synaptic activation and plasticity following LTP induction in vivo (Fukazawa et al., 2003). Following 2 h HFS of the MPP, F-actin (**Fig. 3a, b**) and synaptopodin (**Fig. 3e**) expression was increased in the MML, i.e. the lamina of MPP fiber projection. The distribution of F-actin fluorescence intensity in the IML, MML, and OML was measured along the granule cell layer (GCL)-

hippocampal fissure axis, starting from the border between GCL and IML up to the hippocampal fissure (**Fig. 3d**). Following HFS, F-actin fluorescence intensity showed a significant elevation in the stimulated MML and a significant reduction in the unstimulated IML and OML, whereas the fluorescence intensity of the total ML was not altered compared to the unstimulated side (**Fig. 3c**).

Taken together, these results show stimulation-dependent and layer-specific accumulation of F-actin within the MML and a concurrent decrease of signal intensity in the adjacent IML and OML following HFS of the MPP. These data indicate a stimulation-induced homosynaptic LTP in the MML (Fukazawa et al., 2003) and a concurrent depression in the IML and OML, which could correspond to heterosynaptic LTD in the OML (Abraham et al., 2007) and a possible similar effect in the IML.

Structural plasticity of dendritic spines in adult newborn granule cells following 2 h high-frequency perforant path stimulation

We then took advantage of existing correlations between spine size and synaptic strength (Alvarez and Sabatini, 2007) to study the effects of HFS on structural spine plasticity we used the same grid-based spine size classification as in **Figure 2b** to discriminate between small (< 0.2 μm²) and large (> 0.2 μm²) spines and again analyzed only those dendritic compartments that could be traced until the cell soma. Using this approach, we were able to study layer-specific changes of spines in the same dendritic tree at the level of individual cells (see Methods). Within the MML, following 2 h HFS, the spine density remained unchanged at any age, both in abGCs and mGCs (**Fig. 4c**). However, we observed a decrease in the density of small spines (**Fig. S1c**) and an increase in density of large spines (**Fig. S1d**) in stimulated abGCs. The result was a significant gain in the percentage of large spines within the ipsilateral MML of abGCs (**Fig. 4d**) at 28 dpi (from 15.55 ± 1.32 % to 24.50 ± 1.35 %), 35 dpi (from 15.83 ± 0.89 % to 22.39 ± 2.35 %), and 77 dpi (from 15.90 ± 2.93 % to 26.48 ± 1.70 %), as well as in mGCs (from 15.49 ± 1.42 % to 30.86 ± 5.61 %). Thus, HFS of the MPP induced structural plasticity and spine enlargement in the MML in abGCs from 28 dpi on as well as in mGCs.

While the total number of spines of abGCs and mGCs also remained unchanged in the adjacent OML (**Fig. 4a**), the density of small spines increased (**Fig. S1a**) and the density of large spines decreased (**Fig. S1b**), resulting in a significant decline in the percentage of large spines in the OML from 35 dpi on (at 35 dpi from 14.31 ± 0.82 % to 8.22 ± 0.33 %, at 77 dpi from 15.73 ± 1.39 % to 8.80 ± 1.28 % and in mGCs from 12.65 ± 1.55 % to 7.02 ± 2.59 %; **Fig. 4b**). Although a similar trend of a decline of large spines was observed in the IML, we found no significant changes in the percentage of large versus small spine size in the IML of abGCs and mGCs (**Fig. 4e, f and Fig. S1e, f**).

These results indicate that HFS of the MPP leads to a robust homosynaptic spine enlargement in the (directly activated) MML in abGCs from 28 dpi on and mGCs. Furthermore, concurrent heterosynaptic spine shrinkage was found in the adjacent OML in abGCs starting at 35 dpi and in mGCs. Interestingly, stimulation-induced spine enlargement in the MML and spine shrinkage in the OML were found on adjacent dendritic segments of the same identified GCs, providing structural evidence for activity-dependent localized spine plasticity in the same neuron under in vivo conditions.

We found a sharp increase of structural spine plasticity between 28 dpi and 35 dpi indicating a critical time window for synaptic integration of abGCs. In order to elucidate the gradual changes of spine size following HFS in more detail, we performed a direct measurement of the largest cross-sectional area of all spine heads in confocal z-stacks of dendritic segments from RV-GFP labeled abGCs at 28 dpi and 35 dpi (**Fig. 5**).

The average area of spine heads in the MML increased from 0.13 ± 0.01 µm² (28 dpi) to 0.160 ± 0.002 µm^2 (35 dpi) in abGCs contralateral to the stimulation. We applied thresholds of 0.15 µm², 0.2 µm², and 0.25 µm² to these datasets to differentiate between small and large spines and to analyze the size changes of larger spines (**Fig. 5 insets**). At 28 dpi, spines in the MML were affected by 2 h HFS (**Fig. 5c**) as indicated by an increase from 14.09 ± 1.65 % to 22.01 ± 1.66 % (threshold of 0.2 µm²). There were no significant changes in the OML (**Fig. 5a**) and the IML (**Fig. 5e**) following HFS. At 35 dpi, abGCs showed

an increase of spine head size in the MML at a threshold of 0.25 µm² from 12.45 ± 0.51 % to 18.24 ± 3.62 % (**Fig. 5d**). In contrast, spines in the OML and IML (**Fig. 5 b and f**) showed a decrease in size at a threshold of 0.2 µm² (OML: 20.19 ± 2.90 % to 10.51 ± 0.70 %; IML: from 11.66 ± 1.08 % to 5.02 ± 0.72 %). The existence of synaptic contacts on labeled abGCs spines within the MML were verified with ultrastructural examination of abGCs at 35 dpi (**Fig. 5g, h**).

In summary, the detailed spine head size measurements (**Fig. 5**) confirmed the grid based size classification with a chosen threshold of 0.2 µm² (**Fig. 4**) and showed once more the suitability of this method to detect homosynaptic structural plasticity in the MML and heterosynaptic plasticity in the OML. Furthermore, the detailed analysis provided significant evidence for additional heterosynaptically induced shrinkage of spines in the IML following HFS in abGCs at 35 dpi.

Cell-specific homeostatic effect of homo- and heterosynaptic changes in spine size

In order to investigate the cell-specific manifestation of homo- and heterosynaptic plasticity-related changes of spines, we analyzed individual cells labeled ipsilaterally following HFS (i.e. fully activated cells, **Fig. 6a, b**) and compared them to GCs within their respective cell age group (abGCs or mGCs) on the contralateral, non-stimulated side. The percentage of large spines in the MML was elevated ipsilaterally in comparison with the percentage on the contralateral side. In addition, the proportion of large spines was decreased in the IML and OML. Some abGCs already exhibited homo- and heterosynaptic structural plasticity at 21 dpi and 28 dpi following HFS on the ipsilateral side (21 dpi: 18.75 ± 3.61 %, 28 dpi: 19.82 ± 2.39 %; **Fig. 6c**). The percentage of homo- and heterosynaptic plasticity-positive cells increased with cell age (35 dpi: 51.28 ± 6.60 %), and reached mature levels in abGCs at 77 dpi (61.67 ± 8.33 %). No further increase (62.22 ± 2.22 %) was found in mGCs (**Fig. 6c**). The relative change in percentage of large spines across all groups showed an average increase of 169.50 ± 8.88 % in the MML, a decrease to 39.95 ± 4.59 % in the IML, and to 49.84 ± 5.72 % in the OML. There were no

significant differences between abGCs of different cell ages or between abGCs and mGCs (**Fig. 6d**).

Percentages of large spines from the IML, MML, and OML of the same dendritic tree were averaged in order to estimate the total structural spine changes of individual abGCs (**Fig. 6a, b**). Interestingly, age-matched comparison between ipsilateral and contralateral GCs revealed no significant relative differences, indicating that the overall percentage of large spines remained stable (**Fig. 6e; see also Fig. 4b, d, f**). Thus, the elevation in the percentage of large spines in the ipsilateral MML by homosynaptic structural plasticity was counteracted by heterosynaptic structural plasticity in the adjacent IML and OML and normalized the degree of structural changes along the dendritic tree.

These findings demonstrate that homo- and heterosynaptic plasticity is present in some abGCs from 21 dpi on and gradually increases to mature levels at 77 dpi.

9.6. Discussion

In this study we show for the first time homosynaptic and heterosynaptic structural plasticity of dendritic spines in abGCs following 2 h stimulation of the perforant path in vivo. This provides novel structural evidence for synaptic plasticity in abGCs, consistent with an active role of abGCs in hippocampal learning and memory (Cameron and Glover, 2014).

Two hour HFS of the MPP led to LTP, associated with a strong Arc expression in the granule cell layer. The stimulated MML exhibited an increase of F-actin and synaptopodin expression as well as a significant enlargement of dendritic spines in abGCs from 28 dpi on, thus revealing robust and layer-specific molecular and structural correlates of a homosynaptic LTP in young abGCs. In addition, LTP following 2 h HFS of the MPP was accompanied by LTD as shown by control stimulation of the LPP. Furthermore, the expression of F-actin was reduced in the adjacent unstimulated OML, the termination site of

the LPP, as well as the unstimulated IML. Dendritic spines of abGCs in the IML and OML showed a significant reduction in size from 35 dpi on, indicating heterosynaptic structural plasticity. In addition, homo- and heterosynaptic structural plasticity was also found on the level of individual abGCs from 21 dpi on, as well as in mature abGCs at 77 dpi, and at similar intensities in developmentally-born GCs.

We conclude that synaptic integration of abGCs into the entorhino-hippocampal pathway is a gradual process and requires at least 4-5 weeks until abGCs exhibit structural plasticity with a capacity comparable to mGCs in response to synaptic activation. The finding of layer-specific homo- and heterosynaptic plasticity within the same dendritic tree of individual GCs can be explained as a homeostatic mechanism on the cellular level in both abGCs and mGCs.

General spine development of abGCs

We analyzed the number and morphology of dendritic spines in RV-GFP-labeled abGCs at 21 dpi, 28 dpi, 35 dpi, and 77 dpi and compared them to AAV-GFP-labeled mGCs located in the contralateral, unstimulated DG. The number of spines increased from 21 dpi on, reaching a maximum density at 77 dpi with no significant differences to mGCs (**Fig 2**). The percentage of large spines was almost constant between 10-15 % throughout all analyzed age groups, indicating that the rate of de novo formation of spines is proportional to their morphological development. Our data is consistent with earlier reports from rats and mice on the time course of spinogenesis in abGCs. The earliest time point of spine formation in abGCs was reported at 16 dpi for rats (Ohkawa et al., 2012) and mice (Zhao et al., 2006). An early sharp increase in spine density was observed between 16-18 dpi in rats (Ohkawa et al., 2012) and about one week later in mice (Zhao et al., 2006; Toni et al., 2007), supporting the general idea that abGCs mature faster in rats than in mice (Snyder et al., 2009). Reports in mice further showed a continuous increase during the following 8 weeks until abGCs reach a plateau at about 70 dpi. Spines can show a prolonged structural maturation, which is modulated by a variety of stimuli (Zhao

et al., 2006; Toni et al., 2007, 2008). Because in our study abGCs at 77 dpi exhibited spine shapes and numbers comparable to mGCs, we conclude that in rats, spine maturation is completed by 11 weeks.

The characterization of spine formation in maturating abGCs is based on the analysis of dendritic segments located in the contralateral DG. The contralateral DG receives limited input from the ipsilateral entorhinal cortex (EC) via direct commissural and indirect multi-synaptic projections. The first pathway is known for only a sparse activation of GCs and lacking the capacity of LTP induction under normal, physiological conditions (Wilson et al., 1979, 1981; Wilson, 1981; Alvarez-Salvado et al., 2014). Our electrophysiological data showed a strong LTP induction of the ipsilateral EC-DG pathway, and no LTP-induction on the contralateral EC-DG pathway (**Fig. 1c**). Furthermore, The contralateral, non-stimulated DG showed no enhancement of Arc-expression in the GCL (**Fig. 1**) as well as no enhancement of the LTP-markers F-actin and synaptopodin (**Fig. 3**) in all stimulation experiments, which clearly indicates the absence of any direct or indirect (multi-synaptic) stimulation strong enough to induce LTP resulting in relevant changes in spine size. However, any possible indirect stimulation of the contralateral DG would likely lead to a potential overestimation of contralateral spine sizes, and thus would lead to an underestimation of the documented effects on the ipsilateral side. We therefore chose the contralateral DG as a valuable control that allowed a direct comparison of the non-stimulated and stimulated side in each animal.

Induction of homo- and heterosynaptic plasticity following 2 h HFS of the medial perforant path

Two types of synaptic plasticity are in the focus of this paper: homosynaptic plasticity and potentiation, which is input-specific and occurs only at directly activated synapses, and heterosynaptic plasticity and depression, which can be induced at synapses that were not active during the induction of homosynaptic plasticity (Abraham et al., 2007). Both forms of plasticity have been well-studied in the DG and can be induced by stimulation of the perforant path in vivo (Abraham et al., 1985; Benuskova and Abraham, 2007; Jedlicka et al., 2015).

Heterosynaptic plasticity has been discussed as a homeostatic mechanism for normalization of synaptic weights and maintenance of synaptic competition (Chistiakova et al., 2015).

In our experiments, HFS of the MPP induced a robust homosynaptic LTP and heterosynaptic LTD of the LPP (also reported by Abraham et al., 2007). LTP induction was accompanied by a layer-specific accumulation of F-actin and synaptopodin in the stimulated MML, which is in agreement with the observations described by Fukazawa and colleagues (Fukazawa et al., 2003) indicating that the applied stimulation protocol and procedure were specific in targeting fibers of the MPP and activated mainly synapses located in the MML. Fukuzawa et al. (2003) showed that LTP induction in the DG by stimulating the perforant path in vivo leads to a long-lasting NMDA receptor-dependent reorganization of F-actin. In addition, they found a layer-specific increase of several marker proteins of synaptic activity, including synaptopodin. Synaptopodin is an actin-binding protein, which is functionally linked to the formation of the spine apparatus and it was demonstrated that synaptopodin deficiency leads to an impairment of LTP (Deller et al., 2003; Jedlicka et al., 2009).

Intriguingly, we also found a significant decrease of F-actin in the adjacent unstimulated IML and OML after stimulation of the MML. F-actin, as a component of the cytoskeleton, is associated with the plasma membrane and organization of the postsynaptic density (PSD) in dendritic spines and plays a crucial role in synaptic plasticity and the definition of spine morphology (Bosch and Hayashi, 2012). Polymerization of actin filaments is required for stable LTP (Kim and Lisman, 1999; Huber and Menzel, 2004) whereas LTD is accompanied by depolymerization of F-actin (Okamoto et al., 2004). Thus, our data suggest that actin could be involved not only in the regulation of homosynaptic LTP, but also heterosynaptic LTD.

Given the well-described role of F-actin and synaptopodin in synaptic plasticity, we conclude that the applied HFS protocol in our study was suitable to induce a robust input-specific homosynaptic structural LTP at directly

stimulated GC synapses of the MML (Fukazawa et al., 2003) and likely a concurrent heterosynaptic structural LTD at the unstimulated GC synapses in the OML (Abraham et al., 2007) and possibly also in the IML (Benuskova and Abraham, 2007; Benuskova and Jedlicka, 2012).

Homo- and heterosynaptic structural changes of spines in abGCs following 2 h HFS

We observed an enlargement of spines in dendritic segments located in the stimulated MML in abGCs from 28 dpi on and shrinkage of spines in the adjacent non-stimulated IML and OML from 35 dpi on. Spine size is positively correlated to the size of the postsynaptic density (PSD) and the number of glutamate receptors, and thus with synaptic strength (Reymann and Frey, 2007). Induction of LTP is associated with spine enlargement (Huber and Menzel, 2004), and LTD with spine shrinkage (Zhou et al., 2004). Induction of homosynaptic LTP and heterosynaptic LTD at the perforant path synapse should consequently manifest in a change of spine size, as found in our study. It is heavily debated if LTP is accompanied by a de novo formation of spines or morphological changes of pre-existing spines (Popov et al., 2004; Wosiski-kuhn and Stranahan, 2012). In fact, this may depend on the plasticity-inducing protocols used in different studies. We could not see a change in the overall number of spines following stimulation, indicating that our LTP protocol did not induce changes in spine density. Importantly, tracing dendritic segments from the cell soma to the hippocampal fissure allowed us to study structural changes following HFS in the IML, MML, and OML within the same cell. GCs with induced heterosynaptic plasticity were identified by showing an enlargement of spines in the MML and shrinkage of spines in the IML and OML in comparison to the contralateral, non-stimulated hemisphere. Heterosynaptic plasticity has been reported previously only in the MML and OML, but not in the IML of the DG. Therefore, to our knowledge, these results provide not only the first evidence for heterosynaptic plasticity in abGCs but also the first experimental evidence for heterosynaptic plasticity at commissural/associational IML synapses, as it has been predicted by computational modeling (Benuskova and Jedlicka, 2012). We found stimulation-induced layer-specific homo- and

heterosynaptic plasticity on neighboring IML, MML, and OML segments of the dendritic tree in individual abGCs and mGCs. About 20 % of abGCs exhibited heterosynaptic plasticity from 21 dpi on, and starting at 35 dpi, there was a sharp increase to ~60 %, with no further change at 77 dpi or in comparison to developmentally-born GCs. The effective relative change of structural spine plasticity was equal between all groups. Interestingly, our data revealed that heterosynaptic shrinkage of spines counteracted homosynaptic spine enlargement. The percentage of large spines in abGCs and mGCs showed no net change along the dendritic tree compared to unstimulated control GCs. These findings support the idea of heterosynaptic plasticity as a homeostatic mechanism for normalization of synaptic weights (Chistiakova et al., 2015) and no de novo formation of spines.

A critical time period for integration of abGCs

Various lines of evidence from several studies point to a critical phase for integration of abGCs in the hippocampal network between 4-6 weeks of cell age (Schmidt-Hieber et al., 2004; Ge et al., 2007; Mongiat et al., 2009; Marin-Burgin et al., 2012; Martínez-Canabal, 2015; Temprana et al., 2015). In this study, the majority of abGCs showed a transition from homo- without heterosynaptic plasticity at 28 dpi to homosynaptic together with concurrent heterosynaptic plasticity from 35 dpi on. In a previous study, we analyzed the time course of LTP induction by expression of IEGs in abGCs following 2 h HFS of the perforant path in adult rats (Jungenitz et al., 2014). De novo transcription of IEGs (e.g. c-fos and Arc) has been shown to be required for long-lasting LTP and synaptic plasticity (Fleischmann et al., 2003; Bramham et al., 2008). We identified a sharp increase in the ability of abGCs to respond to LTP stimulation with expression of IEGs between 28 dpi and 35 dpi (Jungenitz et al., 2014). Taken together, our findings imply a rapid period of synaptic integration of abGCs between 28 dpi and 35 dpi.

Between 4-6 weeks of age, abGCs pass through a critical time window that is characterized by an enhanced synaptic plasticity with a lowered threshold for LTP (Schmidt-Hieber et al., 2004; Ge et al., 2007). During this critical phase,

coupling and response to feedback inhibition through GABAergic interneurons is weak, but during maturation GCs become gradually integrated into inhibitory circuits (Temprana et al., 2015). This transition may support a higher excitability in immature, but an increased inhibition in mature GCs. Using rabies virus-mediated retrograde tracing, evidence of early local connections to the hippocampal network has been reported, as well as long range afferent projections from the entorhinal cortex via the perforant path in a rapidly increasing quantity from 21 dpi on, providing evidence for increasing connectivity through the critical phase of 4-6 weeks (Vivar et al., 2012; Deshpande et al., 2013).

We conclude that during their development, abGCs pass through a process of structural maturation until the 3rd week, followed by a gradual integration into the hippocampal network at a critical time period between 4-5 weeks of age, and a further synaptic maturation until 11 weeks when abGCs appear to be comparable to developmentally born mGCs. The finding of robust homo- and heterosynaptic structural plasticity during the critical time period of synaptic integration is consistent with the general view that abGCs contribute to hippocampus-specific forms of learning and memory (Cameron and Glover, 2015).

9.7. Methods

Animals

Adult male Sprague-Dawley rats (8 - 13 weeks, 220 - 450 g; Charles River, Sulzfeld, Germany) were housed under standard laboratory conditions in large rat cages (30 cm x 40 cm). All animal experiments were performed in conformance with German guidelines for the use of laboratory animals.

Retrovirus production

HEK293T cells were co-transfected with pCAG-GFP, pCMV-GP and pCMV-VSV-G (3:2:1) plasmids by Calcium-Phosphate precipitation. The media containing retrovirus was collected 48 h after transfection. Cell debris was

removed from the supernatant by centrifugation at 3200 x g for 10 min and filtration through a 0.22 µm filter. The retrovirus was concentrated by ultra-centrifugation at 160000 x g for 2 h (Sorvall WX Ultracentrifuge and SureSpin 630 swinging bucket rotor; Thermo Fisher Scientific, Waltham, MA, U.S.A.). The retroviral pellet was resuspended in 200 µl phosphate buffered saline (PBS; Sigma-Aldrich, St. Louis, MO, U.S.A.), aliquoted and stored at -80 °C. The titer was at 10^5 colony forming units.

Adeno-associated virus production

HEK293T cells were co-transfected with pDP1rs, pDG and GFP-vector-plasmid (6:4:1) by Calcium-Phosphate precipitation. The transfected cells were collected 48 h after transfection. Cells were washed (2 times) by centrifugation at 1500 x g for 5 min and resuspended in PBS. The viral particles inside the cells were set free by multiple freeze thaw cycles (4 times). The supernatant was collected and washed by centrifugation at 3200 x g for 10 min. The AAV containing supernatant was aliquoted and stored at -80 °C.

Intra-hippocampal viral *in vivo* injection

All surgical procedures were performed under deep Medetomidin (Domitor; Pfizer, New York City, NY, U.S.A.), Midazolam (Dormicum; Roche, Basel, Switzerland) and Fentanyl (Janssen Pharmaceutica, Beerese, Belgium) anesthesia (150 µg Medetomidin, 2 mg Midazolam, 5 µg Fentanyl per kg body weight i.m. initially and additional injections as needed), in agreement with the German law on the use of laboratory animals. Animals were placed in a Kopf stereotaxic device (Kopf instruments, Tujunga, CA, U.S.A.). Two small holes (1.5 - 2.0 mm diameter) were drilled in the skull at -3.8 mm from Bregma and 2.2 mm laterally at both hemispheres. A NanoFil syringe (World Precision Instruments, Inc., Sarasota, FL, U.S.A.) with a 35 gauge beveled needle (NF35BV-2; World Precision Instruments) was used to slowly inject 0.75 µl of the viral solution at 3.2 mm and 3.7 mm below the brain surface into the dentate gyrus (both hemispheres).

Retrovirally-mediated labeling of abGCs is a well-established method (van Praag et al., 2002) utilized by an increasing number of publications characterizing adult neurogenesis. GFP expression of AAV-transduced GCs was controlled by a Synapsin I promotor. Synapsin I is increasingly active when synapse formation starts (Valtorta et al., 2011). The AAV lacks cell type specificity in general, but expression of GFP is limited to mature neurons with established synapses only. AAV-GFP-labeled GCs were identified by their morphology, and to further ensure that predominantly developmentally and perinatally born GCs were analyzed, we selected AAV-GFP-labeled GCs based on their location in the upper half of the GCL, as it has been shown that abGCs remain located in the inner part of the GCL (Radic et al., 2015). Therefore, and because perinatally born GCs form the dominant population of GCs, we assume that AAV-GFP-labeled GCs represent the pool of developmentally-born GCs (mGCs).

Perforant path stimulation *in vivo*

All surgical procedures for perforant path stimulation were performed under deep urethane anesthesia (1.25 g/kg body weight s. c. initially and additional injections as needed; 250 mg urethane/ml 0.9 % saline; Sigma-Aldrich), in agreement with the German law on the use of laboratory animals. Surgery and stimulation procedures were performed as previously described (Jungenitz et al., 2014). In short, animals were placed in a Kopf stereotaxic device (Kopf instruments). Rectal temperature was maintained at $37.0 \pm 0.5\,°C$. Two small holes (1.5 - 2.0 mm diameter) were drilled in the skull and a bipolar stainless steel stimulating electrode (NE-200; Rhodes Medical, Woodland Hills, CA, U.S.A.) was placed in the angular bundle of the perforant path (coordinates from lambda: L: 4.5 mm; AP: +0.5 mm; V: -3.5 mm measured from the surface of the brain). Glass microelectrodes (1.5 mm outer diameter) were pulled on a Zeitz (München, Germany) electrode puller, filled with 0.9 % saline, and placed in the dorsal blade of the granule cell layer (coordinates from bregma: L: 2.0 mm, AP: -3.5 mm, V: -3.5 mm). The vertical tip position of the recording electrode was optimized under low voltage perforant path control stimulation pulses using the characteristic shape of the evoked potentials.

Subsequently, high-frequency stimulation (HFS) maximally evoked population spikes and induced robust long-term potentiation (LTP) as has been described in detail before (Steward et al., 1998; Jungenitz et al., 2014). HFS was applied for 2 h. One HFS train consisted of 8 pulses (500 µA, 0.1 ms pulse duration) of 400 Hz once per 10 s. 2 h HFS was applied in RV-GFP transduced animals 21 dpi (n = 4), 28 dpi (n = 6), 35 dpi (n = 5) and 77 dpi (n = 4) and in AAV-GFP (n = 3) transduced animals 14 dpi. Directly after 2 h of HFS, rats were deeply anesthetized with urethane, and transcardially perfused with a fixative containing 4 % PFA in 0.1 M PBS, pH 7.4. Brains were removed and postfixed for up to 18 h.

LTP induction at the MPP is known to generate heterosynaptic LTD at the LPP (Abraham et al., 1985, 2007). In a separate experimental group (n = 6 animals), a second concentric stimulation electrode was placed in the LPP (coordinates from lambda: L: 5.5 mm; AP: +0.5 mm; V: -3.5 mm measured from the surface of the brain) to concurrently record evoked field potentials in the DG by stimulation of the LPP or MPP. The medio-lateral position of the lateral stimulation electrode in the LPP was optimized and confirmed by low intensity paired pulse stimulation at 20 ms interpulse interval, which is known to result in paired pulse facilitation and increase of the second slope by LPP and not by MPP stimulation (Petersen et al., 2013). HFS was applied to the MPP as described above. Control stimulation pulses were applied separately either to the MPP (500 µA, 0.1 ms pulse duration, 10 s interpulse interval) or the LPP (800 µA, 0.1 ms pulse duration, 10 s interpulse interval) to evoke and record field potentials before, during and after HFS.

In order to estimate the effects of HFS of the MPP on the contralateral EC-DG pathway, an additional stimulation and recording electrode were placed on the opposite, contralateral hemisphere at laterally-inversed positions mentioned above (n = 3 animals). Control stimulation pulses (500 µA, 0.1 ms pulse duration, 10 s interpulse interval) were applied separately either to the ipsilateral or the contralateral MPP to evoke and record field potentials before, during and after HFS. For the analysis of the slope of evoked field potential,

only the early component of the response was measured to avoid contamination by the population spike.

Tissue preparation

Serial frontal sections of the hippocampus (300 µm) were cut with a vibratome, washed in 0.1 M TRIS buffered saline (TBS; AppliChem, Darmstadt, Germany), and stored at −20 °C in cryoprotectant solution (30 % ethylene glycol, 25 % glycerin in PBS). 300 µm serial frontal sections were used to allow reconstructions of complete GC dendritic trees (not in the focus of this study). Subsequently, sections were cut to 50 µm with a vibratome, washed in 0.1 M TBS, and stored at -20 °C in cryoprotectant solution. All histological examinations were performed on 50 µm sections.

Immunohistochemistry

Free-floating sections were washed in TBS, blocked with 5 % bovine serum albumin (BSA; New England BioLabs, Ipswich, MA, U.S.A.) containing 0.1 % Triton X-100 for 1 h at room temperature to reduce non-specific staining and incubated in primary antibody solution containing 2 % BSA, 0.25 % Triton X-100, 0.1 % NaN_3 in 0.1 M TBS for 48 h at room temperature. The following primary antibodies were used: anti-Arc (rabbit, polyclonal, 1:1000; Synaptic Systems, Göttingen, Germany), anti-GFP488 (mouse, 1:500, fluorescence-labeled Alexa 488; Sigma-Aldrich), anti-Synaptopodin (guinea pig, polyclonal, 1:1000; Synaptic Systems). For fluorescence-immunohistochemical detection, sections were incubated with secondary fluorescence-labeled antibodies (1:1000; Alexa 488, 568; Vector Labs., Burlingame, CA, U.S.A.) for 24 h at room temperature.

For detection of F-actin, free-floating sections were washed in TBS, blocked with 5 % BSA for 1 h at room temperature, and incubated with Phalloidin-Alexa 568 (1:200; MoBiTec, Göttingen, Germany) for 24 h at room temperature.

Immunohistochemical quantification

For expression analysis of Arc expression, all GFP-labeled granule cells located on a section (ipsilateral and contralateral) were imaged using a confocal microscope (Nikon Eclipse80i; Nikon, Shinagawa, Tokyo, Japan) and a 40x oil immersion objective (N.A. 1.3; Nikon) with a step distance of 2 µm.

For analysis of F-actin expression, image stacks (step distance of 5 µm, 6 images) were acquired from 2 frontal sections of the ipsilateral and contralateral dentate gyrus molecular layer (3 image stacks per section, suprapyramidal and infrapyramidal blade) using a confocal microscope (Nikon Eclipse 80i; Nikon) and a 20x objective (N.A. 1.3; Nikon). The field zoom was adjusted to include the molecular layer from the granule cell-inner molecular layer-border to the hippocampal fissure. Image stacks were rotated and cropped to align samples using ImageJ (website: imagej.nih.gov/ij/). Profiles of the mean fluorescence-intensity were measured from the first image (showing the section surface) of each image stack using ImageJ. Due to differences in the length between molecular layer samples, fluorescence-intensity profiles were resampled to 100 data points using Matlab (MathWorks, Natick, MA, U.S.A.). The mean fluorescence-intensity of the complete molecular layer showed no significant differences between the ipsilateral and contralateral hemispheres and was therefore used to normalize the fluorescence-intensity profiles. Profiles were divided into the inner, middle and outer molecular layer (IML: 1 - 27, MML: 28 - 64, OML: 65 - 100) and further averaged into two data points per layer, which were used for statistical analysis.

Image acquisition and analysis of dendritic spines

For dendritic spine analysis, segments of GFP-labeled granule cells were imaged using a confocal microscope (Nikon Eclipse 80i; Nikon) and a 60x oil immersion objective (N.A. 1.3; Nikon) with a 5x field zoom and a step distance of 0.5 µm. Only dendritic segments with a visual connection to the cell soma were used for imaging, to ensure a reliable analysis of layer specific differences within the same cell. Only GFP-labeled cells located in a section with robust Arc expression were used. The imaging window for IML located dendritic segments

was set adjacent to the GCL, for the OML close to the hippocampal fissure (with a distance of 5 to 10 µm from the fissure), and the MML in the center between the IML and the OML. 2 - 4 segments were imaged per cell and layer.

The length of a sampled dendritic segment was measured in a z-projection by manual tracing the center of the dendritic shaft (the mean length was approximately 42 µm). Spines were counted in the image stack. Only spines exhibiting a visible spine neck and head were used for the analysis. Spine morphology and size is highly dynamic and correlated to the size of the postsynaptic density (PSD) and the number of glutamate receptors (Alvarez and Sabatini, 2007). Small spines exhibit the ability to potentiate, whereas large spines are more stable and associated with larger synapses. In the literature, large spines with bulbous heads and head diameters > 0.6 µm are also referred to as mushroom-spines (Sorra and Harris, 2000). Accordingly, we classified spines into small and large spines using a grid overlay with a grid element size set to 0.2 µm² (square diagonal ~0.6 µm, see **Fig. 2b**). Spines were assigned to the class of small spines when the spine head appeared visually smaller than a grid element or to the class of large spines when visually larger than a grid element. The number of spines was normalized to the length of the dendritic segment (#/µm).

The specific spine size was measured by manually tracing the largest cross-sectional area of the spine head using Fiji (Schindelin et al., 2012) and a graphic tablet (Wacom, Kazo, Saitama, Japan). In average, 60 spines per ABGC and layer were measured from 3 ipsi- and 3 contralateral cells at 28 dpi and 5 ipsi- and 5 contralateral cells at 35 dpi.

GFP-labeled GCs shown in **Fig. 2a and Fig. 6a** were edited in order to isolate the cells from surrounding fluorescent structures.

Electron Microscopy

Deeply anesthetized rats were transcardially perfused with a fixative containing 4 % PFA (in 0.1 M PBS, pH 7.4), 2 % glutaraldehyde (Polysciences Europe GmbH, Eppelheim, Germany) and 0.1 M sodium cacodylate buffer

(Science Services, München, Germany). Brains were removed and postfixed for up to 18 h. Serial frontal sections of the hippocampus (50 µm) were cut with a vibratome.

Sections were washed in TBS, incubated in 0.1 % NaBH4 (Sigma-Aldrich) and blocked with 5 % BSA containing 0.1 % Triton X-100 for 1 h at room temperature to reduce non-specific staining. Antibody solutions contained 2 % BSA, 0.25 % Triton X-100 in 0.1 M TBS. For detection of GFP-labeled cells, anti-GFP (goat, 1:500, 18 h, room temperature; Acris, Herford, Germany) was used as primary antibody and a biotinylated anti-Goat IgG (1:200, 60 min room temperature; Vector Laboratories, Burlingame, CA) as secondary antibody. After washing in TBS, sections were incubated in avidin-biotin-peroxidase complex (ABC-Elite, Vector Laboratories) for 90 min (room temperature) and reacted with nickel-diaminobenzidine solution (Vector Laboratories) for 2 - 15 min (room temperature). Sections were silver-intensified by the following steps: incubation in 3 % hexamethylenetramine (Sigma-Aldrich), 5 % silvernitrate (AppliChem) and 2.5 % di-sodiumtetraborate (Sigma-Aldrich) for 10 min (60 °C); 1 % tetrachlorogold (AppliChem) solution for 3 min and 2.5 % sodiumthiosulfate (Sigma-Aldrich) for 3 min. Between each step, sections were washed thoroughly in distilled water.

After staining, the sections were washed in cacodylate buffer, osmicated (0.5 % OsO_4 (Plano, Wetzlar, Germany) in cacodylate buffer), dehydrated (1 % uranyl acetate (Serva, Heidelberg, Germany) in 70 % ethanol), and embedded in durcupan (Sigma-Aldrich). Sections were collected on single-slot Formavar-coated copper grids and examined using a Zeiss electron microscope (Zeiss EM 900).

Statistical analysis

Data management, statistical analysis, and visualization were done with Microsoft Excel (Microsoft, Redmond, Washington, U.S.A.) and GraphPad Prism 6 (Graphpad Software, San Diego, CA, U.S.A.). Statistical comparisons were calculated with the two-sided Wilcoxon rank-sum test **(Fig. 3, 4, 5, 6, S1)**, the Kruskal-Wallis with Dunn's comparison test **(Fig. 2, 6)**, the two-way ANOVA

with Bonferroni correction **(Fig. 3)**, or the Friedman with Dunn's multiple comparison test **(Fig. 2)**. Significance level was set at $P < 0.05$. Group values are reported as means ± SEM.

9.8. References

Abraham WC, Bliss TVP, Goddard G V (1985) Heterosynaptic changes accompany long-term but not short-term potentiation of the perforant path in the anaesthetized rat. J Physiol 363:335–349.

Abraham WC, Logan B, Wolff A, Benuskova L (2007) "Heterosynaptic" LTD in the dentate gyrus of anesthetized rat requires homosynaptic activity. J Neurophysiol 98:1048–1051.

Alvarez V a, Sabatini BL (2007) Anatomical and physiological plasticity of dendritic spines. Annu Rev Neurosci 30:79–97.

Alvarez-Salvado E, Pallarés V, Moreno A, Canals S (2014) Functional MRI of long-term potentiation: imaging network plasticity. Philos Trans R Soc Lond B Biol Sci 369:20130152.

Benuskova L, Abraham WC (2007) STDP rule endowed with the BCM sliding threshold accounts for hippocampal heterosynaptic plasticity. J Comput Neurosci 22:129–133.

Benuskova L, Jedlicka P (2012) Computational modeling of long-term depression of synaptic weights: Insights from stdp, metaplasticity and spontaneous activity. Neural Netw World 22:161–180.

Bosch M, Hayashi Y (2012) Structural plasticity of dendritic spines. Curr Opin Neurobiol 22:383–388.

Bramham CR, Worley PF, Moore MJ, Guzowski JF (2008) The immediate early gene arc/arg3.1: regulation, mechanisms, and function. J Neurosci 28:11760–11767.

Cameron HA, Glover LR (2014) Adult Neurogenesis: Beyond Learning and Memory. Annu Rev Psychol 66:1–29.

Cameron HA, Glover LR (2015) Adult Neurogenesis: Beyond Learning and Memory*. Annu Rev Psychol 66:53–81.

Chistiakova M, Bannon NM, Chen J-Y, Bazhenov M, Volgushev M (2015) Homeostatic role of heterosynaptic plasticity: models and experiments. Front Comput Neurosci 9:1–22.

Clelland CD, Choi M, Romberg C, Clemenson GD, Fragniere A, Tyers P, Jessberger S, Saksida LM, Barker R a, Gage FH, Bussey TJ (2009) A functional role for adult hippocampal neurogenesis in spatial pattern separation. Science (80-) 325:210–213.

David G. Amaral, Scharfman HE, Lavenex P (2007) The dentate gyrus: fundamental neuroanatomical organization (dentate gyrus for dummies). Prog Brain Res 153:390–394.

Deller T, Korte M, Chabanis S, Drakew A, Schwegler H, Stefani GG, Zuniga A, Schwarz K, Bonhoeffer T, Zeller R, Frotscher M, Mundel P (2003) Synaptopodin-deficient mice lack a spine apparatus and show deficits in synaptic plasticity. Proc Natl Acad Sci U S A 100:10494–10499.

Denny CA, Kheirbek MA, Alba EL, Tanaka KF, Brachman RA, Laughman KB, Tomm NK, Turi GF, Losonczy A, Hen R (2014) Hippocampal memory traces are differentially modulated by experience, time, and adult neurogenesis. Neuron 83:189–201.

Deshpande A, Bergami M, Ghanem A, Conzelmann K-K, Lepier A, Götz M, Berninger B (2013) Retrograde monosynaptic tracing reveals the temporal evolution of inputs onto new neurons in the adult dentate gyrus and olfactory bulb. Proc Natl Acad Sci U S A 110:E1152–E1161.

Fleischmann A, Hvalby O, Jensen V, Strekalova T, Zacher C, Layer LE, Kvello A, Reschke M, Spanagel R, Sprengel R, Wagner EF, Gass P (2003) Impaired long-term memory and NR2A-type NMDA receptor-dependent synaptic plasticity in mice lacking c-Fos in the CNS. J Neurosci 23:9116–9122.

Fukazawa Y, Saitoh Y, Ozawa F, Ohta Y, Mizuno K, Inokuchi K (2003) Hippocampal LTP is accompanied by enhanced F-actin content within the dendritic spine that is essential for late LTP maintenance in vivo. Neuron 38:447–460.

Gage FH (2010) Mammalian neural stem cells. Science (80-) 287:1433–1438.

Ge S, Yang C-H, Hsu K-S, Ming G-L, Song H (2007) A critical period for enhanced synaptic plasticity in newly generated neurons of the adult brain. Neuron 54:559–566.

Huber L, Menzel R (2004) Structural basis of long-term potentiation in single dendritic spines. Nature 429:761–766.

Jedlicka P, Benuskova L, Abraham WC (2015) A Voltage-Based STDP Rule Combined with Fast BCM-Like Metaplasticity Accounts for LTP and Concurrent "Heterosynaptic" LTD in the Dentate Gyrus In Vivo. PLOS Comput Biol 11:e1004588.

Jedlicka P, Schwarzacher SW, Winkels R, Kienzler F, Frotscher M, Bramham CR, Schultz C, Bas Orth C, Deller T (2009) Impairment of in vivo theta-burst long-term potentiation and network excitability in the dentate gyrus of synaptopodin-deficient mice lacking the spine apparatus and the cisternal organelle. Hippocampus 19:130–140.

Jungenitz T, Radic T, Jedlicka P, Schwarzacher SW (2014) High-frequency stimulation induces gradual immediate early gene expression in maturing adult-generated hippocampal granule cells. Cereb Cortex 24:1845–1857.

Kempermann G, Song H, Gage FH (2015) Neurogenesis in the Adult Hippocampus. Cold Spring Harb Perspect Biol 7:a018812.

Kim CH, Lisman JE (1999) A role of actin filament in synaptic transmission and long-term potentiation. J Neurosci 19:4314–4324.

Marin-Burgin a., Mongiat L a., Pardi MB, Schinder a. F (2012) Unique Processing During a Period of High Excitation/Inhibition Balance in Adult-Born Neurons. Science (80-) 335:1238–1242.

Martínez-Canabal A (2015) Rewiring, forgetting and learning. Commentary: A critical period for experience-dependent remodeling of adult-born neuron connectivity. Front Neurosci 9:710–717.

Mongiat L a, Espósito MS, Lombardi G, Schinder AF (2009) Reliable activation of immature neurons in the adult hippocampus. PLoS One 4:e5320.

Nakashiba T, Cushman JD, Pelkey K a, Renaudineau S, Buhl DL, McHugh TJ, Barrera VR, Chittajallu R, Iwamoto KS, McBain CJ, Fanselow MS, Tonegawa S (2012) Young dentate granule cells mediate pattern separation, whereas old granule cells facilitate pattern completion. Cell 149:188–201.

Oh WC, Parajuli LK, Zito K (2015) Heterosynaptic Structural Plasticity on Local Dendritic Segments of Hippocampal CA1 Neurons. Cell Rep 10:162–169.

Ohkawa N, Saitoh Y, Tokunaga E, Nihonmatsu I, Ozawa F, Murayama A, Shibata F, Kitamura T, Inokuchi K (2012) Spine Formation Pattern of Adult-Born Neurons Is Differentially Modulated by the Induction Timing and Location of Hippocampal Plasticity. PLoS One 7:e45270.

Okamoto K-I, Nagai T, Miyawaki A, Hayashi Y (2004) Rapid and persistent modulation of actin dynamics regulates postsynaptic reorganization underlying bidirectional plasticity. Nat Neurosci 7:1104–1112.

Petersen RP, Moradpour F, Eadie BD, Shin JD, Kannangara TS, Delaney KR, Christie BR (2013) Electrophysiological identification of medial and lateral perforant path inputs to the dentate gyrus. Neuroscience 252:154–168.

Popov VI, Davies H a., Rogachevsky V V., Patrushev I V., Errington ML, Gabbott PL a, Bliss TVP, Stewart MG (2004) Remodelling of synaptic morphology but unchanged synaptic density during late phase long-term potentiation (LTP): A serial section electron micrograph study in the dentate gyrus in the anaesthetised rat. Neuroscience 128:251–262.

Radic T, Al-Qaisi O, Jungenitz T, Beining M, Schwarzacher SW (2015) Differential structural development of adult-born septal hippocampal granule cells in the Thy1-GFP mouse, nuclear size as a new index of maturation. PLoS One 10:e0135493.

Reymann KG, Frey JU (2007) The late maintenance of hippocampal LTP: requirements, phases, "synaptic tagging", "late-associativity" and implications. Neuropharmacology 52:24–40.

Schindelin J, Arganda-Carreras I, Frise E, Kaynig V, Longair M, Pietzsch T, Preibisch S, Rueden C, Saalfeld S, Schmid B, Tinevez J-Y, White DJ, Hartenstein V, Eliceiri K, Tomancak P, Cardona A (2012) Fiji: an open-source platform for biological-image analysis. Nat Methods 9:676–682.

Schmidt-Hieber C, Jonas P, Bischofberger J (2004) Enhanced synaptic plasticity in newly generated granule cells of the adult hippocampus. Nature 429:184–187.

Snyder JS, Choe JS, Clifford MA, Jeurling SI, Hurley P, Brown A, Kamhi JF, Cameron HA (2009) Adult-Born Hippocampal Neurons Are More Numerous, Faster Maturing, and More Involved in Behavior in Rats than in Mice. J Neurosci 29:14484–14495.

Sorra KE, Harris KM (2000) Overview on the structure, composition, function, development, and plasticity of hippocampal dendritic spines. Hippocampus 10:501–511.

Steward O, Wallace CS, Lyford GL, Worley PF (1998) Synaptic activation causes the mRNA for the IEG Arc to localize selectively near activated postsynaptic sites on dendrites. Neuron 21:741–751.

Temprana SG, Mongiat L a, Yang SM, Trinchero MF, Alvarez DD, Kropff E, Giacomini D, Beltramone N, Lanuza GM, Schinder a F (2015) Delayed Coupling to Feedback Inhibition during a Critical Period for the Integration of Adult-Born Granule Cells. Neuron 85:116–130.

Toni N, Laplagne DA, Zhao C, Lombardi G, Ribak CE, Gage FH, Schinder AF (2008) Neurons born in the adult dentate gyrus form functional synapses with target cells. Nat Neurosci 11:901–907.

Toni N, Sultan S (2011) Synapse formation on adult-born hippocampal neurons. Eur J Neurosci 33:1062–1068.

Toni N, Teng EM, Bushong E a, Aimone JB, Zhao C, Consiglio A, van Praag H, Martone ME, Ellisman MH, Gage FH (2007) Synapse formation on neurons born in the adult hippocampus. Nat Neurosci 10:727–734.

Valtorta F, Pozzi D, Benfenati F, Fornasiero EF (2011) The synapsins: Multitask modulators of neuronal development. Semin Cell Dev Biol 22:378–386.

van Praag H, Schinder A, Christie B, Toni N (2002) Functional neurogenesis in the adult hippocampus. Nature 415:1030–1034.

Vivar C, Potter MC, Choi J, Lee J-Y, Stringer TP, Callaway EM, Gage FH, Suh H, van Praag H (2012) Monosynaptic inputs to new neurons in the dentate gyrus. Nat Commun 3:1107.

Wilson RC (1981) Changes in translation of synaptic excitation to dentate granule cell discharge accompanying long-term potentiation. I. Differences between normal and reinnervated dentate gyrus. J Neurophysiol 46:324–338.

Wilson RC, Levy WB, Steward O (1979) Functional Effects of Lesio-Induced Plasticity: Long Term Potentiation in Normal and Lesion-Induced Temporodentate Connections. Brain Res 176:65–78.

Wilson RC, Levy WB, Steward O (1981) Changes in translation of synaptic excitation to dentate granule cell discharge accompanying long-term potentiation. II. An evaluation of mechanisms utilizing dentate gyrus dually innervated by surviving ipsilateral and sprouted crossed temporodentate inp. J Neurophysiol 46:339–355.

Wosiski-kuhn M, Stranahan AM (2012) Transient increases in dendritic spine density contribute to dentate gyrus long-term potentiation. Synapse 66:661–664.

Zhao C, Teng EM, Summers RG, Jr. M, G.l, Gage FH (2006) Distinct morphological stages of dentate granule neuron maturation in the adult mouse hippocampus. J Neurosci 26:3–11.

Zhou Q, Homma KJ, Poo MM (2004) Shrinkage of dendritic spines associated with long-term depression of hippocampal synapses. Neuron 44:749–757.
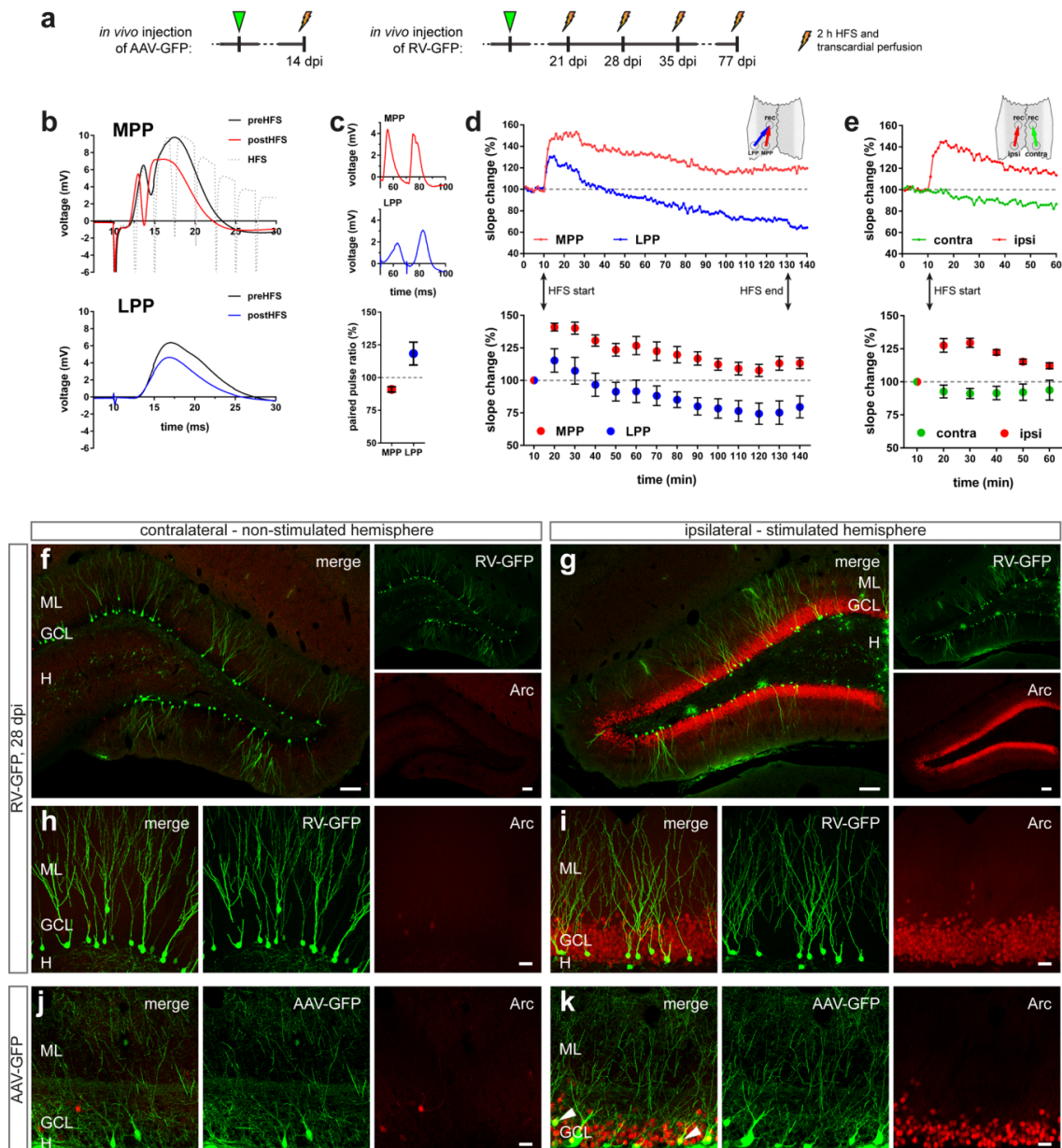
9.9. Figures with legends

Figure 1 Expression of Arc in GFP-labeled young (RV-GFP) and mature (AAV-GFP) GCs following 2 h HFS. (a) Local bilateral intra-hippocampal injections of a murine leukemia virus (RV-GFP, CAG promotor) or an adeno-associated virus (AAV-GFP, synapsin promotor) were performed for GFP-labeling (green) of abGCs **(f-i)** or mature neurons **(j, k)**, respectively. Subsequently, HFS was applied (8 pulses at 400 Hz) to the medial perforant path (MPP). **(b)** In order to estimate homosynaptic induced LTP and heterosynaptic induced LTD, evoked local field potentials of GCS by

MPP stimulation and lateral perforant path (LPP) stimulation were recorded in the DG before application of MPP HFS (black), during MPP HFS (grey dotted line) and following MPP HFS (MPP: red, LPP: blue). **(c)** Low intensity paired pulse stimulation with 20 ms interpulse-interval of the LPP resulted in paired pulse disinhibition and enlargement of the second pulse. **(d)** HFS of the MPP induced LTP via the MPP and LTD via the LPP (top: single animal time course, bottom: group time course). **(e)** Unilateral MPP HFS induced a strong LTP, which was restricted to the ipsilateral hemisphere (top: single animal time course, bottom: group time course). **(g, i, k)** Induction of LTP was accompanied by strong expression of Arc (red) in the ipsilateral granule cell layer (GCL) of the DG, including RV-GFP- and AAV-GFP-labeled GCs. **(f, h, j)** In contrast, the contralateral GCL showed only very sparse Arc labeling. White arrows indicate AAV-GFP- and Arc-labeled GCs. Number of animals: **(c, d)** n = 6, **(e)** n = 3. Scale bars: **(f, g)** 100 µm, **(h-k)** 25 µm. EC, entorhinal cortex; H, hilus; ML, molecular layer.
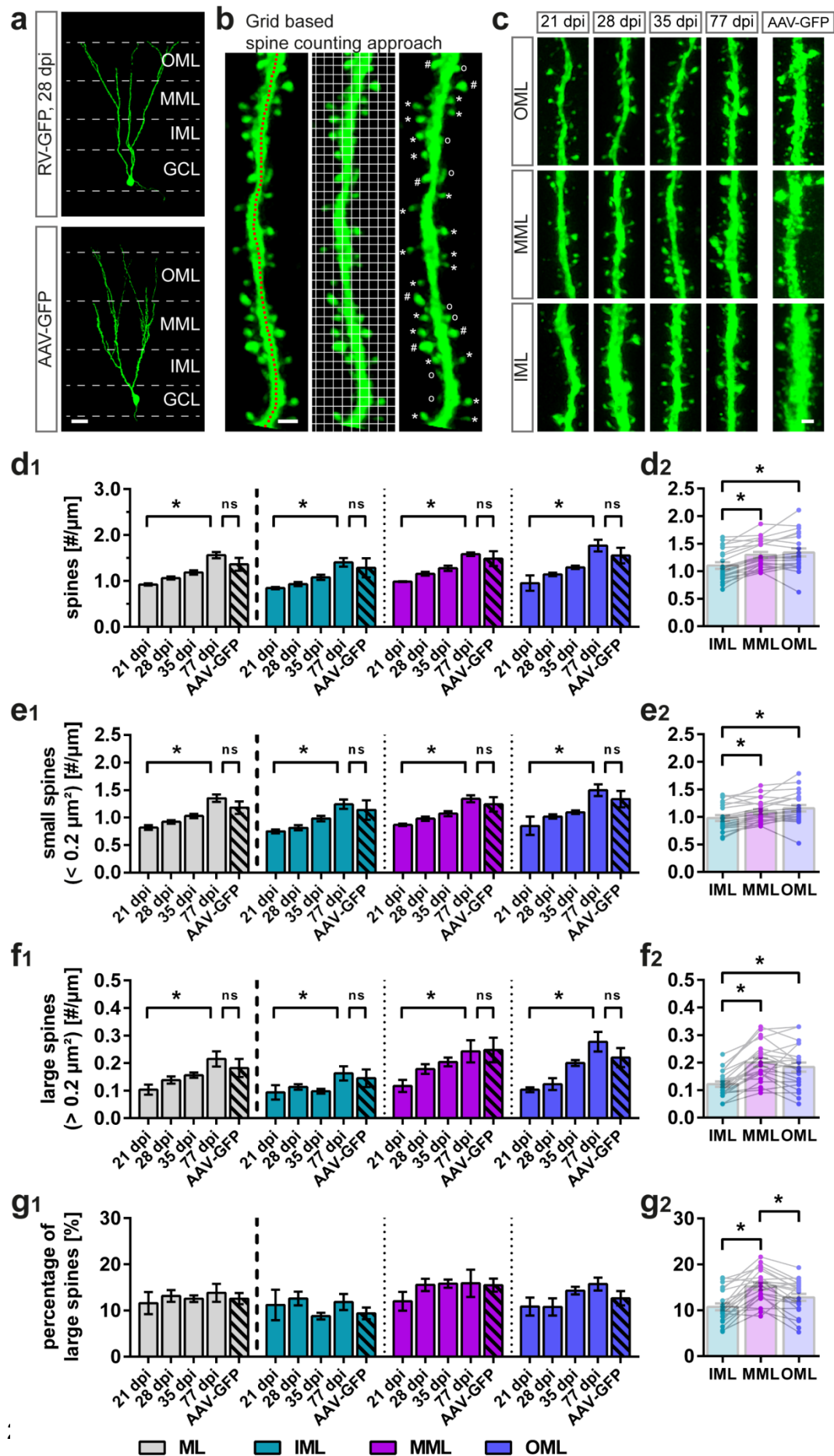
◄ **Figure 2 Time course of dendritic spine development in abGCs. (a)** Sample RV-GFP-labeled abGC at 28 dpi and AAV-GFP-labeled mGC, used to quantify dendritic spines in the inner (IML), middle (MML), and outer (OML) molecular layer during the development of abGCs and in mGCs. **(b)** The length of a dendritic segment was measured in a z-projection (left image, red dotted line), and a grid-based approach (middle image, grid size 0.2 µm²) was used to determine the density of spines in general and to differentiate between small (< 0.2 µm², indicated by stars) and large (> 0.2 µm², indicated by dashes) spines (right image). Spines without a spine neck and head were excluded from analysis (indicated by open circles). **(c)** Samples of dendritic segments from 21 - 77 dpi abGCs and mGCs showing spines in the IML, MML, and OML. **(d_1)** Density of spines in RV-GFP-labeled abGCs in the complete ML from 21 - 77 dpi and in AAV-GFP-labeled mGCs. **(d_2)** Density of spines per layer. **(e_1)** Density of small spines. **(e_2)** Density of small spines per layer. **(f_1)** Density of large spines. **(f_2)** Density of large spines per layer. **(g_1)** Percentage of large spines was calculated as relative amount of large spines from spine density. **(g_2)** Overall percentage of large spines per layer. $n_{21\ dpi} = 3$, $n_{28\ dpi} = 6$, $n_{35\ dpi} = 5$, $n_{77\ dpi} = 4$, $n_{AAV-GFP} = 4$. **(d_1-g_1)** Kruskal-Wallis with Dunn's multiple comparisons test (21 dpi vs. 77 dpi, 77 dpi vs. mGCs): *$P < 0.05$. **(d_2-g_2)** Friedman with Dunn's multiple comparisons test (IML vs. MML, IML vs. OML, MML vs. OML): *$P < 0.05$. Scale bars: **(a)** 25 µm, **(b, c)** 1 µm. GCL, granule cell layer; H, hilus.
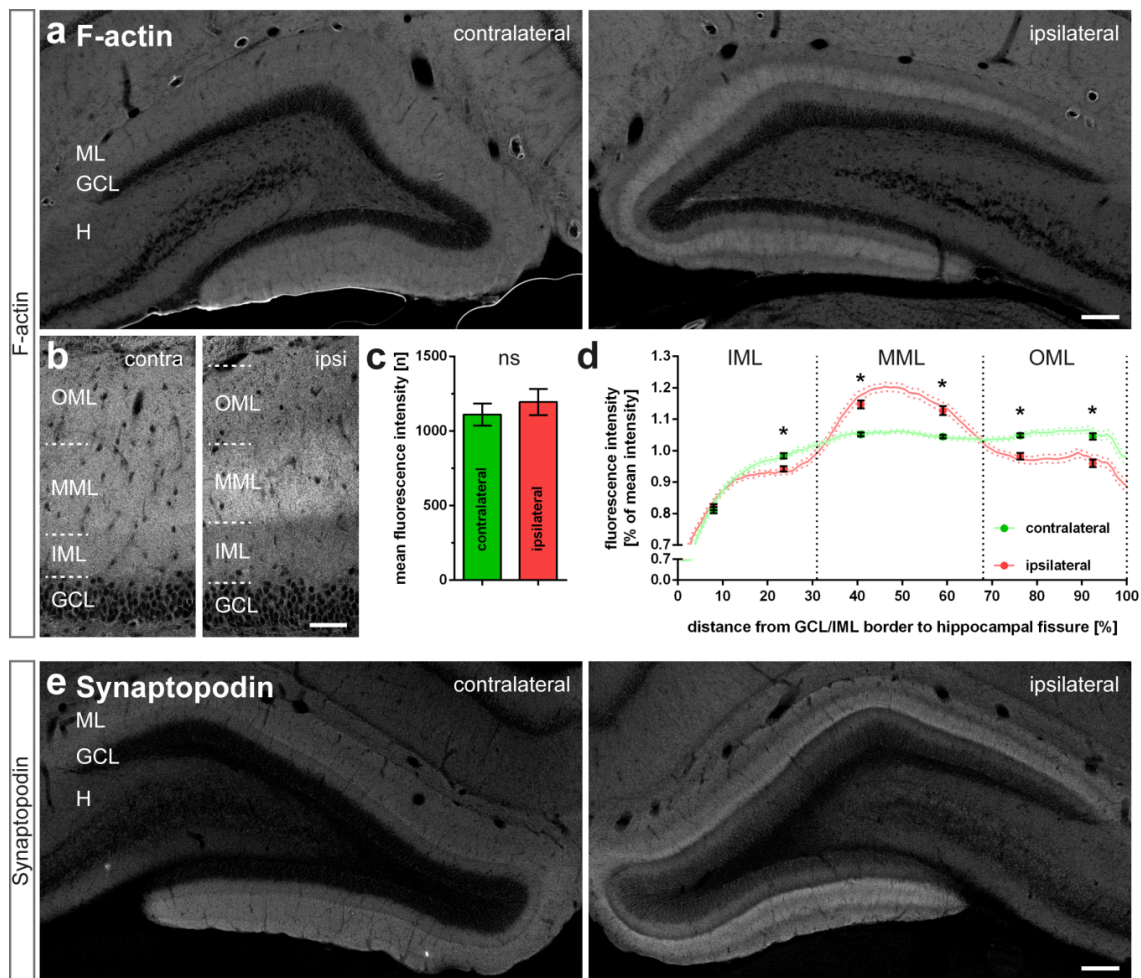
Figure 3 F-actin and synaptopodin are enhanced in the MML following 2 h HFS of the medial perforant path. (a, b) Expression of F-actin following 2 h HFS. **(c)** Immunofluorescence intensity of the entire ML was not altered following HFS in the stimulated (ipsilateral, red) versus unstimulated (contralateral, green) side. **(d)** Normalized intensity profiles obtained across the ML (from the GCL-IML-border to the hippocampal fissure) revealed layer-specific changes of F-actin expression on the stimulated (ipsilateral, red line) side compared to the contralateral side (green line). **(e)** Note layer-specific changes of synaptopodin expression on the stimulated (ipsilateral) side. Number of animals: $n_{F-actin} = 21$. **(c)** Two-sided Wilcoxon rank-sum test: *P < 0.05. **(d)** Two-way ANOVA with Bonferroni correction: *P < 0.05. Scale bars: **(a, e)** 100 µm, **(b)** 50 µm. ipsi, ipsilateral; contra, contralateral; GCL, granule cell layer; H, hilus; ML, molecular layer.
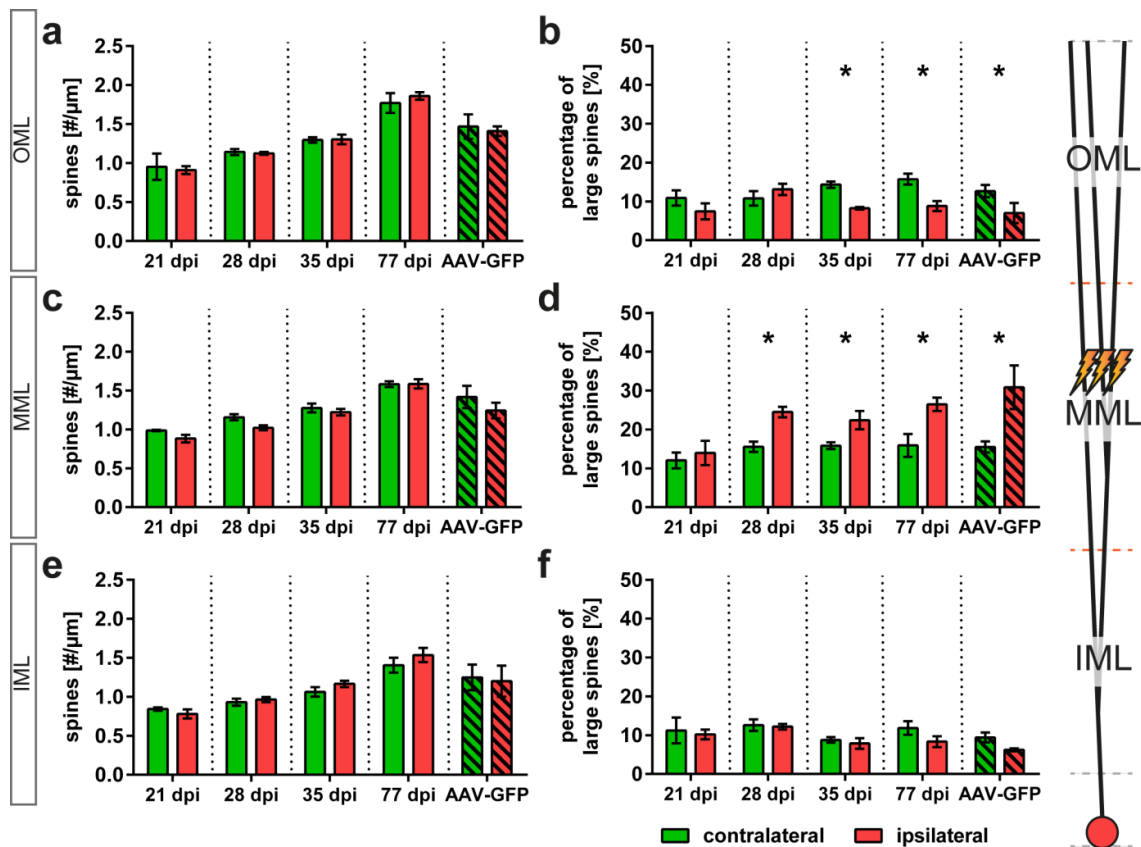
Figure 4 Percentage of large spines is increased in the MML and decreased in the OML following 2 h HFS of the medial perforant path. The medial perforant path was stimulated with a strong HFS protocol for 2 h to induce LTP in the ipsilateral middle molecular layer (MML). Dendritic spines of RV-GFP-labeled abGCs (21 - 77 dpi), or AAV-GFP-labeled mGCs were analyzed in a layer-specific approach. The contralateral, non-stimulated hemisphere was used as a control. **(a)** Spine density in the outer molecular layer (OML) was not altered following HFS. **(b)** The percentage of large spines showed a significant decrease in abGCs from 28 dpi on and in mGCs. **(c)** Spine density in the MML did not change following stimulation at any age neither in abGCs, nor in mGCs. **(d)** The percentage of large spines significantly increased in abGCs from 28 dpi on and in mGCs. **(e, f)** In this analysis, spines in the inner molecular layer (IML) were not significantly affected by HFS (but see also **Fig. 5b**). $n_{21\ dpi} = 3$, $n_{28\ dpi} = 6$, $n_{35\ dpi} = 5$, $n_{77\ dpi} = 4$, $n_{AAV-GFP} = 4$. Two-sided Wilcoxon rank-sum test: *$P < 0.05$.
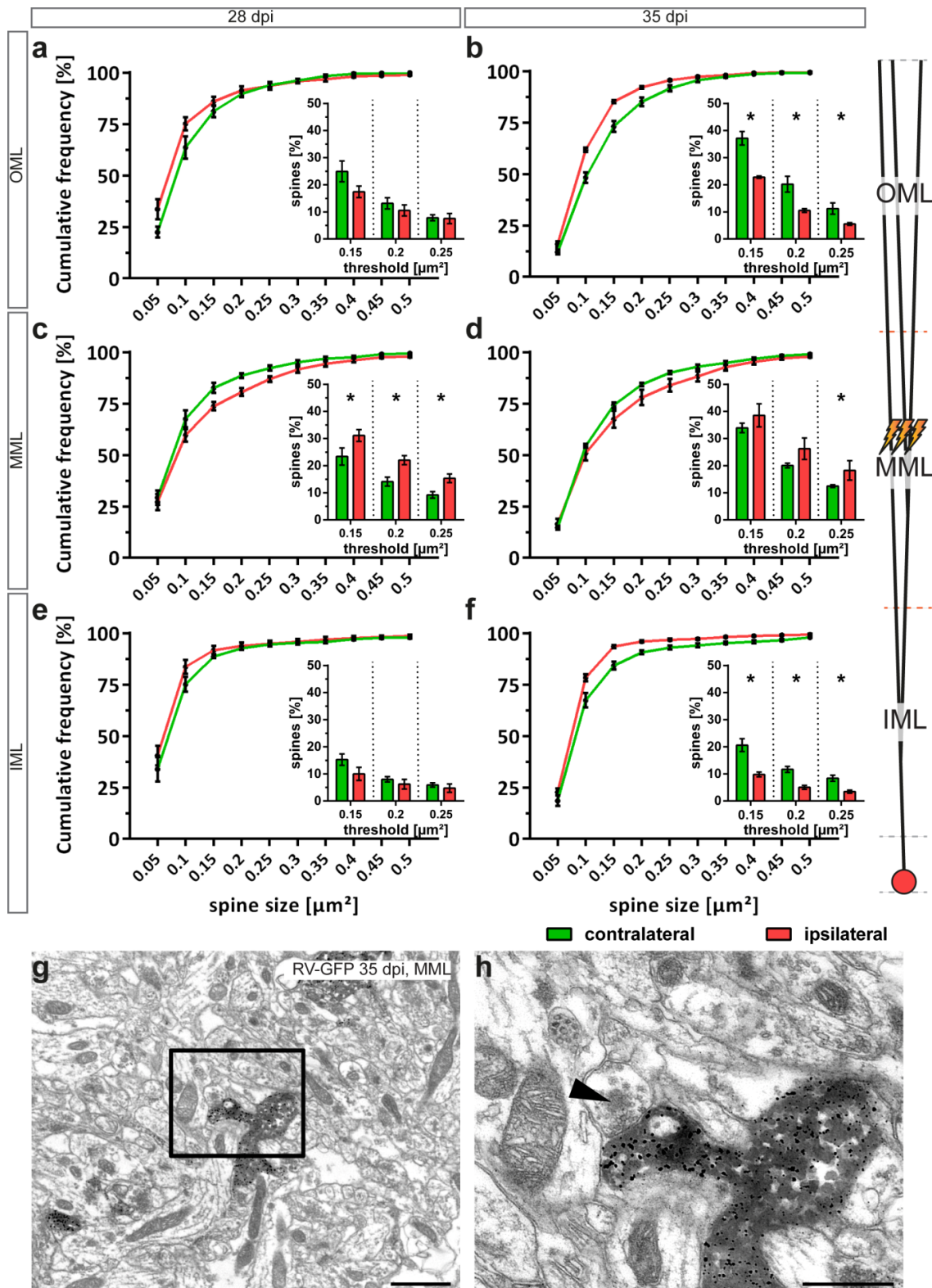
Figure 5 Layer-specific spine size histograms confirm HFS-induced spine plasticity in 28 dpi and 35 dpi abGCs. (a-f) Cumulative fractions of spine head sizes (largest cross-sectional areas) with HFS (red, ipsilateral) and without HFS (green, contralateral) in OML **(a, b)**, MML **(c, d)**, and IML **(e, f)**. Insets identify the amount of

spines larger than the following thresholds: $0.15\ \mu m^2$, $0.2\ \mu m^2$, and $0.25\ \mu m^2$. Significant homosynaptic structural plasticity in the MML of 28 dpi **(c)** and 35 dpi **(d)** abGCs, as well as significant heterosynaptic plasticity in the IML **(f)** and OML **(b)** of 35 dpi abGCs. **(g)** Electron micrograph illustrating an immuno-labeled cross-section of a dendritic segment located in the MML with a spine of a RV-GFP-labeled abGC (35 dpi). **(h)** Enlarged area from g (black rectangle). The spine forms a synapse with an unlabeled axon terminal (black arrow). $n_{28\ dpi} = 6$, $n_{35\ dpi} = 5$. Two-sided Wilcoxon ranksum test: *$P < 0.05$. Scale bars: **(g)** 1000 nm, **(h)** 500 nm.
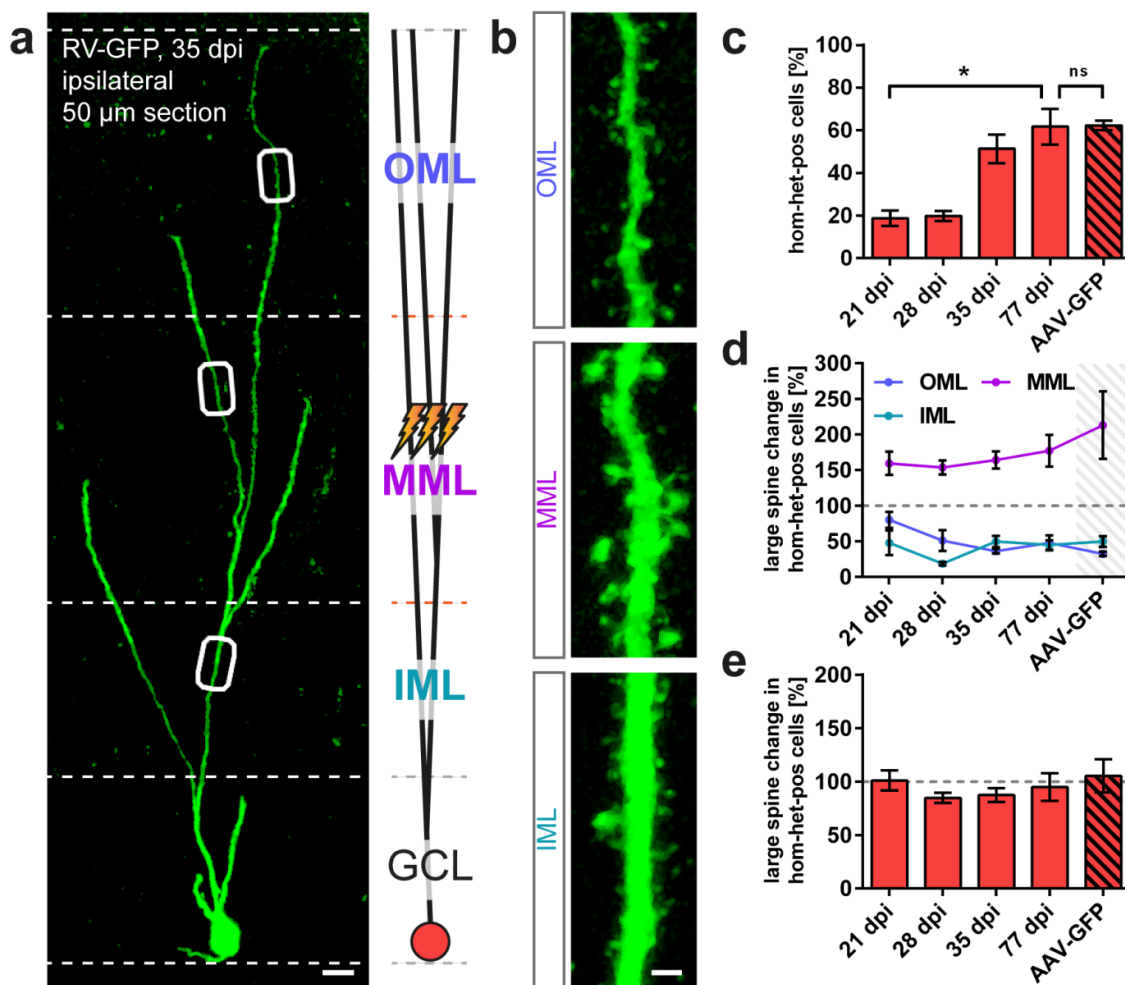
Figure 6 Homo- and concurrent heterosynaptic structural plasticity is induced within the same dendritic tree of individual GCs following 2 h HFS. (a) Homo- and heterosynaptic structural remodeling of spines was analyzed in dendritic segments of the same GC. **(b)** GCs exhibiting homosynaptic structural plasticity in the MML, heterosynaptic structural plasticity in the IML and OML following HFS were identified from the entire population of analyzed cells. **(c)** Fraction of abGCs exhibiting structural homosynaptic spine enlargement and heterosynaptic spine shrinkage (hom-het-pos cells). **(d)** Similar changes in large spines of hom-het-pos GCs in the MML, IML, and OML in all age groups. **(e)** Overall percentage of large spines along the entire dendritic tree (comprising IML, MML, and OML) in relation to the contralateral side, indicating that structural heterosynaptic spine shrinkage in the IML and OML counteracted induction of homosynaptic spine enlargement in the MML. $n_{21\,dpi} = 3$, $n_{28\,dpi} = 6$, $n_{35\,dpi} = 5$, $n_{77\,dpi} = 4$, nAAV-GFP = 4. **(c, d)** Kruskal-Wallis with Dunn's multiple comparisons test (21 dpi vs. 77 dpi, 77 dpi vs. AAV-GFP): *$P < 0.05$. **(e)** Two-sided

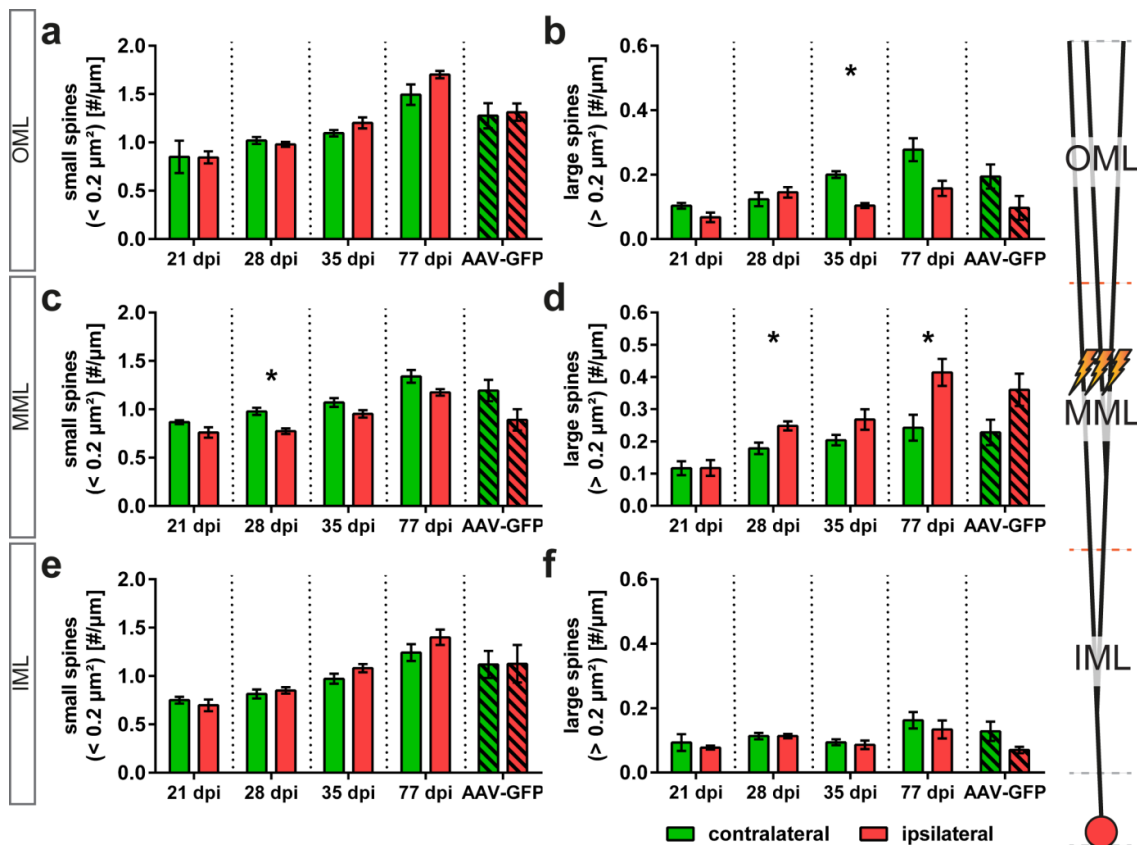Wilcoxon rank-sum test: *P < 0.05. Scale bars: **(a)** 10 µm, **(b)** 1 µm. GCL, granule cell layer.

Figure S1 The number of large spines is increased in the MML and decreased in the OML following 2 h HFS of the medial perforant path. (a) Small spines in the outer molecular layer (OML) were not affected by stimulation at any age. **(b)** Large spines were significantly increased at 35 dpi. **(c)** Small spines decreased in the middle molecular layer (MML) at 28 dpi following stimulation. **(d)** Large spines were significantly increased at 28 dpi and 77 dpi. **(e, f)** Spines in the inner molecular layer (IML) were not affected by HFS and showed no structural changes. $n_{21\ dpi} = 3$, $n_{28\ dpi} = 6$, $n_{35\ dpi} = 5$, $n_{77\ dpi} = 4$, $n_{AAV-GFP} = 4$. Two-sided Wilcoxon rank-sum test: *$P < 0.05$.

Danksagung (Acknowledgments in German language)

Im Folgenden möchte ich die Gelegenheit ergreifen und mich bei allen nachstehenden Personen bedanken, die mich durch die Zeit meiner Doktorarbeit begleitet haben, indem sie mir mit wissenschaftlichen Rat zur Seite standen oder mich mit ihrer Freundschaft unterstützten.

Ich bedanke mich bei meinem wissenschaftlichen Betreuer PD Dr. med. Stephan Schwarzacher für die Bereitstellung dieses faszinierenden Promotionsthemas und seine fortwährende Unterstützung während meiner Doktorarbeit. Die vielen intellektuellen und persönlichen Gespräche werden mir immer in Erinnerung bleiben. Ich habe unsere Dialoge stets als Ermutigung und Motivation empfunden.

Des Weiteren möchte ich mich bei Prof. Dr. med. Thomas Deller für die stete Unterstützung meiner Doktorarbeit bedanken. Seine außerordentlich sachkundigen, erfahrenen und wertvollen Anregungen und Ratschläge habe ich immer geschätzt.

Ebenfalls bedanke ich mich bei Prof. Dr. Manfred Kössl aus dem Fachbereich der Biowissenschaften für seine Betreuung meiner Doktorarbeit.

Großer Dank gebührt auch Dr. med. Peter Jedlicka und Dr. Hermann Cuntz für ihre Unterstützung und kritischen Diskussionen, Expertise und kreativen Ideen. Die TREES toolbox hat große Teile meiner Doktorarbeit erst möglich gemacht.

Zu Dank verpflichtet bin ich auch unseren beiden TAs Anke Biczysko und Ute Fertig für ihre Hilfe bei der histologischen Aufarbeitung meiner zahlreichen Präparate und der professionellen Erstellung elektronenmikroskopischer Aufnahmen.

Mein außerordentlicher Dank gilt Martina Hütten, nicht nur für ihre Hilfe im Umgang mit der alltäglichen Bürokratie, sondern auch dafür, dass sie mir den Spaß am Tennis vermitteln konnte.

Ein ganz besonderer Dank geht an meine beiden Mitdoktoranden Tijana Radic und Marcel Beining für diese aufregende Zeit, aus der eine tief empfundene Freundschaft hervorgegangen ist. In der heutigen Welt ist die erfolgreiche Bearbeitung komplexer wissenschaftlicher Themen nicht mehr im Alleingang zu bewältigen. Freundschaft und Vertrauen sind dafür essentiell. Und natürlich auch das Feierabendbierchen!

Ich möchte mich auch bei allen aktuellen und ehemaligen Kollegen und Freunden aus dem Institut der klinischen Neuroanatomie für die hilfreichen wissenschaftlichen Diskussionen und die freundliche Atmosphäre bedanken: Alban Avdiu, Aline Blistein, Andreas Vlachos, Andreas Strehl, Charlotte Nolte-Uhl, Christos Galanis, Daniel Brühl, Denise Becker, Domenico Del Turco, Estifanos Ghebremedhin, Gabriela Hengel, Gerlind Schuldt, Heike Korff, Jessica Schlaudraff, Ju Won Chae, Julia Muellerleile, Kendrick Yap, Lars Hildebrandt-Einfeldt, Laurent Willems, Mandy Paul, Marie-Christine Beyer, Matej Vnencak, Mathias Singer, Maximilian Lenz, Meike Hick, Michael Rietsche, Nadine Zahn, Namrata Mohapatra, Rainer Wenzel, Sabine Schiener, Silvia Rodrìguez Rozada, Steffen Platschek, Sylvia Cienciala und Viktor Beeg Moreno.

An dieser Stelle möchte ich mich auch bei meinen alten Freunden aus Magdeburg und Frankfurt bedanken: Alexander, Clemens, Eike, Martin, Moyo und Przemyslaw. Auch wenn das Leben für uns unterschiedliche Richtungen genommen hat, bleibt die Zeit, die wir gemeinsam verbracht haben einfach unvergesslich.

Ein ganz besonderer Dank geht an meine Eltern. Ihr habt mir durch eure bedingungslose Unterstützung das Studium der Biologie erlaubt und meine anschließende Doktorarbeit erst ermöglicht.

Tief verbunden und dankbar bin ich meiner Freundin, Marie-Violet, für ihre emotionale Unterstützung und ihr unendliches Verständnis während des Schreibens dieser Doktorarbeit.

Acknowledgments

I want to take the chance and thank a number of people who scientifically contributed to my PhD thesis with their good advice or with their friendship.

I would like to thank my supervisor Dr. med. Stephan Schwarzacher for this fascinating research topic and for his support. The numerous scientific and personal conversations will remain in my memory. I always perceived our dialogues as encouragement and motivation.

Furthermore, I also want to thank Prof. Dr. med. Thomas Deller. I always appreciated his extraordinarily knowledgeable, experienced and valuable suggestions.

I want to thank my second supervisor Prof. Dr. Manfred Kössl in the Department of Biological Sciences for his support.

Big thanks belong to Dr. med. Peter Jedlicka and Dr. Hermann Cuntz for their critical discussions, expertise and creative ideas. The TREES toolbox made large parts of my thesis possible.

I would also like to acknowledge our technical assistents Anke Biczysko and Ute Fertig, for their help on the histological preparation of my endless specimen and for the professional creation of electron micrographs.

My special thanks go to Martina Hütten, not only for her help in dealing with everyday bureaucracy, but also for showing me that tennis can be fun.

A very special thank you goes to my two fellow PhD students Tijana Radic and Marcel Beining. This was an exciting time of my life which resulted in a deeply felt friendship. In today's world, the successful processing of complex scientific topics is no longer manageable alone. A trustful friendship and of course, an after-work beer are essential!

I want to thank all current and former colleagues and friends of the Institute of Clinical Neuroanatomy for their helpful scientific discussions and the friendly atmosphere: Alban Avdiu, Aline Blistein, Andreas Vlachos, Andreas Strehl,

Erklärung über Anteile der Autoren an den Publikationen

High-frequency stimulation induces gradual immediate early gene expression in maturing adult-generated hippocampal granule cells. Cereb Cortex. 2014 Jul;24(7):1845-57

	Entwicklung und Planung	Durchführung der einzelnen Experimente	Erstellung der Datensammlung und Abbildungen	Analyse / Interpretation der Daten	Verfassen des Manuskripts
Jungenitz, Tassilo	40 %	80 % *in vivo* Stimulation und Ableitungen, BrdU Injektionen, Schnitte, Immunfärbung, konfokale Mikroskopie, Bildverarbeitung	100 %	60 % Analyse-Skripte für Auswertungen, Interpretation	60 %
Radic, Tijana	15 %	20 % Schnitte, Immunfärbung	-	20 % Interpretation	10 %
Jedlicka, Peter	15 %	-	-	10 % Interpretation	15 %
Schwarzacher, Stephan W.	30 %	-	-	10 % Interpretation	15 %

Datum/Ort   Datum/Ort

Unterschrift Promovend   Unterschrift Betreuer

Differential structural development of adult-born septal hippocampal granule cells in the Thy1-GFP mouse, nuclear size as a new index of maturation. PLoS One. 2015 Aug 12;10(8):e0135493

	Entwicklung und Planung	Durchführung der einzelnen Experimente	Erstellung der Datensammlung und Abbildungen	Analyse / Interpretation der Daten	Verfassen des Manuskripts
Radic, Tijana	20 %	30 % BrdU Injektionen, Schnitte, Immunfärbung	40 % Fig. 2, Fig. 3	30 % Analyse, Interpretation	30 %
Al-Qaisi, Omar	20 %	40 % BrdU Injektionen, Schnitte, Immunfärbung, konfokale Mikroskopie, Bildverarbeitung	20 % Fig. 1	20 % Analyse, Interpretation	20 %
Jungenitz, Tassilo	20 %	30 % BrdU Injektionen, Schnitte, Immunfärbung	40 % Fig. 4, Fig. 5	30 % Analyse, Interpretation	25 %
Beining, Marcel	5 %	5 % Histologische Auswertung	-	10 % Interpretation	10 %
Schwarzacher, Stephan W.	30 %	-	-	10 % Interpretation	15 %

Datum/Ort   Datum/Ort

Unterschrift Promovend   Unterschrift Betreuer

Adult-born hippocampal granule cells exhibit a critical period of dendritic reorganization and remain structurally distinct from perinatally born granule cells. Brain Struct Funct., first online 11 August 2016

	Entwicklung und Planung	Durchführung der einzelnen Experimente	Erstellung der Datensammlung und Abbildungen	Analyse / Interpretation der Daten	Verfassen des Manuskripts
Beining, Marcel	15 %	55 % Virale Injektionen, Schnitte, Immunfärbung, 2-Photonen und konfokale Mikroskopie, Bildverarbeitung, Rekonstruktion, *Morphologisches Modell	70 % Fig. 1C-D, Fig. 2, Fig. 3, Fig. 4, Fig. 5, Fig. S1-S3	60 % Analyse-Skripte für Re-konstruktionen, Interpretation	40 %
Jungenitz, Tassilo	10 %	35 % Wie MB, nur ohne * und zusätzlich noch *in vivo* Stimulation und Ableitung	30 % Fig. 1A-B, Fig. 6	20 % Interpretation	10 %
Radic, Tijana	5 %	10 % Schnitte, Immunfärbung	-	-	5 %
Deller, Thomas	5 %	-	-	-	10 %
Cuntz, Hermann	20 %	-	-	5 % Interpretation	10 %
Jedlicka, Peter	15 %	-	-	5 % Interpretation	10 %
Schwarzacher, Stephan W.	30 %	-	-	10 % Interpretation	15 %

Datum/Ort Datum/Ort

Unterschrift Promovend Unterschrift Betreuer

Structural homo- and heterosynaptic plasticity in adult newborn rat hippocampal granule cells. Submitted research article.

	Entwicklung und Planung	Durchführung der einzelnen Experimente	Erstellung der Datensammlung und Abbildungen	Analyse / Interpretation der Daten	Verfassen des Manuskripts
Jungenitz, Tassilo	20 %	55 % Virale Injektionen, Schnitte, Immunfärbung, 2-Photonen und konfokale Mikroskopie, Bildverabrietung, Spinerekonstruktion, *in vivo Stimulation und Ableitung, *Spinezählung, *EM Bilder	70 % Fig. 1A-E, Fig. 2D-G, Fig. 4, Fig. 5, Fig. 6, Fig. S1	60 % Analyse-Skripte für Spine-auswertung, Interpretation	40 %
Beining, Marcel	10 %	35 % Wie TJ, nur ohne *	30 % Fig. 1F-K, Fig. 3	20 % Interpretation	15 %
Radic, Tijana	10 %	10 % Schnitte, Immunfärbung	-	-	5 %
Deller, Thomas	5 %	-	-	-	10 %
Cuntz, Hermann	5 %	-	-	5 % Interpretation	10 %
Jedlicka, Peter	15 %	-	-	5 % Interpretation	5 %
Schwarzacher, Stephan W.	35 %	-	-	10 % Interpretation	15 %

Datum/Ort   Datum/Ort

Unterschrift Promovend   Unterschrift Betreuer

Erklärung

Ich erkläre hiermit, dass ich mich bisher keiner Doktorprüfung im Mathematisch-Naturwissenschaftlichen Bereich unterzogen habe.

Frankfurt am Main, den …..(Datum und Unterschrift)

Versicherung

Ich erkläre hiermit, dass ich die vorgelegte Dissertation über

„Functional integration and structural development of adult newborn hippocampal granule cells" (deutscher Titel : „Funktionelle Integration und strukturelle Entwicklung von adult neugebildeten hippocampalen Körnerzellen")

selbständig angefertigt und mich anderer Hilfsmittel als der in ihr angegebenen nicht bedient habe, insbesondere, dass alle Entlehnungen aus anderen Schriften mit Angabe der betreffenden Schrift gekennzeichnet sind.

Ich versichere, die Grundsätze der guten wissenschaftlichen Praxis beachtet, und nicht die Hilfe einer kommerziellen Promotionsvermittlung in Anspruch genommen zu haben.

Frankfurt am Main, den ………………………… (Datum und Unterschrift)

Curriculum vitae

Professional experience

September 2010 -
present

Doctoral Researcher, Clinical Neuroanatomy, Goethe University, Frankfurt am Main (Germany)

January 2010 -
August 2010

Research Assistant, Clinical Neuroanatomy, Goethe University, Frankfurt am Main (Germany)

August 2007 -
April 2008

Research Assistant, Institute of Neurology (Edinger Institute), Goethe University, Frankfurt am Main (Germany)

June 2003 -
January 2005

Research Assistant, Fraunhofer Institute for Factory Operation and Automation, Magdeburg (Germany)

Academic career

September 2010 -
present

Postgraduate studies, Clinical Neuroanatomy, Goethe University, Frankfurt am Main (Germany)

October 2004 -
January 2010

Degree in Biology (Dipl.-Biol.), Clinical Neuroanatomy, Goethe University, Frankfurt am Main (Germany) title of diploma thesis: "Aktivierung neugebildeter Körnerzellen des Gyrus dentatus im adulten Organismus durch hochfrequente Stimulation des Tractus perforans", grade 1.2

Scientific publications

Miroci H, Schob C, Kindler S, Ölschläger-Schütt J, Fehr S, **Jungenitz T**, Schwarzacher SW, Bagni C, Mohr E (2012) Makorin ring zinc finger protein 1 (MKRN1), a novel poly(A)-binding protein-interacting protein, stimulates translation in nerve cells. J Biol Chem 287:1322–1334.

Jedlicka P, Vnencak M, Krueger DD, **Jungenitz T**, Brose N, Schwarzacher SW (2013) Neuroligin-1 regulates excitatory synaptic transmission, LTP and EPSP-spike coupling in the dentate gyrus *in vivo*. Brain Struct Funct.

Jungenitz T, Radic T, Jedlicka P, Schwarzacher SW (2014) High-frequency stimulation induces gradual immediate early gene expression in maturing adult-generated hippocampal granule cells. Cereb Cortex 24:1845–1857.

Radic T*, Al-Qaisi O*, **Jungenitz T***, Beining M, Schwarzacher SW (2015) Differential structural development of adult-born septal hippocampal granule cells in the Thy1-GFP mouse, nuclear size as a new index of maturation. PLoS One 10:e0135493. (* joint first-authors)

Beining M*, **Jungenitz T***, Radic T, Deller T, Cuntz H, Jedlicka P, Schwarzacher SW (2016) Adult-born dentate granule cells show a critical period of dendritic reorganization and are distinct from developmentally born cells. Brain Struct Funct. Epub ahead of print (* joint first-authors)

Submitted manuscripts

Jungenitz T*, Beining M*, Radic T, Deller T, Cuntz H, Jedlicka P, Schwarzacher SW (submitted) Structural homo- and heterosynaptic plasticity in adult newborn rat hippocampal granule cells. (* joint first-authors)

Radic T, **Jungenitz T**, Singer M, Beining M, Cuntz H, Vlachos A, Deller T, Schwarzacher SW (submitted) Time-lapse imaging reveals highly dynamic structural maturation of postnatally born dentate granule cells in organotypic entorhino-hippocampal slice cultures.

Scientific conferences, meetings and workshops attended

21. – 24.09.2016   111th Annual Meeting of the Anatomical Society, Göttingen (Germany)
Poster presentation: Adult neurogenesis in the rat hippocampus: structural development and activity-related homo- and heterosynaptic plasticity of adult newborn dentate granule cells. Jungenitz T, Beining M, Radic T, Deller T, Cuntz H, Jedlicka P and Schwarzacher SW.

22. – 24.06.2016   rmn² (rhine main neuroscience network) 4th biennial meeting, Oberwesel (Germany)
Poster presentation: Dynamic structural development, activity-related dendritic plasticity and homo- and heterosynaptic plasticity of adult newborn dentate granule cells in the rat hippocampus. Jungenitz T, Beining M, Radic T, Deller T, Cuntz H, Jedlicka P and Schwarzacher SW. (awarded best poster prize)

23. – 25.09.2015   31. Arbeitstagung der Anatomischen Gesellschaft / 110th Annual Meeting, Würzburg (Germany)

6. – 8.05.2015   Adult Neurogenesis: Evolution, Regulation and Function; Dresden (Germany)
Poster presentation: Structural development and plasticity of adult newborn hippocampal dentate granule cells. Jungenitz T, Beining M, Radic T, Jedlicka P, Schwarzacher SW.

5. - 11.09.2014   route28, Fraunchiemsee (Germany)

5. - 9.07.2014   9th FENS Forum of Neuroscience, Milan (Italy)
Poster presentation: Structural prerequisites for functional integration of adult newborn dentate granule cells in the hippocampus. Jungenitz T, Beining M, Radic T, Schwarzacher SW.

25. - 27.06.2014	rmn² (rhine main neuroscience network) 3rd biennial meeting, Oberwesel (Germany) **Poster presentation:** Structural prerequisites for functional integration of adult newborn dentate granule cells in the hippocampus. Jungenitz T, Beining M, Radic T, Schwarzacher SW.
12. - 17.05.2014	Keystone Symposia: Adult Neurogenesis, Stockholm (Sweden) **Poster presentation:** Structural prerequisites for functional integration of adult newborn dentate granule cells in the hippocampus. Jungenitz T, Beining M, Radic T, Schwarzacher SW.
22.11.2013	ICNF Mini-Symposium, Frankfurt am Main (Germany) **Poster presentation:** Gradual immediate early gene expression and synaptic integration of adult newborn granule cells in the hippocampus. Jungenitz T, Radic T, Jedlicka P, Schwarzacher SW.
24. - 26.06.2013	Eurogenesis, Bordeaux (France) **Poster presentation:** Gradual immediate early gene expression and synaptic integration of adult newborn granule cells in the hippocampus. Jungenitz T, Radic T, Jedlicka P, Schwarzacher SW.
9. - 13.04.2013	15th International Neuroscience Winter Conference, Sölden (Austria) **Poster presentation:** Gradual synaptic integration of maturing adult-generated hippocampal granule cells. Jungenitz T, Radic T, Jedlicka P, Schwarzacher SW.
14. - 18.07.2012	8th FENS Forum of Neuroscience, Barcelona (Spain) **Poster presentation:** Structural development and functional integration of newborn granule cells in the adult hippocampus. Jungenitz T, Al-Qaisi O, Jedlicka P, Schwarzacher SW.

20. - 22.04.2012   rmn² (rhine main neuroscience network) 2nd biennial meeting, Oberwesel (Germany)
Poster presentation: Structural and functional maturation of adult newborn hippocampal granule cells. Jungenitz T, Al-Qaisi O, Deller T, Schwarzacher SW.

23. - 26.03.2012   Joint meeting of Anatomical Societies, Frankfurt am Main (Germany)

25.11.2011   ICNF Mini-Symposium, Frankfurt am Main (Germany)
Poster presentation: Structural and functional maturation of adult newborn hippocampal granule cells. Jungenitz T, Al-Qaisi O, Deller T, Schwarzacher SW.

24. - 26.11.2010   rmn² (rhine main neuroscience network) 1st biennial meeting, Oberwesel (Germany)
Poster presentation: Adult newborn hippocampal granule cells show increasing reactivity to perforant path stimulation with structural maturation. Schwarzacher SW, Jungenitz T, Deller T.

27.11.2009   ICNF Mini-Symposium, Frankfurt am Main (Germany)

6. - 7.03.2009   ICNF Symposium, Frankfurt am Main (Germany)